NUREG/CR-5853
EGG-2670

Investigation of the Applicability and Limitations of the ROSA Large-Scale Test Facility for AP600 Safety Assessment

Prepared by
M. G. Ortiz, J. E. Fisher, J. M. Cozzuol,
T. J. Boucher, S. M. Sloan, S. M. Modro

Idaho National Engineering Laboratory
EG&G Idaho, Inc.

Prepared for
U.S. Nuclear Regulatory Commission

AVAILABILITY NOTICE

Availability of Reference Materials Cited in NRC Publications

Most documents cited in NRC publications will be available from one of the following sources:

1. The NRC Public Document Room, 2120 L Street, NW., Lower Level, Washington, DC 20555

2. The Superintendent of Documents, U.S. Government Printing Office, P.O. Box 37082, Washington, DC 20013-7082

3. The National Technical Information Service, Springfield, VA 22161

Although the listing that follows represents the majority of documents cited in NRC publications, it is not intended to be exhaustive.

Referenced documents available for inspection and copying for a fee from the NRC Public Document Room include NRC correspondence and internal NRC memoranda; NRC bulletins, circulars, information notices, inspection and investigation notices; licensee event reports; vendor reports and correspondence; Commission papers; and applicant and licensee documents and correspondence.

The following documents in the NUREG series are available for purchase from the GPO Sales Program: formal NRC staff and contractor reports, NRC-sponsored conference proceedings, international agreement reports, grant publications, and NRC booklets and brochures. Also available are regulatory guides, NRC regulations in the *Code of Federal Regulations*, and *Nuclear Regulatory Commission Issuances*.

Documents available from the National Technical Information Service include NUREG-series reports and technical reports prepared by other Federal agencies and reports prepared by the Atomic Energy Commission, forerunner agency to the Nuclear Regulatory Commission.

Documents available from public and special technical libraries include all open literature items, such as books, journal articles, and transactions. *Federal Register* notices, Federal and State legislation, and congressional reports can usually be obtained from these libraries.

Documents such as theses, dissertations, foreign reports and translations, and non-NRC conference proceedings are available for purchase from the organization sponsoring the publication cited.

Single copies of NRC draft reports are available free, to the extent of supply, upon written request to the Office of Administration, Distribution and Mail Services Section, U.S. Nuclear Regulatory Commission, Washington, DC 20555.

Copies of industry codes and standards used in a substantive manner in the NRC regulatory process are maintained at the NRC Library, 7920 Norfolk Avenue, Bethesda, Maryland, for use by the public. Codes and standards are usually copyrighted and may be purchased from the originating organization or, if they are American National Standards, from the American National Standards Institute, 1430 Broadway, New York, NY 10018.

NUREG/CR-5853
EGG-2670

Investigation of the Applicability and Limitations of the ROSA Large-Scale Test Facility for AP600 Safety Assessment

Prepared by
M. G. Ortiz, J. E. Fisher, J. M. Cozzuol,
T. J. Boucher, S. M. Sloan, S. M. Modro

Idaho National Engineering Laboratory
EG&G Idaho, Inc.

Prepared for
U.S. Nuclear Regulatory Commission

AVAILABILITY NOTICE

Availability of Reference Materials Cited in NRC Publications

Most documents cited in NRC publications will be available from one of the following sources:

1. The NRC Public Document Room, 2120 L Street, NW., Lower Level, Washington, DC 20555

2. The Superintendent of Documents, U.S. Government Printing Office, P.O. Box 37082, Washington, DC 20013-7082

3. The National Technical Information Service, Springfield, VA 22161

Although the listing that follows represents the majority of documents cited in NRC publications, it is not intended to be exhaustive.

Referenced documents available for inspection and copying for a fee from the NRC Public Document Room include NRC correspondence and internal NRC memoranda; NRC bulletins, circulars, information notices, inspection and investigation notices; licensee event reports; vendor reports and correspondence; Commission papers; and applicant and licensee documents and correspondence.

The following documents in the NUREG series are available for purchase from the GPO Sales Program: formal NRC staff and contractor reports, NRC-sponsored conference proceedings, international agreement reports, grant publications, and NRC booklets and brochures. Also available are regulatory guides, NRC regulations in the *Code of Federal Regulations*, and *Nuclear Regulatory Commission Issuances*.

Documents available from the National Technical Information Service include NUREG-series reports and technical reports prepared by other Federal agencies and reports prepared by the Atomic Energy Commission, forerunner agency to the Nuclear Regulatory Commission.

Documents available from public and special technical libraries include all open literature items, such as books, journal articles, and transactions. *Federal Register* notices, Federal and State legislation, and congressional reports can usually be obtained from these libraries.

Documents such as theses, dissertations, foreign reports and translations, and non-NRC conference proceedings are available for purchase from the organization sponsoring the publication cited.

Single copies of NRC draft reports are available free, to the extent of supply, upon written request to the Office of Administration, Distribution and Mail Services Section, U.S. Nuclear Regulatory Commission, Washington, DC 20555.

Copies of industry codes and standards used in a substantive manner in the NRC regulatory process are maintained at the NRC Library, 7920 Norfolk Avenue, Bethesda, Maryland, for use by the public. Codes and standards are usually copyrighted and may be purchased from the originating organization or, if they are American National Standards, from the American National Standards Institute, 1430 Broadway, New York, NY 10018.

NUREG/CR-5853
EGG-2670
R4

Investigation of the Applicability and Limitations of the ROSA Large-Scale Test Facility for AP600 Safety Assessment

Manuscript Completed: October 1992
Date Published: December 1992

Prepared by
M. G. Ortiz, J. E. Fisher, J. M. Cozzuol,
T. J. Boucher, S. M. Sloan, S. M. Modro

Idaho National Engineering Laboratory
Managed by the U.S. Department of Energy

EG&G Idaho, Inc.
Idaho Falls, ID 83415

Prepared for
Division of Systems Research
Office of Nuclear Regulatory Research
U.S. Nuclear Regulatory Commission
Washington, DC 20555
NRC FIN L2513
Under DOE Contract No. DE-AC07-76ID01570

ABSTRACT

A comparison of the thermal hydraulic behavior of the Advanced Passive 600 MW(e) (AP600) and the Rig of Safety Assessment (ROSA) Large-Scale Test Facility (LSTF), under similar initial and boundary conditions, was developed through computer simulations of selected accident scenarios for the Nuclear Regulatory Commission. The purpose of the comparison was to develop criteria to evaluate the capability of a scaled integral facility to perform an AP600 safety assessment. It was concluded that ROSA LSTF, with a minimum of required modifications, is capable of reproducing most of the phenomena and behavior expected of AP600; distortions become important for slow transients and cases in which the nonsymmetric behavior of AP600 is relevant.

CONTENTS

LIST OF FIGURES

LIST OF TABLES

EXECUTIVE SUMMARY

Westinghouse Electric Company will submit the Advanced Passive 600 MW(e) (AP600) nuclear power plant design to the United States Nuclear Regulatory Commission (NRC) for certification in 1992. In contrast to current generation reactors, this design features passive safety-grade systems for accident mitigation, relying on gravity-driven flow or stored energy such as gas pressurized accumulators or electric batteries. Therefore, the driving forces for the safety functions are small compared to the pumped power of conventional safety systems, and the performance of these systems may be adversely affected by relatively minor variations of system parameters, such as temperature or pressure caused by system or phenomena interactions. Also, the operation of the passive safety systems poses challenging computational problems to current thermal-hydraulic system analysis codes.

Therefore, the need for an integral test facility was identified for evaluation of AP600 safety systems performance and for assessment and validation of computer analysis codes. Among existing integral test facilities, NRC identified the Rig of Safety Assessment (ROSA) Large-Scale Test Facility (LSTF) as a potential candidate to be modified and used to perform confirmatory testing of AP600 high-pressure system behavior. The Idaho National Engineering Laboratory (INEL) was contracted to evaluate the potential suitability and limitations of ROSA, appropriately modified, to perform AP600 testing.

Comparison Criteria

To conduct the study, the INEL performed Reactor Excursion and Leak Analysis Program simulations of a selected set of transients, with AP600 and ROSA (modified) models subjected to the same initial and boundary conditions, and compared the results. The comparison of trends, events, magnitudes, and timing focused on three important aspects of the AP600 safety systems performance:

- Continuity of safety injection
- Depressurization rate
- Coolant inventory and distribution.

Transient Scenarios

The specific transients selected were

- A 3-in. diameter break in the cold leg
- A 1-in. diameter break in the cold leg
- A 3-in. diameter break in the pressure balance line
- Two cases of steam generator tube ruptures (one and three tubes)
- A main steam line break.

These transients were selected because they are design basis accident scenarios, they challenge the passive safety features of AP600, and the list of processes and governing mechanisms believed to participate in these transients spans over a wide range of important phenomena.

ROSA Modifications

The ROSA model used in the calculations was modified several times to determine the kinds of changes that may be required of ROSA to increase the fidelity of its simulation of AP600. Minor changes were also made to conduct sensitivity calculations, to elucidate the relative importance of some component or mechanism. The major changes were classified in four levels, described as follows:

I First-level modifications were derived by mere inspection of the two designs, selecting only those deemed essential. These modifications included the addition of the passive safety features not present in ROSA: core makeup tank (CMT) and appropriate pressure balance lines (PBLs), a passive residual heat removal system with simulated secondary cooling, automatic

depressurization system (ADS) Stages 1 through 3 on top of the pressurizer, ADS Stage 4 on the hot leg, and minimization of the pump loop seals.

II Second-level modifications were derived from the analysis of the first simulations. These included a properly scaled AP600 pressurizer, a surge line, and a surge line connection.

III Third-level modifications included all of the above modifications plus significant changes to the LSTF configuration: one cold leg was split to incorporate two CMTs instead of one.

IV The forth-level modifications were the result of the initial analyses, more in-depth inspection of the plant design differences, and discussions with representatives of the Japan Atomic Energy Research Institute, which owns ROSA. These include Levels I and II, appropriate upper head flow paths, an in-containment refueling water storage tank, and two CMTs whose cold leg PBLs are connected to the same cold leg for most transients but to cold legs on different loops for the nonsymmetric PBL break scenario.

An initial series of calculations was performed with various combinations of the above modifications (Levels I, II, and III). The primary purpose of these calculations was to aid in identifying the modifications to the ROSA facility that would improve its simulation of the AP600 system (Level IV). All the ROSA scenarios were simulated with the first level of model changes. The second level of changes was tested on the 3-in. cold leg break scenario; and the third level of changes was tested on the 3-in. PBL break. All of the changes incorporated into the model are feasible and correspond to the available piping and the physical configuration of ROSA.

After the initial calculation effort, several ROSA simulations were performed with a model that included all the most important modifications suggested by the initial effort and several additional changes (Level IV). These calculations included a 3-in. cold leg break case, a 1-in. cold leg break case, and a 3-in. PBL break case. The intent of this final set of calculations was to verify the improvement in system response with all modifications included in the model.

Conclusions

The comparisons of the behavior of ROSA with the first level of modifications indicate that ROSA is capable of reasonably representing AP600 behavior during the early portion of most transients. The behavior in slow transients or the latter part of fast transients was distorted mainly because of the larger friction and metal mass to volume ratio of scaled facilities. The capability of ROSA to simulate AP600 can be improved with minor modifications, such as in the upper head flow paths and adding the proper pressurizer (as in the second level of changes).

Because of its single cold leg and CMT PBL configuration, the ROSA modified to the first level of changes was not capable of capturing the nonsymmetries of AP600. The complexity of AP600 safety system interactions made ROSA with the third-level changes behave even more distorted than the base case (Level I).

Incorporating into the ROSA model all the most important modifications suggested by the analysis effort (i.e., fourth-level changes) improved the simulation of the AP600 plant. Even in the PBL break, in which the configuration was decidedly different than AP600, the nonsymmetric behavior expected of the CMTs appeared to be well represented. It should be mentioned that AP600 design modifications were made by Westinghouse during the course of this analysis. The results shown here no longer correspond to an accurate description of AP600 behavior. However, the changes are not expected to bring about new phenomena or sharper distortions.

ACRONYMS AND INITIALS

ADS	automatic depressurization system
AP600	Advanced Passive 600 MW(e)
CMT	core makeup tank
ECC	emergency core cooling
INEL	Idaho National Engineering Laboratory
IRWST	in-containment refueling water storage tank
JAERI	Japan Atomic Energy Research Institute
LSTF	Large-Scale Test Facility
MSLB	main steam line break
NRC	Nuclear Regulatory Commission
o.d.	outside diameter
PBL	pressure balance line
PCCS	passive containment cooling system
PRHR	passive residual heat removal
PSIS	passive safety injection system
PWR	pressurized water reactor
RCP	reactor coolant pump
RELAP5	Reactor Excursion and Leak Analysis Program
ROSA	Rig of Safety Assessment
S signal	safety injection actuation signal

Investigation of the Applicability and Limitations of the ROSA Large-Scale Test Facility for AP600 Safety Assessment

1. INTRODUCTION

Westinghouse Electric Company will submit the Advanced Passive 600 MW(e) (AP600) nuclear power plant design to the United States Nuclear Regulatory Commission (NRC) for certification in 1992. In contrast to current generation reactors, this design features passive safety-grade systems for accident mitigation, relying on gravity-driven flow or stored energy such as gas pressurized accumulators or electric batteries. Therefore, the driving forces for the safety functions are small compared to the pumped power of conventional safety systems, and the performance of these systems may be adversely affected by relatively minor variations of system parameters, such as temperature or pressure caused by system or phenomena interactions. Also, the operation of the passive safety systems poses challenging computational problems to current thermal-hydraulic system analysis codes. Therefore, the need for an integral test facility was identified for evaluation of AP600 safety systems performance and for assessment and validation of computer analysis codes.

The most effective integral system testing requires a facility that can simulate a whole accident sequence, from high-pressure events, through the depressurization phase, and into low-pressure, long-term cooling. Another approach is to use separate integral facilities for high-pressure and low-pressure events. The second approach may allow use of existing facilities with appropriate modifications. NRC identified the Rig of Safety Assessment (ROSA) Large-Scale Test Facility (LSTF), operated by the Japan Atomic Energy Research Institute (JAERI), as a candidate for the high-pressure and depressurization event integral testing. The Idaho National Engineering Laboratory (INEL) was contracted by NRC to evaluate the potential suitability and limitations of ROSA, appropriately modified, for AP600 testing. The objectives of this effort were to formulate comparison criteria to evaluate ROSA's capabilities to represent AP600, to perform the appropriate calculations and comparisons, to make a recommendation of the required ROSA modifications, and to apply the formulated criteria to the comparison to produce an evaluation of ROSA's suitability for AP600 safety assessment. Note that this was not an absolute evaluation of ROSA as an integral test facility but rather as a potential facility for a very special application. This report documents the results of this effort.

AP600 is a complex system that has and exhibits interactions between components that are not present in current generation reactors. ROSA LSTF, with the minimum modifications required to resemble AP600, exhibits a similarly intricate interactive character. It is not feasible that the comparison of a few simulations would be enough to accurately identify all the sources of distortion and their respective magnitude; effort was devoted to answer as many questions as was allowable by the information available; thus, parts of the report are very rich in detail. In some appropriate cases, sensitivity calculations were performed to elucidate important effects. Also, the simulation may not have captured everything that could happen in a real scenario and could only give an approximation of what can be expected.

The Reactor Excursion and Leak Analysis Program 5 (RELAP5)/MOD2.5 was used to simulate and analyze AP600 and ROSA response to postulated transients. The code had clearly identified deficiencies, mainly with respect to the new and unique features of AP600. The answers obtained are in need of the very assessment they were used to evaluate. These deficiencies are currently being investigated, and a code

enhancement program has been implemented to address these concerns. In the meantime, however imperfect the tool, it was applied equally to both systems (AP600 and ROSA). Also, while the plant simulated behavior may require the assessment to define its accuracy, the behavior differences observed point to system differences that need to be taken into account in the evaluation of ROSA's applicability to simulate AP600 phenomena.

Section 2 of this report discusses the features and differences of AP600 and ROSA and their respective code input models. In Section 2, the different levels of design (model) modifications required of ROSA for the comparisons are presented. Section 3 presents the comparison criteria developed for this task and the selection of the postulated transients for the comparisons between the two systems. Sections 4 discusses in detail the results of the modified ROSA calculations and their comparison to AP600 simulations. Section 5 discusses the simulations conducted to verify the recommended modifications, as resulted from the inspection of Section 2, the analysis of Section 4, and discussions with representatives of JAERI. Section 6 is a summary evaluation of the suitability of ROSA to produce the expected AP600 phenomena.

2. MODEL DESCRIPTION

ROSA LSTF is a 1/48-volumetrically scaled, full-height, full-pressure simulator of a conventional Westinghouse-type four-loop (3,423 MW thermal power) pressurized water reactor (PWR); it does not have the advanced passive safety features of the AP600 design.[1,2] To examine the feasibility of using ROSA for the AP600 safety assessment, a revised RELAP5 model of ROSA was developed based on available information about AP600 plant design and the existing ROSA facility configuration. This section presents an overall description of the two designs, their differences, and the modifications and scaling considerations used to develop the revised ROSA model. Specific AP600 design information is omitted in this report because of its proprietary status.

2.1 AP600 Design

AP600 is a Westinghouse two-loop PWR design. Each loop has one hot leg, one inverted U-tube steam generator, two reactor coolant pumps, and two cold legs per loop. The major difference between the AP600 and typical PWR designs is the passive nature of AP600 safety and support systems, which rely solely on gravitational forces. The passive safety system of AP600 consists of[3,4,5,6]

- Two spherical, high-pressure, accumulator tanks.
- Two core makeup tanks (CMTs), which replace the high-pressure injection system.
- One in-containment refueling water storage tank (IRWST) that replaces the safety grade, low-pressure injection system.
- A full-pressure, full-decay power, passive residual heat removal (PRHR) system, which has a heat exchanger submerged in the IRWST and replaces the auxiliary feedwater system.
- The automatic depressurization system (ADS), which consists of a series of valves that open in stages as the level in the CMTs drop. The first three stages of ADS valves vent the pressurizer into the IRWST through spargers. The fourth stage vents the hot leg directly into the containment.
- The containment itself, which includes the passive containment cooling system (PCCS) and a sump valve that returns the liquid to the primary coolant system.

All valves in the safety system are either check, fail-safe, air-operated valves or motor-operated valves supplied from redundant battery banks.

During normal operation, the tops of the CMTs are connected to the top of the pressurizer and one cold leg each, through the pressure balance lines (PBLs). The pressurizer PBL vents the pressurizer to the top of the CMT, while the connection through the cold leg PBL is normally closed with a motor valve. The CMT connection to the passive safety injection system (PSIS) line is also closed during normal operation with a motor-operated valve. The safety injection actuation (S) signal opens these valves and causes the CMTs to vent to the cold leg through the PBLs and to the PSIS line on the bottom of the CMTs, thus injecting liquid into the vessel downcomer.

In addition to the aforementioned system differences, AP600 reactor coolant pumps (RCPs) are encased into the primary and the bottom of the steam generator outlet plenum. There is no loop seal for these pumps.

2.2 ROSA LSTF

ROSA includes two symmetric primary loops, each containing one cold leg, one hot leg, an inverted U-tube steam generator, and an RCP. Each ROSA loop represents two of the reactor loops lumped together. The loop horizontal legs were sized to conserve the scaled volume as well as the ratio of length to the square root of diameter, $L/D^{0.5}$, in order to simulate the two-phase

flow regime transitions.[7] The inverted U-tube steam generators are full length and contain 141 tubes. Tube thickness, outside diameter (o.d.), and length are identical to those of the reference PWR. Note that the reference PWR for ROSA has steam generator design differences from those used in U.S. Westinghouse four-loop plants. A pressurizer is connected to one of the hot legs. The ROSA vessel includes an annular downcomer and contains 1,064 full-length rods capable of operating at 10 MW, or 14% of scaled full power for the reference PWR. The heater rod dimensions and pitch are the same as for the 17 x 17 fuel assembly used in the reference PWR core. Emergency core cooling (ECC) components, typical of those in the reference PWR, are included in ROSA.

2.3 Required Modifications and Scaling Considerations

The ROSA LSTF system is full height.[8] The facility scaling is time preserving, and the time and length ratios are equal to one. The volume ratio, the product of the area ratio times the length ratio, makes ROSA about 1:30 of AP600. Thus, appropriate scaling ratios (~1 for height, ~1/30 for volume, ~1/5.5 for area) were used to determine the scaled dimensions of the AP600 components that are to be simulated with ROSA. Figure 1 illustrates the comparison between the relative elevation of the components of the two designs (figures appear after the references, before the appendix).

As ROSA is different from AP600, several levels of modifications were implemented in the revised ROSA RELAP5 model.

The first level of modifications corresponded to obvious differences in the two designs, found by mere inspection. The most important modification was the addition of the passive safety systems (i.e., one CMT; corresponding PBL; a PRHR system with simulated, forced, secondary cooling; ADS Stages 1, 2, and 3 on top of the pressurizer; and ADS Stage 4 on the hot leg), all of which ROSA did not have, and reduction of the loop seal between the steam generator and the pump. The two CMTs of AP600 were lumped as one in ROSA, because ROSA had only one cold leg per loop and one available reactor vessel penetration.

Despite these modifications, some important differences remained as a result of the ROSA configuration. The most important were

- The volume of each steam generator, which was scaled to represent two steam generators of the reference PWR, had a secondary volume about 36% overscaled in reference to AP600. In addition to this, the tube walls, o.d., and total surface area were also oversized with respect to AP600.

- Loop piping flow area, of both hot and cold legs, was twice the appropriate AP600 scaled value. Fluid volume of the hot leg was about 20% greater than ideally scaled, whereas the cold leg fluid volume was about a factor of two greater, even with a reduced pump suction height.

- An additional scaling distortion in the loop piping as well as in other plant components was the excessive metal volume to fluid volume ratio that is inherent to any reduced scale facility. The effect of this distortion is for plant structures to become a greater source (or sink) for heat transfer to fluid in the system than would occur in a full size system.

- The pressurizer was well scaled volumetrically, but its height was about one-third that of the AP600 pressurizer, and the flow area was more than twice the scaled AP600 pressurizer area.

- Since ROSA only had one cold leg per loop, the two CMTs of AP600 would have to be lumped into one as well. This would prevent ROSA from representing any asymmetric behavior associated with the dual cold leg, dual CMT configuration of AP600.

- There was no IRWST in ROSA, therefore the PRHR secondary was modeled initially as forced cooling.

- The flow paths through the reactor vessel upper head were different. ROSA presented a higher flow resistance and a different flow configuration.

A second and a third level of modifications were tested in response to these remaining differences between the two systems and their relative effect on how the behavior of the two systems differed. In addition to these, minor changes were also made and examined as sensitivity calculations.

The second level of changes replaced the original ROSA pressurizer with a full-height pressurizer, volume scaled to the AP600 pressurizer. Sensitivity calculations demonstrated that for the transients selected, the effect of the larger hot and cold leg was not very important. Yet this second level was still unable to fully represent the nonsymmetric behavior of the PBL break.

In the third level of modifications, one of the ROSA cold legs was split to accommodate two CMTs with the corresponding PBLs.

If ROSA were ideally scaled, all its components would be 1/30th of the volume of the actual plant. This was not the case and some differences remained. Table 1 summarizes the scaling of ROSA components and those of an ideally scaled facility, according to the volume ratio between ROSA and AP600. In some cases (where components were additions), the assumed dimensions were those of the next available commercial size, thus the ratios were not exactly 1.0.

As a result of the analyses and discussions with JAERI, a fourth level of modifications was recommended. These included all of the Level I and II modifications plus the modifications of the upper head flow paths, two CMTs and thus two sets of PBLs and direct vessel injections, and an IRWST.

2.4 RELAP5 Input Models

2.4.1 AP600 Input Model. A preliminary RELAP5 AP600 input deck was developed, containing models for all of the major primary, secondary, and passive safety systems' components. The design data for the deck represented the best available information effective September 1990. The salient features of the AP600 system previously described were incorporated in the RELAP input deck.

The AP600 RELAP5 deck had 276 hydrodynamic volumes, 396 junctions, and 293 heat structures, as shown in Figure 2. Both loops were explicitly modeled, including the hot leg, the steam generator, and two cold legs and associated pumps. Loop A had the pressurizer and the PRHR system connections. The B loop cold legs had the CMT pressure balance line connections. The steam generators were F type; the models were taken from an existing RELAP deck and modified to incorporate the known design features of the AP600 steam generators. The RCP models contained the AP600 homologous curves for single-phase operation. Two-phase head and torque multipliers and degradation data were from Combustion Engineering pump data. Hydraulic torque and inertia were set to obtain AP600 design values for pump heating and coastdown characteristics.

The reactor vessel model was detailed and contained representation of all internal components. Hydraulic volumes represented the downcomer, the lower plenum, the core, the reflector, the guide tubes, the upper plenum, and upper head regions. Heat structures represented the fuel, the reflector, the core barrel, and the metal masses of the vessel, lower and upper heads, and guide tubes and other structures in the upper plenum and upper head regions. The downcomer was a pseudo-two-dimensional component represented by a ring of eight annular sectors connected using crossflow junctions in the horizontal direction, as shown in Figure 3. This modeling scheme allowed a limited multidimensional flow representation. Horizontal momentum flux and spatial acceleration were neglected but temporal

Table 1. Summary comparisons of component scaling.

Item	ROSA LSTF/ideal volume scaled facility
Fuel rod outer diameter	1.00
Length	1.00
Pitch	1.00
Number of active rods	0.85
Total heat transfer area	0.85
Total core flow area	0.92
Bundle hydraulic diameter	1.00
Steam generator tube inner diameter	1.27
Wall thickness	2.79
Average length	1.12
Fitch	1.31
Material (stainless steel/Inconel 690)	
Number of tubes	0.76
Total inner heat transfer area	1.16
Total outer heat transfer area	1.33
Total primary flow area	1.23
Total primary volume	1.42
Steam generator inlet plenum volume	0.94
Steam generator outlet plenum volume	0.94
Steam generator secondary riser hydraulic diameter	0.99
Riser flow area	1.35
Total volume	1.36
Single loop hot leg volume	1.23
Single loop cold leg volume (full pump suction)	2.96
[1.2-m (3.96-ft) pump suction]	1.97
Vessel volume	0.95
Downcomer volume	0.84
Pressurizer volume	0.95
Primary side total volume	1.00
Hot leg flow area	2.11
Length	0.58
Lumped cold leg flow area	2.09
Length (full pump suction)	1.90
[1.2-m (3.96-ft) pump suction]	1.19
Downcomer flow area	0.79
Length	1.06
Pressurizer flow area	2.41
Length	0.35
Pressurizer surge line flow area	1.00
Length	1.02
Lumped CMTs cylinder region area	1.00
Cylinder region metal surface area	0.71

Table 1. (continued)

Item	ROSA LSTF/Ideal volume scaled facility
Overall length	1.00
Total volume	1.00
Lumped CMT header area	1.03
Length	1.00
Lumped CMT discharge line area	1.03
Length	1.00
Lumped pressurizer PRL flow area	1.01
Length	1.00
Lumped cold leg PRLs area	1.03
Length	1.00
Lumped safety injection common lines area	1.03
Length	1.00
PRHR pipe inner diameter	1.24
Wall thickness	1.76
Length	1.11
Number of tubes	1.00
Total inner heat transfer area	1.28
Total outer heat transfer area	1.48
Total primary flow area	1.55
Total primary volume	1.73
Single loop lumped pump	
Locked rotor resistance	
Loop A	1.56
Loop B	1.45

acceleration and friction terms were included. The lower plenum, core, and upper plenum hydraulic volumes were also pseudo-two-dimensional: two parallel flow paths were provided to accommodate differences brought about by asymmetries in the responses of the two loops. All major vessel bypass paths were included except for outlet nozzle leakage. Because of the elevated cold leg configuration, this path could not be represented without imposing a severe courant limit on the calculation time step. Flow through this path was incorporated in the upper head cooling spray bypass. Other bypass paths were the guide tube flow, the core cavity bypass, and the reflector cooling flow.

The passive safety features were modeled using Westinghouse design data (for elevations, liquid volumes, and line losses) available at the time of this study (no details of ADS piping losses were available). The RELAP5 accumulator model did not include the capability for spherical geometry; thus, these were modeled as cylinders. The containment was included as a volume; however, heat transfer across the containment walls was not included in the model. Therefore, containment pressure during transients was expected to be overpredicted.

2.4.2 ROSA Input Model. A base ROSA input deck was modified (according to the aforementioned levels of changes) to include the passive safety features of AP600 and to better represent some aspects of the AP600 system configuration. The additions included the ADS system and associated piping, one CMT and the

associated pressurizer and cold leg PBL and safety injection line, and the PRHR heat exchanger and piping. Effort was spent to ensure that the elevation of connections of the passive safety features to ROSA system components matched as closely as possible the elevations of corresponding connections in the AP600 system. Effort was also spent considering the physical feasibility of the proposed changes in the real plant. The ADS, the PRHR, and associated piping modeling from the AP600 input deck were scaled by reducing flow areas and were then incorporated directly into the ROSA model. Three stages of ADS connected to the top of the pressurizer, and the fourth stage connected to the nonpressurizer loop hot leg. All four stages of ADS were modeled as discharging directly to the atmosphere, since no IRWST existed in ROSA. The PRHR lines were connected to the pressurizer surge line near the junction with the hot leg and to the outlet side of the steam generator in the pressurizer loop.

To represent the PRHR heat exchanger, JAERI proposed using a heat exchanger with controlled secondary flow to allow simulating a range of heat transfer conditions. Thus, the shell side of the PRHR heat exchanger was modeled as a heat transfer coefficient boundary condition. The heat transfer coefficient value chosen was representative of natural circulation convection with vertical geometry.

The single CMT and associated piping used in the ROSA model were scaled to represent the two CMTs and two sets of piping in the AP600 system. The CMT cold leg PBL connected to the cold leg of the nonpressurizer loop, and the pressurizer PBL connected to the top of the pressurizer. The safety injection line connected the CMT/accumulator discharge roughly at the elevation of the bottom of the cold leg.

The ROSA accumulator was fairly well scaled to simulate the two accumulators in the AP600 system. The accumulator was repositioned to represent the injection location and elevation of the AP600 accumulators.

The RCP suction heights were reduced as much as possible while maintaining the present position of the pumps in the ROSA system. With this change, the bottom of the pump suctions was about 0.5 m (1.65 ft) below the cold leg center line. All of the above modifications corresponded to a first level of ROSA modifications, the base deck that was used for all selected transients.

The second level of modifications to the ROSA deck were tested as sensitivity cases to elucidate sources of distortion. The ROSA pressurizer was substituted with a full height pressurizer volume scaled to the AP600 pressurizer and was used for one 3-in. CLB calculation. This same calculation was repeated with yet another level of modification that included the properly area-scaled hot leg (in addition to the pressurizer). Also, the ROSA downcomer was renodalized to a semi-two-dimensional downcomer (radial and vertical volumes cross connected) to approximate that of the AP600 model. Finally, the third level of changes was implemented to examine the possibility of capturing the nonsymmetric AP600 behavior during a PBL break.

It was initially assumed that physical modifications to ROSA would likely not include an IRWST. Thus, the IRWST was not included in the ROSA input deck for the first set of calculations. Later, after the first analyses and discussions with JAERI, an IRWST was considered and included in the model.

The control logic and trip setpoints used in the AP600 model to represent the plant control system were duplicated in the ROSA input model. Where necessary, trip setpoints were modified to account for differences in component geometry between the AP600 and ROSA systems. A nodalization diagram of the modified (base case) ROSA input deck is shown in Figure 4.

3. SELECTION OF EVALUATION CRITERIA AND POSTULATED TRANSIENTS

To determine whether ROSA LSTF could capture the key phenomena of AP600 and would be able to provide data for code assessment, a group of transients was selected to compare the results of simulating AP600 and ROSA undergoing the same transient. It was assumed that the selected transients would fall into the design basis accident classification and should exhibit a wide range of phenomena and behavior for code assessment.

The proposed criteria for the comparison attended to the following issues related to safety systems:

- Ability of the systems to provide continuous safety injection
- Depressurization capabilities and timing
- Primary system coolant inventory and distribution.

Thus, the modified ROSA simulations were examined to determine, in general, if

- The CMTs provided core cooling with a similar injection pattern as AP600
- The system depressurization rate followed AP600 depressurization
- The primary coolant inventory and distribution resembled that of AP600.

In addition to these main aspects of the comparison, effort was made to establish that the governing mechanisms present in both systems were the same or similar.

A working table of initiating events and relevant phenomena was drafted (Table 2) to help elucidate the important issues and required experiments for AP600 safety assessment. This table was and continues to be used to determine what transients to calculate. For this report, the following transient scenarios were selected, all of which challenged the performance of the unique safety features of AP600:

- Three-inch-diameter CLB
- One-inch-diameter CLB
- PBL break
- SG single-tube and three-tube ruptures
- Main steam line break (MSLB).

This set of transients corresponded to the first three types of initiating events of Table 2: small break loss-of-coolant accidents, steam generator tube rupture, and MSLB. They presented a broad variety of conditions to challenge the passive safety systems during the high-pressure and depressurization phases of an accident. ROSA was not being considered for simulation of the low-pressure, long-term cooling events. These transients did not include single failures in addition to the initiating event.

An integral test facility test does not provide data for specific model validation. Its objective is rather the determination of biases; evaluation of components, processes or phenomena interactions; and the identification of any new phenomenon that may not have been considered in the design of the plant or the development of the simulation code. Therefore, it is important that the integral facility exhibits the important events and the major trends (key phenomena) expected in the prototype as well as their timing.

In reality, two sources of distortion are expected to affect the fidelity with which the integral facility can represent the plant: scale distortions, scaled facilities are smaller and thus will exhibit more friction, a higher metal mass/volume ratio, and higher heat losses to the environment; and unless the facility is a scaled replica of the plant, it will have configuration differences that will distort its representation of the prototype.

Table 2. Summary of transient initiating events and relevant phenomena

Full-pressure events	Phenomena
Steam generator tube rupture	Natural circulation in PRHR system
	Effects on noncondensable nitrogen from accumulators (heat transfer, system pressure)
	Mass and energy transfer between primary and secondary
	Manometer effect between CMT and pressurizer
	Recirculation to CMTs
	Effect of PRHR system performance on SG safety relief valves
	Local condensation in PBL from pressurizer and PRHR system tubes
	Interaction between accumulators and CMTs
	Asymmetries and loop dependencies
Small break loss-of-coolant accident	Check valve behavior in PBL and drain lines of CMTs
	Draining characteristics of CMTs
	Local condensation in PBL from pressurizer and PRHR system tubes
	Interaction between accumulators and CMTs
	Natural circulation in the PRHR system
	Asymmetric loop behavior
	Thermal effects in the PRHR and CMT systems due to large temperature gradients
	Condensation in CMTs and PBL
	Manometer effect between CMT and pressurizer
	Interaction between primary safety and containment
	Entrainment through pressurizer surge line to ADS valves
	Effects on noncondensible nitrogen from accumulators (heat transfer, system pressure)
	Temperature gradients in PRHR system and CMTs
	Recirculation to CMTs
	Locked rotor pump resistance effect
	Siphoning of IRWST water through first three stages of ADS when fourth stage opens
	Asymmetric behavior for CLBs
	Integral system effects dependent on break location; asymmetries, effects on CMTs, etc.
Steam line break	Additional asymmetry induced by PRHR system cooling
	Boron transport to the core

Table 2. (continued).

Full-pressure events	Phenomena
	Boron dilution due to flow to CMTs (recirculation path)
	Pressurized thermal shock due to temperature gradients and poor mixing
	Natural circulation in the PRHR
	Manometer effect between CMT and pressurizer
	Recirculation to CMTs
	Local condensation in PBL from pressurizer and PRHR system tubes.
Loss of feedwater/ feedwater line break	Check valve behavior in PBL and drain lines of CMTs
	Draining characteristics of CMTs
	Local condensation in PBL from pressurizer and PRHR system tubes
	Interaction between accumulators and CMTs
	PRHR performance (and overcooling)
	Natural circulation in the PRHR system
	Competing natural circulation loops (PRHR system, CMTs, SGs)
	Asymmetric loop behavior
	Thermal effects in the PRHR system and CMT systems
	Condensation in CMTs and PBL
	Manometer effect between CMT and pressurizer
	Effects of having pumps on or off
	IRWST mixing/stratification
	Entrainment in pressurizer surge line
Inadvertent pump trip	Asymmetric system response
	PRHR system performance (including natural and forced circulation)
	Local condensation in PBL from pressurizer and PRHR system tubes
	Interaction between accumulators and CMTs
Inadvertent ADS operation	Entrainment through pressurizer surge line to ADS valves
	Check valve behavior in PBL and drain lines of CMTs
	Draining characteristics of CMTs
	Local condensation in PBL from pressurizer and PRHR system tubes
	Interaction between accumulators and CMTs
	Natural circulation in the PRHR system
	Asymmetric loop behavior
	Thermal effects in the PRHR system and CMT systems
	Condensation in CMTs and PBL

Table 2. (continued).

Full-pressure events	Phenomena
	Manometer effect between CMT and pressurizer
	Interaction between primary safety and containment
	Effects on noncondensibles (heat transfer, system pressure)
	Temperature gradients in PRHR system and CMTs
	Recirculation to CMTs
	Locked rotor pump resistance effect
	Siphoning of IRWST water through first three stages of ADS when fourth stage opens
	Asymmetric behavior for CLBs
Excess feedwater	Additional asymmetry induced by PRHR system cooling
	Boron transport to the core
	Boron dilution due to flow to CMTs (recirculation path)
	Pressurized thermal shock due to temperature gradients and poor mixing
	Natural circulation in the PRHR system
	Manometer effect between CMT and pressurizer
	Recirculation to CMTs
	Local condensation in PBL from pressurizer and PRHR system tubes
	Interaction between accumulators and CMTs
Anticipated transient without scram	Check valve behavior in PBL and drain lines of CMTs
	Draining characteristics of CMTs (when there is overpressure discharge through safety relief valves)
	Local condensation in PBL from pressurizer and PRHR system tubes
	Interaction between accumulators and CMTs
	Effect of ADS initiation due to radiation release through safety relief valves
	PRHR system performance (and overcooling)
	Natural circulation in the PRHR system
	Competing natural circulation loops (PRHR system, CMTs, steam generators)
	Asymmetric loop behavior due to CMT and PRHR system
	Boron dilution due to flow to CMTs (recirculation path)
	Boron transport to the core
	Thermal effects in the PRHR and CMT systems

Table 2. (continued).

Full-pressure events	Phenomena
	Condensation in CMTs and PBL
	Manometer effect between CMT and pressurizer
	IRWST mixing/stratification
	Phase separation phenomena in pressurizer in relation to ADS and mass loss

ROSA has both of these sources of distortion. The RELAP5/MOD2.5 code was used through system calculations to provide estimates of the magnitude of the effects those distortions cause in the response of ROSA relative to the response of AP600. As mentioned in the previous section, a minimum configuration change of ROSA is required for a satisfactory comparison. From the analyses, additional minor changes are recommended (typical pressurizer and upper head flow paths) to improve ROSA's approximation of AP600.

4. CALCULATIONS, RESULTS, AND DISCUSSION

Safety evaluations for small break loss-of-coolant accidents are primarily concerned with criteria such as maintaining sufficient system mass inventory (particularly in the vessel) and providing adequate core cooling. For the AP600 design, the ultimate satisfaction of these criteria is dependent upon the operation and interaction of the passive safety systems. The passive safety systems can be divided into two major categories: those that are necessary to bring the system (in a safe manner) to conditions conducive to long-term core cooling (ADS stages to accelerate depressurization, PRHR system heat removal, and CMT injection to maintain the vessel inventory), and those that are necessary to maintain long-term, core cooling (IRWST injection and containment cooling). The former are important during the high-pressure phase of the transient, while the latter are important for the low-pressure, long-term phase. The passive safety systems applicable to high-pressure considerations are the CMTs, the PRHR system, the accumulators, and the four ADS stages. The objective of these passive safety systems is to maintain system inventory and depressurize the system in a manner that maintains adequate core cooling and facilitates establishment of long-term core cooling.

This section discusses comparisons of the AP600 and ROSA calculations for the transient scenarios selected and highlights the performance of the high pressure passive safety features. Similarities and differences in the response of the two systems and their possible causes are described in detail.

4.1 Three-Inch Cold Leg Break

Calculations simulating a 3-in.-diameter CLB, of the pressurizer side loop, were performed for both the AP600 and the modified (first-level) ROSA LSTF systems. This location was selected because the ROSA system response for this case would better simulate AP600 response than if the break were situated in a CMT side cold leg. Since there was only a single cold leg in each loop of the ROSA LSTF system, simulating a break in the CMT side cold leg would not capture the asymmetric response of the two CMT side cold legs and CMT trains expected in the AP600 system. Additionally, a break in a pressurizer side cold leg in the AP600 system was expected to cause the two cold legs connected to the CMTs to experience the same boundary conditions during the transient. As a result, the transient response of the two CMT side cold legs and the two sets of PBLs/CMTs/ECC lines would be the same. With this in mind, the CMT side cold leg response and the PBL/CMT/ECC line response in the ROSA facility was expected to be most representative of AP600 behavior for the pressurizer side CLB.

For the 3-in. CLB analysis, a single AP600 calculation was performed, along with several ROSA calculations. The ROSA calculations included (a) a base case using the first-level modified ROSA LSTF model described in Section 2.4.2; (b) a case in which the ROSA pressurizer and surge line were replaced with a pressurizer and surge line scaled directly to the AP600 pressurizer (second level); (c) a case in which the ROSA pressurizer, surge line, and hot leg were replaced with components scaled to the corresponding AP600 components; (d) a case with a multi-channel downcomer instead of the single channel used in the base case model; and (e) a case in which the PBLs and ECC line form losses were modified to provide better agreement of the ROSA/AP600 ECC flow. The results of comparisons of the AP600 calculation and the various ROSA calculations are presented in Sections 4.1.2 through 4.1.6. This discussion is preceded by a brief description of the conduct of the calculations. A final section (Section 4.1.7) discusses the applicability of ROSA LSTF for 3-in. CLB experiments.

4.1.1 Calculation Conduct. Performance of RELAP5 calculations involved a two-step process. The process included establishing a steady state with appropriate initial and boundary conditions and then initiating the transient from that steady state with proper trip setpoints and control functions being represented. In establishing the initial steady states for these calculations, -IVex-

pected AP600 system thermal-hydraulic operating conditions were used.

The AP600 steady state was set at nominal full power (1,933 MW) and flow conditions. The base case ROSA conditions were adjusted to match, as closely as possible, those for AP600, given the constraints of reduced power and flow capabilities in the ROSA facility. The ROSA steady state was established at the facility power limit of 10 MW (roughly 16% of scaled AP600 full power).[a] The [illegible] leg temperatures in the ROSA [illegible] were obtained the same as in AP600 by [illegible] pumps to give 16% of the scaled loop flow. The secondary pressure (saturation temperature) was adjusted (i.e., increased relative to a full power case) to allow energy removal from the primary system at the reduced core power rate. The ROSA steady state secondary pressure and temperature matched the values in the AP600 calculation reasonably well. However, if the ROSA steam generators incorporated thin wall U-tubes (as used in AP600), the secondary pressure would be considerably higher than in AP600 to allow removal of heat at the reduced core power rate. The thicker steam generator U-tube walls in ROSA require lower secondary pressure to achieve the same result. Primary pressure was the same for both AP600 and ROSA calculations. The pressurizer level for the ROSA base case was set to provide the appropriate scaled AP600 liquid volume. (In the base case ROSA model, the pressurizer elevation and height were different than in AP600.) For those ROSA calculations that included the scaled AP600 pressurizer, the initial pressurizer level was the same as in AP600. The PBL, CMT, accumulator, and ECC line fluid initial conditions were the same for both cases, with the CMT and accumulator temperatures set at a containment temperature of 311 K (100°F).

The transient part of the calculation was initiated by tripping open a valve with an appropriately sized area to represent the break. For the AP600 calculation, the break was located near the downcomer inlet in one of the two parallel cold legs in the loop containing the pressurizer. For the modified ROSA calculations, the break was located near the downcomer inlet in the single cold leg in the loop containing the pressurizer, and the break area was scaled by the ROSA/AP600 area scaling ratio. Both breaks were modeled as crossflow junctions with the break junction connected to Volume 280-01 for the AP600 calculation (Figure 2) and Volume 448-01 for the ROSA calculation (Figure 4). For the ROSA transient calculations, trips and controls were as specified for the AP600 system.

The comparisons presented in this section cover the time period from the initiating event (break at time zero) through 2,500 seconds. In the AP600 calculation, all four stages of ADS had opened and IRWST flow had been initiated by about 2,500 seconds. Since in the ROSA calculation the IRWST was not simulated, the calculation was terminated at 2,500 seconds after all four stages of ADS had opened.

4.1.2 AP600/ROSA Base Case 3-In. Cold Leg Break Comparison. The AP600 and ROSA base case 3-in.-diameter CLB calculations were analyzed with the primary objective being the identification of similarities and differences in the response of the two facilities, especially with respect to the behavior of the passive safety systems. The results of this analysis indicated good agreement in many aspects of the primary system response and passive safety feature behavior. In particular, the early primary side depressurization, the CMT circulation and draining, the PRHR system flow response, and ADS Stages 1 and 2 initiation and flow rates were well represented by the ROSA calculation. However, differences in the primary depressurization and fluid temperature distribution in the intermediate and late portion of the calculations resulted in considerable differences in the core vapor generation rate and

a. Initially, several ROSA 3-in. CLB calculations were performed with 100% of the scaled AP600 core power and loop flow (both of which could not be obtained in the ROSA facility). The purpose of these initial calculations was to help identify differences in ROSA/AP600 system responses without the added distortions caused by dissimilar initial conditions. The ROSA calculations discussed herein were performed as they would be conducted in the ROSA facility.

vessel mass inventory. This was especially true once Stage 3 of ADS had opened. The following paragraphs describe the areas of agreement and difference for the two calculations. A brief overview of the general system response is presented first, followed by a comparison of the system response for the two cases.

4.1.2.1 General System Response. The AP600 and ROSA system response to the 3-in. CLB was characterized by an early depressurization phase that was controlled primarily by the break and steam generator primary/secondary coupling, followed by a later phase in which depressurization was mainly controlled by the action of the ADS. The sequence of events for each calculation is listed in Table 3.

Scram occurred shortly after rupture on a low-pressurizer pressure signal. The same signal terminated feedwater flow to and steam flow from the steam generator secondaries, tripped off the primary cooling pumps, and opened valves in the cold leg PBLs and CMT outlet lines. At this point, liquid began to circulate through the cold leg PBLs and CMTs, but the CMTs did not begin to drain until later in the transient, that is, even though cold CMT water was injected into the primary, there was no voiding at the top of the CMT because the water was replenished with hot primary water from the cold legs through the PBL connection. Nevertheless, the effect was to add mass to the primary system.

The primary system initially depressurized fairly rapidly due to flow out the break and continuing heat transfer to the SG secondary. As the pressurizer emptied and the hot leg fluid reached saturation, the depressurization rate slowed. Shortly thereafter, the primary pressure equilibrated with the secondary pressure and remained at the secondary pressure for several minutes. During this period, the secondaries continued to represent a heat sink for primary fluid, although total heat transfer was low because of the small primary-to-secondary temperature difference. Also during this period, voiding in the steam generator U-tubes and in the cold legs continued.

Break uncovery occurred about 30 seconds before the U-tubes were completely voided and caused a slight decrease in the primary pressure. However, significant further depressurization of the primary did not occur until the U-tubes became completely voided. Once this happened, the primary became thermally decoupled from the secondary, while a clear path to the break, through the hot leg and the U tubes, was established for steam generated in the core region. The primary pressure once again began to decrease at a fairly rapid rate. Also, because the intact side cold legs (to which the PBLs were attached) had voided, the liquid flow natural circulation path, consisting of the cold legs, the PBLs, the CMTs, and the ECC injection lines, was interrupted. When this occurred, the CMT liquid level began to drop. Lowering the CMT levels initiated ADS, which further increased the primary depressurization rate. Accumulator flow began immediately following first-stage ADS actuation.

The system continued to depressurize as the second, third, and fourth stages of ADS were activated. Containment pressure (or atmospheric pressure in the case of the ROSA calculation) was reached at roughly 25 minutes.

4.1.2.2 Passive Safety Features Response. Comparison of the AP600 and ROSA calculation results indicated that the initial system response was in good agreement for the two calculations. Also, timing of events and flow rates associated with the passive safety features agreed well up to the point of activation of third-stage ADS. The break flow and integrated break flow for the two cases are compared in Figures 5 and 6.[b] The ROSA break flow was only slightly higher in the early part of the transient, and total flows out the break over the duration of the transient agreed very well. Break uncovery occurred at the same time (about 370 seconds) for both cases, as shown in Figure 7, which compares the break volume vapor void fraction.

b. Where applicable, ROSA calculation parameters were multiplied by the appropriate AP600/ROSA scaling factor to allow direct comparison of calculation results.

Table 3. Comparison of events for AP600 and ROSA 3-in. CLB RELAP5.

Transient event	Timing for AP600 full-power, initial-condition calculation (sec)	Normalized AP600 primary system mass inventory (%)	Timing for ROSA reduced-power, initial-condition calculation (sec)	Normalized ROSA primary system mass inventory (%)
Break initiation	0.0	100	0.0	100
Scram (Pprz = 1875 psia)	~13.6	95	~15.2	95
PBL/CMT circulation began	~15	95	~15.2	95
CMT draining began	372.0	39	390.0	36
First stage ADS activated	576.0	36	640.0	39
PRHR flow began	576.0	36	640.0	39
Accumulator injection began	582.0	36	674.0	40
Second stage ADS activated	1137.0	57	1114.0	53
Third stage ADS activated	1281.0	45	1286.0	44
Fourth stage ADS activated	1644.0	21	2096.0	44
CMTs empty	~1950	23	~2450	34
IRWST injection began	~2478	21	NA	NA

Response of the CMTs and associated PBLs were also in good agreement for most of the transient. Figures 8 and 9 compare the cold leg and pressurizer PBL flow rates for the two cases. Flow was initiated in both lines at about 15 seconds when ECC line valves were opened on a low pressurizer pressure signal. Flow rates in both lines were lower in the ROSA calculation as a result of the higher line resistance associated with smaller pipe sizes.[c] However, flow termi-

c. The PBLs and ECC lines used in the ROSA model were scaled to represent the two sets of lines in the AP600 system. Each line in the ROSA model was given twice the scaled area of the corresponding line in the AP600 model. Form loss coefficients for line inlet and outlet, valves, and pipe bends were kept the same for both models.

nated in each line at about the right time and with the same cause. In both cases, steam flow through the pressurizer PBL ceased once first stage ADS was activated.

At this point, pressurizer pressure decreased rapidly, and the pressurizer PBL check valve reset. The check valve remained closed for the duration of the transient in both cases. Also, in both cases, liquid flow in the cold leg PBLs continued until the CMT side cold legs voided (at about 370 seconds in AP600 and 390 seconds in ROSA). Once the CMT side cold legs voided, the source of liquid for the cold leg PBL was removed, and steam was drawn into the line. Note that mass continued to be added to the RCS. It was the voiding of the cold leg at the PBL suction that allowed the CMT levels to begin to drop. Prior to this, liquid was circulated (siphoned) from the cold leg, through the cold leg PBLs and CMTs, and into the vessel downcomer. Figure 10, which compares the CMT liquid levels for the two cases, shows that the CMTs remained liquid full until about 370 and 390 seconds, respectively, for AP600 and ROSA, while Figure 11, which compares the CMT outlet flow for the two cases, shows that there was considerable flow through the CMTs during the same period.

Once the CMTs began to drain, flow increased out the CMTs. The higher CMT flow rates continued until accumulator flow began. Initiation of accumulator flow pressurized the ECC line downstream of the CMT check valve and effectively interrupted CMT draining until the accumulators were empty. Total accumulator mass flow for the two cases is shown in Figure 12. The accumulator began to inject somewhat later in ROSA (about 674 seconds versus 582 seconds in AP600) because the primary system depressurized at a slower rate in ROSA. Also, because the nitrogen volume in the ROSA accumulator was oversized, given the scaled liquid volume, the accumulator depressurized at a somewhat lower rate than in AP600 (because the differential change in gas pressure was smaller for a given loss of liquid volume). This gave a higher accumulator liquid flow rate in ROSA, but for a shorter duration.[d]

After the accumulator flow ceased, the CMTs continued to drain. Notice that while the ROSA CMT flow rate (Figure 11) was generally lower than in AP600 (again as a result of the higher PBL/ECC line resistances in ROSA), the duration of flow was longer. The net effect was that the ROSA CMT draining response agreed very well with AP600, at least until about 1,600 seconds. At this point, the ROSA calculation exhibited another interruption of CMT flow, which did not occur in the AP600 calculation.[e] The cause of this flow cessation has been identified as a code error, and such a flow cessation would likely not occur in the facility. CMT flow was reestablished at about 1,890 seconds. The flow cessation had the effect of delaying the activation of fourth-stage ADS (see below) and emptying of the CMT. The CMT emptied at about 2,450 seconds in ROSA, as compared to about 1,950 seconds in AP600.

Draining of the CMTs activated the four stages of ADS as well as initiated PRHR flow. First-stage ADS and PRHR flow were activated on a CMT level of 75%, while ADS Stages 2, 3, and 4 were activated on levels of 60, 50, and 25%, respectively. Figures 13 through 16 compare ADS flow rates for the four stages for each case, while Figure 17 compares PRHR flow response. Because the CMT level response for the two cases was very similar, the timing of activation of the first three stages of ADS and initiation of PRHR flow agreed very well. (As described above, the timing of fourth stage ADS opening was delayed in ROSA because of the delay in draining of the CMT). Also, there was good agreement for the magnitudes of the ADS Stages 1 and 2 flow rates and for the PRHR flow rates. However, the magnitude of ADS Stages 3 and 4 flow rates in ROSA was quite different than for AP600. This is illus-

d. The ROSA accumulator could be modified using a standpipe arrangement to provide for injection of a properly scaled liquid volume while at the same time allowing a properly scaled nitrogen volume.

e. The reduction of flow that began at about 1,800 seconds in the AP600 calculation occurred as a result of emptying of the CMTs.

trated in Figure 18, which compares the total integrated flow out all four ADS stages. As shown in the figure, there was excellent agreement in total flow exiting the system through the ADS until after activation of Stage 3. The impact of the difference in ADS Stages 3 and 4 flow responses was that the AP600 calculation exhibited a significantly lower vessel mass inventory in the later part of the transient. The reasons for the differences between the two calculations are discussed in the following paragraphs.

4.1.2.3 Distortions. As discussed in Section 2.3, the ROSA facility exhibited several differences with respect to an ideally scaled AP600 simulator. While no single difference has been identified as being the main cause of distortions between the AP600 and ROSA calculations, the cumulative effects of the various differences resulted in appreciable distortions in the overall system response for the 3-in. CLB scenario. The system pressure during the intermediate portion of the transient tended to remain elevated in the ROSA calculation. Also, the ROSA calculation exhibited a higher core inlet subcooling, which resulted in a lower vapor generation rate in the core region. The difference in core vapor generation in turn resulted in differences in ADS flow response and loss of vessel inventory for the two calculations. The effects of the various distortions on the system response are highlighted below by comparing the system depressurization response for the two cases and identifying those aspects of the system thermal-hydraulic behavior that led to the observed pressure response differences.

The pressurizer pressure response for the AP600 and ROSA calculations is compared in Figure 19. Initial agreement was excellent. Between about 400 and 1,300 seconds the ROSA pressure remained well above that AP600. Comparison of primary and secondary pressures for the two cases and the voiding response of the steam generator U-tubes and the cold legs shows why this occurs. Figure 20 compares the pressurizer pressure with the steam generator secondary pressures for AP600, while Figure 21 shows the same parameters for ROSA. As explained previously, the primary pressure initially decreased fairly rapidly until it equilibrated with the secondary pressure. The primary then remained at the secondary pressure for several minutes while primary side fluid continued to be lost out the break. Notice that in both cases, the primary pressure began to decrease gradually at about 375 seconds. Recall that this is about the time that break uncovery occurred (see Figure 7). However, more rapid depressurization was delayed until the steam generator U-tubes and cold legs had become almost completely voided, providing a clear path for steam generated in the core to exit the system. Figure 22 shows the collapsed liquid level in the steam generators for the AP600 case, while Figure 23 shows the void fractions in one of the intact cold legs (response of the other intact cold leg is identical). Both the steam generators and intact cold legs were voided by about 400 seconds.

At this time, the primary system pressure began to decrease at a fairly rapid rate (Figure 20) in the AP600 calculation. The ROSA calculation exhibited a similar response, but voiding of the steam generators was delayed by about 100 seconds. The steam generator collapsed liquid levels for this case are shown in Figure 24, while Figure 25 presents the void fractions in the horizontal section of the intact cold leg, and Figure 26 shows the void fraction at the bottom and on the upflow side of the pump suction leg. The intact cold leg and pump suction upflow was essentially completely voided by 400 seconds, and the bottom of the suction exhibited a high void fraction (which should represent little resistance to steam flow). However, the steam generator upflow sides did not void until just after 500 seconds. The delay in voiding was attributed to the differences in steam generator configuration between ROSA and AP600. The ROSA steam generator primary side volume was oversized by about 40% relative to the AP600 steam generators. Also, the top of the tube sheet was about 1.5 m (4.95 ft) lower in ROSA, and the tops of the U-tubes were about 0.4 m (1.32 ft) higher. Each of these factors contributed to the delay in steam generator voiding in ROSA. Again, the primary pressure (Figure 21) began to decrease at a more rapid rate after complete voiding of the

steam generator occurred. Returning to Figure 19, immediately after the steam generators voided and before first-stage ADS activation, the depressurization rate in ROSA was considerably lower than in AP600.

Two sources of distortion may have been responsible for the slower depressurization of ROSA. The first source of distortion was inherent of scaled facilities and had to do with the energy stored by the structure (i.e., in ROSA the metal-to-fluid volume ratio and the structural-heat-transfer-surface-area-to-fluid volume ratio are considerably larger than in AP600). On a scaled basis, more energy was available in the ROSA structure. This had the effect of reducing the cool-down (and corresponding contraction) of the primary liquid, which tended to maintain a higher system pressure. The second source of distortion was specific to ROSA and had to do with the different configuration of the upper head flow paths available to the reactor coolant. The sketch below illustrates this difference (no exact information is included due to the proprietary status of AP600 design).

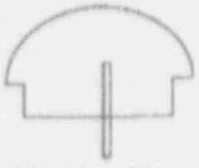

The upper head in ROSA acted as a *pressurizer*, maintaining the pressure higher than in AP600. This effect was most noticeable in a slower transient, such as the 1-in. CLB scenario that follows in the next section of this report.

The difference in pressure response during the intermediate part of the transient for the AP600 and ROSA calculations was indicative of considerable differences in other aspects of the system thermal-hydraulic behavior, including the core region vapor generation rate and the vessel mass inventory. The total core region (lower plenum, core, and upper plenum) vapor generation for the AP600 and ROSA calculations is shown in Figure 27. Figure 28 compares the vessel mass inventory for the two cases. It is evident from these figures that the amount of steam generated in the core region in AP600 was significantly greater than in ROSA (especially after about 600 seconds), and the vessel mass inventory was depleted to a greater extent in AP600 as a result. The higher vapor generation in AP600 was a direct result of a lower degree of subcooling of the core liquid. Comparison of the fluid temperature and saturation temperature at midcore for AP600 and ROSA (Figures 29 and 30) illustrates the significant difference in subcooling leading to the difference in vapor generation rates. Liquid at midcore in AP600 was at saturation, while ROSA continued to exhibit considerable subcooling. The lower core subcooling in AP600 appeared to be associated with a considerably higher steam flow in the intact cold legs, which tended to heat the downcomer liquid. This difference is described as follows.

Recall that steam generated in the core (along with entrained liquid) can escape from the primary through one of three main paths. First, it can pass into the hot leg, through the surge line/pressurizer, and then out the ADS. Second, it can pass through the break side hot leg, into the broken cold leg, and directly out the break. Third, it can pass through the hot legs, into the intact cold legs, then into the downcomer, and finally out the break. It is flow through this third path that impacts the downcomer fluid temperature and, correspondingly, the core fluid temperature. Steam entering the downcomer from the intact cold legs mixes with the downcomer liquid,[f] which is then heated. The amount of heating depends on the loop steam flow rate. In ROSA, the loop steam flow that eventually entered the downcomer passed through the single intact cold leg. In AP600, a much higher steam flow rate into the downcomer was distributed among the three intact cold legs. Figure 31 compares the total mass entering the downcomer from the intact cold

f. Because of the CMT and accumulator flow, the downcomer remained mostly full of subcooled liquid.

legs for the two calculations. For comparison, the figure includes the total mass leaving the downcomer through the broken cold leg. Flow from the downcomer to the break was comparable for the two cases until about the time the third stage of ADS opened. However, flow into the downcomer from the three intact cold legs in the AP600 calculation was significantly higher[g] than that from the single intact cold leg in the ROSA calculation.

As implied above, the primary impact of the difference in steam flow into the downcomer was its effect on the downcomer fluid temperature and the corresponding degree of subcooling of liquid entering the core region. Figure 32 compares the fluid temperatures in the downcomer just below the cold leg elevation for the ROSA and AP600 calculations. The fluid temperature in AP600 was as much as 120 K higher than in the ROSA calculation during the intermediate portion of the transient. The core inlet fluid temperatures and corresponding saturation temperatures are shown in Figure 33. The effect of the higher steam flow rates in AP600 was readily observable as a higher core inlet temperature (as much as 40 K) in AP600 after about 700 seconds. This effect, combined with the lower system pressure in AP600, resulted in the relatively large differences in subcooling, observed in Figure 33. Note that the ECC injection into the downcomer did not significantly impact the difference in subcooling at the core inlet. In both cases, the total ECC mass (CMT and accumulator fluid) being injected into the downcomer and the temperature of that fluid was comparable. Figure 34 shows the total integrated ECC line flow for both cases, and Figure 35 shows the fluid temperatures in the ECC line near the vessel. Again, these parameters agreed well during the period when maximum subcooling differences were observed at the core inlet.

g. In AP600, of the total flow into the downcomer shown in Figure 28, 50 to 60% of the flow passed through the intact cold leg on the break side of the system, and the remainder passed through the two cold legs on the intact side of the system. This represents a different flow pattern for the two facilities, for in ROSA only the intact loop offered a flow path to the downcomer.

The effects of several other distortions in the ROSA facility are not as readily apparent in the 3-in. CLB calculation results described above. Particular areas of concern include the ROSA pressurizer configuration and the loop piping flow area distortion described in Section 2.3.

The pressurizer in ROSA was well scaled volume-wise to the AP600 pressurizer, but its height was much shorter and its diameter was much larger than it would have been if properly flow-area scaled. Additionally, the bottom of the ROSA pressurizer was situated at a higher elevation than in AP600 (see Figure 1). These distortions were likely to affect the system response in two ways. First, the oversized diameter would lead to lower steam velocities in the pressurizer once ADS was activated. This would affect the amount of liquid entrained in the steam flow out the ADS and could impact the primary system transient liquid inventory. Second, the pressurizer configuration and the elevation of the bottom of the pressurizer, relative to AP600, could distort the primary side mass distribution for the two systems. As an example, a liquid level just below the ROSA pressurizer represented a level well into the AP600 pressurizer. For such a case, more liquid would be situated high in the AP600 system than for an equivalent level in ROSA.

The loop piping flow area in ROSA was oversized by a factor of 2.1. The concern with the loop flow area distortion was primarily related to the hot leg region. Due to the oversized hot legs in ROSA, the liquid and vapor velocities would be smaller than those in AP600. This could affect entrainment of liquid in the hot leg as well as into the surge line and pressurizer when the ADS was activated. Again, this could impact the primary side liquid inventory. Another effect of the reduced velocities in the hot legs was that it could influence the voiding response of the steam generators, which, as indicated above, was delayed relative to AP600. To address these concerns, two additional ROSA 3-in. CLB calculations were performed. One calculation included a properly scaled pressurizer and surge line, with the remainder of the model being unchanged. The second included the properly scaled pressurizer and surge line, along with a properly scaled hot leg flow

area. In this second calculation, the connection of the pressurizer surge line to the hot leg was represented identically to that in the AP600 model. The results of these calculations are presented in Sections 4.1.3 and 4.1.4.

Finally, there was concern about the possible effect of differences in the ROSA and AP600 input models rather than to actual physical plant differences. First, the downcomer in the ROSA input deck is modeled as a single channel, while in the AP600 deck it is modeled with eight separate, but connected, channels. This difference affects the mixing of steam and liquid in the downcomer and the corresponding subcooling of that fluid as it passes into the core region. To investigate this effect, the ROSA downcomer was renodalized as a multichannel like the AP600 model. It was determined that the distortion caused by this nodalization difference was very small. The results of a 3-in. CLB calculation using the multichannel ROSA model are discussed in Section 4.1.5. The second concern was related to the PBL/ECC line resistances in the ROSA model. These lines were flow-area scaled to their counterparts in the AP600 model. Because line resistances for the small pipes used in the ROSA model were higher than in the AP600, flow through the CMT system was lower than required in the base case calculation. A 3-in. CLB calculation was performed in which form loss coefficients in the PBLs and ECC line were reduced to allow a better match of the CMT system flow. This change provided a slightly better agreement between ROSA and AP600. The results of this calculation are presented in Section 4.1.6.

4.1.3 Full-Height Pressurizer. As discussed above, results of the AP600 and ROSA base case 3-in. CLB calculations showed a significant discrepancy in ADS Stage 3 flow as well as system mass loss after Stage 3 was activated. One possible contributor to these differences was liquid de-entrainment in the ROSA pressurizer because of its over-scaled flow area. To assess the impact of this distortion, a sensitivity calculation was performed using a full-height, volume-scaled pressurizer and surge line. Results indicate the system's response was not significantly affected by changing the pressurizer. The responses for the actual and full height pressurizer cases were very similar with only minor small quantitative and timing differences observed. As shown in Figures 36 and 37, the ADS Stages 1, 2, and 3 integrated total mass loss and surge line integrated mass flow responses were very similar for the two ROSA calculations. The full-height pressurizer had very little effect on the ADS Stages 1, 2, and 3 total mass loss.

4.1.4 Full-Height Pressurizer and Area-Scaled Hot Legs. As a followup to the scaled pressurizer calculation, another ROSA sensitivity calculation was performed using a properly scaled hot leg flow area. The ROSA hot leg flow area was oversized by a factor of 2.1. This would result in significantly lower liquid and vapor velocities in the hot legs, which could effect liquid entrainment and flow to the pressurizer/ADS. The purpose of this calculation was to assess the impact of the hot leg area distortion on the ADS flow response as well as other system parameters. The model used for the calculation also included the appropriately scaled pressurizer and surge line described in Section 4.1.3. All other system components and operating conditions were identical to those for the base case.

The ROSA scaled hot leg calculation showed considerable improvement in the ADS flow response relative to the base case. However, other system parameters were not significantly affected nor were the types of phenomena occurring in the system. Figure 38 compares the total integrated ADS mass flow rate (all four stages) for the AP600 and ROSA base case calculations and for the ROSA case with scaled hot leg. The better agreement for the ROSA scaled hot leg and AP600 cases was primarily due to improved calculation of the ADS Stages 3 and 4 response. Figures 39 and 40 compare the integrated ADS Stages 3 and 4 mass flow rates for the three cases. By the latter part of the transient, roughly 30% more fluid passed through Stage 3 ADS with the area-scaled hot leg. This was in considerably better agreement with the AP600 calculation than were the base case results. Also, Stage 4 ADS was activated sooner in the ROSA area scaled hot leg

case, again improving the comparison with the AP600 calculation. However, the change in hot leg area did not appreciably affect the rate of mass loss through Stage 4 ADS. In both cases, total mass through Stage 4 ADS in any equal time increment was about the same and significantly higher than in the AP600 calculation. This is consistent with the fact that the ROSA ADS flow was being discharged to atmospheric pressure, while the AP600 ADS was being discharged to the higher pressure containment.

The response of the remainder of the system showed relatively little effect due to the scaled hot leg. Figure 41 compares the vessel normalized mass inventory for the three cases. While there were small differences in mass inventory for the ROSA cases, neither calculation showed the degree of mass loss that occurred in the latter part of the AP600 calculation. The lower vessel depletion exhibited in the ROSA calculations was attributed to the significantly lower core vapor generation rate associated with a higher degree of core inlet subcooling. Figure 42 compares the total vessel vapor generation rates for the three cases, while Figure 43 compares the core inlet fluid temperatures. Both parameters show relatively little effect of the scaled hot leg. Figure 44, which compares the total liquid volume in the pressurizer, indicates some improvement in the latter part of the transient. However, the effects were small. Finally, Figure 45 shows the CMT liquid level for the three cases. The ROSA scaled hot leg case did not exhibit the flow cessation that occurred in the latter part of the CMT drain down in the base case. This improved the agreement with the AP600 calculation and allowed Stage 4 ADS activation earlier than in the base case, as indicated above.

4.1.5 Multi-Channel Downcomer. A ROSA-IV sensitivity calculation was performed to evaluate the effect of modeling the downcomer with a pseudo-two-dimensional (more nodes) representation, as was done in the AP600 model. The sensitivity calculation was performed for the 3-in. CLB scenario. The primary effect of the renodalized downcomer was poorer mixing; thus, colder liquid flow at the reactor core inlet during the depressurization sequence as accumulator liquid was injected into the downcomer and flowed into the lower plenum and core regions. This reduced-temperature liquid resulted in slightly lower vessel vapor generation rate, thereby reducing the ADS system mass flow rate. The effect was small and the finer nodalization did not improve the comparison between AP600 and ROSA-IV.

4.1.6 Reduced Pressure Balance Line/ECC Line Resistance. Because of the higher line resistance obtained by area scaling the PBLs and ECC line, flow through the CMT system was somewhat lower for the ROSA calculations than required. To assess the effect of the lower CMT flow, a 3-in. CLB calculation was performed in which form loss coefficients in the PBLs and ECC lines were arbitrarily reduced to match the CMT flow in the AP600 calculation. With the exception of the change in form loss coefficients, the model used for the calculation was identical to the model described in Section 4.1.4, including the scaled pressurizer, the surge line, and the hot legs.

The modification to the PBL and the ECC line loss coefficients gave better agreement for the total CMT flow and temperature response but had only minor effects on other aspects of the system behavior. Figure 46 compares the total CMT flow rate for the AP600 calculation and the ROSA calculations with the scaled pressurizer and the hot legs and with the reduced PBL/ECC line loss coefficients. As indicated in the figure, the change in loss coefficients resulted in a higher CMT flow than in the previous case and gave excellent agreement with the AP600 CMT flow over most of the injection period. The higher CMT flow rate also improved the CMT temperature response comparison. Figure 47 presents the fluid temperature at the bottom of the CMT for the three cases. With the higher flow rate, the tank temperature increased at about the same rate (although somewhat earlier) as in the AP600 calculation and to a more representative level before the tank emptied.

The principal effect of the higher CMT flow on the remainder of the system was a small reduction

of the bulk primary side temperature. This in turn resulted in a somewhat lower primary side saturation pressure and temperature. Figure 48 compares the core inlet fluid temperature and corresponding saturation temperature for the two ROSA calculations. The effect of the higher CMT flow was a somewhat earlier reduction in core inlet fluid temperature and about a 10 to 15 K reduction in saturation temperature. The change in subcooling at the core inlet had little effect on the net vapor generation in the core. Figure 49 shows the core vapor generation rate for the AP600 and ROSA calculations and exhibits little difference for the two ROSA cases. Finally, the higher CMT flow led to an earlier depletion of the CMT mass inventory (1,825 versus 2,125 seconds). This allowed the vessel mass inventory to begin to decrease somewhat earlier for the high CMT flow case. This is shown in Figure 50, which compares the vessel normalized mass inventory for the three cases.

4.1.7 Applicability of ROSA for 3-In. Cold Leg Break Experiments. The AP600 and ROSA 3-in. CLB analysis indicates that the modified ROSA facility, with first level changes, provides representative results for the major aspects of the primary system response and passive safety feature behavior. The early primary side depressurization, CMT circulation and draining, PRHR flow response, and ADS Stages 1 and 2 initiation and flow rates were well represented in the calculations using the modified ROSA model. Additionally, phenomena occurring during the transient were similar for both facilities. System configuration differences and scaling distortions inherent to scaled facilities affect the agreement in the longer term system response.

Analyses of the effects of modifications to the ROSA system, beyond those described in Section 2.3, indicate the following. Incorporation of a properly scaled pressurizer and surge line would likely have little effect on the system response and phenomena in a 3-in. CLB simulation. However, that this is not true for the 1-in. CLB. Inclusion of area scaled hot legs in ROSA would likely improve simulation of the hot leg response as well as that of the Stages 3 and 4 ADS. These improvements would be in the form of closer agreement in the magnitude of variables and timing of events. However, the types of phenomena occurring in the system would not be expected to change with this modification.

4.2 One-Inch Cold Leg Break

Because of its small size, the 1-in.-diameter break had a lesser influence on system pressure response than did larger breaks. Factors such as steam generator and core/vessel heat transfer played a more important role in the system depressurization response for this case. Therefore, the system response for the 1-in. break was quite different from that for the 3-in. break described in Section 4.1.

Calculations simulating a 1-in. CLB were performed for both the AP600 and modified ROSA facilities. The purpose of these calculations was to assess the similarities and differences in system behavior for a case in which system distortions could have a greater impact on transient response. As was the case for the 3-in. CLB calculations, the break was assumed to occur in a cold leg of the loop containing the pressurizer. With the exception of the break size, conduct of the calculations was the same as described for the 3-in. CLB calculations (Section 4.1.1). Comparisons presented in this section cover the time period through 6,000 seconds, which included activation of all four stages of ADS.

The results for the 1-in. CLB calculations showed that overall trends in system response were similar for the two facilities. However, the calculations exhibited differences in the phenomena occurring during the transient. Distortions in the ROSA facility had a more pronounced effect over the course of this transient than was evident in the 3-in. break case. The distortions with most impact were the difference in vessel upper head initial conditions and the pressurizer configuration. As stated in Section 2.3, the two facilities incorporated different flow paths to and from the vessel upper head. In the AP600 system (as it was known when the calculations were conducted), flow into the upper head was such that the upper head fluid temperature was at roughly the cold leg

temperature during normal operation. For ROSA, it was at about the hot leg temperature. Also, the bottom of the pressurizer in ROSA was situated at a higher elevation than in AP600. Thus, similar liquid levels in the two systems may have corresponded to different liquid inventory distribution. These distortions affected both the voiding response of the primary system and the timing of events during system depressurization. Differences in timing are indicated in Table 4, which lists the sequence of events for both cases.

The differences in system response for the two facilities are highlighted in the following subsections.

4.2.1 System Response for 1-in. Cold Leg Break. Both the ROSA and AP600 1-in. cold leg break calculations exhibited the general characteristics of a small break transient in an AP600 type system. Figure 51 compares the pressurizer pressure for both cases and illustrates these characteristics. They are as follows:

1. An initial, relatively slow decrease in primary system pressure and eventual equilibration of the primary with the secondary pressure

2. An extended period during which the primary pressure remained at about the secondary pressure while primary fluid continued to exit the system through the break

3. Initiation of CMT draining once the primary liquid inventory had decreased sufficiently

4. Activation of ADS on CMT level decrease, which reestablished rapid primary depressurization, with the pressure quickly decreasing to containment pressure (AP600) or atmospheric pressure (ROSA).

While the pressure response for the two cases exhibited similar trends, there were several areas of disagreement. First, during the period of about 400 to 800 seconds, the pressure in the ROSA calculation was considerably higher than in AP600. Second, from about 500 to 2,000 seconds, the pressure in AP600 exhibited an oscillatory response that did not occur in ROSA. Finally, ADS was activated earlier in the AP600 calculation than in ROSA (3,357 versus 4,326 seconds). These areas of disagreement suggest differences in phenomena leading to the particular response observed. As identified earlier, differences between the two facilities affected the phenomena occurring in the system and the progress of the transient. The resulting differences in system response as well as the similarities are described next.

In both cases, the initial depressurization was similar. The hottest fluid in the system at rupture was in the pressurizer. As the system initially depressurized, the pressurizer fluid flashed and began to drain into the hot leg. While this process was in progress, fluid in other parts of the primary remained subcooled and no voiding occurred. The volume of fluid exiting the break was made up by the volume of pressurizer fluid entering the hot leg. Subcooling in the primary persisted until the pressurizer and surge line were essentially empty. After this point, the response observed in the AP600 and ROSA calculations became quite different.

In the AP600 calculation, after the pressurizer emptied, the hottest fluid in the system was in the upper core region. Vapor generation began in this region shortly after the pressurizer emptied. The density differences between the hot core/hot leg fluid and cooler cold leg/downcomer fluid resulted in a natural circulation flow from the vessel towards the steam generators. The steam generated in the core thus migrated to the steam generators, where it collected at the tops of the

Table 4. Comparison of event timing for AP600 and modified ROSA LSTF 1-in. cold leg break RELAP5 calculations.

Event	Time (seconds)	
	AP600	ROSA
Break	0	0
Scram	108	140
PBL/CMT circulation began	186	214
CMT draining began	2,520	3,550
First stage ADS	3,357	4,326
PRHR flow began	3,357	4,326
Second stage ADS	3,516	4,520
Accumulator flow began	3,567	4,558
Third stage ADS	3,600	4,608
Fourth stage ADS	3,813	4,862
CMTs empty	4,200	5,200
IRWST flow began	4,600	NA

U-tubes. This steam did not initially condense because the primary temperature was equilibrated with the secondary. As steam continued to collect in the U-tubes, the resulting steam binding first slowed and then brought the natural circulation flow to a stop. While the natural circulation flow was decreasing, the core liquid heated up to saturation. As further decay heat was added, it caused a slight increase in the primary system pressure (Figure 51), along with a corresponding increase in system saturation temperature. The increase in primary saturation temperature reestablished primary-to-secondary heat transfer in the steam generators, which led to condensation of some of the steam. The condensation reduced the effect of the steam binding, and natural circulation flow was reestablished. As a result, however, cool liquid from the downcomer and lower core moved upward in the core. The cool liquid displaced saturated fluid, and vapor generation in the core region ceased. After a short period, the cool liquid was heated to saturation, and vapor generation began once again. This phenomenon occurred in a cyclic fashion over a period of about 25 minutes and was accompanied by a partial periodic voiding and refill of the upper core, hot legs, and steam generators. The volume occupied by the steam condensed in the steam generators was made up by subcooled liquid draining into the upper plenum from the vessel upper head region. The cyclic behavior ended once the upper head had drained. Continuing loss of fluid out the break eventually led to initiation of draining of the CMT. This was followed by activation of the ADS, which quickly depressurized the system. The presence of liquid in the pressurizer (which partially refilled shortly after its initial draining) contributed to earlier initiation of CMT draining and activation of ADS than was observed for the ROSA calculation.

In the ROSA calculation, fluid in the core and hot legs remained subcooled for an extended period beyond emptying of the pressurizer. This was a result of flashing of hot fluid in the vessel upper head, which held the system pressure above the saturation pressure of the core fluid. The vessel upper head fluid temperature in ROSA was initially at roughly the core outlet temperature. Because of the small flow rates through the upper head, this fluid remained hot even after the core power trip resulted in a cooldown of the core fluid. Thus, immediately after the pressurizer drained, the hottest fluid in the system was in the

upper head. As this fluid flashed, upper head liquid was forced into the upper plenum region. The volume of liquid exiting the primary through the break during this period was made up by the draining of the upper head, and little voiding of the remainder of the primary was observed. Continued [illegible] of the upper head liquid resulted in cooling of the remaining fluid and eventually the upper head fluid temperature dropped to about that of the core outlet. At this point, net vapor generation in the core region began, along with a gradual voiding of the remainder of the primary. Voiding of the upper parts of the system to the level of the cold legs then allowed the CMT to begin draining. ADS activation followed shortly thereafter, and the primary quickly depressurized to atmosphere. The oscillatory behavior observed in the AP600 calculation was not seen in the ROSA calculation. Also, the ROSA pressurizer remained empty during the intermediate phase of the calculation (it did not begin to refill until after initiation of ADS). This resulted in a considerable delay in ADS initiation (relative to AP600), as there was more liquid in the remainder of the primary system that was to be removed before CMT draining began.

To summarize, the AP600 and ROSA calculations exhibited considerable differences in the overall system response and phenomena observed for the 1-in. CLB transient. While the trends in overall system response were similar for the two cases, the phenomena occurring in the transient were strongly affected by differences in the upper head initial conditions and response as well as by the pressurizer configuration. As the discussion above is limited to describing the general course of events for the two cases, details of the processes and phenomena involved have not been included. A more detailed description of these items is presented next.

4.2.1.1 Effects of Upper Head Response for 1-in. Cold Leg Break. The general trend in system depressurization was similar for the AP600 and ROSA 1-in. CLB calculations. However, the phenomena that occurred during the depressurization were different for the two cases. One system component that not only exhibited different response but also affected phenomena occurring in other parts of the system was the upper head. Upper head vapor generation in ROSA acted to hold a higher primary pressure (than in AP600) during the period immediately following the emptying of the pressurizer and surge line. The higher pressure prevented substantial voiding of the primary while the upper head drained. In AP600, the lack of significant vapor generation in the upper head allowed the primary pressure to fall to the saturation pressure of the core outlet fluid. As a result, vapor generation in the upper core began early. The period of interest is the first 2,000 seconds of the transient. By 2,000 seconds, the upper head was completely drained in AP600 and the level was down to the elevation of the top of the "inverted top hat" in ROSA.[h]

As indicated previously, the differences in system response for the two cases may have been initiated primarily because of differences in the vessel upper head initial conditions and the response of the upper head fluid temperature shortly after rupture. Figures 52 and 53 compare the upper head fluid temperatures (at various elevations) and the core outlet fluid temperature for the ROSA and AP600 cases, respectively. The point to note in these figures is that the upper head fluid temperatures in ROSA were consistently higher than the core outlet fluid temperature, while the reverse was true for much of the period in AP600. The effect of this difference occurred since the pressurizer and surge line were initially empty.[i] In the ROSA calculation, the decreasing system pressure resulted in the upper head fluid temperature becoming saturated by about

h. The "inverted top hat" portion of the ROSA upper head (Volume 140 in the ROSA nodalization shown in Figure 4) was closed off from the upper plenum and therefore could not drain directly into the upper plenum. The flow path from the upper head to the upper plenum was from the top volume (Volume 152 in Figure 4) and represented the guide tube flow path. The inverted top hat fluid could not escape the upper head unless it flashed/boiled off.

i. The pressurizer and surge line were completely drained by about 250 seconds in the ROSA calculation and 300 seconds in the AP600 calculation.

275 seconds. The fluid temperature then remained at saturation for the duration of the period of interest. This is illustrated in Figure 54, which compares the fluid and saturation temperatures in the top volume[j] of the upper head for ROSA. Figures 55 and 56 show similar parameters in the top and bottom volumes of the upper head for the AP600 calculation. However, unlike ROSA, fluid in the upper volume remained subcooled until after 1,200 seconds,[k] and (with the exception of the period between 380 and 520 seconds) the lower volume remained subcooled until almost 1,700 seconds.[l]

The impact of the upper head temperature difference for the two cases was in how it affected the response of the remainder of the system. In ROSA, the saturated upper head fluid flashed, which tended to hold up the primary pressure. This maintained subcooling in the remainder of the primary. The lack of vapor generation in AP600 allowed the system pressure to drop to the saturation pressure of the core outlet fluid, and early boiling in the core region was observed (see Section 4.2.1.2). Figure 57 compares the total upper head vapor generation rates for the two cases. In the ROSA calculation, vapor generation began when the fluid became saturated (at about 275 seconds) and persisted at a fairly substantial rate until well after 800 seconds. In AP600, except for a few brief periods during which vapor was generated, the subcooling in the upper head acted to condense steam (as indicated by the negative vapor generation rate). Figure 58, which is a blowup of the pressurizer pressures for the two cases, shows the effect of the difference in upper head vapor generation. The ROSA pressure was considerably higher between 300 and 750 seconds and corresponded to the saturation pressure of the upper head fluid. The higher primary pressure caused the core outlet fluid to remain well subcooled. Figure 59, which compares the core outlet fluid temperature with the corresponding saturation temperature, shows the degree of subcooling. On the other hand, the AP600 pressure (Figure 58) was controlled by saturation of fluid at the core outlet. The oscillatory pressure response was associated with periods of vapor generation when fluid in the upper core region was saturated. Figure A-56, which compares the core outlet fluid and saturation temperatures for the AP600 case, shows that the temperature alternated between being saturated and well subcooled. The cause of this response is discussed in detail in the following subsection.

4.2.1.2 Pressure Plateau Phase System Response. The previous subsection described the difference in upper head response for the two 1-in. CLB cases and the impact of the upper head response on the system pressure. Partially as a result of the difference in system pressure response, phenomena occurring in the primary system were different for the two cases. Of particular interest is the primary side pressure oscillation (and the phenomena associated with it) that occurred in the AP600 calculation but not in the ROSA calculation. The pressure oscillation did not significantly change the overall system depressurization response. However, as stated above, the phenomena occurring in the two facilities during the period encompassing the oscillations were different. This can be important from a code assessment standpoint, because the phenomena in the experiment will not be representative of those likely to occur in the full size plant. This section describes the differences in primary side phenomena during the period following the emptying of the pressurizer/surge line and before initiation of ADS.

As indicated in Figure 58, the pressure in the AP600 calculation began to oscillate after

j. Similar response was observed in the upper head middle and lower volume fluid temperatures, although at slightly later times as the fluid in these volumes was initially somewhat cooler than the top volume.

k. By 1,200 seconds, the upper head liquid level has decreased below the level of the upper volume, which then contained only saturated steam.

l. The increase in fluid temperature in both upper head volumes, after about 150 seconds, was due to upper plenum fluid entering the upper head. This occured after primary pumps begin to coastdown. Prior to pump coastdown, flow was directed from the upper head into the upper plenum.

500 seconds, with a period of 100 to 200 seconds and a peak-to-valley magnitude of roughly 0.25 MPa (36 psi). As described in Section 4.2.1, the oscillations were associated with vapor generated in the core being condensed somewhat later in the steam generators. Immediately after rupture, fluid in the core region was subcooled. As the system pressure dropped, the upper core fluid became saturated, and vapor generation began. This is illustrated in Figure 61, which compares the core outlet fluid and saturation temperatures and includes the net core vapor generation rate. This vapor migrated from the core region, into the loops and steam generators. Figures 62 and 63 show the vapor void fraction in the intact and broken loop hot legs and the collapsed liquid levels in the two steam generators and indicate the accumulation of steam in these regions on a periodic basis.[m] As steam was being generated, the primary pressure and corresponding saturation temperature were increasing. Steam on the primary side of the steam generators became hotter than the secondary fluid, and primary-to-secondary heat transfer[n] began to increase. This is illustrated in Figure 64, which compares the primary pressure and break side steam generator primary-to-secondary heat transfer. As the heat transfer continued, steam in the steam generators was condensed and the pressure began to fall. Coincidentally, natural circulation flow was reestablished, and subcooled liquid from lower parts of the core moved upwards through the core, displacing the saturated two-phase mixture that allowed the steam generation to occur. Figure 65 compares the core collapsed liquid level and the system pressure. Note that the core level recovered very quickly as soon as the pressure began to decrease The movement of subcooled liquid into the upper core shut down the steam generation until the liquid could be heated saturation once again (see Figure 61). The process repeated itself for a period of about 20 minutes.

The ROSA calculation did not exhibit the oscillatory behavior of the AP600 calculation. As indicated in Figure 66, the vapor generation rate in the core region was small during the first 2,000 seconds of the transient (compare to Figure 61). Recall from above that the core region fluid remained somewhat subcooled during this period as a result of the pressurizer effect of the upper head. Thus, there was only a gradual buildup of steam in the hot legs and steam generators. Figures 67 and 68 show the vapor void fractions in the hot legs and the collapsed liquid levels in the steam generators for this case and illustrate the slow buildup. Once steam began to occupy the steam generators, heat transfer to the secondary (Figure 69) and the corresponding condensation of steam was minimal. This is at least in part due to the thicker tube walls in the ROSA steam generator. Thicker walls would tend to damp out any effects that would contribute to an oscillatory type behavior. This is because a larger primary-to-secondary temperature difference in ROSA would be required to obtain a response that occurs at a lower temperature difference in AP600.

4.2.1.3 Effect of Pressurizer Response in 1-in. Cold Leg Break. The delayed initiation of ADS in the ROSA calculation was a direct result of the difference in pressurizer response that occurred during the first 2,000 seconds of the transient. In the ROSA calculation, the pressurizer emptied early in the transient (at about 100 seconds) and remained empty until after the initiation of ADS flow. In the AP600 calculation, the pressurizer emptied at roughly the same time as in ROSA but then partially refilled as a result of vapor generation in the core region. Figure 70 compares the pressurizer collapsed liquid level for the two case. In the AP600 calculation, prior to the time of ADS activation, about 12 m^3 (39.6 ft^3)of liquid was effectively removed from the remainder of the primary system. This allowed an earlier draining of the CMTs and a corresponding earlier initiation of ADS flow in the AP600 case. Notice that while the ROSA pressurizer was empty, the level of liquid in the

m. Notice that there was an almost complete refilling of the steam generator and hot legs following each period of steam generation. The liquid necessary to accomplish this refill came from draining of the upper head.

n. Note that before the increase in primary pressure/saturation temperature, the primary-to-secondary temperature differential was small. Thus, little heat was being transfer to the secondary.

surge line corresponded to the same elevation as the level of fluid in the AP600 pressurizer. This was illustrated in Figure 71, which compares the pressurizer/surge line collapsed level for the two cases.

4.2.2 Applicability of ROSA LSTF to 1-in. Cold Leg Break Experiments. The results of the AP600 and ROSA 1-in. CLB calculations suggest the likelihood of differences in the transient response of the two systems. While the overall trends in primary depressurization were similar, phenomena that occurred during the transient and event timing were different. The principal distortions contributing to differences were the vessel upper head and the pressurizer.

The fourth level of modifications to the ROSA facility, including addition of a properly scaled pressurizer and changing the upper head flow path configuration, would likely improve comparison of the transient response for the 1-in. CLB case. With respect to upper head modifications, initial conditions and transient flow response comparison could be improved by increasing the flow through the upper head and by using a representative upper head-to-upper plenum flow path and area. Such a change would likely eliminate the pressurizer effect of the current upper head and would allow the earlier core outlet fluid temperature saturation observed in the AP600 calculation. However, it is not evident that such a change would result in the pressure oscillations observed in the AP600 calculation. With respect to the pressurizer modification, a scaled pressurizer would likely improve the event timing comparison for the two cases. However, this change would not necessarily affect phenomena occurring in the system.

4.3 Pressure Balance Line Break

A 3-in. break in one of the cold leg PBLs was imposed in this calculation. The break was located in the vertical portion of the PBL between the top of the cold leg and the valve connecting this line to the header piping at the top of the CMT. In terms of the code input models, for both the AP600 and ROSA the break junction was located at the outlet of Volume 857-03. For the ROSA calculation, the break area was scaled by the overall ROSA/AP600 scaling factor of about 1:30.

As stated previously, the main feature that distinguished plant response to this break location as compared to a "normal" 3-in. CLB was the asymmetric draining rate of the CMTs. Scoping calculations have shown that during a "normal" CLB of this size, the draining of the two CMTs is nearly identical. For the PBL break, however, the draining of the CMT associated with the affected PBL was delayed. With the break in the cold leg PBL, vapor flowed from the pressurizer, through the pressurizer PBL, and into the cold leg PBL, where it then escaped through the break. The effect of this flow was to reduce the pressure at the top of the affected CMT relative to the nonaffected CMT. Initiation of draining of the affected CMT was thus delayed.

There were two limitations in the ROSA model used for the PBL break calculation described in this section. First, in the ROSA model with the first level modifications, the two CMTs and two sets of PBLs of AP600 were simulated with a single lumped CMT and one set of PBLs. Therefore, any asymmetric CMT phenomena could not be simulated. This inability to simulate asymmetries, given only Level I modification, would limit the utility of ROSA in simulating PBL break transients. Second, the downcomer portion of the ROSA input model was represented by one-dimensional components. On the other hand, the AP600 downcomer was represented by a quasi-two-dimensional model. This difference in the two models appeared to affect the calculation of several phenomena (including break flow rate), as is discussed later.

An attempt was made to upgrade the ROSA modifications to a third level (split cold leg beyond the pump, renodalized downcomer, two CMTs, and two sets of PBLs) in order to address some of the limitations of the model. The results of a calculation made with this third level modification model (see the appendix of this report)

Table 5. Calculated sequence of events (in seconds).

Event	AP600	ROSA
Break opened	0	0
Reactor scram signal	11	12
Feedwater off, turbine stop valves began to close (main steam isolation valves began to close in ROSA)	11	12
Reactor coolant pump trip signal	11	12
S signal	19	21
First stage ADS actuated	695	904
Second stage ADS actuated	1,190	1,696
Third stage ADS actuated	1,335	1,890
Fourth stage ADS actuated	1,720	2,376
Accumulator flow began	745	920
Accumulator flow ended	1,060	1,130

showed a more distorted response, particularly timing-wise, than with level one modifications. These results indicated that splitting the cold legs downstream of the pump, and thereby allowing use of two sets of CMTs/PBLs, was not an acceptable alternative to the Level I modification.

4.3.1 System Response. The general sequence of events in both AP600 and ROSA PBL break calculations was similar, as demonstrated in Table 5. However, the actual timing of events, such as ADS actuation and accumulator injection, was delayed in the ROSA calculation because the level decline in the single CMT in ROSA was different than in the unaffected CMT in AP600. This was due to the lumping of the CMTs and PBLs in the ROSA model. For this break location, the effect of lumping the CMTs and PBLs is that the ROSA CMT behavior was not representative of either the affected or unaffected AP600 CMT.

The overall progression of the transient was illustrated by the primary system pressure response (Figure 72). Both AP600 and ROSA depressurized rapidly to the saturation pressure. Further system depressurization was caused by different events for ROSA and AP600, leading to a different time of departure from the plateau. In ROSA, the break flow began a rapid transition to nearly single phase vapor beginning at about 500 seconds (Figure 73), thus causing ROSA to begin to depressurize again at that time. However, the transition to nearly single phase vapor flow for AP600 did not occur until after first stage ADS was opened; and because the two first stage ADS valves were bigger than the break, the effect of single phase break flow was overshadowed by the depressurization due to vapor flow through the ADS valves.

The early transition to nearly all vapor break flow in ROSA was attributable to differences in fluid conditions in the downcomer region where the cold legs were connected. The mass flow rate at the affected cold leg connection to the reactor vessel (Figure 74) indicated that, for both calculations, flow reversal occurred at 180 seconds. Once flow reversal occurred in the affected cold leg, the main contribution to the break was from the vessel downcomer. The liquid fraction in the downcomer volume connected to the affected cold leg is shown in Figure 75. The figure indicates that although the liquid fraction in the AP600 volume initially decreased faster,[o] the ROSA volume actually emptied earlier (at ~600

o. The unaffected CMT did not provide much net mass because of recirculation back to the CMT through the PBL.

seconds). As a consequence, the break void fraction in ROSA reached one at ~600 seconds (Figure 73).

Another difference evident from the event sequence was that actuation of first stage ADS was delayed in the ROSA calculation. Since ADS actuation was dependent on CMT level, the delay pointed to discrepancies in CMT behavior. The CMT collapsed liquid level (Figure 76) shows that, although the ROSA CMT began to drain sooner than the unaffected CMT of AP600, the rate of level decline was much slower and thus caused the delay in first stage ADS. The ROSA CMT began to drain sooner because the break in the PBL made it more difficult to set up a recirculation mode that maintained the CMT level. As opposed to the AP600 unaffected CMT, which in the first 400 seconds was providing flow to the downcomer (Figure 77), most of that liquid was recirculated via the cold leg and PBL back to the CMT to keep it full. On the other hand, the level dropped more gradually in ROSA because of venting of much of the vapor through the pressurizer PBL to the break. (Although the break in ROSA was the same size as that in AP600, the pressure balance lines were twice as large since they were lumped together. This meant that more vapor could flow from the pressurizer through the ROSA PBL than in any one AP600 PBL.)

The openings of the second, third, and fourth stages of ADS were delayed in the ROSA calculation, also due to differences in CMT level response. The ROSA CMT collapsed liquid level showed an increase in the period from 1,050 to 1,150 seconds, which the unaffected AP600 CMT did not. This increase in CMT level followed accumulator injection (Figure 78) and was a result of large condensation rates in the PBL and CMT. Condensation occurred as cold accumulator water was circulated from the downcomer out the cold leg connection (cold leg temperature became ~120 K subcooled) and into the PBL. Condensation lowered the pressure throughout the PBL and at the top of the CMT. Since the break was still choked at this time, the induced low pressure caused some of the liquid entrained from the cold leg to flow past the break into the upper portion of the PBL and CMT, where it caused further condensation and a subsequent rise in the CMT level. This refilling phenomena was not seen in either AP600 CMT: the unaffected CMT of AP600 did not have a break in the PBL, which would tend to cause accumulator liquid to flow toward it; the affected AP600 CMT remained full until 1,200 seconds because the break vented all the vapor coming from the pressurizer/CMT PBL, so any condensation in its PBL did not affect the CMT level.

Besides the obvious differences in event timing, the ROSA calculation showed a core heatup, which the AP600 calculation did not. Figures 79 and 80 show the cladding temperatures for the two calculations, where Cladding 1 is in the bottom volume of the core and Cladding 6 is in the top volume of the core. Although the ROSA CMT was providing some mass makeup for the primary system (~10,000 kg by 400 seconds), the heatup occurred because the mass lost through the break in ROSA was much greater than in AP600 (Figure 81). Also, the decrease in core collapsed liquid level to below 40% (Figure 82) represented a more severe condition in ROSA than in AP600 because of the relative elevation of the core inside the vessels of the two facilities; the AP600 core was lower than the ROSA core. Thus, for the same percentage of mass lost from both vessels, the corresponding collapsed liquid level in the ROSA vessel would be closer to the top of the core. The heatup was mitigated by the initiation of continuous CMT flow. Although a single unique cause was not identified for the lower core level depression in ROSA, the major contributor was believed to be the difference in upper head configuration. The ROSA downcomer to upper head leak path was much smaller than the scaled downcomer to upper head spray path in AP600, meaning there was less vapor communication (and thus less pressure equalization) between the core and the downcomer. This type of condition could have led to a more pronounced core level depression.

As mentioned in the prior discussion about the core heatup, the mass lost through the break in the ROSA calculation exceeded that in the AP600

calculation. As shown by the break mass flow rate (Figure 83), this was true for the first 500 seconds of the transient, particularly from 250 to 350 seconds. The flow in this period was greater because the fluid in the affected cold leg became 10 K subcooled (Figure 84) due to the injection of CMT water into the downcomer. It appeared that the AP600 calculation did not show a similar increase during CMT injection because of increased thermal mixing (and hence a higher fluid temperature) due to the two-dimensional downcomer nodalization. In the AP600 downcomer model, the passive safety injection (PSI) lines were not connected to the same stack of volumes as the cold legs (as in the ROSA model) but were removed by one azimuthal volume from them. This meant that ECC fluid entering the vessel needed to mix in more than one volume before leaving the vessel through the affected cold leg. Furthermore, even outside the time when this "hump" in break flow occurred, the ROSA break flow rate exceeded that of AP600 because the ROSA case showed a lower void fraction at the break. Based on the results of several ROSA modeling sensitivity studies in which the form loss factor at the junction from the cold leg to the PBL was varied, it was concluded that the reduced losses in the ROSA model, because of the lumping of the PBLs and thus a connection to a single cold leg, was a contributing factor. When a form loss factor was input at this junction, the saturated break flow (from ~150 to 400 seconds, excluding the hump) was closer to that of AP600. After 500 seconds, the ROSA break flow became less than that of AP600 because the ROSA downcomer volume connected to the cold legs, emptied sooner than that of AP600, as discussed previously. Once the corresponding AP600 downcomer volume emptied at 700 seconds, the flow rates exhibited the same type of behavior. Each flow rate exhibited an increase during the time of accumulator injection because of an increase in the downcomer level and decrease in downcomer fluid temperature.

An indicator of the effect on the system of the discrepancies in break flow rate and timing of ADS actuation was the total primary system mass inventory shown in Figure 85. Because the ROSA break flow was initially larger than that of AP600, the ROSA mass inventory dropped more than that of AP600. Additionally, because ADS actuation was delayed in ROSA, the final mass inventory was greater than that for AP600 because less mass had been lost through those valves (Figure 86).

Because of possible concerns about the scaling of the ROSA pressurizer for AP600 simulations, a final point of interest is the pressurizer level response. The ROSA pressurizer was about the correct volume for AP600 simulation, but the shape was shorter and fatter than a true scaled representation of the AP600 pressurizer. Despite these differences, the general response of the pressurizer collapsed liquid level was the same in both cases (Figure 87). The only significant discrepancy between the two calculations was that the AP600 pressurizer refilled to about 10% after it first emptied and before first stage ADS was actuated. Later in the transient, as the ADS stages were activated, the levels in the two cases responded similarly. Both showed an increase after the first stage of ADS was opened because of liquid entrainment into the pressurizer from the hot leg. However, when the second and third stages of ADS were opened, the level in both cases showed a dramatic decrease because more liquid was entrained out through the ADS valves (due to a large increase in vapor velocity in the pressurizer) than could be made up for by entrainment from the hot leg.

4.3.2 Applicability Concerns. The major applicability concern for ROSA simulation of this transient was the lumping of the CMTs and PBLs. Since a PBL break caused asymmetric passive safety system response, any lumping of these systems would cause distortions. The first-level modification calculation demonstrated that the one ROSA CMT behaved differently than either the affected or unaffected CMT of AP600. This resulted in a difference in timing of ADS, which further resulted in an incorrect prediction of primary system mass inventory, at the end of the transient. Further, an over-prediction of liquid discharge through the break (resulting from CMT and PBL lumping distortions), in combination with the geometric distortion of the ROSA

Table 6. Steam generator single-tube rupture scenario.

Event	Time (sec) AP600	ROSA
Initiated single-tube rupture	0	0
Reactor scramed, tripped reactor coolant pumps and turbine valve (closed main steam valve in ROSA)	132	107
S signal, initiated CMT flow	522	546
Steam generator low level, initiated PRHR	5,500	7,192
ADS actuation	NA	NA

core being located higher in the vessel than that of AP600, contributed to the calculation of a core heatup in ROSA and not AP600.

4.4 Steam Generator Tube Ruptures

Calculations of single-tube and three-tube rupture cases were performed with both AP600 and ROSA models. The tube ruptures were simulated in the AP600 model by adding a break junction between the "A" steam generator outlet plenum and the bottom of the downcomer, in a manner similar to the ROSA break simulation hardware arrangement. The break areas used were twice the combined flow area of the number of tubes ruptured to represent double-ended breaks. The ROSA break models represented the actual break simulation hardware presently available. This was done so that any differences between actual tube rupture response and those due to simulation in a test facility could be evaluated. The ROSA input model, modified to the first level of changes described in Section 2, was used for these calculations.

4.4.1 Single-Tube Rupture. Table 6 lists the sequence of events for the steam generator single-tube rupture scenario.

The primary system pressure response comparison is shown in Figure 88. The calculated RCS pressure response was nearly identical for the two simulations for about the first 2,000 seconds. This demonstrated that the ROSA steam generator tube rupture simulation hardware did not introduce noticeable distortion into the system depressurization. Therefore, the times of reactor scram and CMT initiation were almost the same. PRHR initiation timing (on steam generator, low-level signal) was later in ROSA. Possible reasons for the delay were the overscaled coolant loop mass and the increased friction loss in the CMT discharge piping and PSIS line.

The CMTs exhibit natural circulation (buoyancy-driven) convection cooling in addition to gravity-driven liquid injection. The natural circulation cooling phenomena is only observed during periods when primary coolant system water level remains above the top of the CMTs. The S signal opens the valves between the CMTs and their respective PSIS lines. At the same time, pressure equalization valves connect the loop cold legs to the tops of the CMTs via the PBLs. Since the CMTs are above the loops and are ~240 K cooler, a buoyancy-driven flow path is established via the PSIS line to the downcomer, through the vessel and around the loop into the cold legs, and back to the CMT via the PBL path.

This phenomenon was observed in the one-tube rupture scenarios in both AP600 and ROSA, as shown in Figure 89. Immediately after the S signal occurred, flow rates in the PSIS line increased to 42 scaled kg/s for ROSA and 52 kg/s for both AP600 CMTs. At the same time, flow rates in the PBLs increased to 33 and 38 kg/s, respectively; the difference was due to the larger friction of the scaled system. The CMTs remained full during this period, as shown in Figure 90. The flow differences were due to different densities of the liquid flowing in the PSIS

and PBLs; the volumetric flow rates needed to be the same for the tanks to remain full.

The CMTs were a source of mass as well; as shown in Figure 91, total CMT inventory decreased about 280,000 kg between flow initiation and 7,000 seconds. Eventually, as the CMT temperature rose and the thermal driving head decreased, the flow rates degraded and the difference between PSIS and PBL flow decreased. The circulating flow ceased when the driving head was overcome by another force. In ROSA, this occurred when PRHR was initiated (and CMT gravity-driven injection began); in AP600, loop cold leg flow was interrupted by the formation of voids in the associated steam generator tubes.

Pressurizer level response is shown in Figure 92. In both calculations, the pressurizer was predicted to empty after ~750 seconds. In AP600, the pressurizer level began to increase due to CMT mass makeup starting at 950 seconds and continued until PRHR initiated. The ROSA pressurizer did not refill, because the inlet to the pressurizer was situated higher in the system, and there was less CMT mass makeup. There were subtle differences in RCS characteristics that slowed the ROSA responses to this transient and made them less pronounced.

Differences in liquid distribution (especially in the pressurizer), and fluid temperature and mixing associated primarily with the downcomer region, resulted in significantly different CMT gravity-driven injection response in the two calculations. As noted, gravity-driven injection from the CMT tank occurred in ROSA at the same time as initiation of PRHR flow. The CMT level decreased quite rapidly after this point in the ROSA calculation. CMT level decrease of 18% in 2,800 seconds, contrasted with a decrease of only 2.5% in 1,000 seconds in AP600 (see Figure 90). This distortion in the predicted ROSA response was influenced by several factors, including the one-dimensional downcomer nodalization and the lack of level in the pressurizer at the time of PRHR initiation. Figure 93 shows the temperature responses in the reactor vessel downcomer cells connected to the cold legs and to the PSIS lines. In the AP600 calculation, PRHR initiation had almost no effect on the downcomer cell connected to the cold leg. However, in ROSA, the two downcomer cell temperatures became the same following PRHR initiation. The different downcomer temperature distribution (and corresponding downcomer head difference) for the two cases was partially responsible for the different CMT drain behavior. The other contributor to the different CMT drain response was the liquid subcooling in the PBL tee that connected the pressurizer and loop pressure balance lines to the CMT vent line. Liquid subcooling in this tee for the two calculations is shown in Figure 94. In AP600, this volume remained subcooled following PRHR initiation, despite the magnitude of the associated cooldown. This was because the pressurizer level provided sufficient static head on the system to maintain subcooled liquid in the tee. Conversely, in ROSA, the corresponding volume became saturated and voiding occurred immediately following PRHR initiation, because there was no liquid level in the pressurizer to provide a static head for subcooling. The effect of this difference, once again, was to allow the CMT to begin to drain earlier in the ROSA calculation.

The primary system mass inventory responses for the two calculations exhibited the same trends until 5,500 seconds, as indicated in Figure 95. Both calculations exhibited a mass decrease until ~750 seconds, at which time CMT draining overcame break flow rate and the masses increased until about 2,800 seconds. The mass increase was about 10,500 kg in AP600 and the equivalent to 6,000 kg in ROSA; the ROSA mass increase was less because of the higher pipe friction and lower draining rate of the CMT. Note that both ROSA and AP600 showed decreasing primary system mass inventories from ~2,800 seconds until the times of PRHR initiation (at about ~5,500 seconds in the AP600 calculation and 7,200 seconds for ROSA). Thereafter, the increased primary system cooling in AP600 caused coolant temperatures to decrease, thus causing primary coolant shrinkage and decreasing pressurizer level. The temperature decrease also reduced saturation pressure, which reduced

break flow, as shown in Figure 96. The ROSA calculation did not follow the same trend as AP600, primarily due to the reduced effect of PRHR cooling. The PRHR heat exchanger heat transfer coefficient specified for the ROSA calculation assumed natural circulation cooling on heat exchanger shell side; an assumption not particularly appropriate for this transient, because the PRHR-side (tube-side) heat transfer occurred at the steam generator safety setpoint temperature (560 K). By contrast, the AP600 IRWST-side (shell side) wall temperature significantly exceeded saturation, and subcooled nucleate boiling occurred in the tank; thus, the heat transfer coefficient boundary condition assumed for the ROSA PRHR heat exchanger model caused underprediction of the actual cooling. The ROSA calculation should be repeated with a more sophisticated representation of shell-side heat transfer in the PRHR heat exchanger.

The timing and magnitude of the cooling effect were different in ROSA, the timing was slower, and the loop temperature changes were smaller (Figure 97). AP600 loop average temperature decreased ~30 K and reached its minimum value at ~2,400 seconds, as the CMT cooling became less than the core decay heat. Temperature then returned to ~564 K at 3,500 seconds. The steam generator safeties opened and removed decay heat until the intact steam generator mass decreased to the low-level setpoint, thereby actuating the PRHR system at 5,500 seconds. In contrast, the ROSA loop average temperature decreased ~17 K, to a minimum of ~555 K at ~3,000 seconds. The steam generator heated up to the safety setpoint between 3,000 and ~5,200 seconds. PRHR was actuated at ~7,200 seconds, 1,700 seconds slower than AP600. The friction pressure drop distortion in the CMT piping and the overscaling of the loops may have both contributed to the calculated differences. In ROSA, the CMT recirculation cooling was effective for a longer period of time because of the lower recirculation flow rate.

Steam generator mass responses, shown in Figure 98, were in close agreement until ~3,500 seconds. The affected side inventories showed nearly identical responses for this period and gradually diverged thereafter. On the intact side, at 1,200 seconds, the AP600 feedwater line emptied into its downcomer; otherwise, the intact side inventories were nearly identical as well.

PRHR initiation was predicted ~1,700 seconds later in ROSA than in AP600, primarily because the coolant loop temperature changes were retarded by a higher ratio of coolant loop-to-CMT mass, as discussed above. The signal for PRHR initiation was low steam generator water level, which occurred in the unaffected loop. The actual low-level setpoint in AP600 is unknown; in the models it was set to 70% of initial (steaming) mass. Figure 99 shows the steam generator secondary pressure response comparisons. In the AP600 calculation, pressure reached the safety valve setpoint slightly earlier. A pressure decay and subsequent return to the safety valve setpoint occurred during the period of CMT natural circulation cooling.

4.4.2 Three-Tube Rupture. Table 7 presents the sequence of events for the steam generator three-tube rupture case.

The three-tube rupture case showed the same trends and distortions as the one-tube case. The initial response characteristics for pressures, system masses, break flow rates, and CMT responses agreed well, as before. The same timing and magnitude distortions were present in RCS temperature and steam generator pressure responses as in the one-tube rupture case. Again, pressurizer level recovery was noted in AP600 but not in ROSA.

The primary system pressure response comparison is shown in Figure 100. The difference in timing of the ADS systems was due to the coolant loop-to-CMT volume ratio distortion, which caused the loop temperature response more slowly, as with the single-tube rupture case. In both cases, first stage ADS initiation quickly caused a rapid increase in CMT flow rate (because of the increased pressure drop between the top of the CMT and the pressurizer), and a relocation of system inventory into the pressurizer, as shown in Figure 101. This pressurizer level peak occurred at 5,800 seconds in AP600 and between 7,300 and 7,550 seconds in ROSA.

Table 7. Steam generator three-tube rupture.

Event	Time (sec) AP600	ROSA
Initiated three-tube rupture	0	0
Reactor scram, trip reactor coolant pumps and turbine valve (main steam valve closed in ROSA)	44	41
S signal, initiated CMT flow	91	135
Steam generator low level, initiated PRHR	5,335	NA
ADS First stage (initiates PRHR in ROSA)	5,742	7,218
ADS Second stage	5,922	7,556
ADS Third stage	5,998	7,644
ADS Fourth stage	6,145	7,947
Accumulator flow initiated	6,000	7,650
Accumulator flow ends	6,235	7,844

Figure 102 shows that about 70% of the total primary system mass was lost from the primary system after ADS actuation. Fluid was carried upward through the pressurizer, and in AP600, out the ADS blowdown lines into the spargers, and out the top of the IRWST into the containment volume. In both AP600 and ROSA, accumulator injection temporarily shut off CMT flow during its injection period. The injection of subcooled accumulator liquid temporarily reversed the system mass loss. Primary mass increased from ~28,000 to ~68,000 kg in AP600, with the fluid going primarily into the vessel downcomer and core regions; there was a lesser mass increase in ROSA. The effect was not as large in the ROSA calculation, but the trend was similar. There was a second inventory increase in AP600 at ~9,000 seconds (Figure 102) due to IRWST injection, shown in Figure 103. Because ROSA has no IRWST, it did not show a comparable increase.

Minor differences occurred in loop flow response for the two calculations. The ROSA intact loop stagnated between 700 and 2,000 seconds, because of voiding in the associated steam generator tubes, shown in Figure 104. The affected loop also stagnated between 6,100 and 7,000 seconds (Figure 105). This phenomenon did not appear in AP600 in this transient but occured during other scenarios.

4.4.3 Summary

4.4.3.1 Scaling Distortions. The major distortion in the ROSA results was the slower response, owing to the higher friction loss of smaller pipes and the overscaling of coolant mass in the primary loops. System depressurization results were remarkably similar for the two cases, which shows that the break simulation hardware used for ROSA tube ruptures was adequate for simulating AP600 depressurization response. The scaling distortion in the pressurizer produced no identified effect, and the steam generator tube thermal conductance distortion showed little or no impact on the response differences.

4.4.3.2 Modeling Differences. A difference occurred in CMT gravity-driven injection response because of the one-dimensional vessel downcomer model in ROSA. This caused early CMT injection flow in the single-tube scenario. Also, there were differences in the PRHR models, which resulted in different cooldown rates, thus affecting break flow rates and other parameters.

4.4.3.3 Applicability of ROSA for Steam Generator Tube Rupture Experiments. Based on the results of comparisons of the AP600 and ROSA steam generator tube rupture calculations, the following conclusion was reached. With first-level modifications, ROSA is capable of capturing the trends and events expected for the AP600 transient. The main distortions appear to be in the timing of events.

4.5 Main Steam Line Break

In present PWRs, the primary concern with the MSLB transient has been the extent of the cooldown of the primary side associated with the blowdown of the steam generator secondary. The cooldown has been of significance both with respect to pressurized thermal shock of the reactor vessel[p] and return to criticality for plants operating at hot standby conditions. An additional concern in the AP600 system will be the transport of borated water from the CMTs to the core, and the mixing of the borated liquid with the nonborated reactor coolant. The addition of the borated water to the core region is relied upon to maintain the core in a shutdown state.

MSLB calculations were performed for both the AP600 and ROSA facilities, and the results have been analyzed. The objective of this effort was to identify similarities and differences for the two facilities in the cooldown response of the primary system and the behavior of the ECC system (both CMT and PRHR) during the transient. The comparisons presented in this section cover the zero through 3,500-second time period, as this period captures the events of interest given the assumed ROSA facility modifications. The calculations were conducted from hot standby initial conditions. At hot standby, the primary side fluid temperature was maintained by pump heating alone (zero core power is assumed). An MSLB at these conditions will result in a greater cooldown of the primary than would occur if the plant were operating at full power and thus represents a more severe transient.

For the AP600 calculation, the initial conditions included full loop flow, with the primary system fluid temperature at the full power core inlet temperature and the system pressure set at 15.5 MPa. For ROSA, the primary side temperature and pressure were set to match those in AP600, but the initial loop flow was limited to the maximum loop flow obtainable in the ROSA system (roughly 25% of full flow scaled from AP600). For both cases, pressurizer liquid inventory was set at a level that would result in the nominal full power operating level if the system were brought up to full power. Initial secondary fluid temperature matched the primary fluid temperature for both cases, and secondary pressure was at the fluid saturation pressure. Secondary liquid level was assumed to be roughly halfway up the separator volume, which is consistent with the normal operating level for hot standby conditions. Steaming on the secondary was sufficient to remove energy added to the primary by pump heating.

For these calculations, the break was located in the steam line piping of the loop without the pressurizer. The break was simulated with a trip valve, which opened instantaneously to the full area of the steam line pipe. However, as the AP600 steam generators will include flow restrictor nozzles at the outlet of the steam dome, the effective break area for a double-ended offset shear MSLB is that of the flow restrictor nozzle. The flow restrictor nozzles are represented in both the AP600 and ROSA RELAP5 models.

4.5.1 Calculation Results. The AP600 and ROSA MSLB calculations exhibited good agreement in the initial phase of the transient but significant differences in the intermediate and latter parts of the transient. The main differences between the two calculations were in the primary side depressurization response and the factors that control that response. Other aspects of system behavior also exhibited significant variations for the two case, but these variations were more in magnitude rather than type of phenomena being observed. The areas of disagreement

p. Improved vessel shielding and reduced neutron flux in the AP600 system should reduce the likelihood of pressurized thermal shock of the reactor vessel.

occurred primarily as a result of differences in structural heat transfer between the two systems and to a lesser extent as a result of variations in intact steam generator heat transfer response. Structural heat transfer plays a more important role in the MSLB transient because of the lack of core power. The following sections describe the similarities and differences for the two calculations. A general overview of the system response is presented first. This is followed by a comparison of the general heat transfer response for the two systems. This section highlights the relative importance of structural heat transfer to the differences in system depressurization between the two calculations.

4.5.1.1 Main Steam Line Break System Response. The initial part of the MSLB transient was characterized by a rapid cooldown and depressurization of the primary system. The early portion of the primary side cooldown and depressurization were similar for both the ROSA and AP600 calculations. The primary-to-secondary heat transfer associated with the blowdown of the affected steam generator dominated the primary side response during this period. At rupture, liquid in the affected steam generator secondary began to flash, forcing fluid out the break. The break flows for the two cases (Figure 106) exhibited good agreement, with the ROSA flow being slightly lower than AP600 early on and somewhat higher later in the blowdown.[q] The blowdown process results in a large transfer of energy from the primary to the secondary in the affected steam generator. Figure 107, which shows the total primary-to-secondary heat transfer rate in the affected steam generator, indicates the same trend and similar magnitudes for the two cases. The large transfer of energy to the affected secondary caused a rapid cooldown of the primary and a corresponding depressurization as the primary liquid contracts. The primary side cooldown is illustrated in Figure 108, which compares the fluid temperature at the inlet to the vessel on the break leg of the system. The initial cooldown was slightly faster for the AP600 case, and the minimum temperature was about 4 K lower than for the ROSA calculation. Figure 109 compares the primary system pressure for the two calculations. Again, the initial pressure responses are in good agreement.

As the transients progressed beyond the initial depressurization and cooldown phase, differences in the primary system response began to develop. This is evident in the primary pressures (Figure 109), which diverge after about 200 seconds. In the ROSA calculation, the primary pressure dropped to the intact side steam generator secondary pressure (Figure 110) and remained at the secondary pressure for the duration of the calculation. In the AP600 calculation, the primary side pressure (Figure 111) dropped well below the pressure of the intact secondary early in the transient and then continued to decrease as the transient progressed. Several factors affected the primary pressure response, including energy removal (or addition) from (or to) the primary in the steam generators, energy removal from the primary due to the CMT and PRHR flows, and energy addition to the primary due to system structure heat transfer. However, as shown in Section 4.5.1.2, the difference in heat transfer from system structures was the primary contributor to the different pressure response for the two cases. Piping heat transfer to the primary fluid was two to three times greater in ROSA than in AP600.[r] In the ROSA calculation, heat transfer to the primary fluid from system structures counteracted the cooling effect of the CMT and PRHR flows. This reduced the rate at which the primary

q. Differences in break flow were attributable to modeling differences for the two systems. The ROSA steam line break was modeled as blowing down directly to atmosphere (constant back pressure). The AP600 steam line break was modeled as blowing down into containment (back pressure increasing with time). Also, length of piping downstream of the flow restrictor nozzle was different for ROSA and AP600.

r. Core power was assumed to be zero for the main steam line break transient. Structure (piping, vessel, etc.) heat transfer is much more influential for this transient, because it represents a significant portion of the total heat transfer occurring in the primary system. In transients with core power, structure heat transfer represents a much smaller contribution to total system heat transfer, and its effects are much less noticeable.

fluid was cooled, and the pressure tended to hang on the intact secondary pressure. In the AP600 calculation, piping heat transfer was less able to maintain the primary fluid temperature, and the CMT and PRHR flows allowed the primary to gradually cool down and depressurize.

Other differences in the two calculations occur primarily in the heat transfer and voiding response of the steam generator on the intact side of the system. In both cases, the intact steam generator became a heat source early in the transient (at about 90 seconds in the AP600 calculation and 200 seconds in the ROSA calculation) and continued as a heat source until about 450 seconds in ROSA and 550 seconds in AP600. This is illustrated in Figure 112, which compares the intact steam generator total heat transfer rate for the two cases. The secondary-to-primary heat transfer led to boiling in the U-tubes once fluid became saturated. Figure 113 shows the net vapor generation in the intact steam generator for the two cases. The higher secondary-to-primary heat transfer in the AP600 calculation after roughly 200 seconds (Figure 112) resulted in significantly more vapor generation. The vapor being generated forced liquid out of the U-tubes. This is indicated in Figures 114 and 115, which show the steam generator upflow and downflow side collapsed liquid levels for the AP600 and ROSA cases.[s] Due to the higher vapor generation rate in the AP600 calculation, roughly 85% of the U-tube inventory was forced out. This compares to only about a 20% inventory depletion in the ROSA intact steam generator. Note that while steam was being generated in the intact steam generator, other parts of the system (with the exception of the pressurizer and surge line) were liquid solid for both calculations. The volume of liquid forced from the steam generator U-tubes was accommodated by a surge of liquid into the surge line and pressurizer. Figure 116 compares the combined pressurizer/surge line collapsed level for the two cases, and Figure 117 compares the pressurizer total liquid volume. Notice that the combined pressurizer/surge line levels recovered to about the same value in both calculations. However, this level in the AP600 system represented a significant volume of liquid being stored in the pressurizer. The same level in the ROSA system was below the inlet of the pressurizer. The volume of the surge line in the ROSA calculation was sufficient to accommodate the much smaller volume of fluid being forced from the intact steam generator.

The response of the passive safety features for the two calculations was generally in good agreement. In both calculations, CMT flow was initiated immediately after rupture on a low steam line pressure signal, and PRHR flow began within the first minute on a low secondary level signal. Figures 118 and 119 compare the CMT flows and PRHR flows, respectively, for the two calculations. CMT flows exhibited the same trends for both cases but as discussed in previous sections, the flow rate was somewhat lower throughout the transient for the ROSA calculation. The PRHR flow in the AP600 calculation increased to a much higher value than for ROSA initially but agreed very well with the ROSA values in the later part of the transient.[t] While there was continuing flow through the CMT in this transient, primary side mass inventory was not lost, and the CMTs remained full. Thus, the ADS valves were not activated during the transient. However,

s. The break side steam generator U-tubes remained liquid solid throughout the transient for both calculations. Blowdown of the secondaries was over by about 600 seconds in each case, and primary-to-secondary heat transfer was effectively zero after this point.

t. The difference in initial PRHR response was likely a result of the manner in which the PRHR heat exchangers were represented in the two models. For the AP600 calculation, the heat exchanger secondary was modeled explicitly. Because the fluid entering the heat exchanger initially was hot, the primary to secondary heat transfer rate was high (subcooled nucleate boiling). The result was a large change in the primary side fluid density, which supported relatively large PRHR flow. In the ROSA calculation, the PRHR heat exchanger secondary was modeled as a boundary condition with a constant heat transfer coefficient representative of an average long-term value for the AP600 calculation. Initial cooling of the fluid was much less, and initial PRHR flow was correspondingly lower than in the AP600 calculation.

because of the decreasing pressure in the AP600 calculation, small, intermittent accumulator flow occurred in the latter part of the transient. This is shown in Figure 120, which compares the accumulator flow rates for the two calculations. The primary pressure remained above the accumulator pressure throughout the ROSA calculation.

4.5.1.2 System Heat Transfer Response for the MSLB. Because the primary remains intact for the MSLB transient, pressure is controlled solely by energy addition to or subtraction from the primary fluid. Energy can be added to the primary fluid by heat transfer from metal structures or by heat transfer from the intact side steam generator secondary, which becomes a heat source early in the transient. Energy is subtracted from the primary through heat transfer to the secondary of the break side steam generator, or by replacement of hot primary fluid with cold CMT or PRHR fluid. The relative magnitude of each of the various heat transfer contributors determines its impact on the pressure response.

Figures 121 through 124 compare the AP600 and ROSA structure heat transfer for the intact and broken loops (excluding the steam generators), the vessel (excluding the core), and the core itself. Figures 125 and 126 compare energy removal through the CMT and PRHR systems. Finally, Figures 107 and 112 show the energy removal or addition through the break side and intact side steam generators. Several points are of interest in these figures. First, structural heat transfer from the loop piping and vessel in the ROSA calculations was as much as two to three times higher than in AP600 and remained consistently higher throughout the calculation. Second, heat removal through the CMT system was in excellent agreement for the two calculations, and except for differences initially, heat removal through the PRHR agreed reasonably well. Third, energy removal through the break side steam generator was in reasonably good agreement for the two cases, with the magnitude in ROSA alternating between being somewhat lower and somewhat higher than in AP600. Fourth, while there were differences in magnitude and direction of heat transfer in the intact steam generator, they occurred early in the transient when the break side steam generator heat transfer far exceeded that of the intact side steam generator.

The likely impact on system pressure of the various heat transfer contributors is put into perspective in Figures 127 and 128. These figures compare all contributions to the primary heat transfer for both calculations. Figure 127 covers the time period of zero to 600 seconds, while Figure 128 covers the period of 500 to 3,500 seconds. All structural heat transfer is combined into a single curve, as is the CMT and PRHR heat removal. Individual curves are maintained for the intact and break side steam generator heat transfer. Recall from above (see Figure 109) that the primary pressures for the two calculations agreed well until about 200 seconds, and after this point the AP600 pressure dropped well below that in ROSA. An evaluation of Figures 127 and 128 indicates that the major difference in heat transfer contributions for the two calculations occurred in the structural heat transfer. While the break side steam generator was the major contributor to heat transfer until about 350 seconds, variations in this parameter were considerably less than those in the structural heat transfer. Also, there was little variation in intact side steam generator heat transfer or in heat removal through the CMT/PRHR after 200 seconds. Therefore, it is evident that the major contributor to the difference in primary pressure response was the difference in structural heat transfer. The higher structural heat transfer in ROSA was the prime contributor to maintaining the higher primary pressure in that calculation.

4.5.2 Applicability of ROSA LSTF for MSLB Experiments. The following conclusions are based on the evaluation of the modified (first level) ROSA and AP600 MSLB calculations. First, the blowdown of the steam generator secondary and corresponding cooldown and early depressurization of the primary system should be reasonably well represented in the ROSA facility. This phase of the MSLB accident is dominated by the large primary-to-secondary heat transfer rate in the affected steam generator, which will likely overshadow the effects of other distortions in the system. Also, the CMT and PRHR flow response should be representative of their counterparts in

the AP600 system. Differences in the CMT and PRHR flow response in the AP600 and ROSA MSLB calculations can be minimized by making the pipe friction losses as similar as possible to those of the AP600 CMT and PRHR piping. Also, a more realistic boundary condition should be specified for the PRHR heat exchanger.

Second, the differences in the intermediate and late primary side pressure response between the ROSA and AP600 MSLB calculations are consistent with the distortions in structure heat transfer inherent to full-height, scaled flow area facilities, such as ROSA. Metal volume to fluid volume ratios in the piping and components in ROSA will be larger than in a full size plant. Metal structures thus will represent a greater heat source in ROSA. This will have more of an influence on primary side response in the MSLB because of the lack of core power for this transient. The greater structure heat transfer in ROSA will likely result in significant differences in the primary pressure response relative to the expected AP600 system response. However, trends, if not magnitude, of other aspects of the primary side behavior should be represented in the ROSA facility.

5. RESULTS OF CALCULATIONS WITH LEVEL IV MODIFICATIONS

The calculation effort described in Section 4 was directed primarily toward evaluating the impact of Level I modifications and identifying aspects of the ROSA system response that were significantly different from the response expected in the AP600 system. Based on this effort, possible changes in ROSA configuration or component design were identified. Several ROSA sensitivity calculations were performed in order to evaluate some of these changes. For these calculations, individual components were modified to better represent an appropriately scaled AP600 component or the configuration used in the AP600 system. The analyses of the calculation results indicated that some of these changes to the ROSA system would improve the comparison with the AP600 plant.

As a followup to the initial effort, several additional ROSA calculations were performed with a model that included the most important modifications suggested by the analyses (Section 4) and by discussions with JAERI and Westinghouse. This fourth level of modifications included the Level I modifications described in Section 2, with the following additions:

1. A full-height pressurizer scaled directly from the AP600 pressurizer; the surge line configuration and connection to the hot leg were made the same as in the AP600 model
2. A modified upper head that included scaled, upper-head cooling spray flow area and an area-scaled drain path between the bottom of the inverted top hat region and the upper plenum
3. PBLs and ECC injection line with modified loss coefficients to offset the pipe wall friction distortion introduced by volume scaling these lines
4. Accumulator liquid and nitrogen volumes scaled to the AP600 accumulators; the assumption here is that a standpipe can be used in the ROSA accumulator to provide the correct total liquid/nitrogen volume
5. A scaled IRWST
6. A quasi-two-dimensional nodalization of the reactor vessel downcomer.

Initially, the impact of the scaled IRWST was not investigated. It was included in this level of modifications because it allowed a useful extension of the calculation into the low pressure portion of the transient. Inclusion of an IRWST in the actual ROSA would provide an overlap of test results with those expected from AP600 low-pressure test facility simulations. The two-dimensional nodalization of the downcomer was included at this point to offer a more direct comparison between the two models.

The ROSA calculations performed with the Level IV modifications included a 3-in. CLB case, a 1-in. CLB case, and a 3-in. PBL break case. These particular cases were selected because they should best spotlight the impact of the modifications made to the input model. The results of these calculations are compared in the following sections with the associated AP600 and original ROSA Level I calculations. The purpose of this effort is to highlight the improvements in response achieved by incorporating the Level IV modifications as well as to identify any differences that may still exist.

5.1 Three-Inch Cold Leg Break

The ROSA 3-in. CLB calculation was rerun with the Level IV modifications described above. Table 8 compares the event timing for the two ROSA calculations and the AP600 calculation. The results of the calculation show a general improvement in timing of events relative to the base case. Initiation of draining of the CMTs began at about the same time in the "all mods" case as in the AP600 case. First-stage ADS and accumulator flow began about 45 to 55 seconds later in the all mods case than in AP600, but these times were still earlier than in the base case. Actuation of Stages 2 and 3 ADS in the all mods case both occurred somewhat earlier than in the AP600 or ROSA base cases, but the 450-second delay (relative to the AP600 case) in actuation of Stage 4 ADS in the bases case was not observed in the all mods case. Emptying of the CMTs occurred at about the same time in the all mods and AP600 cases; again, an improvement over the delay in draining was observed in the ROSA base case.

Table 8. Comparison of event timing for AP600 and modified ROSA 3-in. CLB RELAP5 calculations.

Event	Time (sec) AP600	ROSA (base case)	ROSA (all mods)
Break	0	0	0
Scram	14	15	15
PBL/CMT circulation began	15	15	15
CMT draining began	372	390	375
First stage ADS	576	640	620
PRHR flow began	576	640	620
Accumulator flow began	582	674	635
Second stage ADS	1,137	1,114	1,050
Third stage ADS	1,281	1,286	1,185
Fourth stage ADS	1,644	2,096	1,540
CMTs empty	1,950	2,450	1,965
IRWST flow began	2,478	NA	3,025

A comparison of other system parameters also indicated improvements with the Level IV modifications. These improvements are described here. The system pressure response for the three cases is shown in Figure 129. During the time period after about 400 seconds, the depressurization of the all mods case occurred somewhat earlier and at a faster rate than in the base case and was more comparable to the depressurization of the AP600 case. The improvement in pressure response was likely due to the improved upper head flow path modelling in the all mods case. The more open upper head-to-downcomer/cold leg region flow path enhanced the net flow of steam from the upper plenum region to the break.

The main factor in the improved response of the passive safety features in the all mods case was the reduction of the PBL and ECC line loss coefficients. This change resulted in a higher total ECC flow rate than in the base case, which again compared more favorably with the AP600 case. Figure 130 shows the total ECC flow rate (combined CMT and accumulator flow) for the three cases. Notice that the magnitude of the ECC flow in the all mods case agreed very well with that in AP600. Additionally, the all mods case did not exhibit the flow cessation that was observed in the base case (between about 1,650 and 1,900 seconds). As a result, the all mods case exhibited a continuous depletion of CMT liquid following second stage ADS actuation. Figure 131 compares the CMT liquid level for the three cases. While the level decreased slightly earlier overall in the all mods case than in AP600, the rate of decrease after Stage 2 ADS actuation was essentially the same.

The ADS response for both the base and all mods cases agreed very well with the AP600 calculation until after actuation of third stage ADS. Figure 132 compares the total integrated ADS flow rate for the three cases. After Stage 3 ADS actuation, the base case exhibited considerably lower total mass loss through the ADS than in AP600. However, the all mods case showed marked improvement over the base case. Total mass loss from the system through ADS for this case increased faster after Stage 3 ADS than in

the base case and was in better agreement with the AP600 case.

Because of the higher total ADS mass loss in the all mods case (relative to the base case), the vessel and system mass inventory response in the later portion of the transient were in better agreement with the same parameters for AP600. Figures 133 and 134 show the vessel and system normalized mass inventory, respectively, for the three calculations. Both figures show a more significant decrease in inventory in the later part of the transient for the all mods and AP600 cases than in the base case. Notice that in addition to the effect of the lower ADS flow in the base case, the higher inventories were, at least in part, due to the delayed CMT draining, which provided fluid to the system later in the transient.

To summarize, the ROSA 3-in. CLB calculation with Level IV modifications showed improvement in the timing of events as well as in the trends of system parameters relative to the base case. The system depressurization and response of the passive safety features all showed better agreement with the AP600 calculated behavior than did the ROSA base case.

5.2 One-Inch Cold Leg Break

As with the 3-in. CLB calculation described in Section 5.1, a 1-in. CLB calculation was also performed with the Level IV modifications. Table 9 compares the calculated sequence of events for the 1-in. all mods and base (Level I) cases, along with that for the AP600 case. The results presented in the table show very little overall difference in the event timing between the Levels I and IV cases. However, some aspects of the system response of the all mods case exhibited significant improvement relative to the base case. For example, the oscillatory behavior of primary pressure seen in the AP600 calculation was also seen in the ROSA all mods case. The improvements in the all mods case are described below.

As shown in Table 9, scram occurred considerably earlier in the all mods case than in the base case and was in better agreement with the AP600 calculation. The difference in timing for the two ROSA cases was due to small differences in the initial pressure response. Figure 135 compares the early system pressure for the three cases and indicates the time of scram for each case as well as the time of the S signal, which results in the initiation of PBL flow and CMT circulation.

As indicated above, an oscillatory type pressure response similar to that in the AP600 1-in. calculation occurred in the ROSA all mods case. Figure 135 compares the system pressure response for the three cases. As shown in the figure, the Level IV modifications had negligible effect on the overall ROSA transient characteristics. However, comparison of the pressure response in the time period between roughly 400 and 2,500 seconds (the expanded region in the figure) indicates pressure oscillation in the all mods case similar to those in AP600. The appearance of the oscillation phenomena in the ROSA all mods case was attributed to the modifications of the upper head flow path configuration and its effect on the upper head initial conditions.

Reduction of the PBL/ECC line loss coefficients in the all mods case resulted in an increased flow in the injection line during the period of CMT circulation, which was in excellent agreement with the AP600 calculation. This is shown in Figure 137, which compares the CMT flow for the three cases. Figure 138 compares the CMT level response. The effect of the Level IV modifications on the level response was limited to slight timing differences. CMT draining started slightly earlier in the all mods case (3,300 versus 3,600 seconds), but the timing for ADS actuation was nearly identical.

Table 9. Comparison of event timing for AP600 and modified ROSA 1-in. cold leg break RELAP5 calculations.

Event	Time (sec) AP600	ROSA (base case)	ROSA (all mods)
Break	0	0	0
Scram	90	140	79
PRL/CMT circulation began	186	214	162
CMT draining began	2,520	3,550	3,300
First stage ADS	3,357	4,326	4,285
Second stage ADS	3,516	4,520	4,460
Accumulator flow began	3,567	4,558	4,545
Third stage ADS	3,600	4,608	4,544
Fourth stage ADS	3,813	4,862	4,824
CMTs empty	4,200	5,200	5,200
IRWST flow began	4,600	NA	6,000

The pressurizer collapsed liquid level response was also improved in the all mods case, as shown in Figure 139. The all mods case exhibited a pressurizer level recovery after about 500 seconds but to a lesser extent than occurred in the AP600 calculation. The ROSA base case exhibited no pressurizer level recovery until quite late in the transient. Figure 140, which compares the combined pressurizer and surge line collapsed liquid level for the three cases, again indicates good agreement between the all mods case and the AP600 calculation, at least during the early part of the transient. Both calculations indicated an immediate level loss at rupture, followed by a level recovery to ~10 m (~33 ft). This again compares to a considerably delayed recovery of the pressurizer/surge line level in the ROSA base case. Between ~1,300 and 1,750 seconds, the level in the all mods case oscillated in response to the system pressure oscillation, which was similar to the behavior in the AP600 calculation. Notice that between ~1,750 and 3,300 seconds, when CMT draining began, the pressurizer level in the all mods case gradually decreased to about 10%. This was about the same as the level in the base case at the time of CMT draining and compared to a level of about 40% in the AP600 case at the equivalent time.

The difference in pressurizer inventory response for the all mods case (as well as the base case) and the AP600 case indicates that differences existed in the mass inventory of the remainder of the system. Figures 141 and 142 show the response of the normalized vessel and system mass inventories, respectively, for the three cases. The normalized vessel mass in the all mods case exhibited better agreement with AP600 than did the base case. This improvement is attributed to the Level IV upper head modifications, which allowed a more representative upper head flow response than occurred with the base case model. On the other hand, the normalized system mass in the all mods case showed no discernable improvement. At the time of ADS actuation, it was at about 40%, the same as in the base case, and compares to 50% in the AP600 case. The differences in system mass between the two ROSA cases and the AP600 case indicate that remaining loop distortion (such as cold leg elevation relative to the CMT) continued to influence the resulting system response. In particular, both the base and

all mods cases exhibited considerable delay in the initiation of draining of the CMTs and actuation of the various ADS stages relative to the AP600 case. The ROSA cold leg elevation was lower (relative to that of the CMT) than in AP600; therefore, this was the probable reason for the CMT draining delay although not specifically investigated in detail.

To summarize, the ROSA 1-in. CLB calculation with Level IV modifications showed little difference in the timing of events relative to the base case calculation. However, other aspects of the all mods system response showed improvement related to the changes made with the Level IV modifications. ECC flow response was in excellent agreement with the AP600 case because of the modifications to the PBL/ECC line loss coefficients, and the level response of the scaled pressurizer was also improved. Likewise, vessel mass inventory fell into excellent agreement with that in AP600 as a result of the improved upper head flow path modeling.

5.3 Three-Inch Pressure Balance Line Break

The ROSA PBL break calculation was repeated with all of the fourth level modifications implemented in the deck. Other modifications to the deck were necessary to simulate this transient more accurately. These included

1. Separate modeling of the two ECC trains (instead of lumping them into one)

2. Connection of each cold leg-to-CMT PBL to a cold leg in a separate loop (rather than connecting each to a branch of a *split* cold leg in one loop)

3. Reduction of the form loss coefficients in the ECCS lines (PBLs, PSIS lines, and accumulator surge lines) to zero because the total line resistance in the ROSA model was much higher than in the AP600 model.

The purpose of this calculation was to demonstrate the effects of including all of the recommended modifications and to identify any more sensitivities (of modeling or design) that need to be investigated when more current AP600 design data is available. The results of this calculation are compared with the AP600 and ROSA base cases in the following sections.

5.3.1 Comparison to AP600 and ROSA Base Case Results. The overall impact of the fourth level modifications was evident in the improved timing of events indicated in the sequence of events (Table 10) and in the pressurizer pressure response (Figure 143).[u] In the base case calculation, all of the major events lagged those of AP600, particularly the timing of ADS actuation. The improvement was primarily due to separate modeling of each CMT, which resulted in better prediction of the timing of the onset of CMT draining, and also the CMT draining response (Figure 144). The better prediction of CMT draining in turn improved the timing of ADS actuation.

Besides the timing of events, several important transient parameters were also greatly improved by the modifications. These include the following (which will be discussed in the remainder of this section):

1. Core collapsed liquid level (and, consequently, cladding temperature)

2. ECC mass flow rate (including IRWST flow)

3. Reactor vessel mass inventory.

---

u. Note that both the AP600 calculation and the ROSA calculation with all modifications were run to 4,000 seconds to reach the time when IRWST injection begins. The ROSA base case calculation was only run to 3,200 seconds because it did not include the IRWST.

Table 10. Comparison of event timing for AP600 and modified ROSA-LSTF 3-in. PBL break RELAP5 calculations.

Event	Time (sec) AP600	ROSA (base case)	ROSA (all mods)
Break opened	0	0	0
Scram signal	11	12	10
Steam generator isolation	11	12	10
Pump trip	11	12	10
Safety signal	19	21	20
First stage ADS	695	904	810
Second stage ADS	1,190	1,696	1,166
Third stage ADS	1,335	1,890	1,388
Fourth stage ADS	1,720	2,376	1,784
Accumulator injection	745–1,060	920–1,130	866–1,290
IRWST injection begins	3,400	NA	3,800

5.3.2 Core Collapsed Liquid Level. In the base case calculation, a core heatup was predicted that did not occur in the AP600 calculation. This was due to a much lower prediction of core collapsed liquid level than in AP600. The calculation of core collapsed liquid level was improved in the current calculation (Figure 145). Unlike the base case model, the fully modified ROSA model had a correctly scaled flow path between the downcomer and upper head and a flow path between the upper plenum and the upper head (as the AP600 design does). These flow paths to the upper head, particularly the correctly scaled one from the downcomer, resulted in more equalization of pressure between the upper plenum and the upper downcomer, and a lesser core level depression than in the base case. Since there was minimal vapor flow from the upper plenum to the downcomer via the upper head in the base case calculation, the pressure buildup in the core tended to depress the core level far below that predicted in the AP600 calculation.

5.3.3 ECC Mass Flow Rate. The timing and magnitude of CMT and accumulator injection were closer to that of AP600 in the current calculation (Figure 146). During the first 700 seconds, because there was only one CMT modeled in the base case, the ECC flow rate (due only to CMT flow) varied off and on. Separate modeling of each CMT and a reduction in the PBL and PSIS line loss coefficients resulted in ECC flow closer to that of AP600. Also, separate modeling of the CMTs resulted in better agreement with AP600 in the period between 2,000 and 2,700 seconds.

However, the ECC flow rate was different in the latter portion of the transient (beyond 3,000 seconds) because IRWST injection was calculated in the modified ROSA case to occur later and to have a smaller magnitude than in AP600. This occurred for two reasons.

First, the boundary pressure of the IRWST (the pressure at the top) was fixed at atmospheric pressure in the ROSA calculation. In the AP600 calculation, the IRWST was connected to the containment, which was allowed to pressurize. Thus, the driving force in the ROSA calculation was about 15 psi less than in AP600. The IRWST

was modeled this way in ROSA because nothing was known about how the pressure in the simulated IRWST was going to be controlled. In the ROSA facility, the best way to avoid this problem was to control the pressure in the simulated IRWST to the same pressure as in the simulated containment (or sump).

Second, and of lesser importance, the piping friction losses in ROSA were much higher than in AP600. Since the form loss coefficients were zero in AP600, they could not be reduced in the ROSA model to compensate for excessive wall friction. This resulted in a more resistant flow path from the IRWST into the PSIS lines, which can affect the timing and magnitude of IRWST injection.

5.3.4 Reactor Vessel Mass Inventory. The agreement with AP600 reactor vessel mass inventory (Figure 147) was improved, mainly as a consequence of better prediction of the timing of ADS actuation. Particularly after 1,000 seconds, the improved timing of second, third, and fourth stage ADS actuation gave much closer agreement in trend and magnitude. However, in the final phase of the transient the delay in IRWST injection in the modified ROSA calculation also delayed the slight recovery in mass inventory seen in the AP600 calculation when the IRWST began to inject.

5.3.5 Sensitivities in the Calculation. There were two main sensitivities connected with this calculation. The first is the IRWST boundary pressure (discussed in the previous section). The timing and magnitude of IRWST injection were greatly affected by the boundary pressure on the IRWST. A suggestion was given to minimize this problem in the test facility.

The second is the modeling of the upper head flow paths. The modeling of the upper head flow paths (particularly the one to the downcomer) was discovered to affect the draining characteristics of the unaffected CMT (Figure 144). In the modified ROSA calculation, the draining of the unaffected CMT was not interrupted when the accumulators injected. Thus, the CMT level did not show the same plateau in the period of accumulator injection as AP600 did. This is an area that should be investigated in future AP600 and ROSA calculations when better AP600 design data is available (so that more about the physical characteristics of the AP600 upper head flow paths is known).

5.3.6 Summary and Conclusions. As expected, the agreement with AP600 was greatly improved when the fourth level of modifications was added to the ROSA input deck. The two changes that had the most effect on the results were the separate modeling of the two ECC trains and the modeling of the flow paths to the upper head. The most improved key parameters were the timing of events, the cladding temperature, and the reactor vessel mass inventory. However, two areas were identified that will require further investigation: what the boundary pressure in the IRWST will be (and how it will be controlled) and how to appropriately model the upper head flow paths.

6. SUMMARY, CONCLUSIONS, AND RECOMMENDATIONS

The analyses presented in earlier sections each included specific conclusions. This section summarizes the general observations made throughout the study.

Throughout the first part of this effort, the following observations were made:

- With the minimum, first-level, of modifications (CMT, PBL, ADS Stages 1 through 4, PRHR, and reduced loop seals), ROSA was able to represent reasonably well the early part of most transients (until about the third stage ADS). As time evolved, or for relatively slow transients (1-in. CLB or one steam generator tube rupture), a number of distortions combined to cause the ROSA behavior to diverge from that of AP600. The difference in the coolant flow path in the upper head was identified as a major contributor to the distortions. A relatively minor, but additional, modification of the ROSA upper head was identified that should improve the fidelity of ROSA simulation.

- It was determined that the nontypical pressurizer of ROSA, its elevation and its surge line connection contributed to some of the differences observed. In particular, the mass distribution of the two systems differed because of the different elevation and shape of these two components. Thus, a second level modification was recommended in which a new pressurizer with the correct elevation and surge line connection is used in ROSA to improve its approximation to AP600.

- Because of its single cold leg per loop and thus single CMT configuration, ROSA with first level modifications could not represent nonsymmetric features of AP600 response. This was observed in the FBL break (Section 4.3) and to a much lesser degree in the other small break loss-of-coolant accident scenarios. An attempt was made to evaluate yet a third level of ROSA modifications, which would include two CMTs and their PBL connections to the two parts of a split cold leg. The results of this evaluation (the appendix) indicate that the system's complexity requires more changes than the ones proposed. The fact that the two CMTs would still share the same vessel penetration introduces additional distortion and makes the simulation differ from AP600. Such modification is thus not recommended.

- Distortions due to scaling (smaller pipes and larger metal mass/volume ratio) are partially responsible for timing differences (more pipe friction, slower flows) and the lesser loss of mass in ROSA than in AP600. Such distortions are not particular to ROSA and would be expected of any scaled facility.

In summary, for the first part of the analysis, ROSA, with the minimal modifications listed earlier as the first level set of changes, can capture most of the behavior and phenomena of AP600, for relatively fast transients, and the data from experiments in ROSA can be used for code assessment. However, ROSA with minimal modifications cannot be expected to capture all phenomena occurring in AP600 nor all features of transient accident sequences, and care should be taken while selecting and analyzing any experiment.

In the second part of this effort, a set of selected scenarios were simulated, using the recommended additional modifications to the ROSA base case. These modifications resulted from the analyses and from discussions with Westinghouse and JAERI. The purpose of the second part of the effort was mainly to verify that the recommended changes indeed improved the simulation and no additional distortions were uncovered or enhanced.

As expected, the agreement with AP600 calculations was greatly improved. The two additional modifications (to the base case or Level I) that appeared to have the most impact were the modeling of two separate ECC trains and the adjustment of the upper head flow paths. Addition of an IRWST allowed the simulation to be carried further, beyond the opening of the fourth stage of ADS.

7. REFERENCES

1 Y. Kukita, Y. Anoda, and K. Tasaka, "Summary of ROSA-IV LSTF First-Phase Test Program—Integral Simulation of PWR Small Break LOCAs and Transients," *Nuclear Engineering and Design, 131*, 1991, pp. 101-111.

2 The ROSA-IV Group, *ROSA-IV Large Scale Test Facility (LSTF) System Description*, JAERI-M 84-237, Japan Atomic Energy Research Institute, January 1989.

3 R. J. Beelman and S. M. Sloan, "Modeling AP600 with RELAP5," *1991 ANS International Topical Meeting on the Safety of Thermal Reactors, Portland, Oregon, July 21–25, 1991.*

4 Westinghouse Electric Corporation, *AP600 Design Parameter List*, NSE-90-0206, Rev. 1/GIN G1D 001, Rev. 1, September 4, 1990.

5 Westinghouse Electric Corporation, *AP600 Plant Description Document*, DE-AC03-86SF16038, January 1989.

6 Westinghouse Electric Corporation, *AP600 Plant Description Document*, DE-AC03-90SF18495, December 1990.

7 N. Zuber, *Problems in Modeling Small Break LOCA*, NUREG-0724, USNRC, 1990.

8 S. M. Modro, T. J. Boucher, V. T. Berta, G. E. McCreery, R. R. Schultz, D. C. Mecham, and S. A. Naff, *Evaluation of Scaled Integral Test Facility Concepts for The AP600*, EGG-NE-10239, May 1992.

Main Text Figures

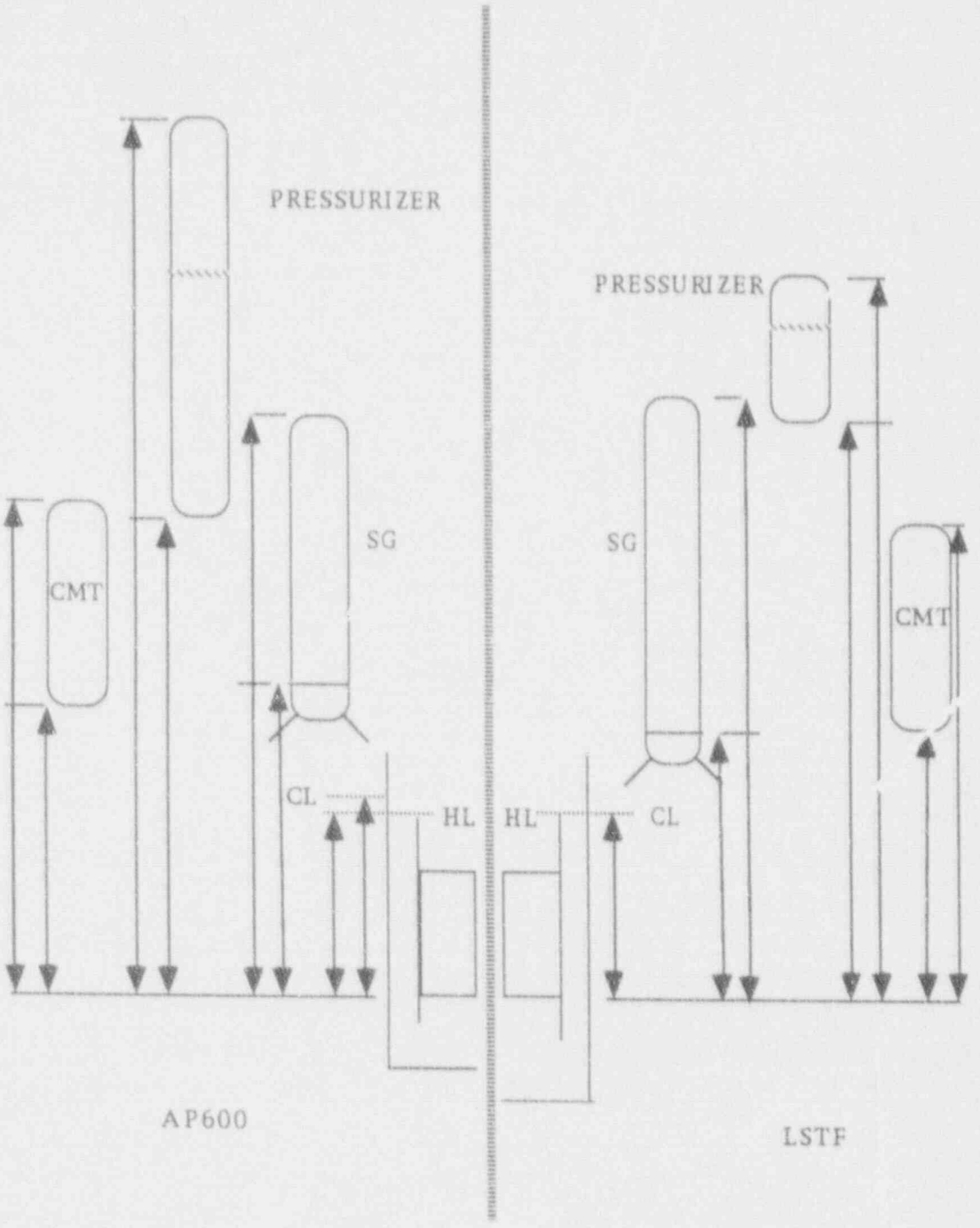

Figure 1. Schematic comparison of system elevations for AP600 and ROSA LSTF.

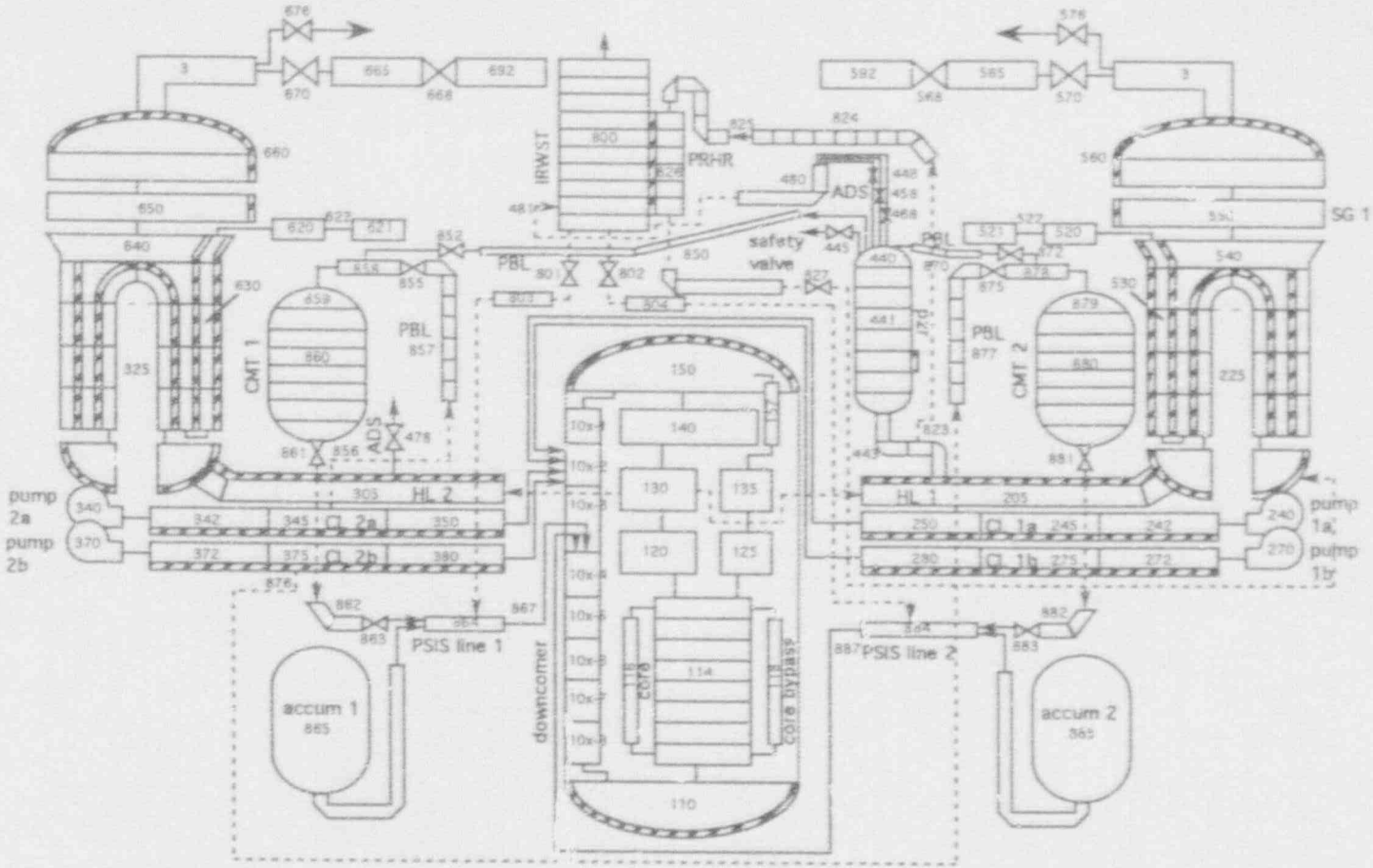

Figure 2. RELAP5 nodalization scheme for AP600.

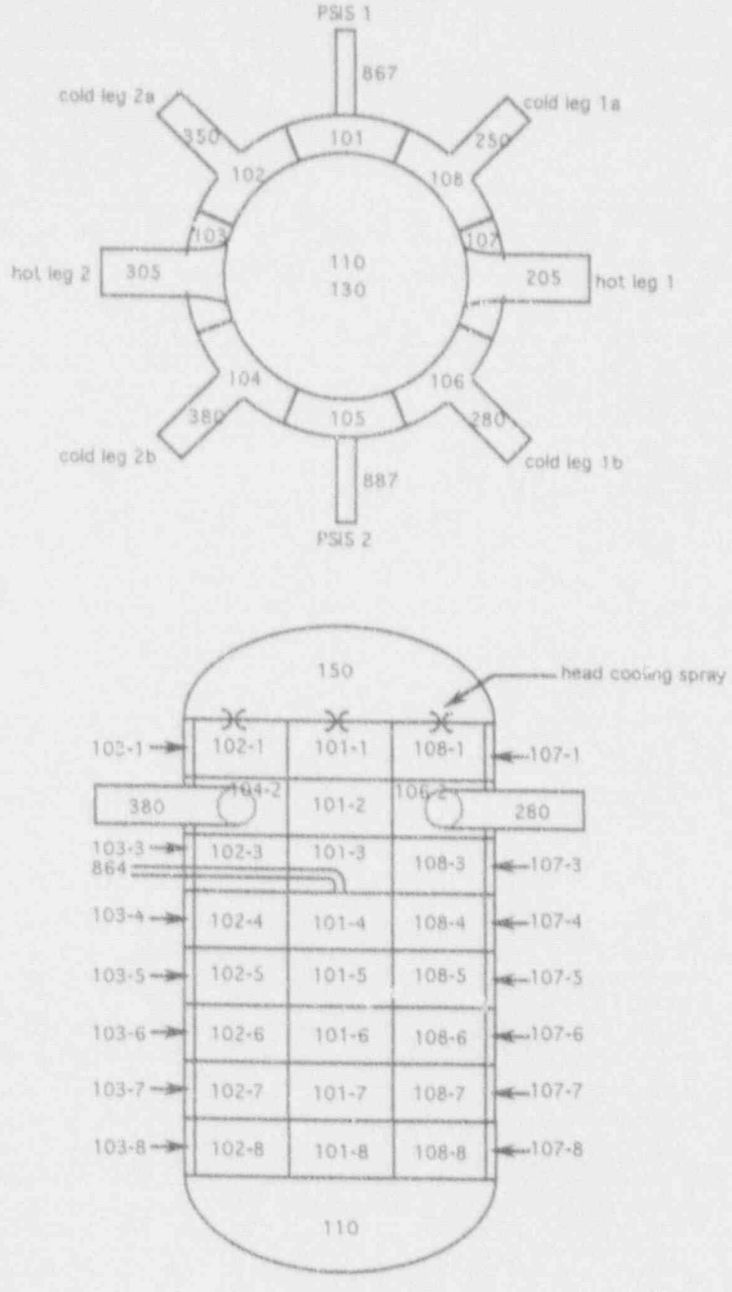

Figure 3. AP600 downcomer nodalization.

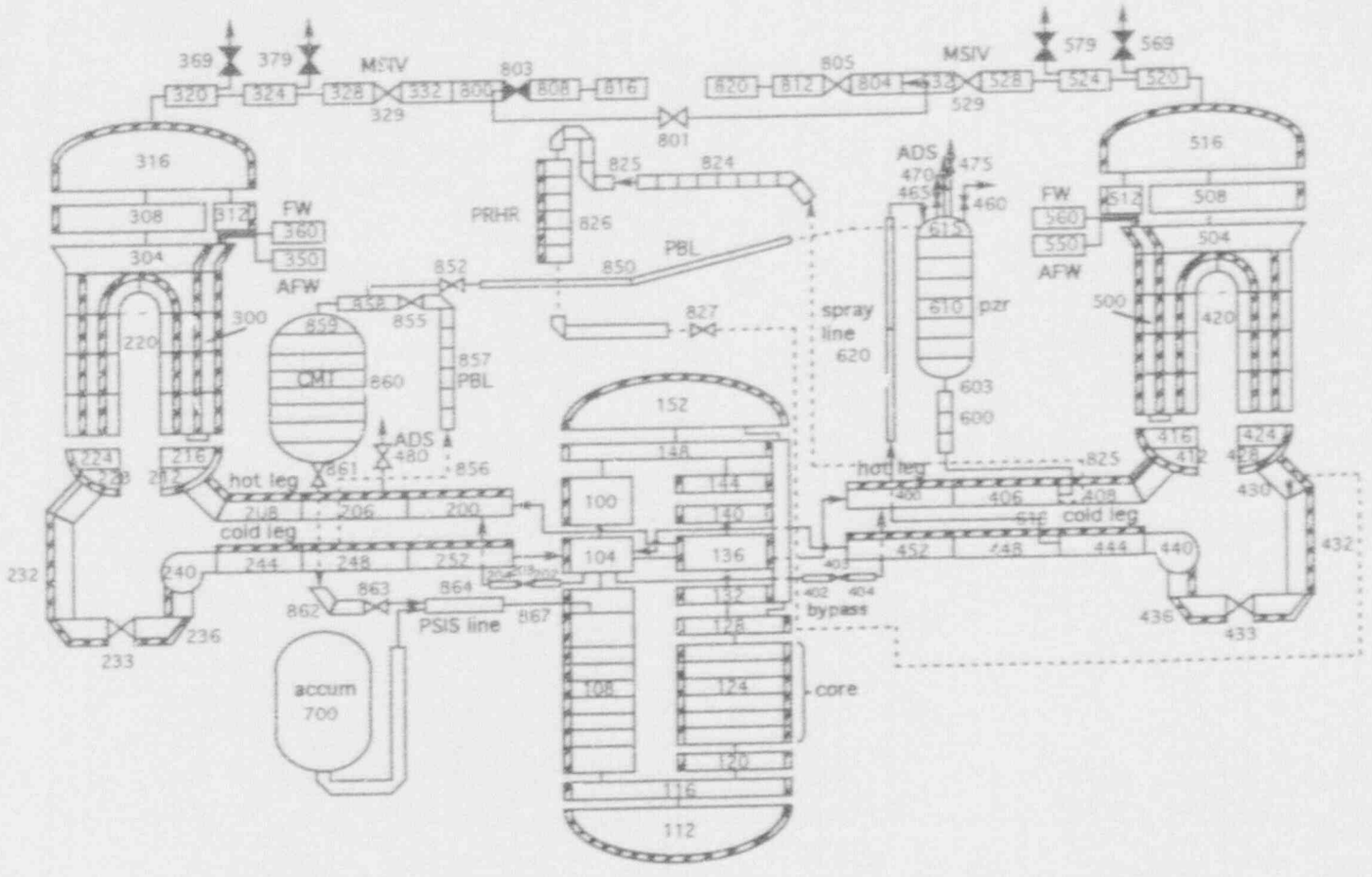

Figure 4. Modified RELAP5 nodalization scheme for ROSA.

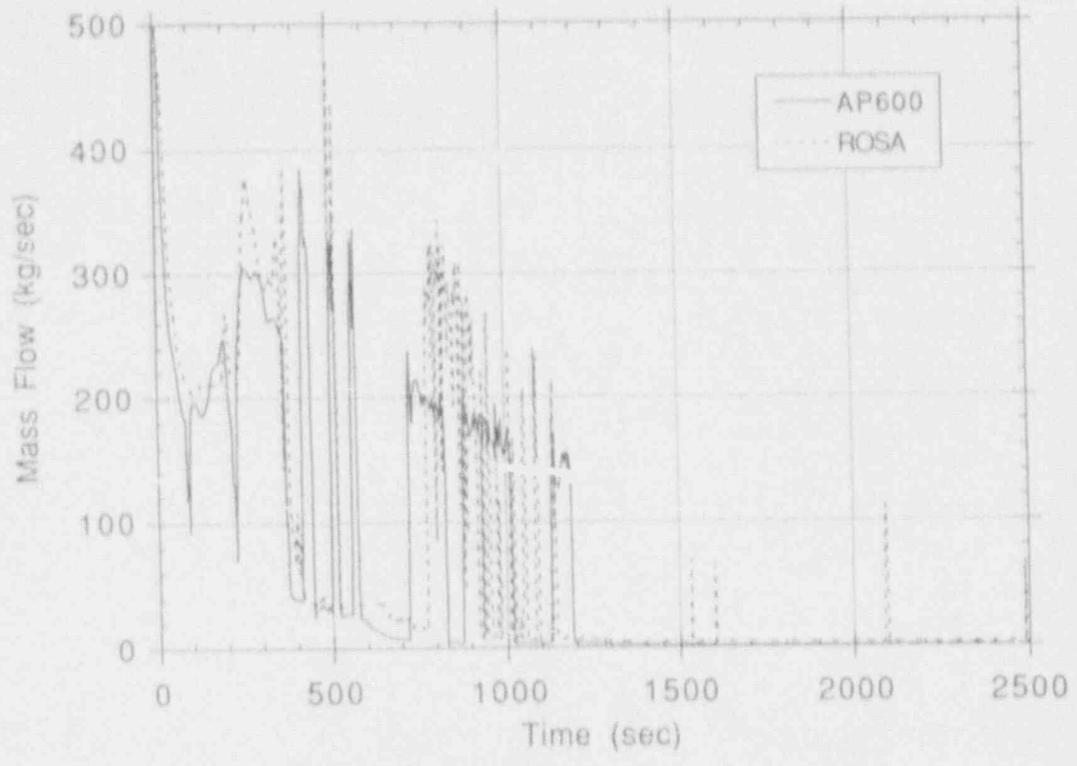

Figure 5. Break mass flow rate for 3–inch CLB calculations.

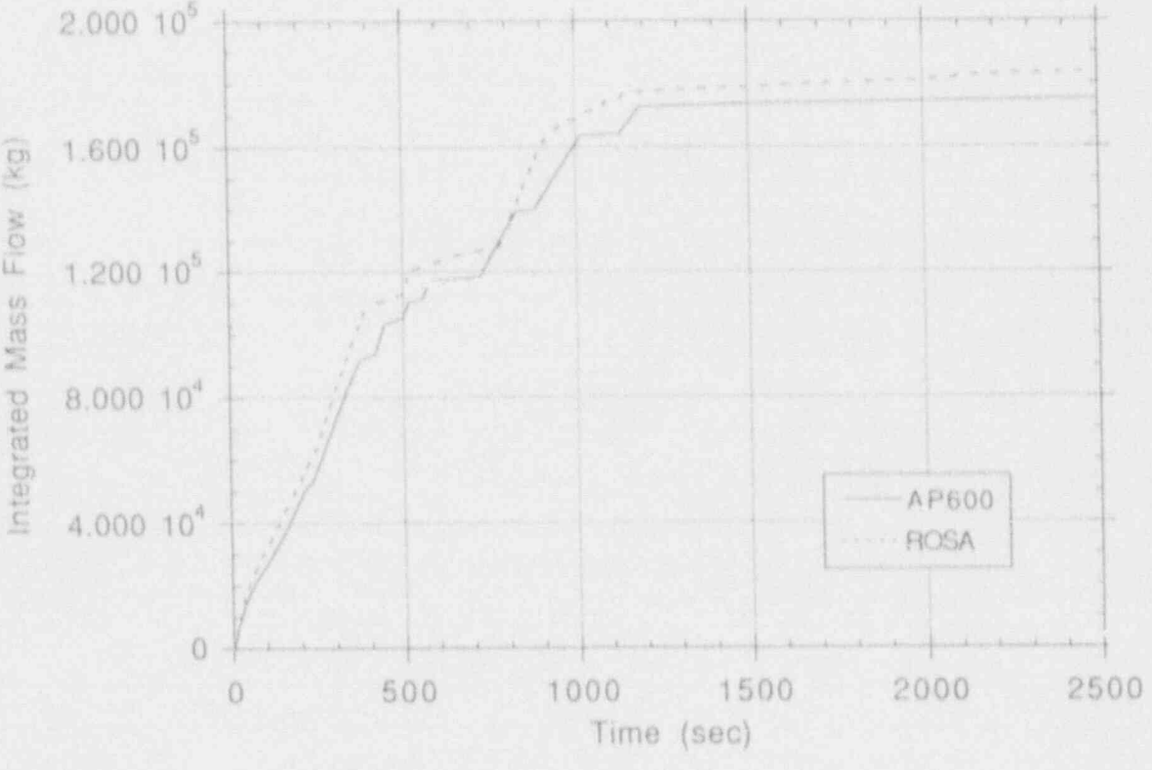

Figure 6. Integrated break mass flow rate for 3–inch CLB calculations.

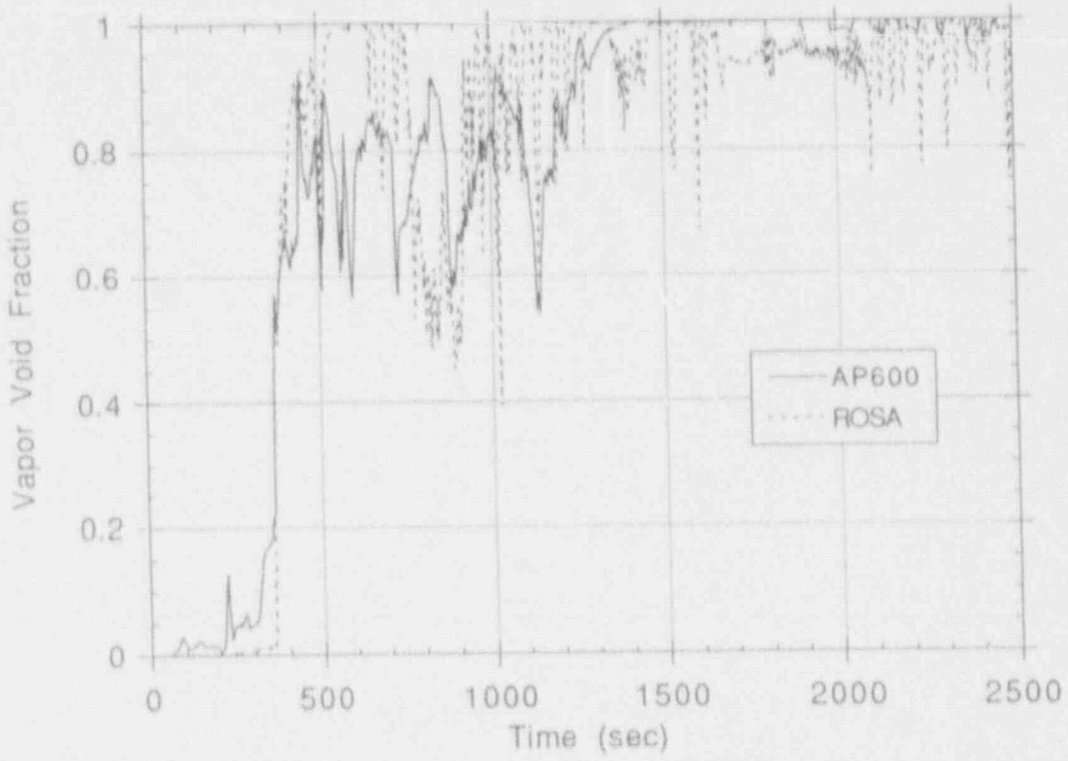

Figure 7. Break volume vapor void fraction for 3–inch CLB calculations.

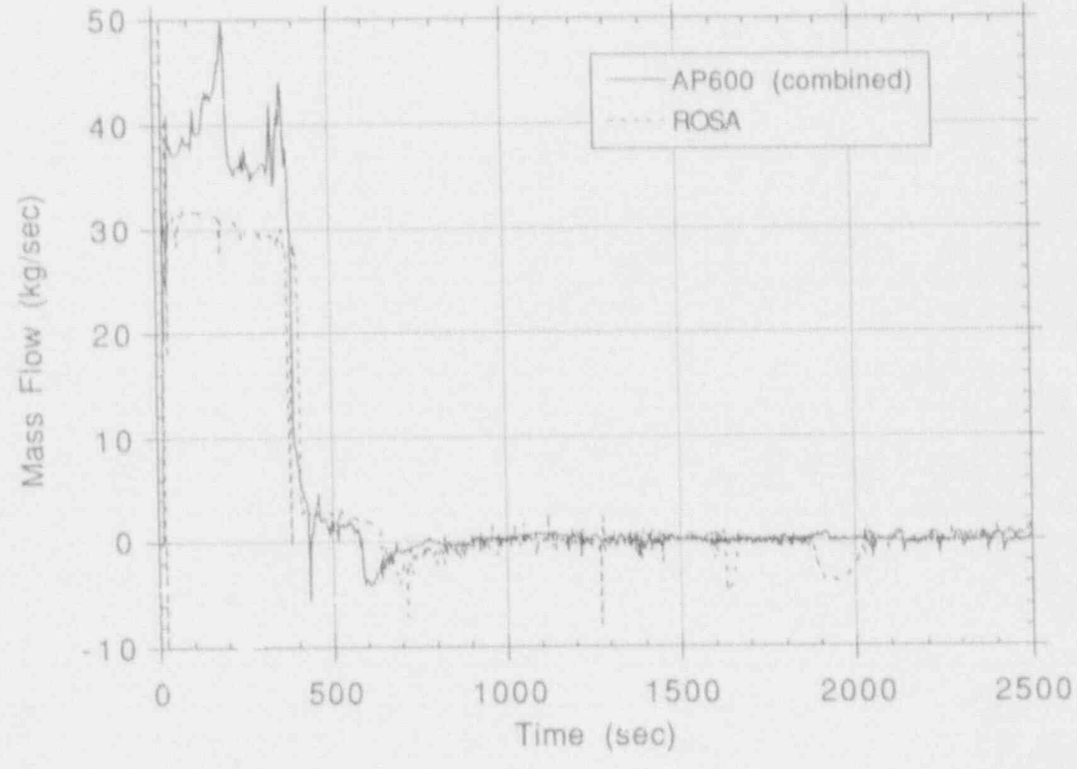

Figure 8. Cold leg pressure balance line mass flow rate for 3–inch CLB calculations.

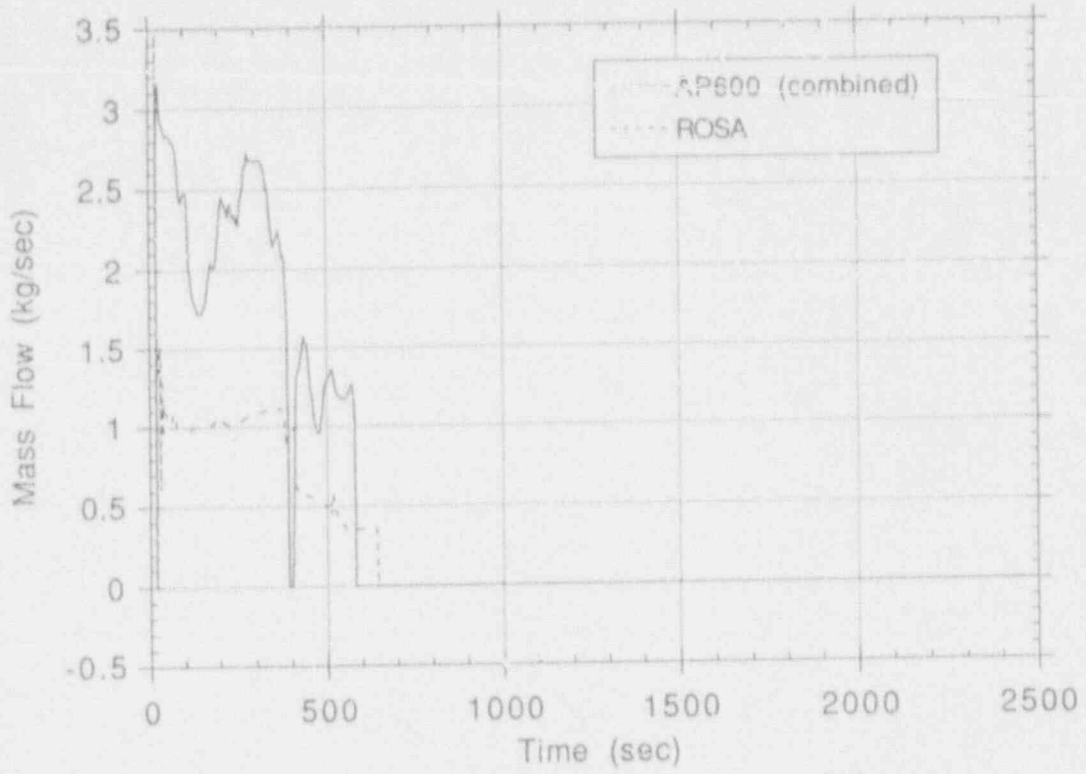

Figure 9. Pressurizer pressure balance line mass flow rate for 3–inch CLB calculations.

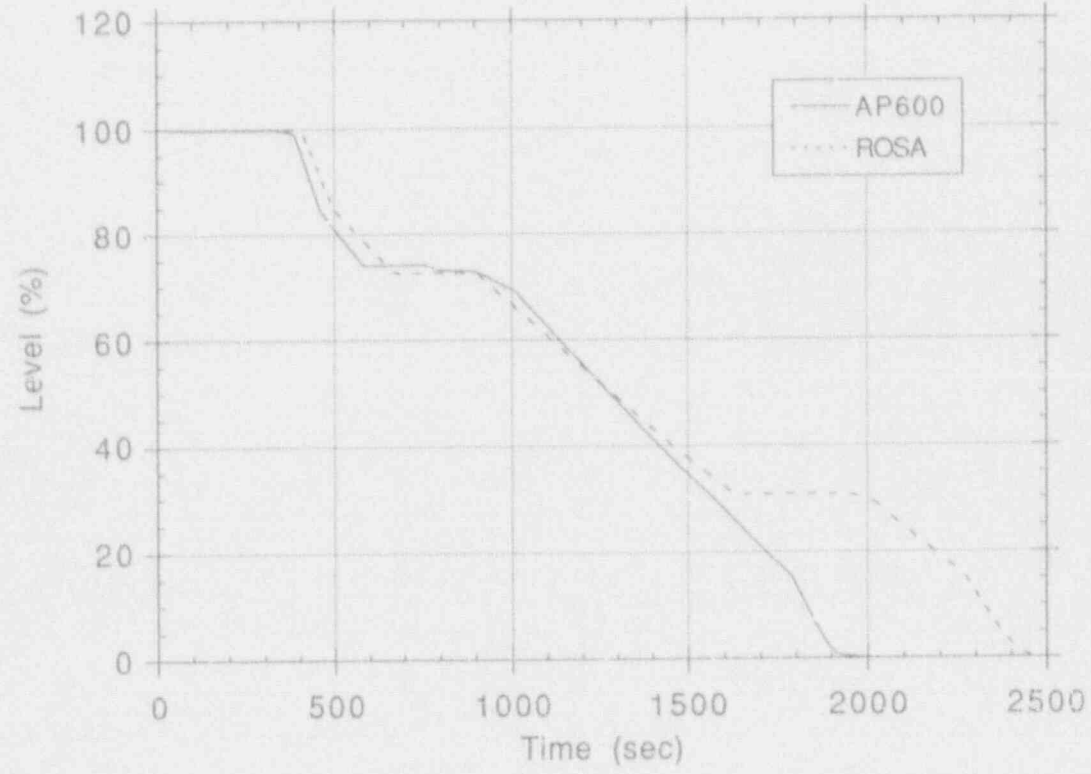

Figure 10. CMT liquid level for 3–inch CLB calculations.

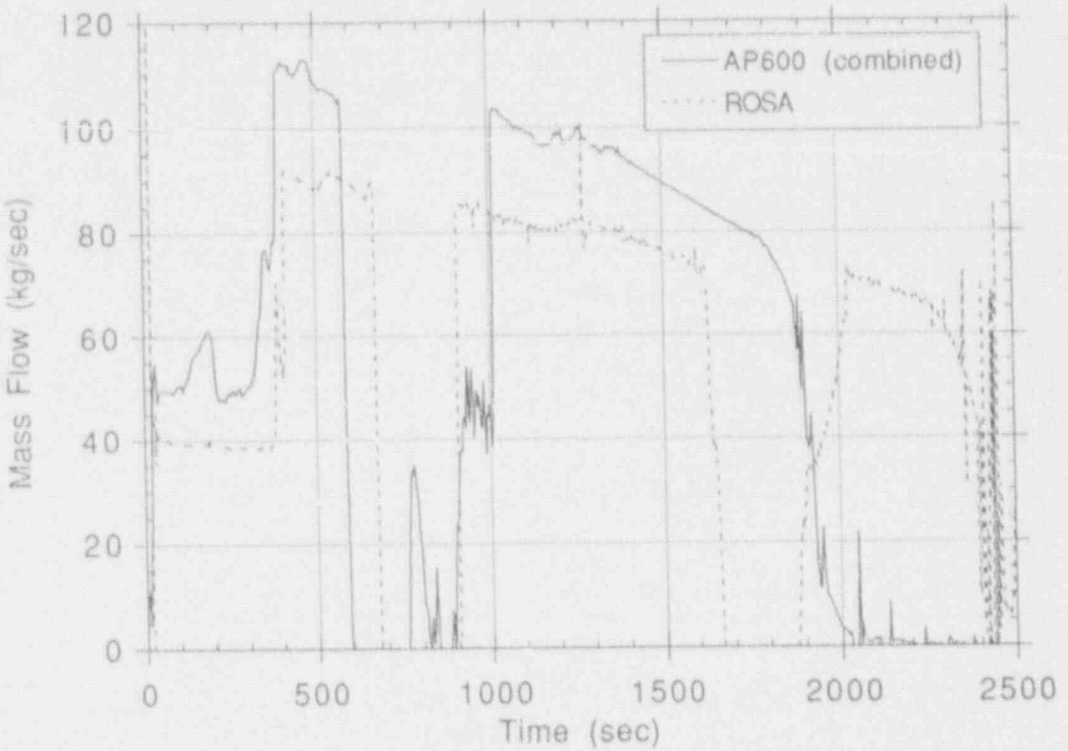

Figure 11. CMT mass flow rate for 3–inch CLB calculations.

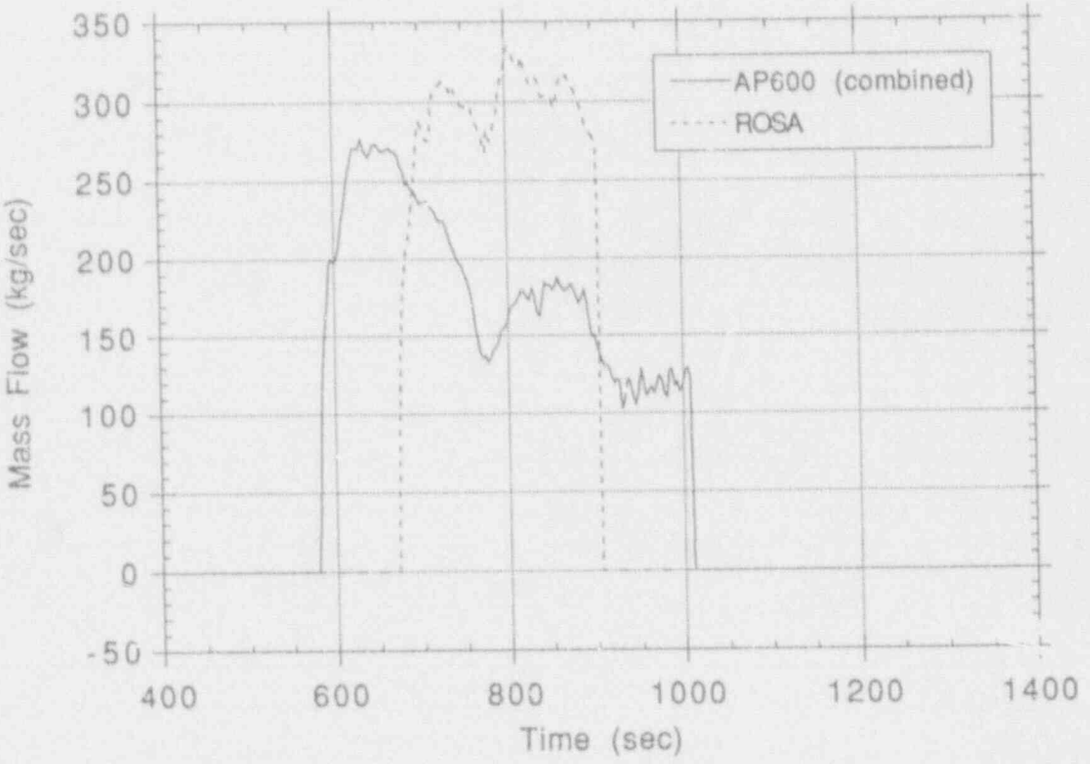

Figure 12. Accumulator mass flow rate for 3–inch CLB calculations.

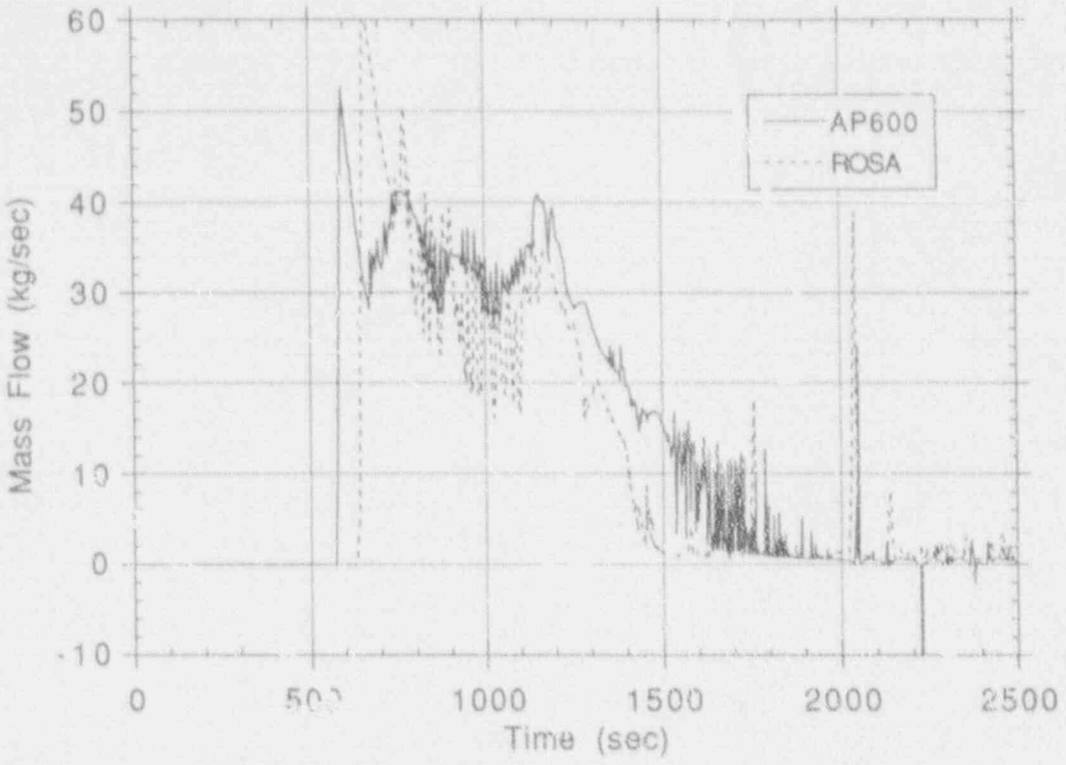

Figure 13. ADS Stage 1 mass flow rate for 3-inch CLB calculations.

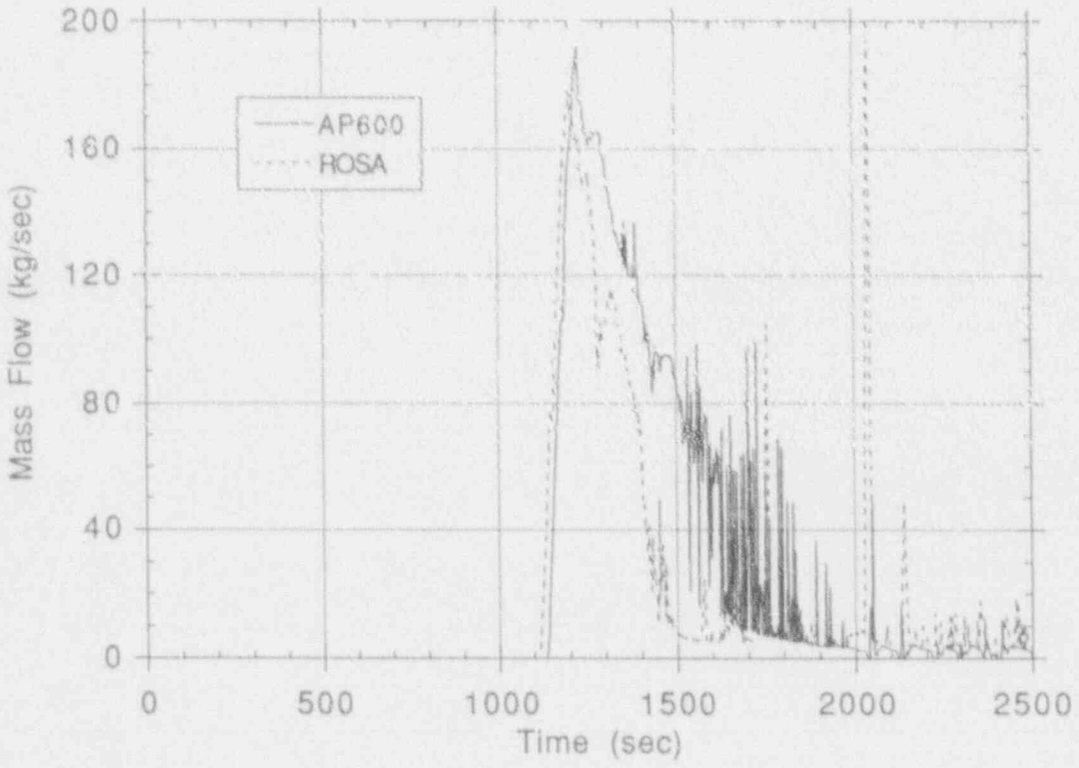

Figure 14. ADS Stage 2 mass flow rate for 3-inch CLB calculations.

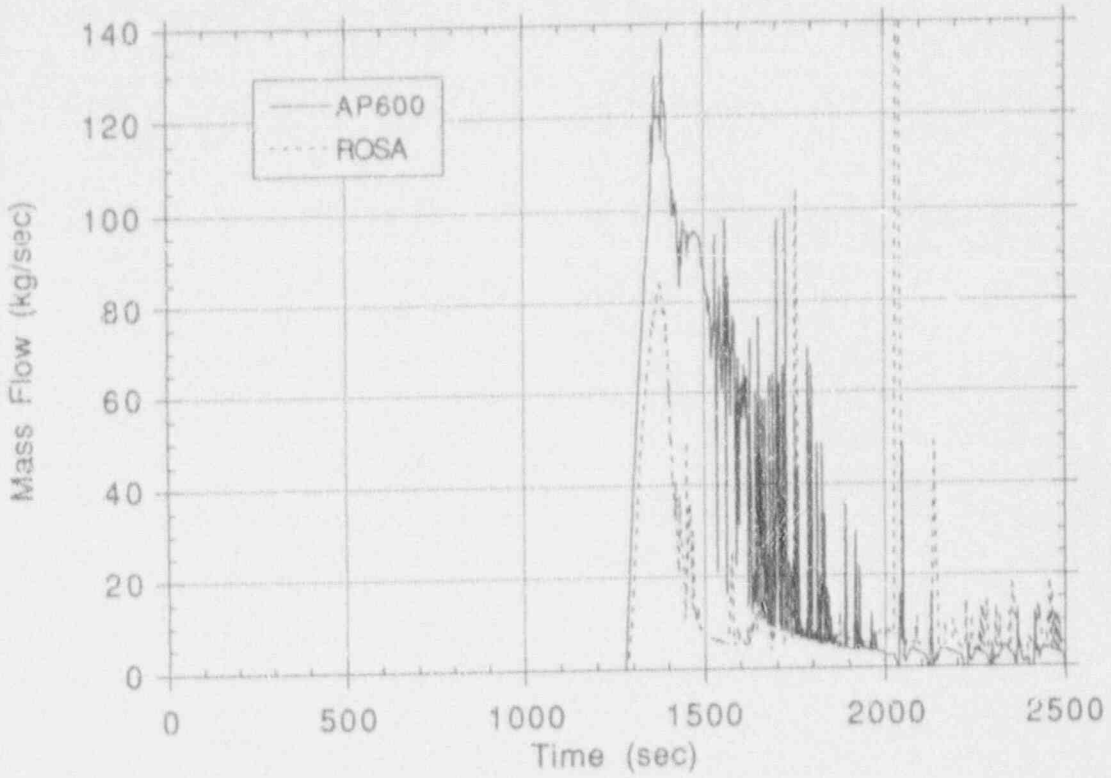

Figure 15. ADS Stage 3 mass flow rate for 3–inch CLB calculations.

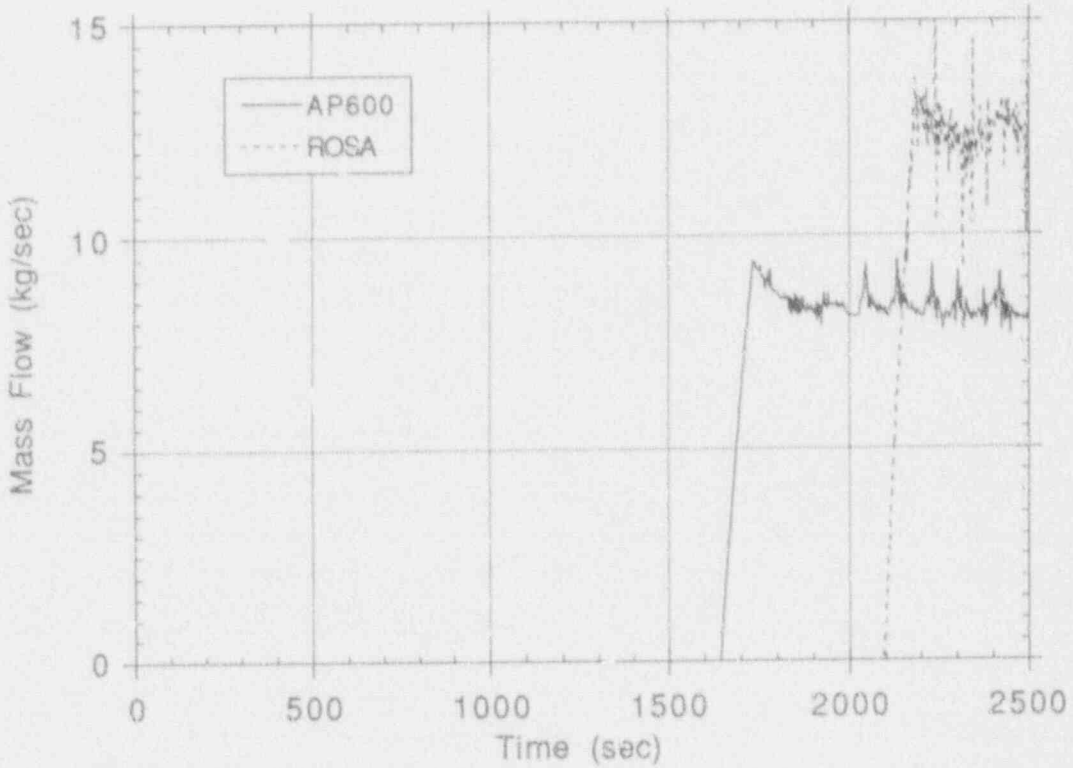

Figure 16. ADS Stage 4 mass flow rate for 3–inch CLB calculations.

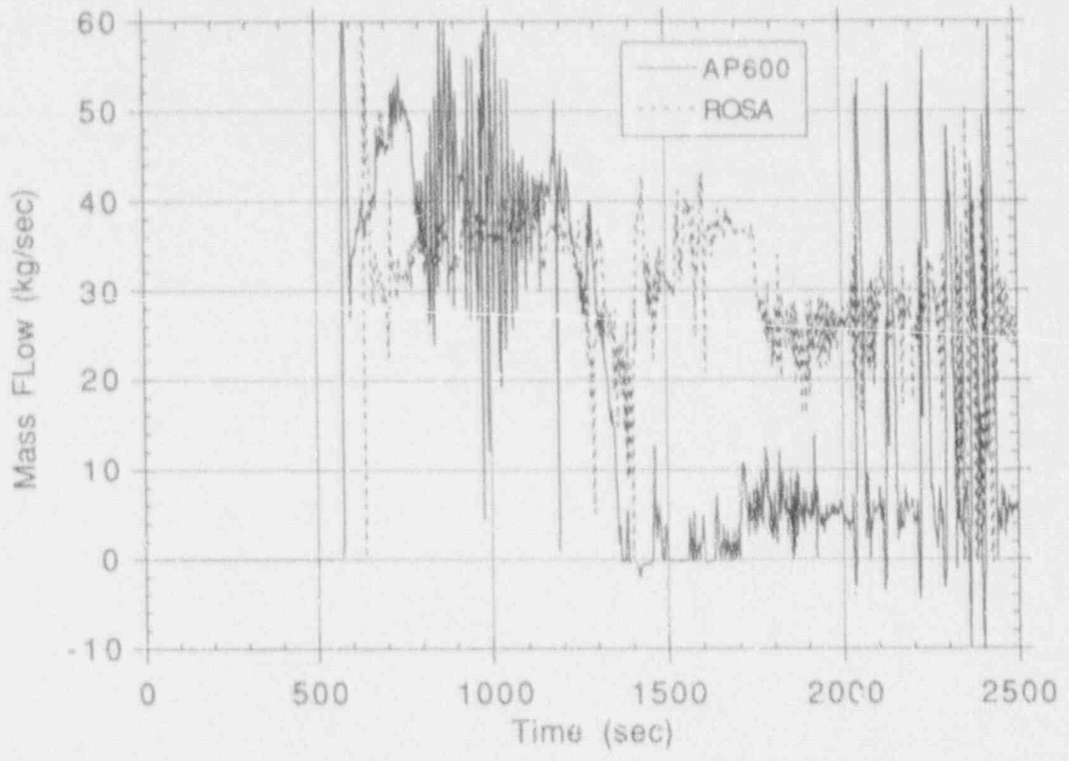

Figure 17. PRHR mass flow rate for 3-inch CLB calculations.

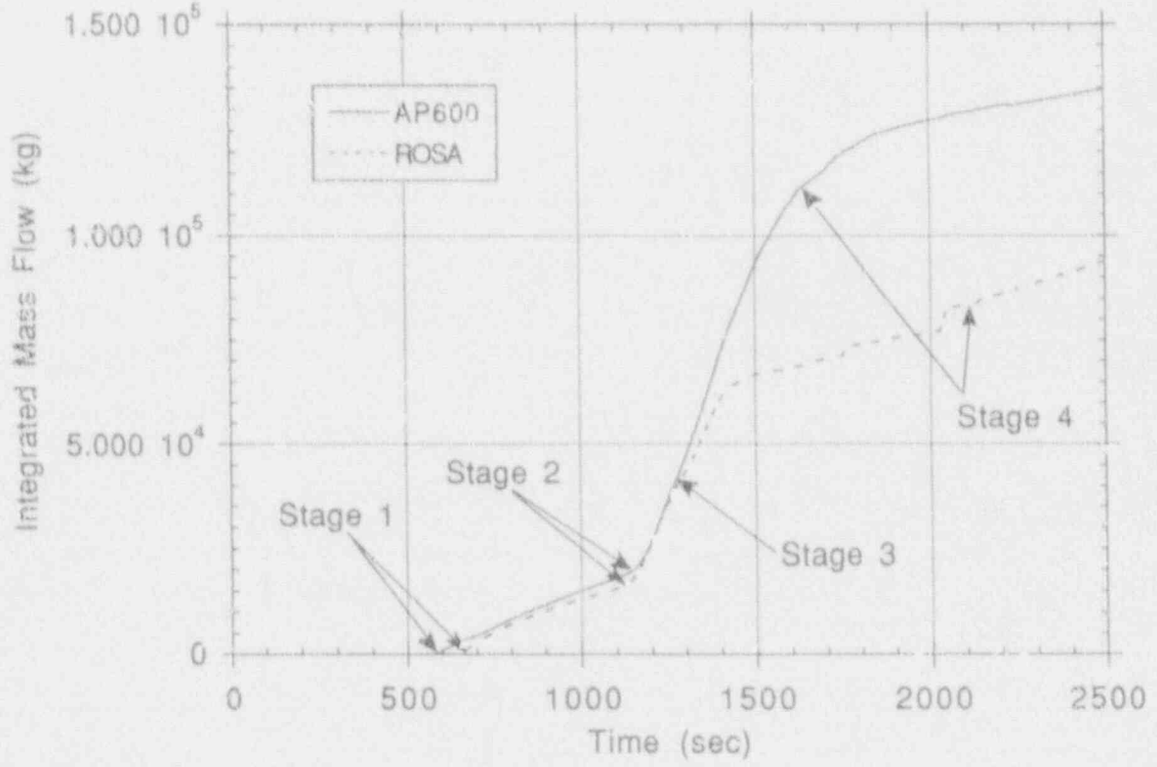

Figure 18. Integrated total ADS mass flow rate for 3-inch CLB calculations.

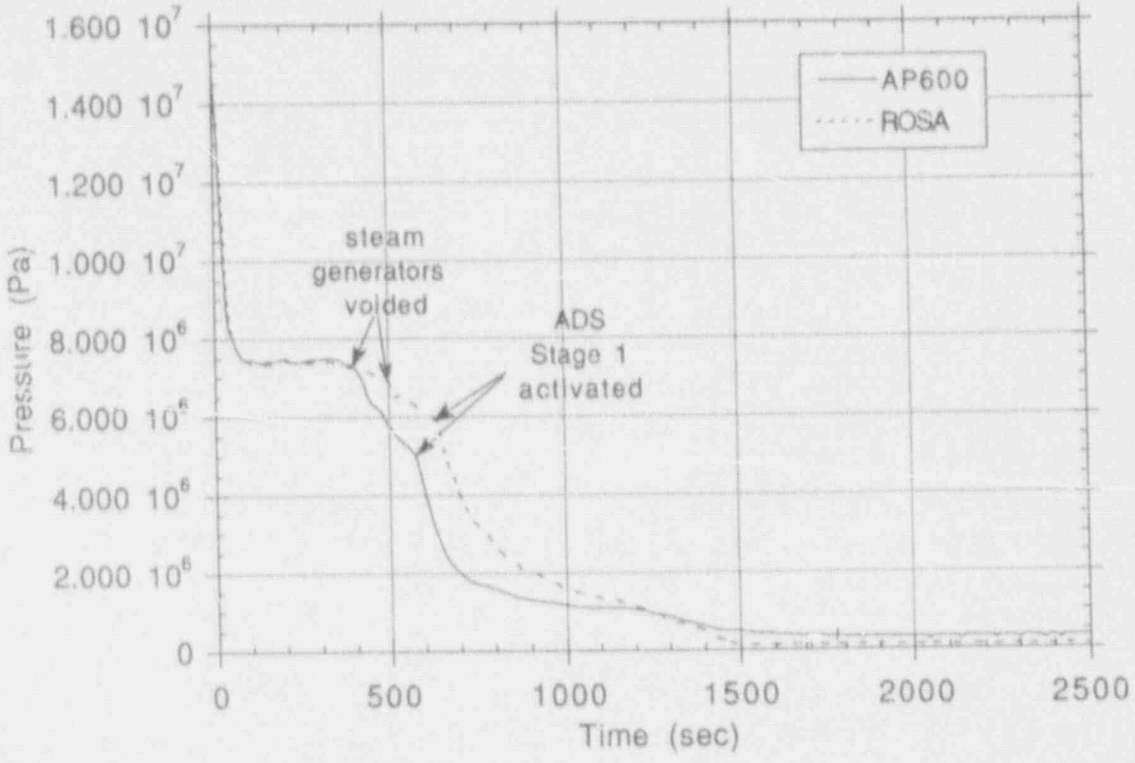

Figure 19. Pressurizer pressure for 3–inch CLB calculations.

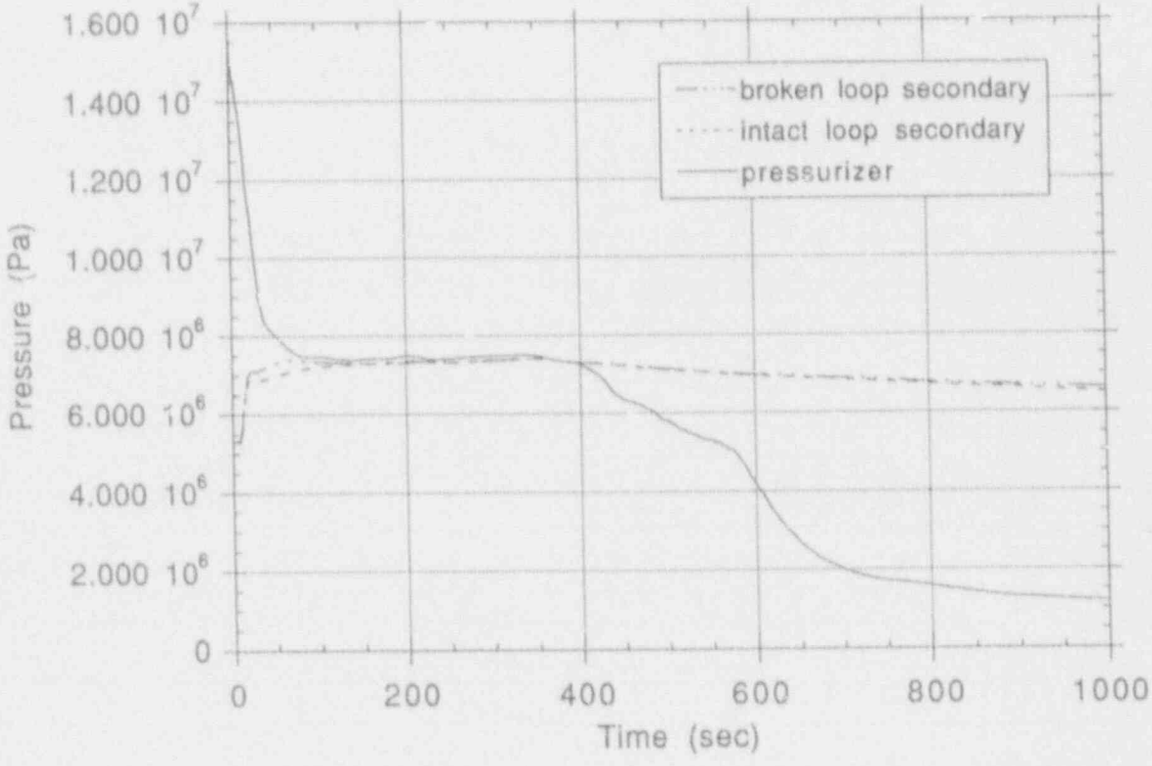

Figure 20. Primary and Secondary pressure for AP600 3–inch CLB calculation.

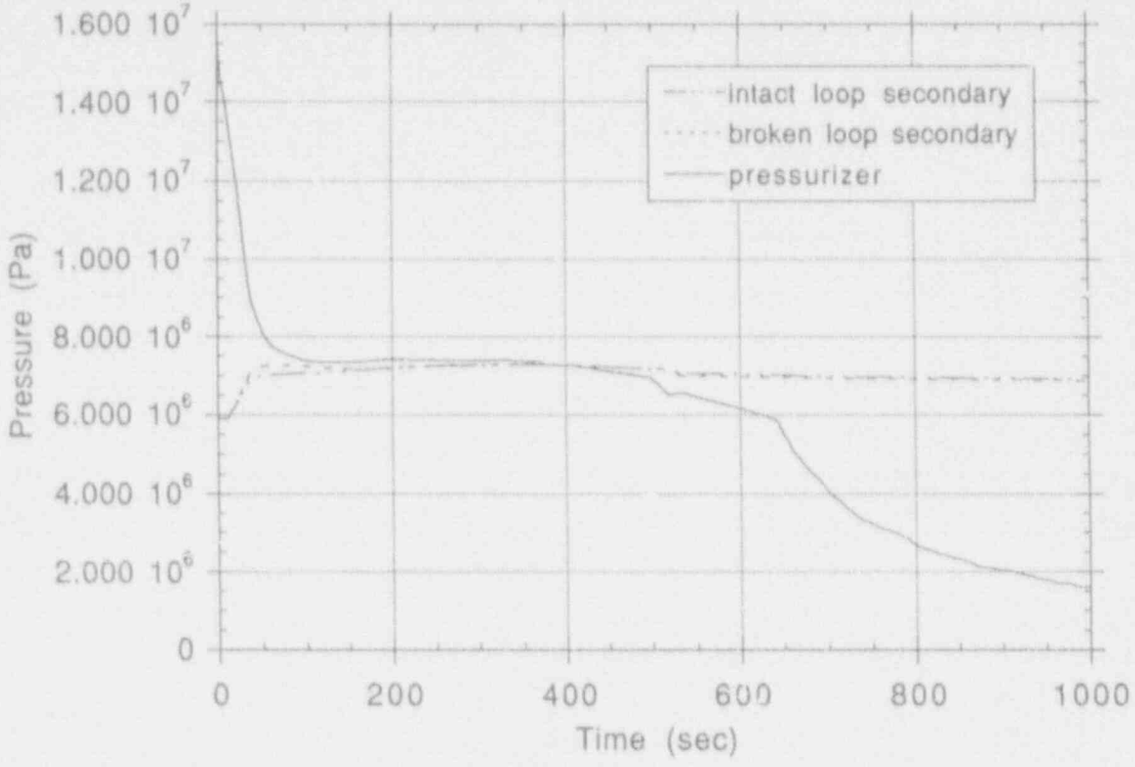

Figure 21. Primary and secondary pressure for ROSA 3–inch CLB calculation.

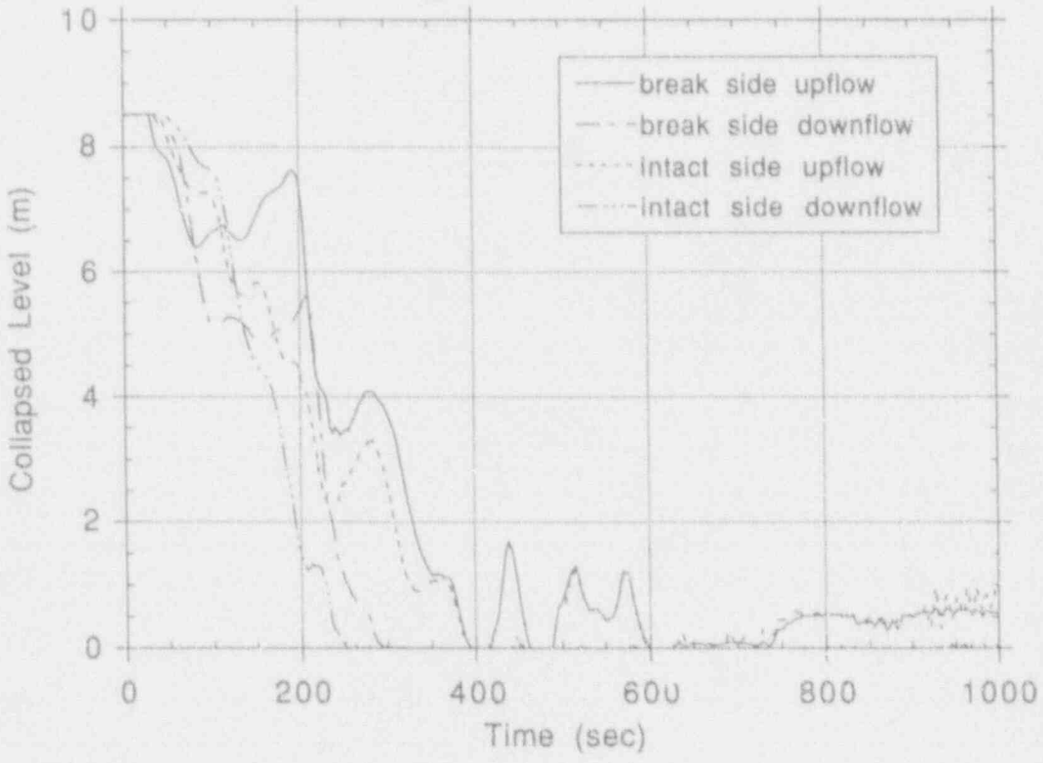

Figure 22. Steam generator U–tube collapsed liquid level for AP600 3–inch CLB calculation.

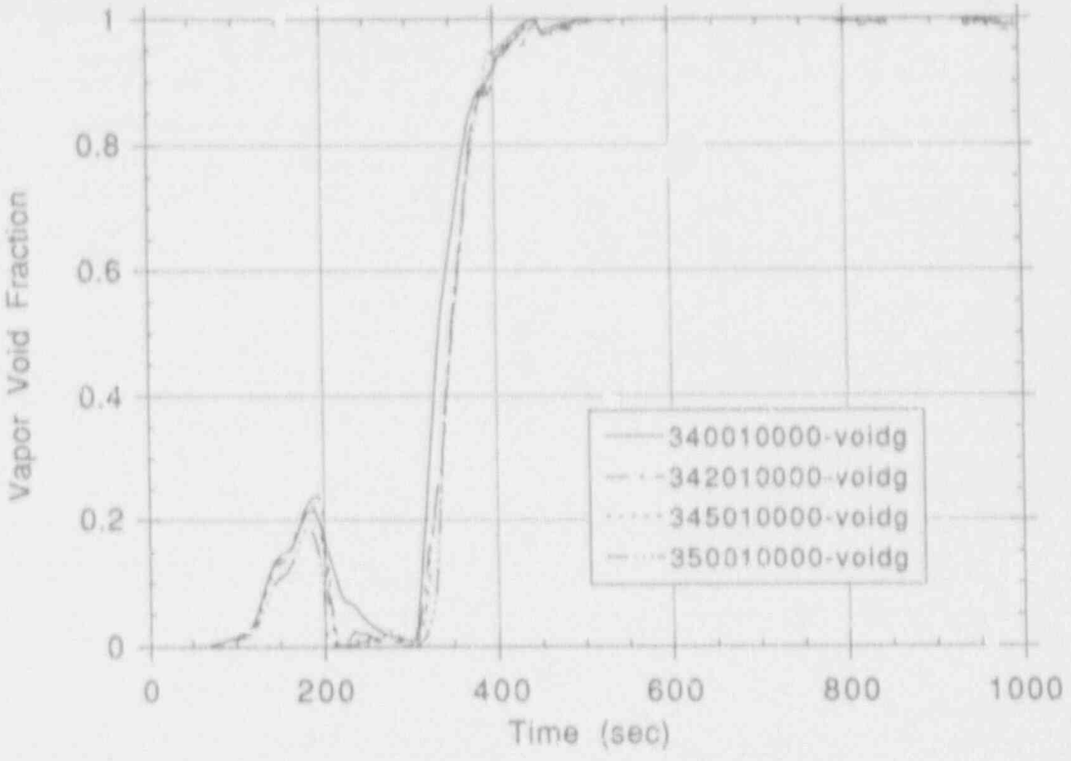

Figure 23. Intact side cold leg (2a) volume vapor void fractions for AP600 3-inch CLB calculation.

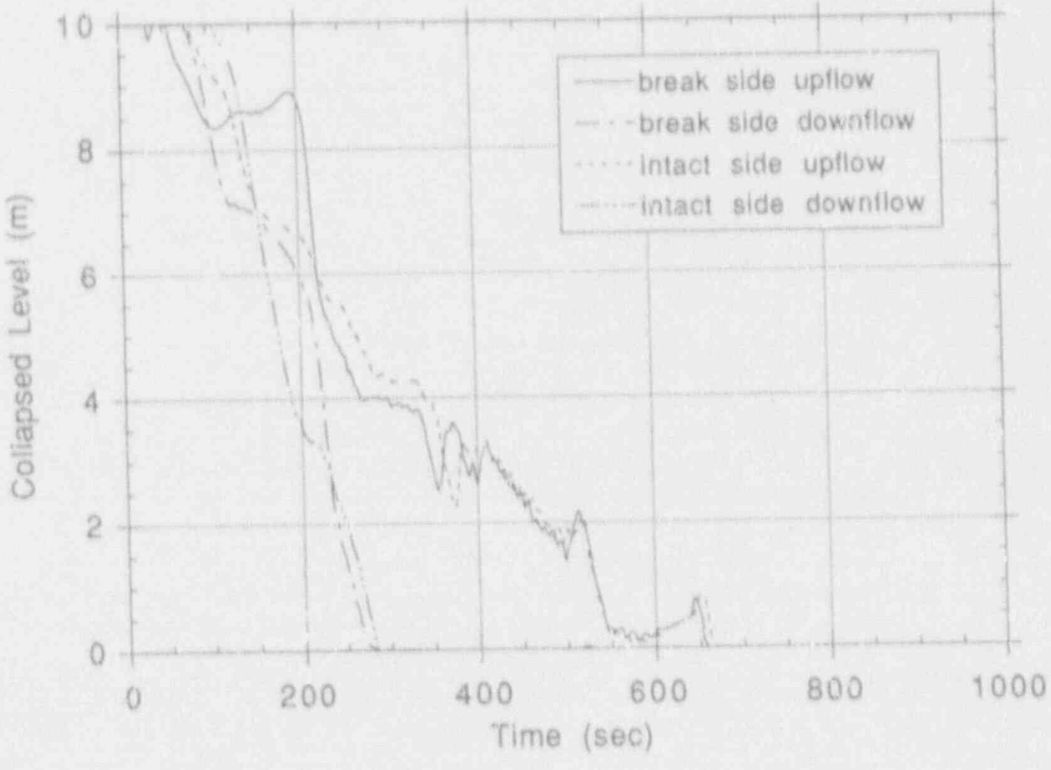

Figure 24. Steam generator U-tube collapsed liquid level for ROSA 3-inch CLB calculation.

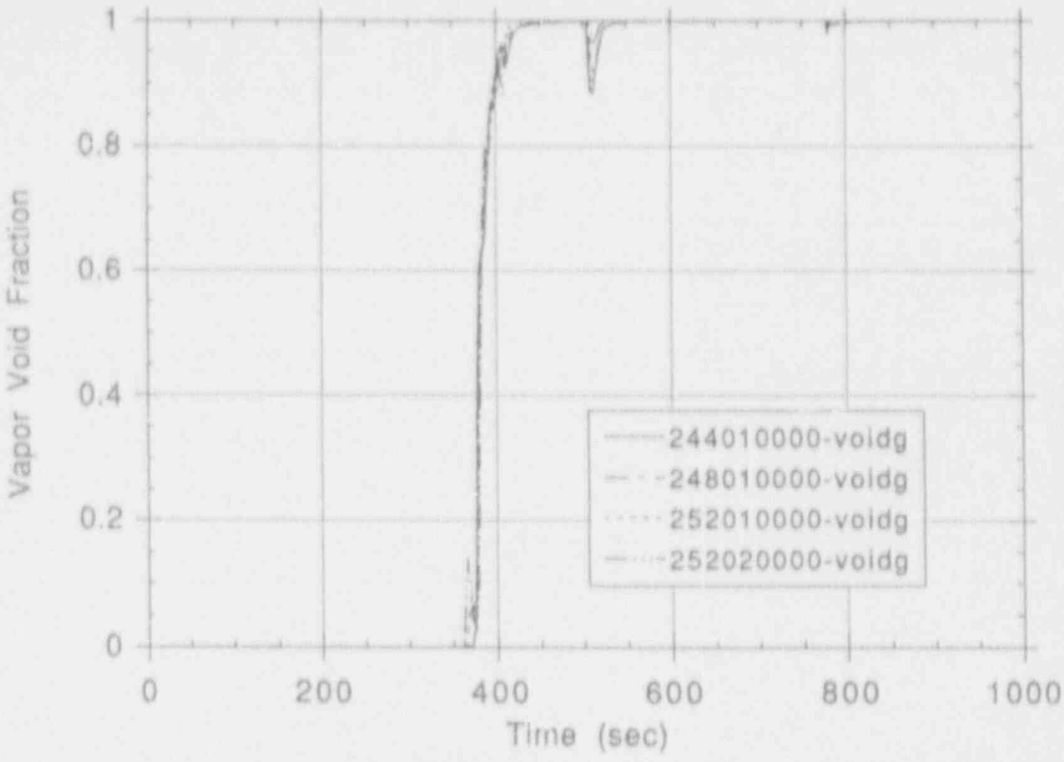

Figure 25. Intact side cold leg volume vapor void fractions for ROSA 3–inch CLB calculation.

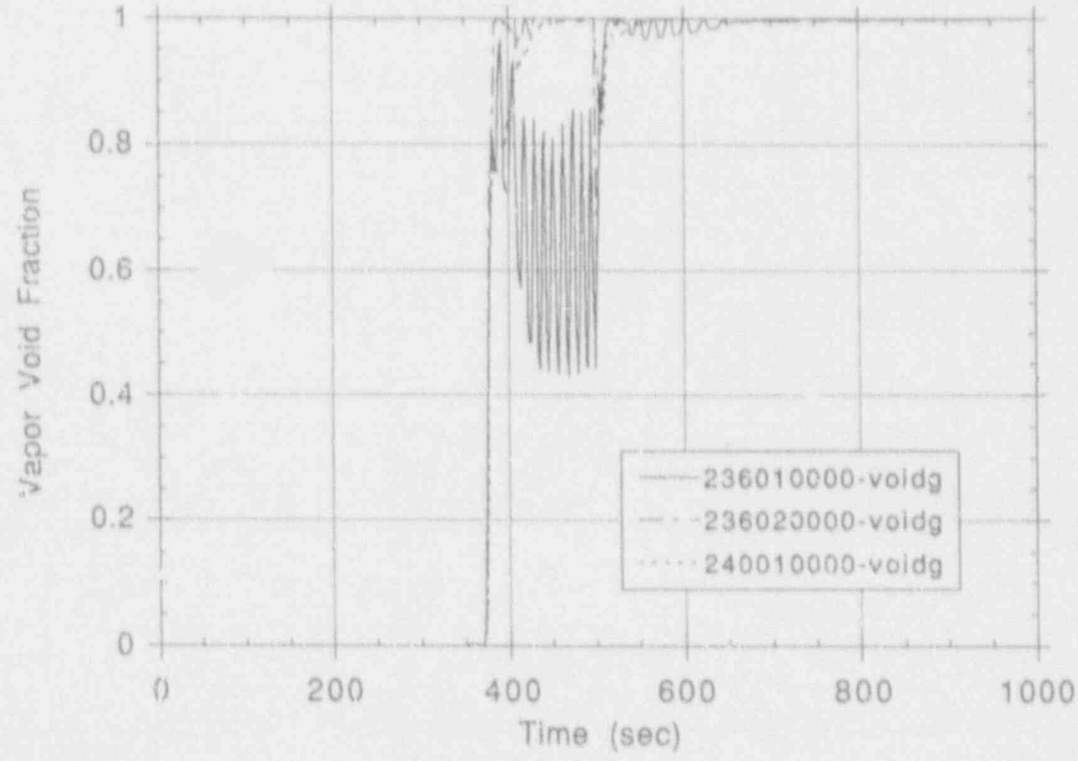

Figure 26. Intact cold leg pump suction upflow volume vapor void fractions for ROSA 3–inch CLB calculation.

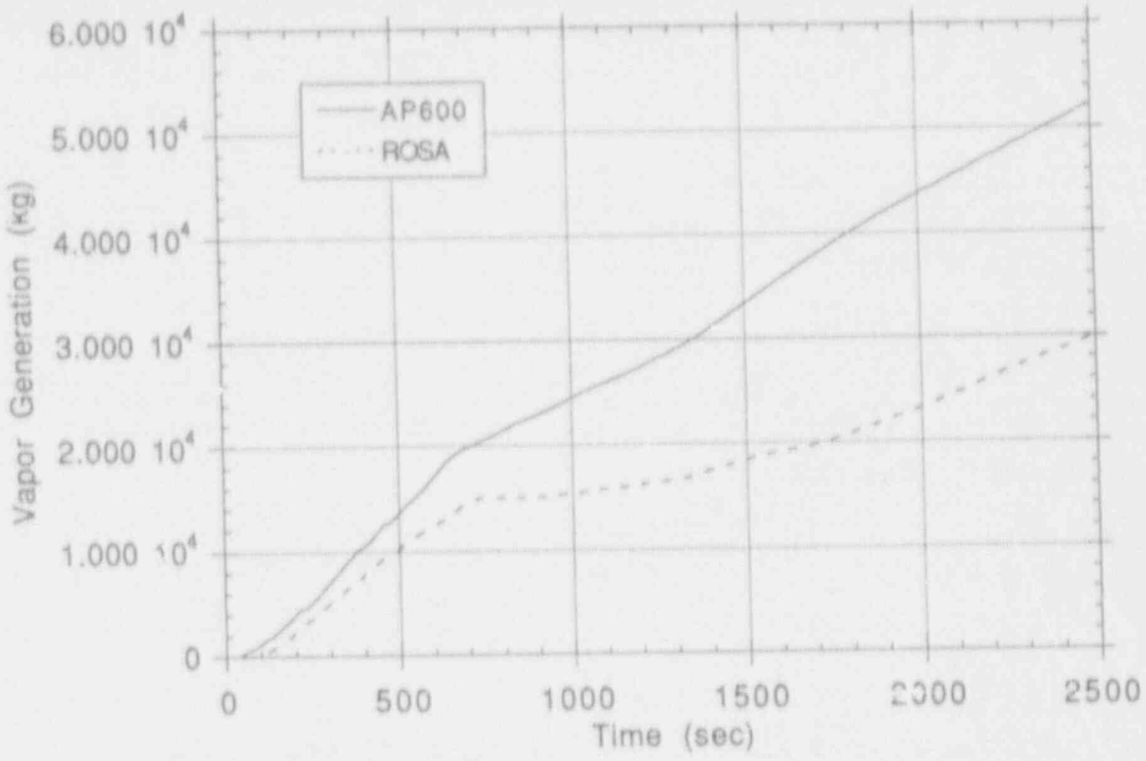

Figure 27. Lower plenum/core/upper plenum integrated vapor generation rate for 3–inch CLB calculations.

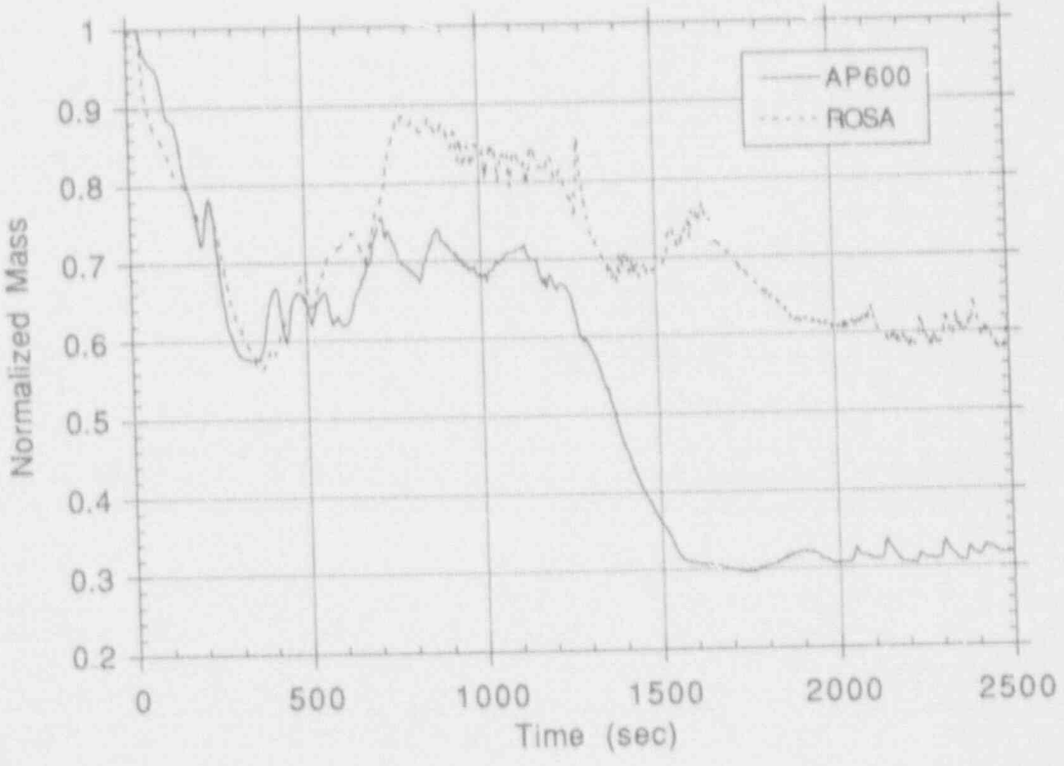

Figure 28. Vessel normalized mass inventory for 3–inch CLB calculations.

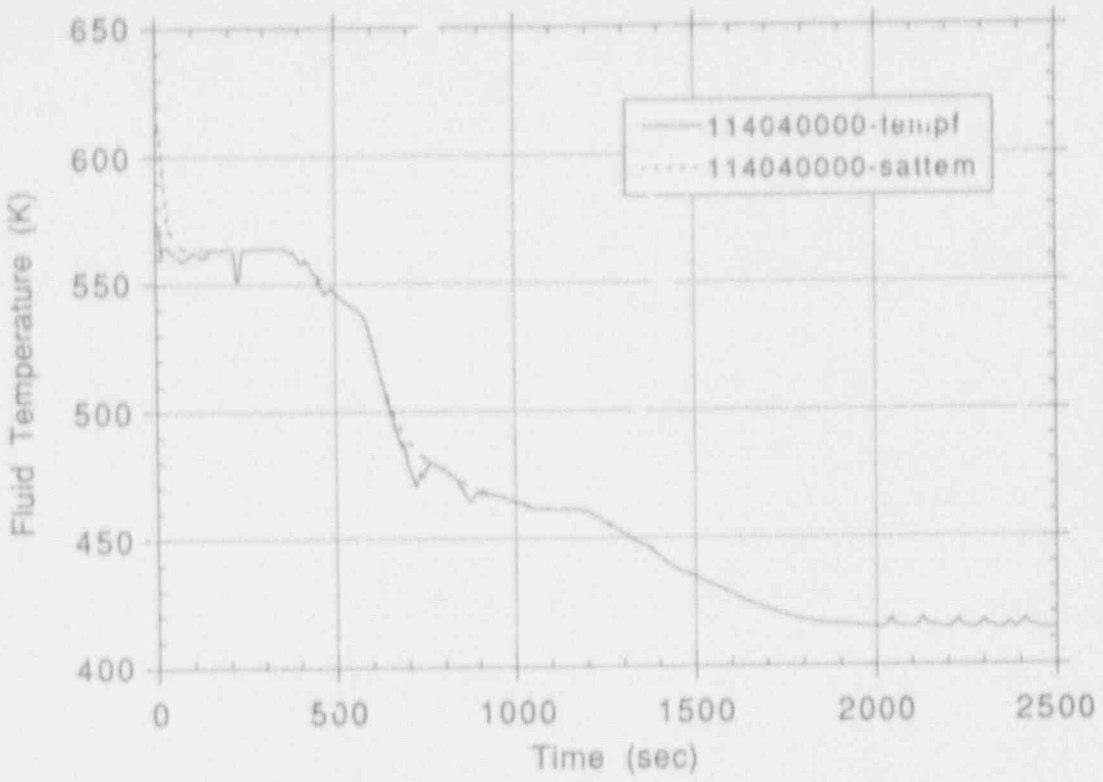

Figure 29. Mid–core fluid and saturation temperature for AP600 3–inch CLB calculation.

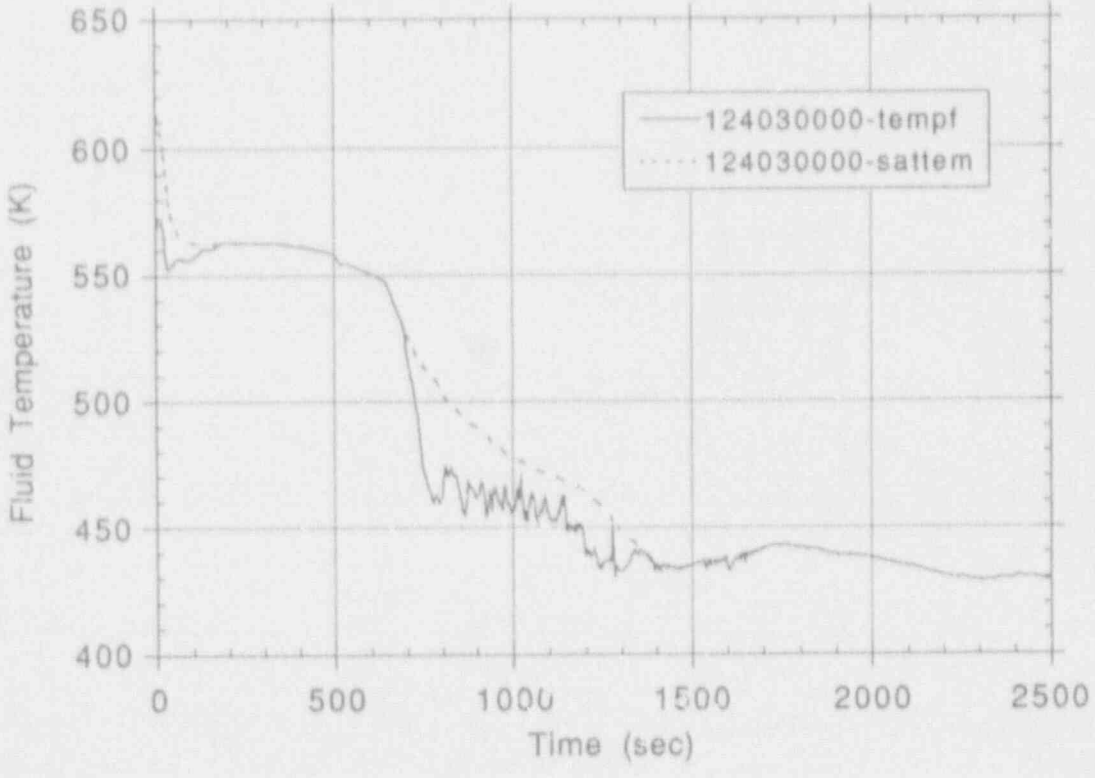

Figure 30. Mid–core fluid and saturation temperature for ROSA 3–inch CLB calculation.

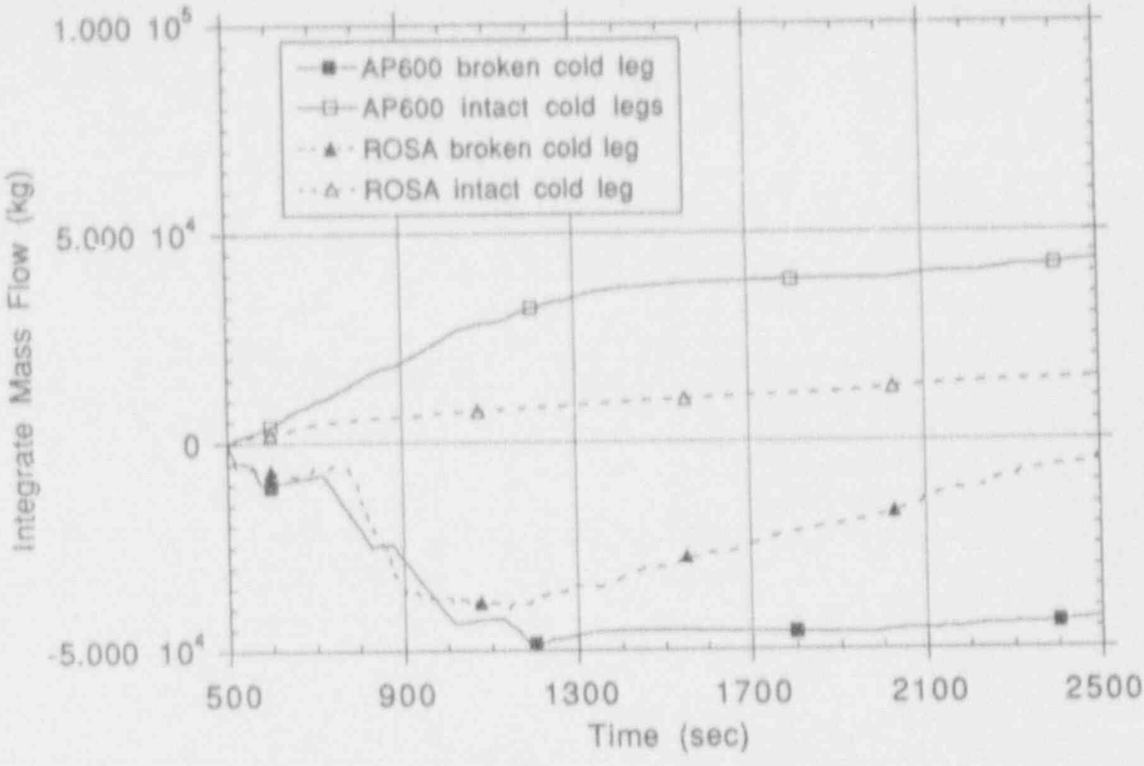

Figure 31. Integrated cold leg mass flow rates for 3–inch CLB calculations.

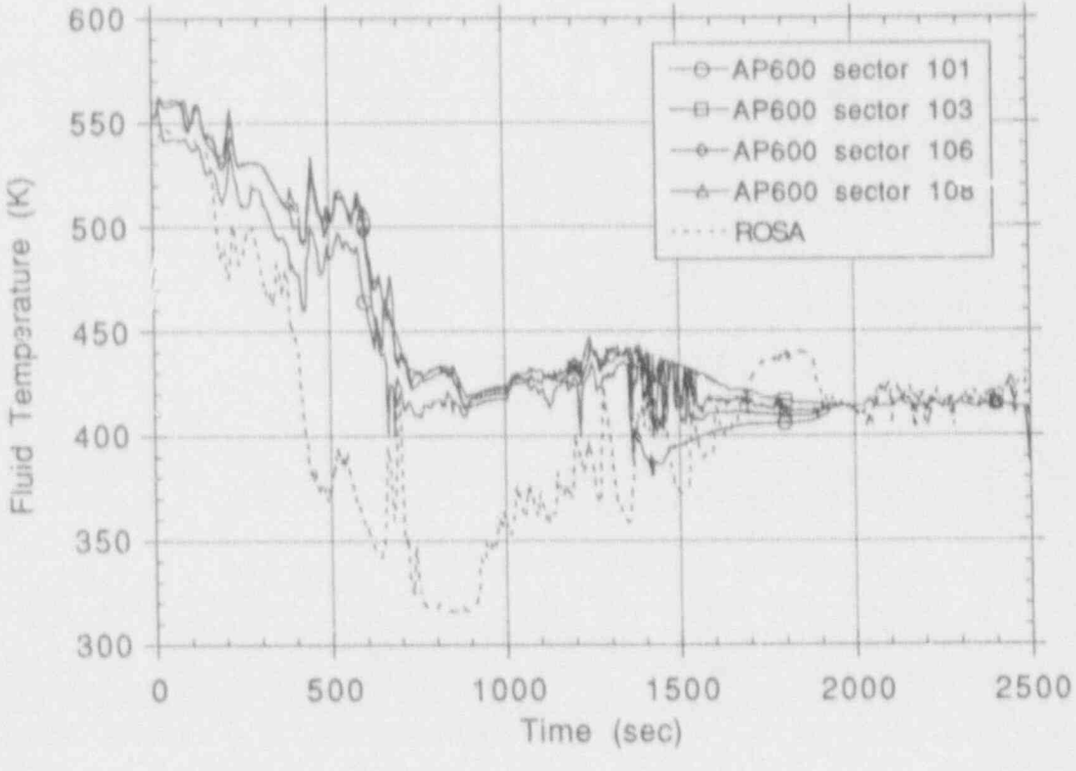

Figure 32. Upper downcomer fluid temperatures for 3–inch CLB calculations.

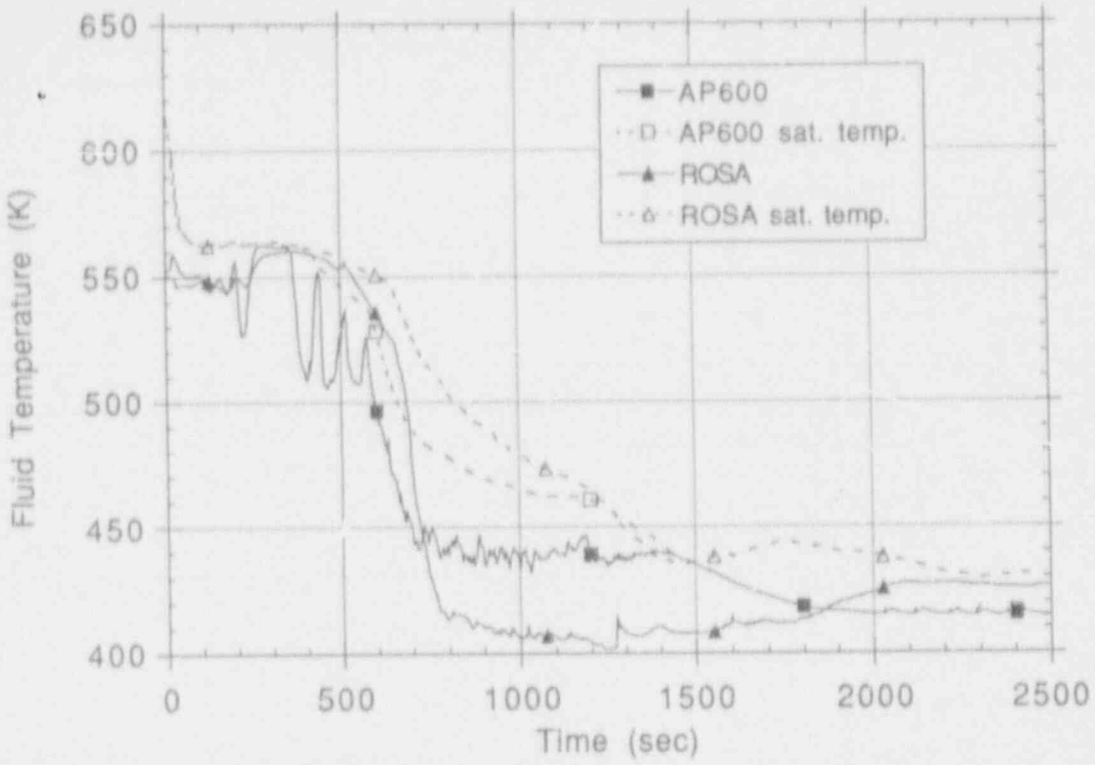

Figure 33. Core inlet fluid and saturation temperatures for 3–inch CLB calculations.

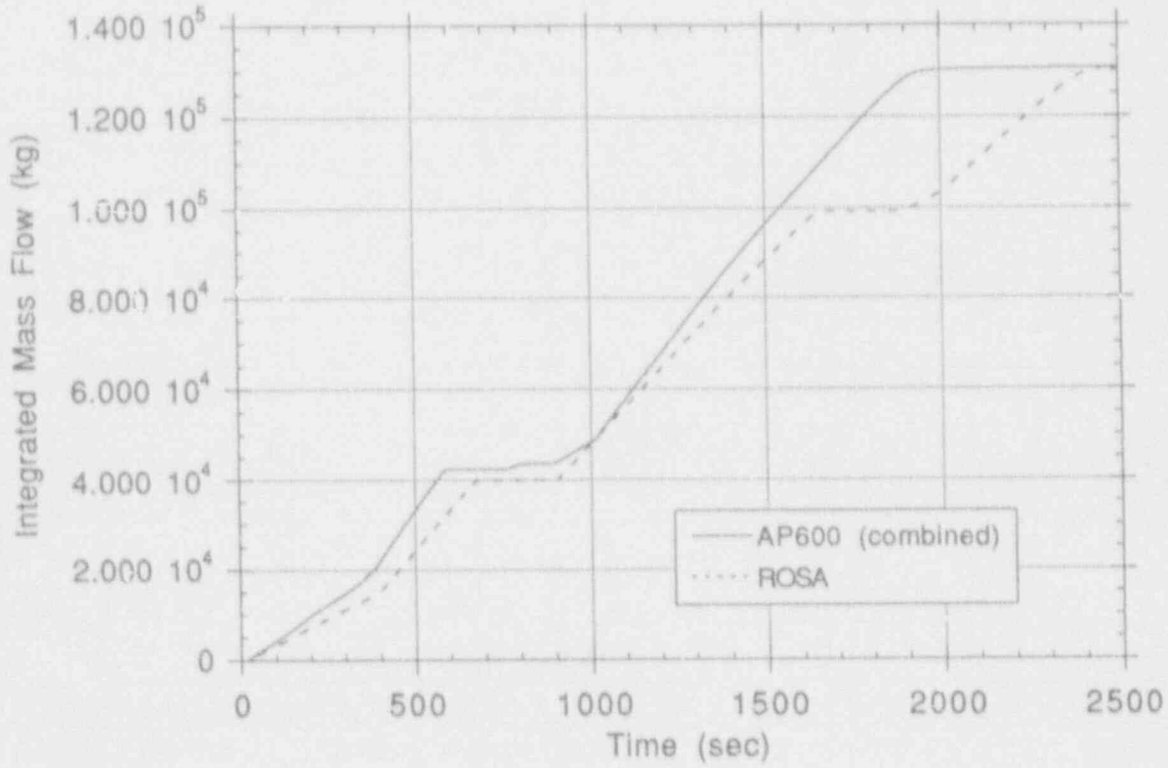

Figure 34. Integrated total ECC line flow for 3–inch CLB calculations.

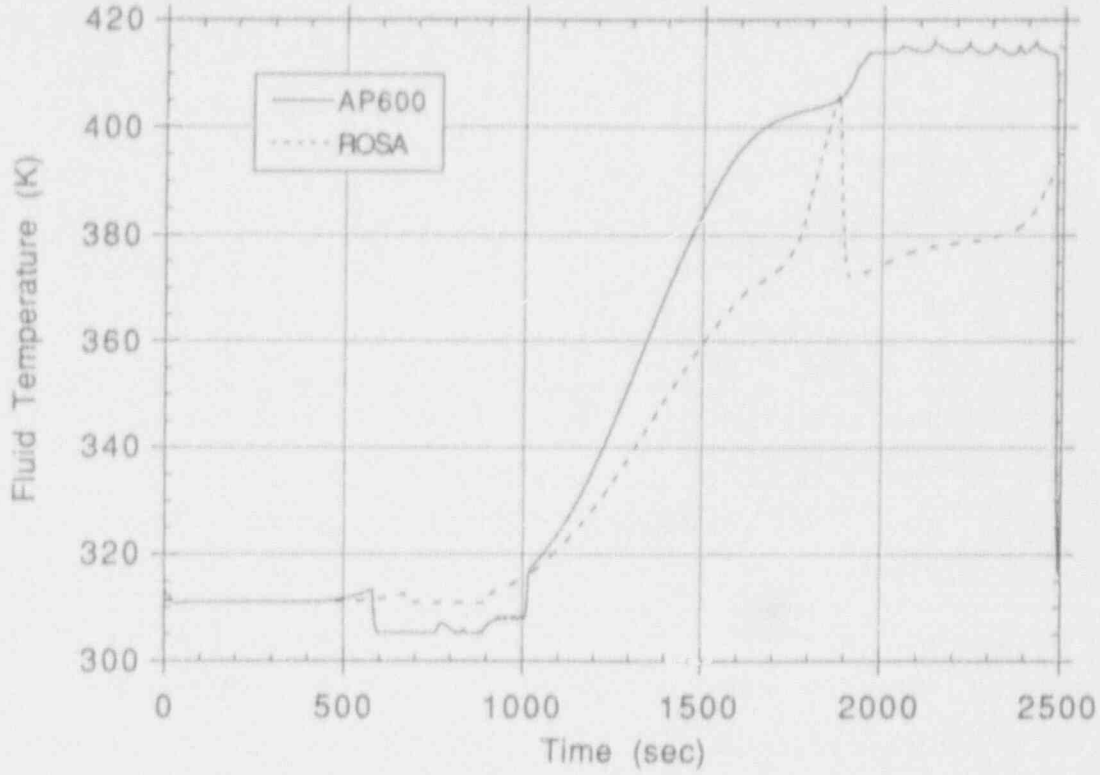

Figure 35. Fluid temperature in ECC line near vessel for 3-inch CLB calculations.

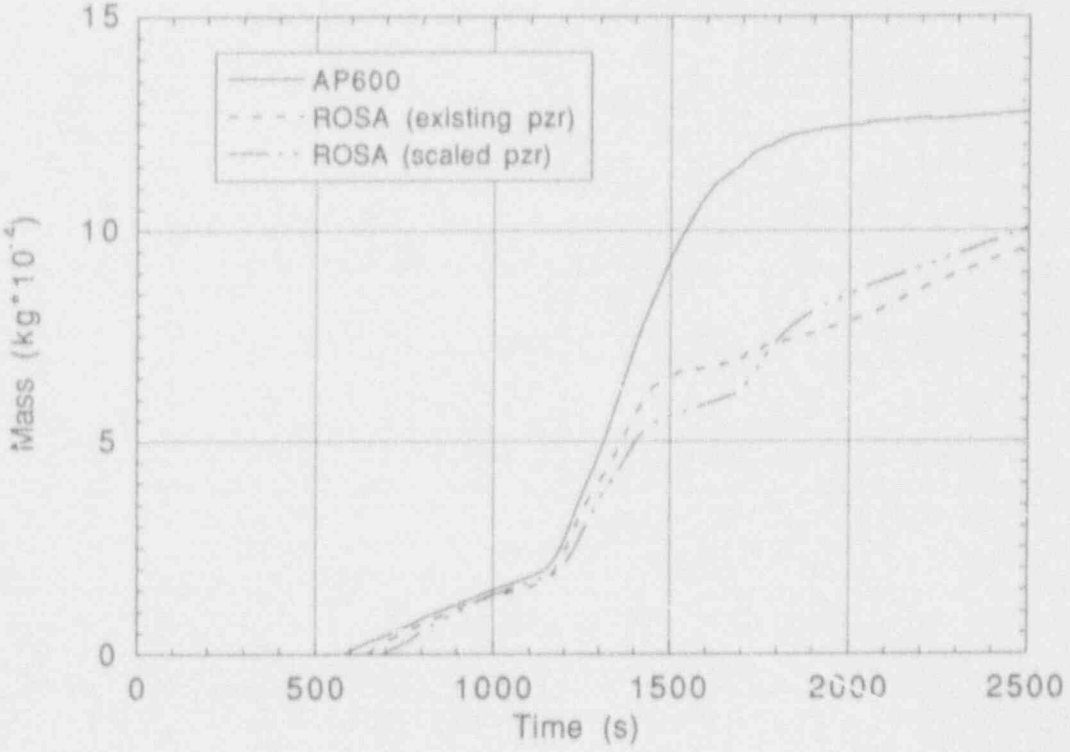

Figure 36. Integrated total ADS Stages 1, 2, and 3 mass flow rate for 3-inch CLB calculations.

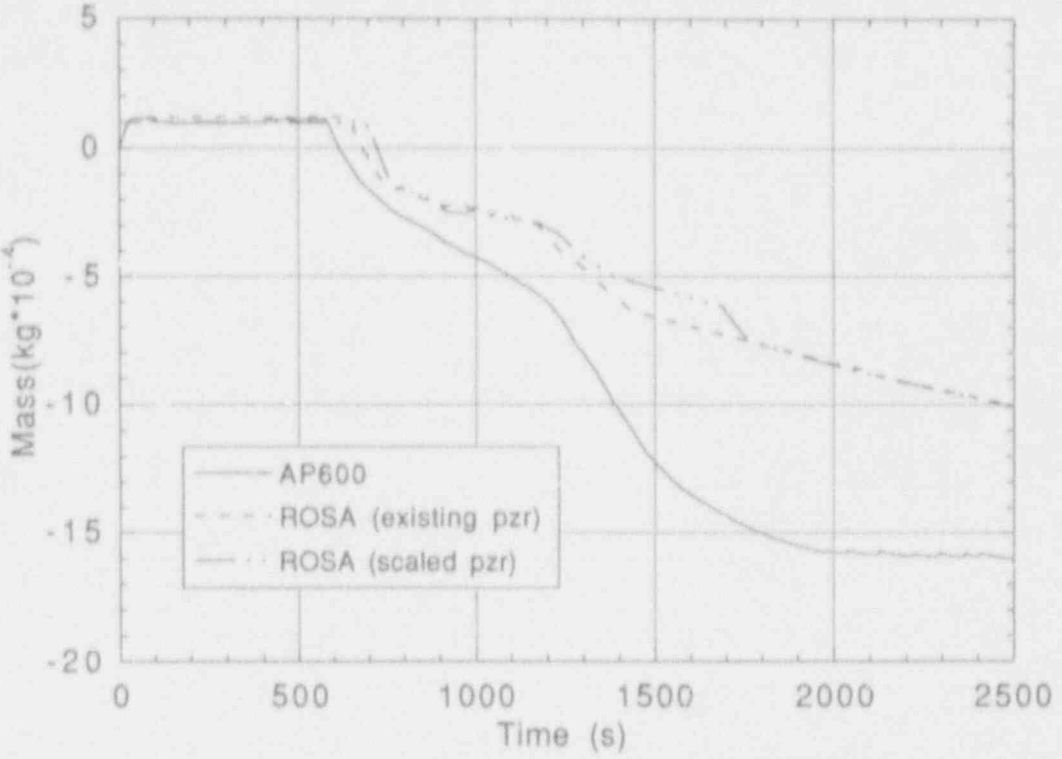

Figure 37. Pressurizer–to–surge line integrated mass flow rate for 3–inch CLB calculations.

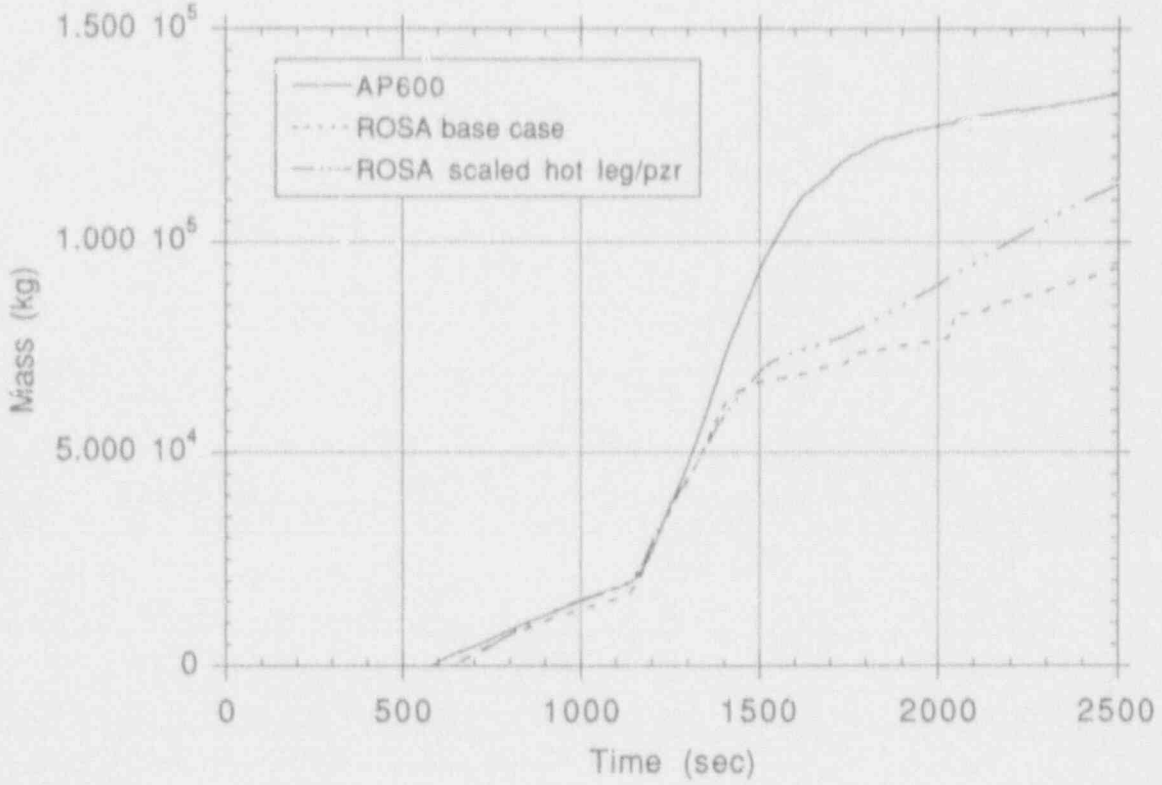

Figure 38. Integrated total ADS mass flow rate for 3–inch CLB calculations.

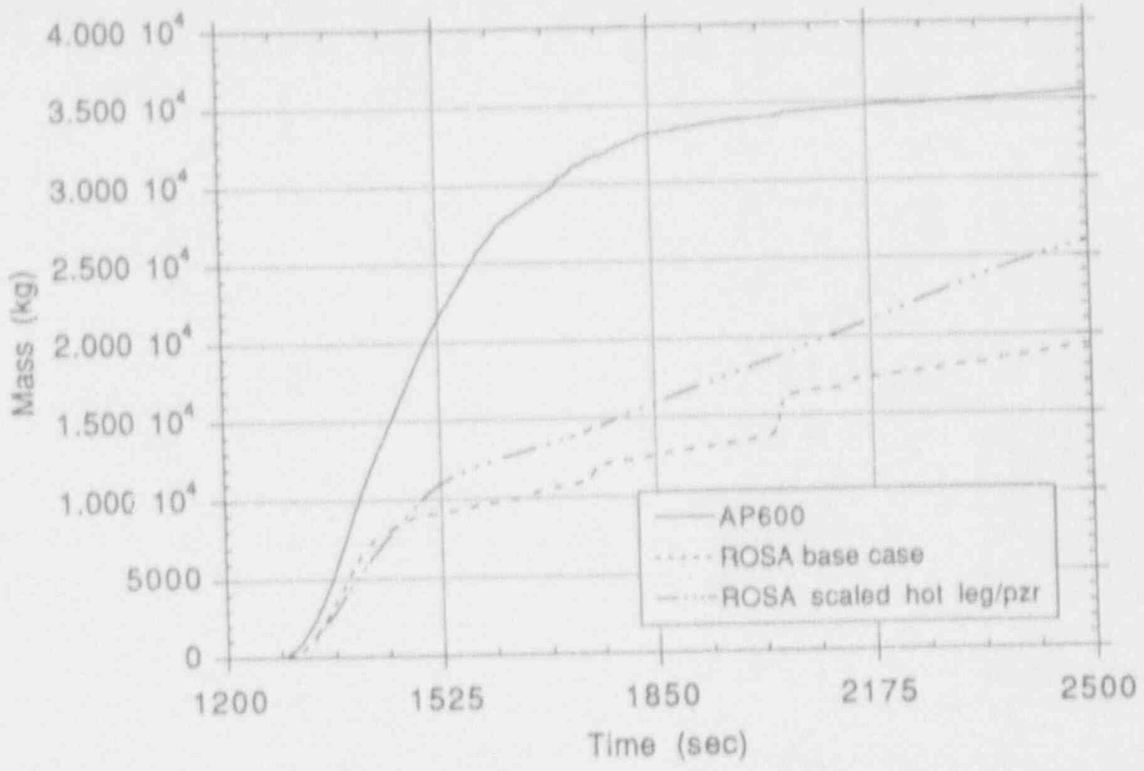

Figure 39. Integrated Stage 3 ADS mass flow rate for 3–inch CLB calculations.

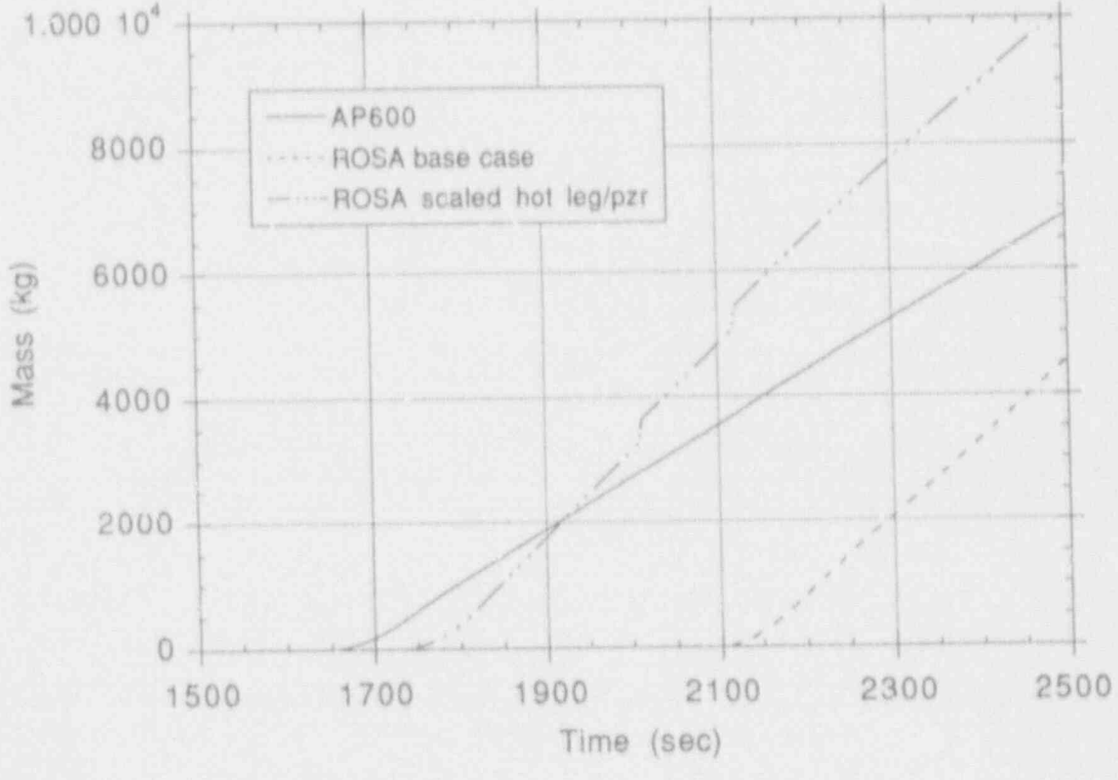

Figure 40. Integrated Stage 4 ADS mass flow rate for 3–inch CLB calculations.

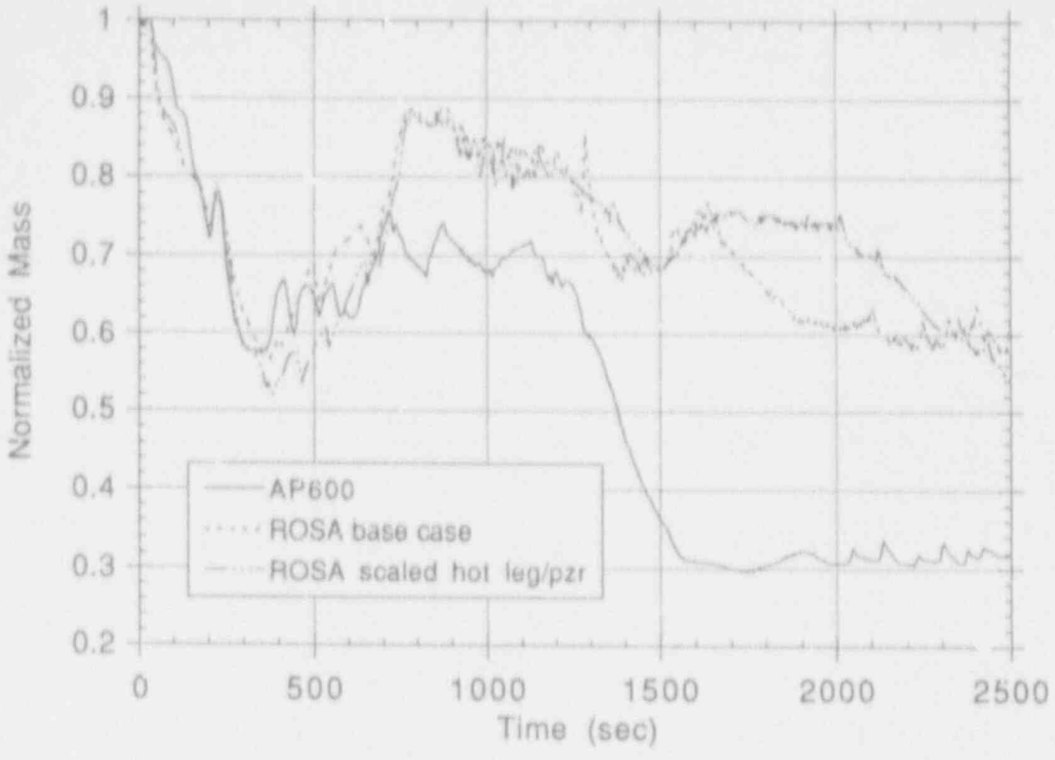

Figure 41. Vessel normalized mass inventory for 3–inch CLB calculations.

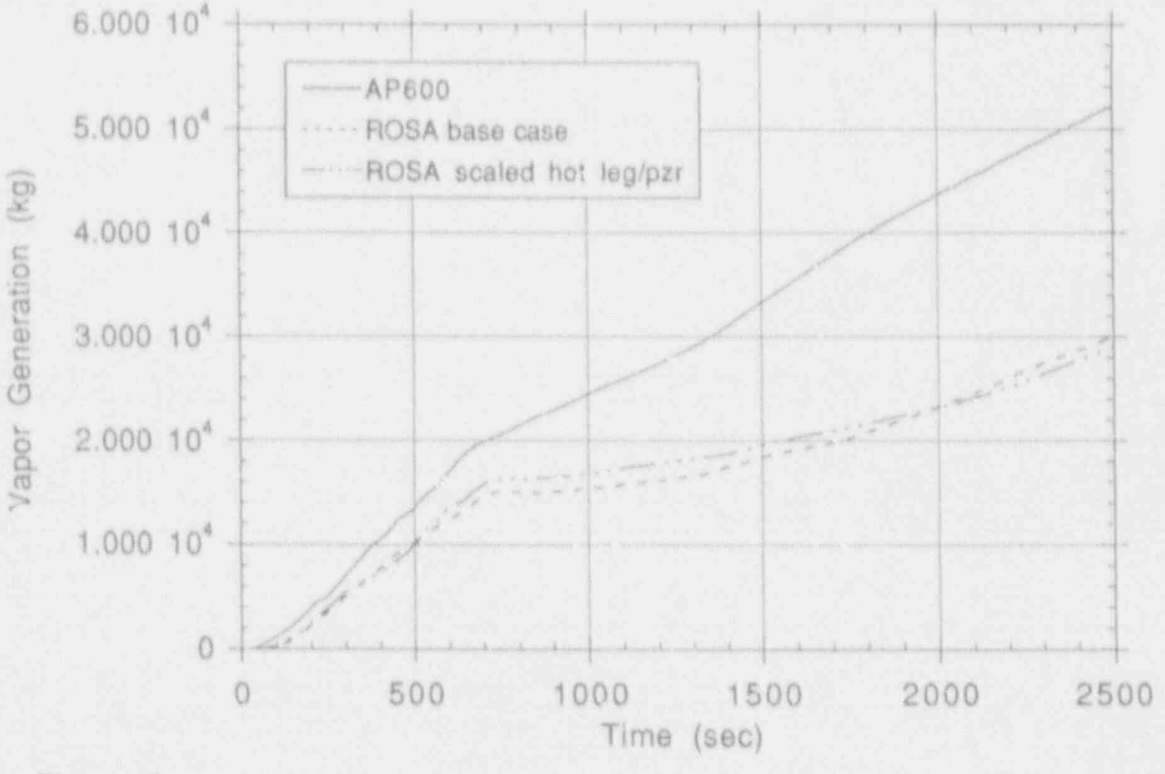

Figure 42. Lower plenum/core/upper plenum integrated vapor generation rate for 3–inch CLB calculations.

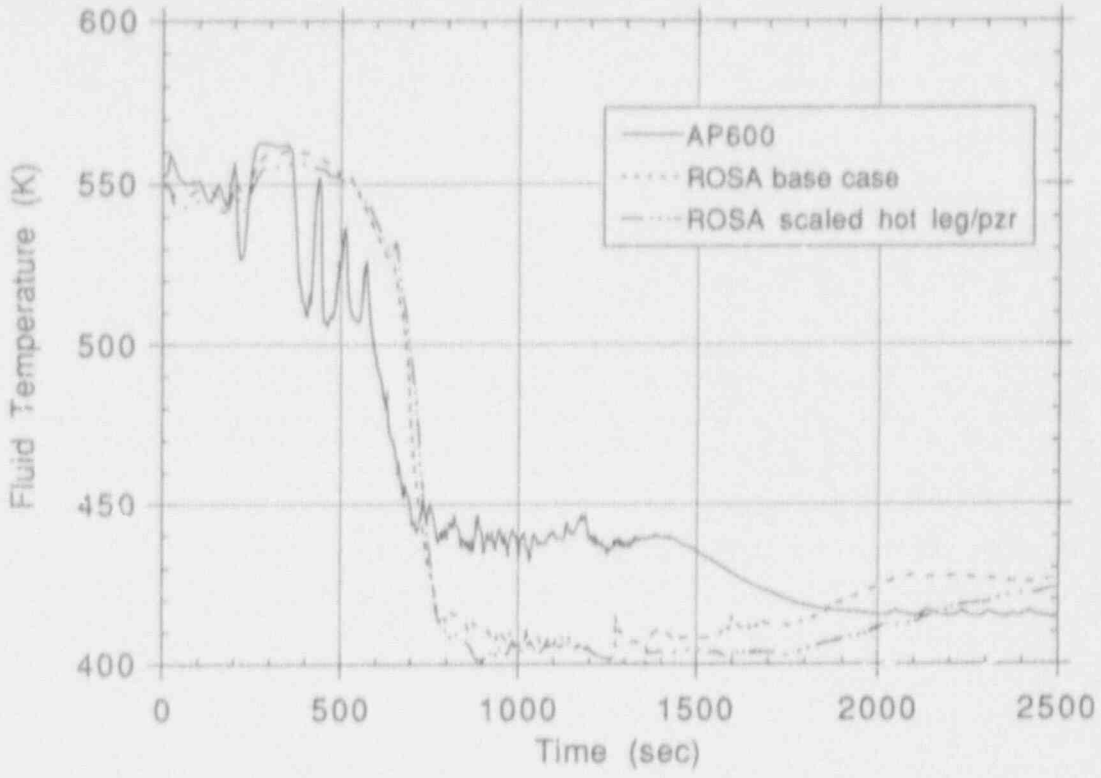

Figure 43. Core inlet fluid temperatures for 3-inch CLB calculations.

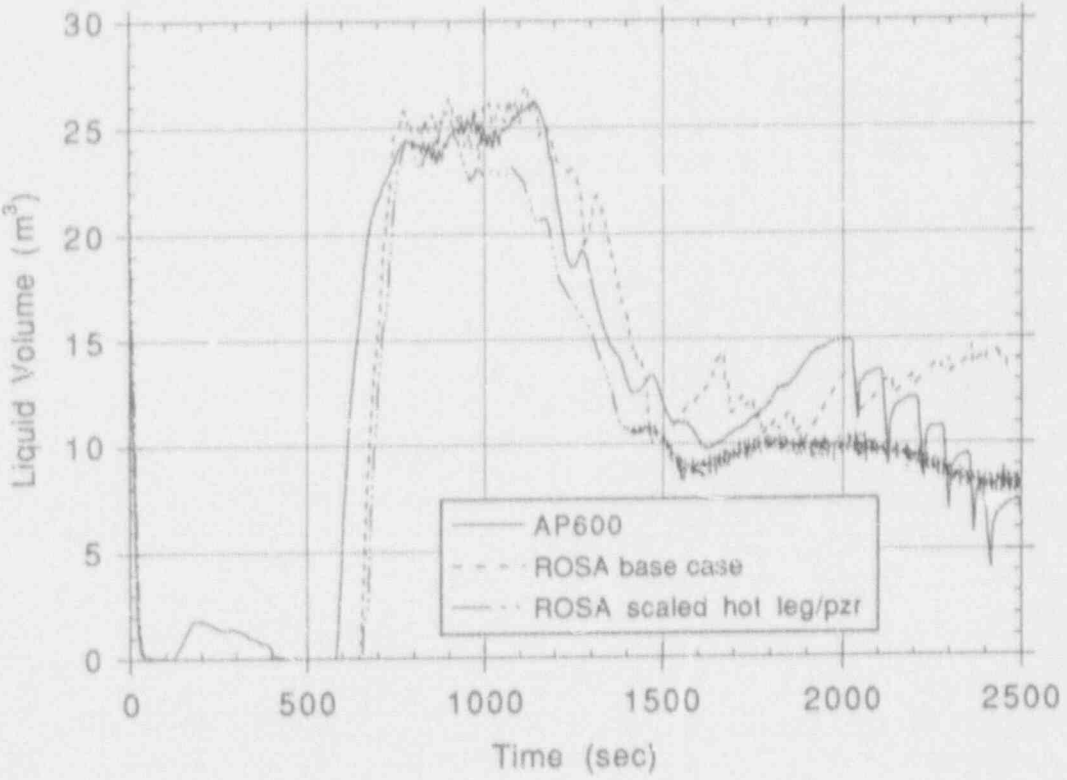

Figure 44. Total pressurizer liquid volume for 3-inch CLB calculations.

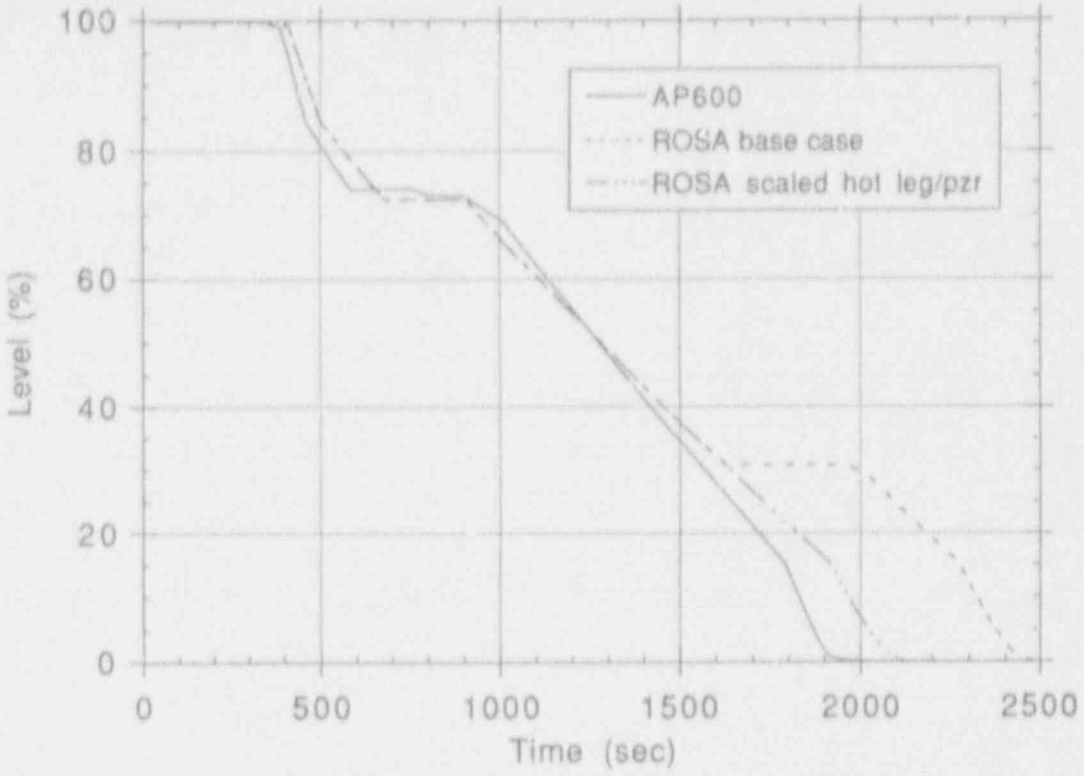

Figure 45. CMT liquid level for 3-inch CLB calculations.

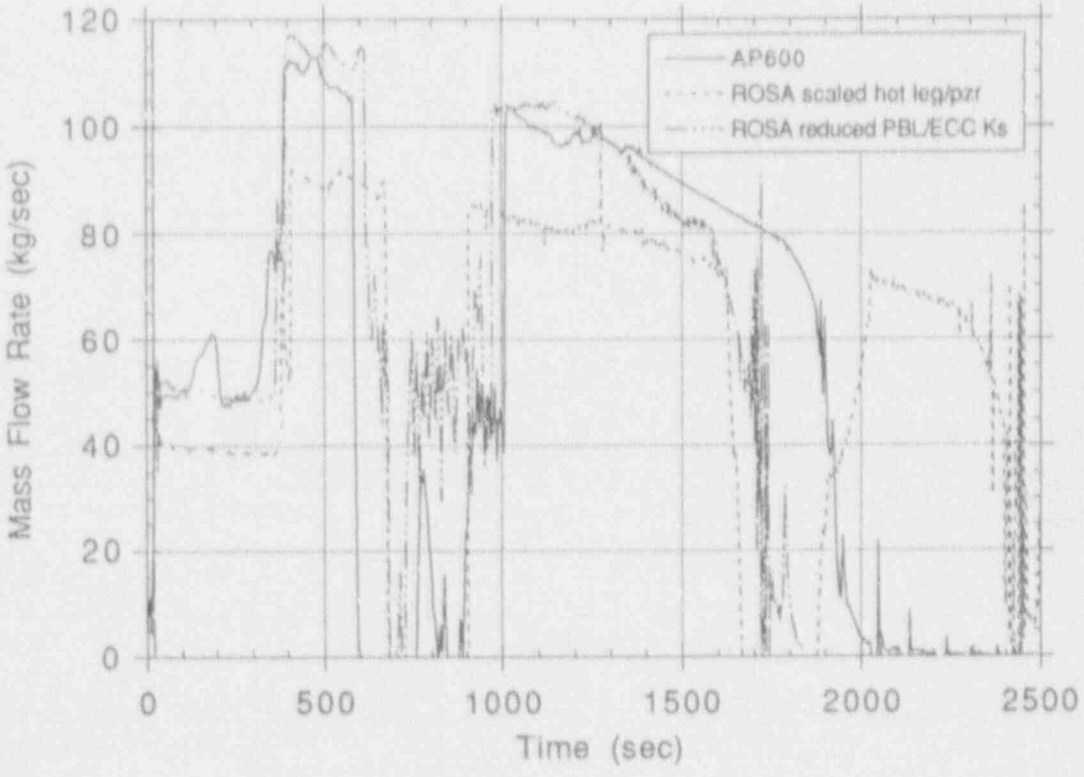

Figure 46. CMT mass flow rates for ROSA and AP600 3-inch CLB calculations.

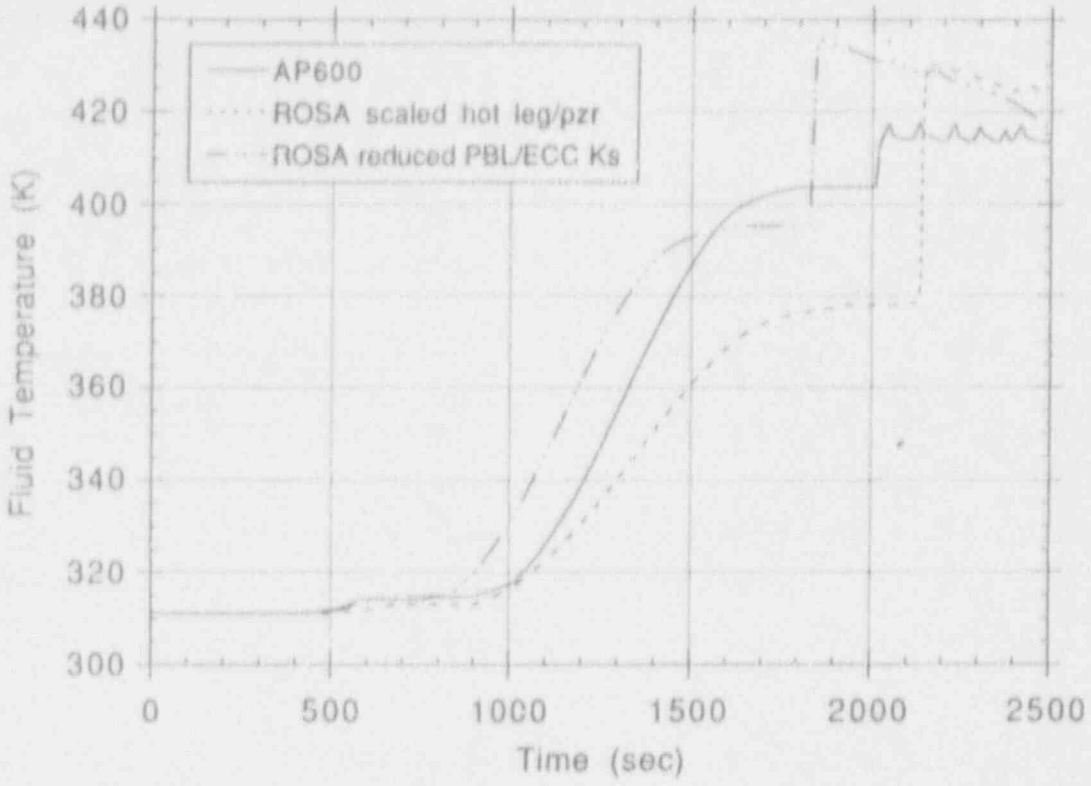

Figure 47. Fluid temperature at bottom of CMT for ROSA and AP600 3–inch CLB calculations.

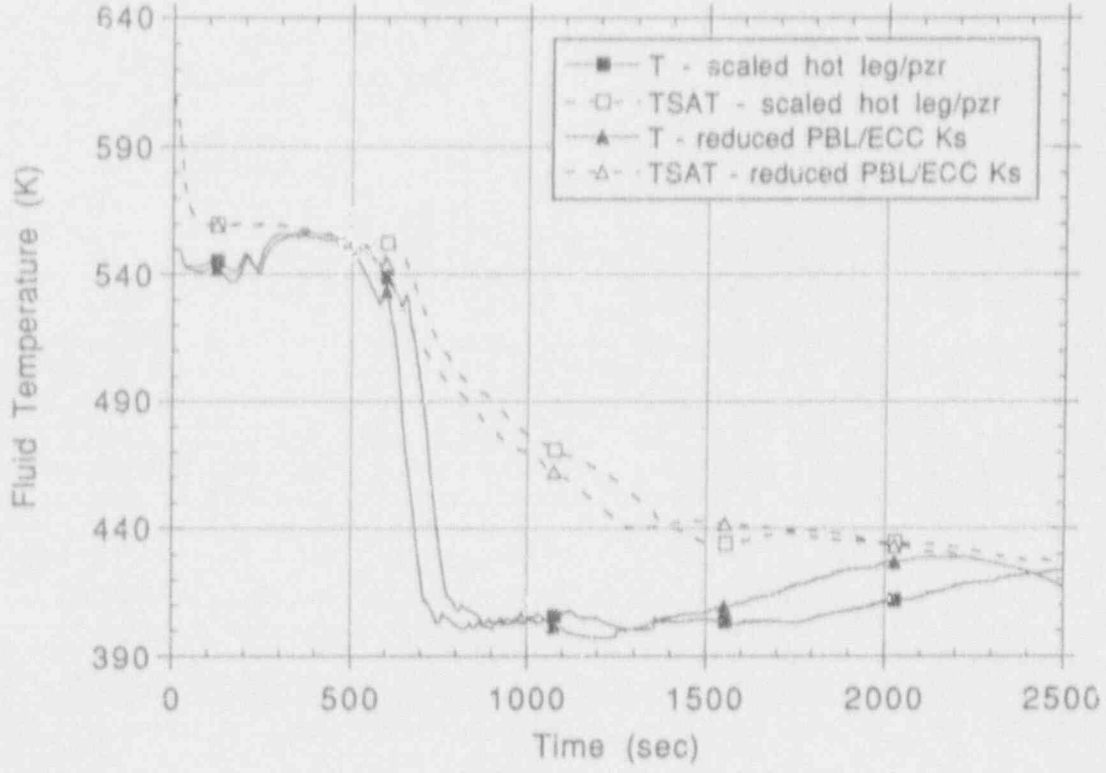

Figure 48. Core inlet fluid temperature and saturation temperature for ROSA 3–inch CLB calculations.

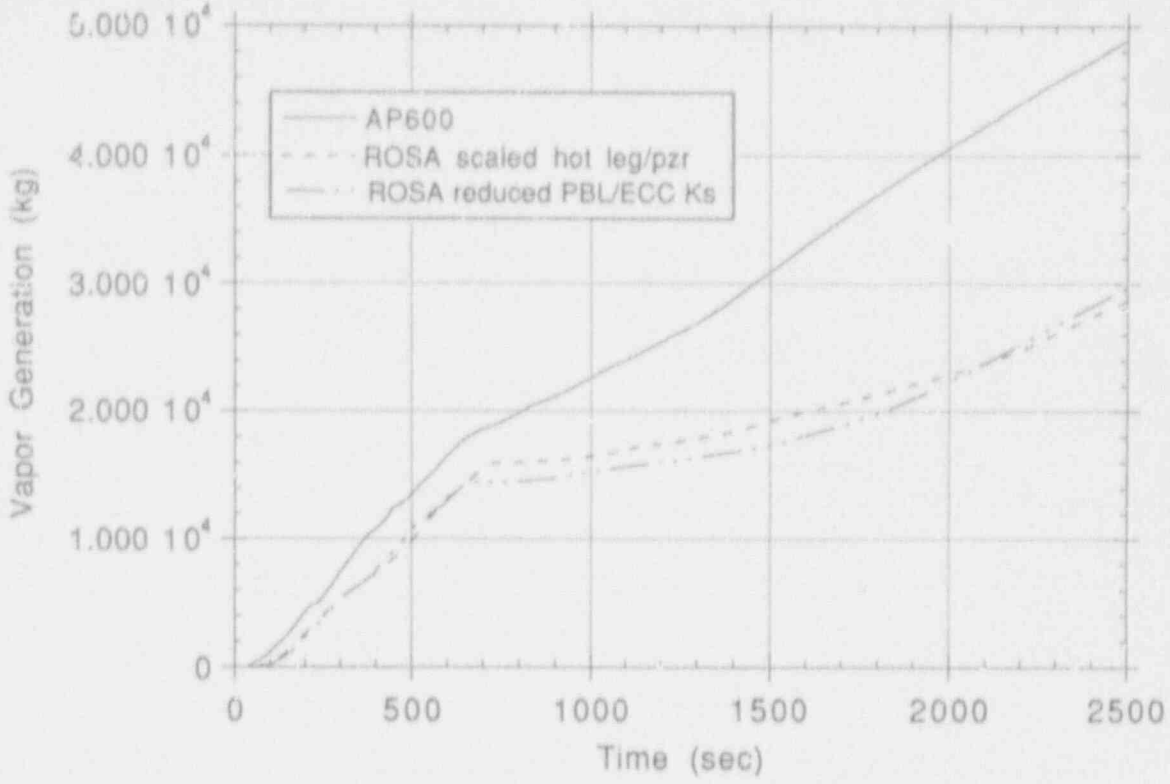

Figure 49. Core vapor generation for ROSA and AP600 MSLB calculations.

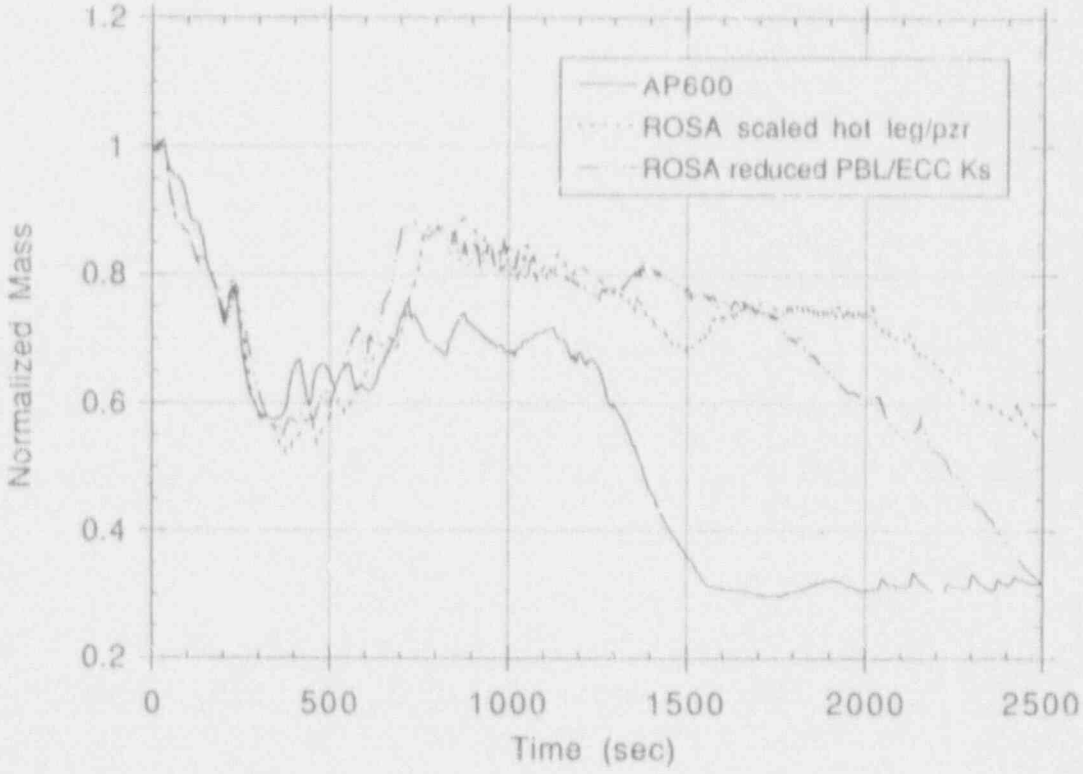

Figure 50. Vessel normalized mass inventory for ROSA and AP600 3-inch CLB calculations.

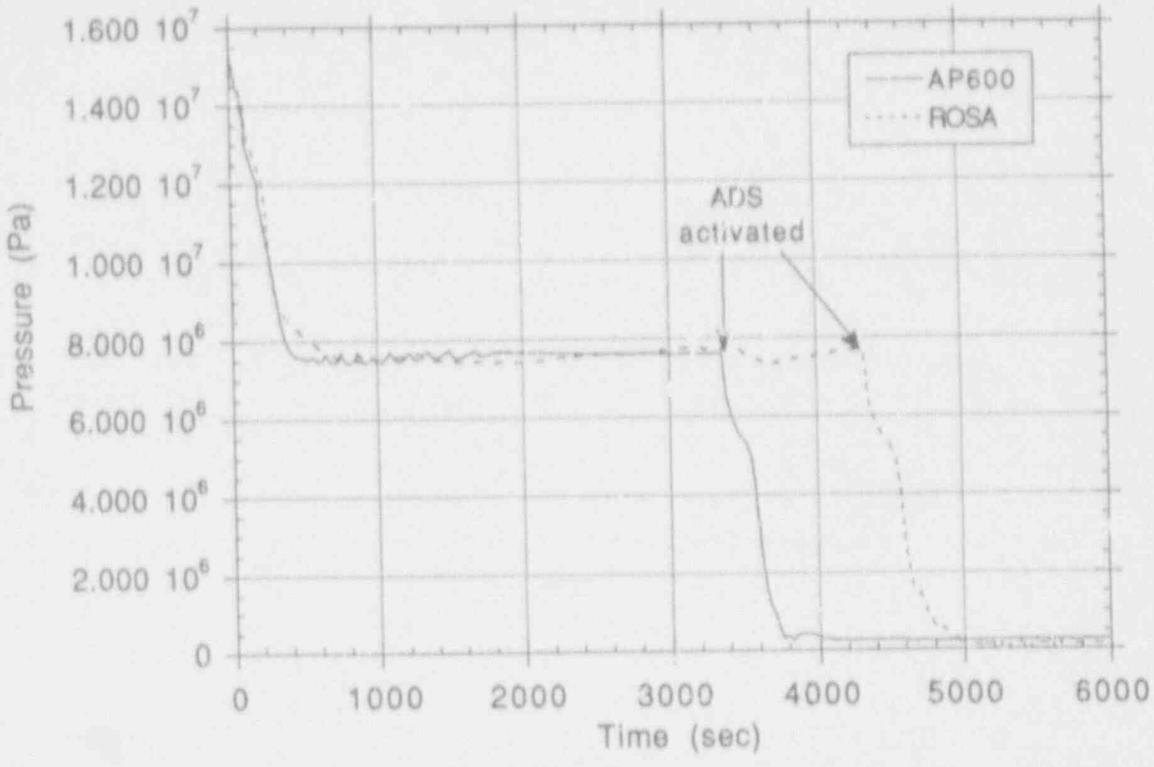

Figure 51. Pressurizer pressures for 1-inch CLB calculations.

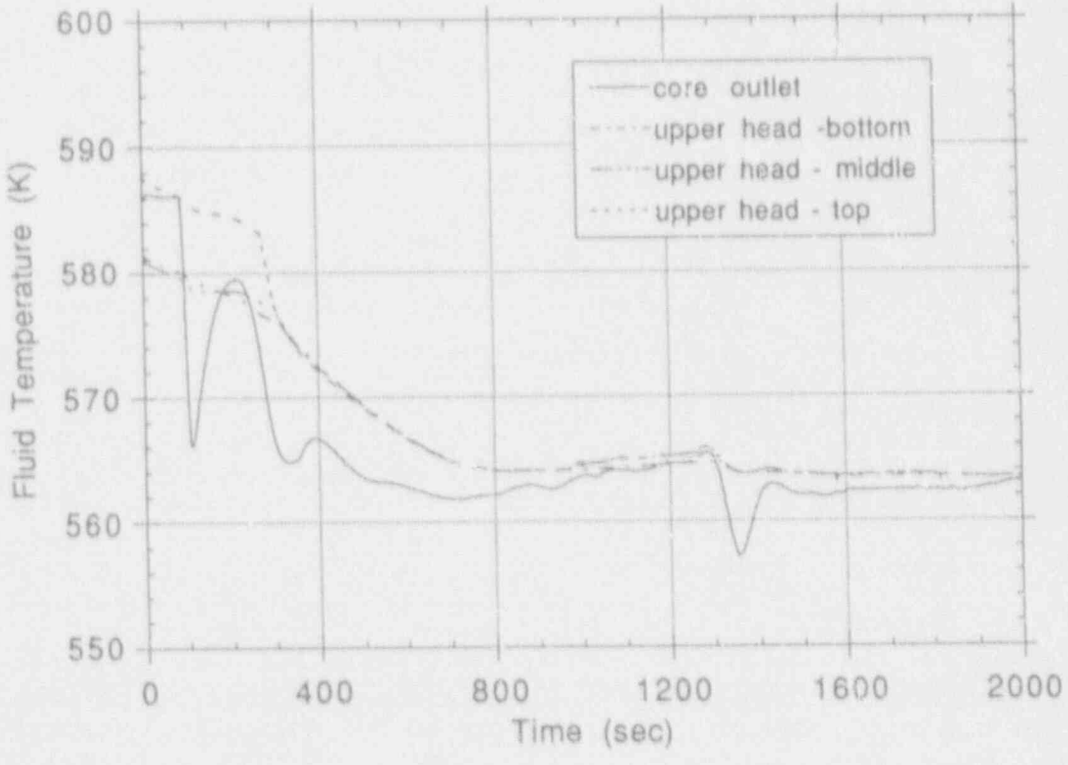

Figure 52. Core outlet and vessel upper head fluid temperatures for ROSA 1-inch CLB calculation.

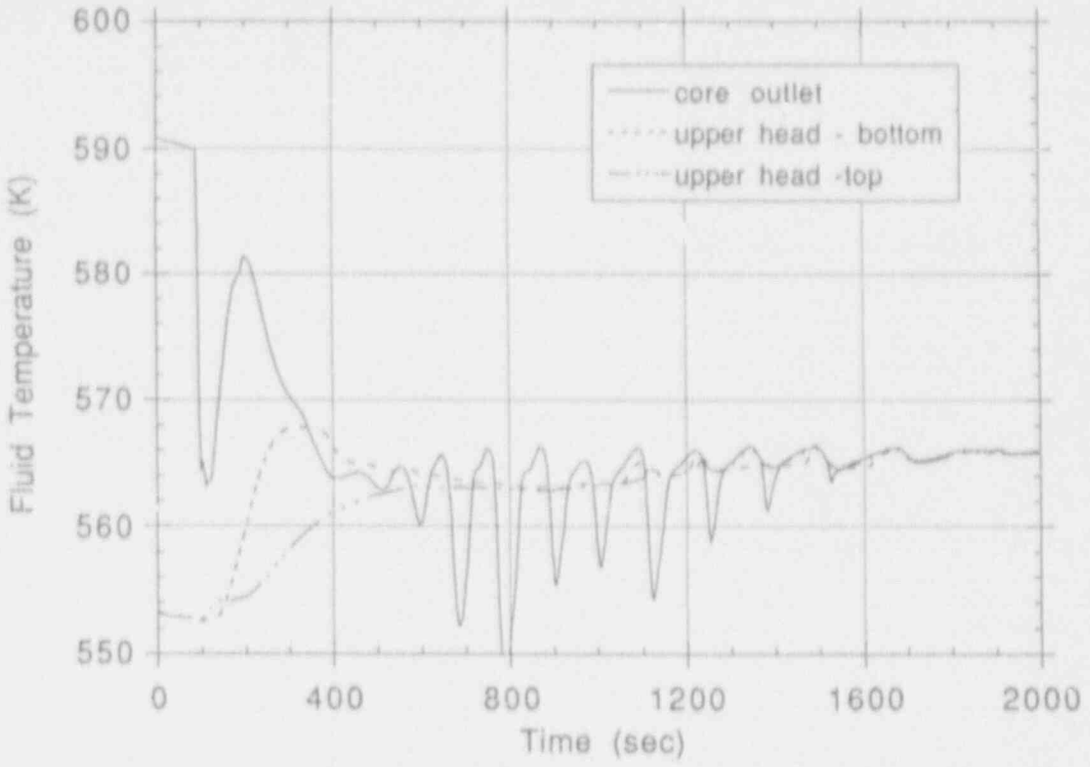

Figure 53. Core outlet and vessel upper head fluid temperatures for AP600 1-inch CLB calculation

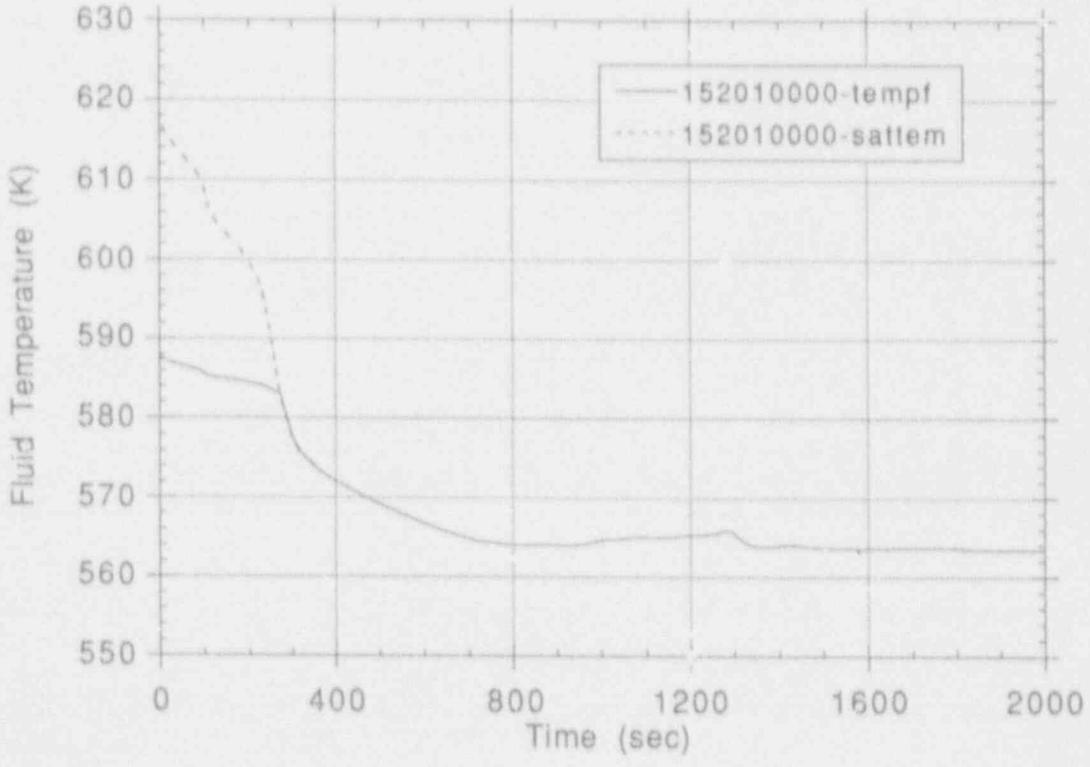

Figure 54. Upper head top volume fluid and saturation temperature for ROSA 1-inch CLB calculation.

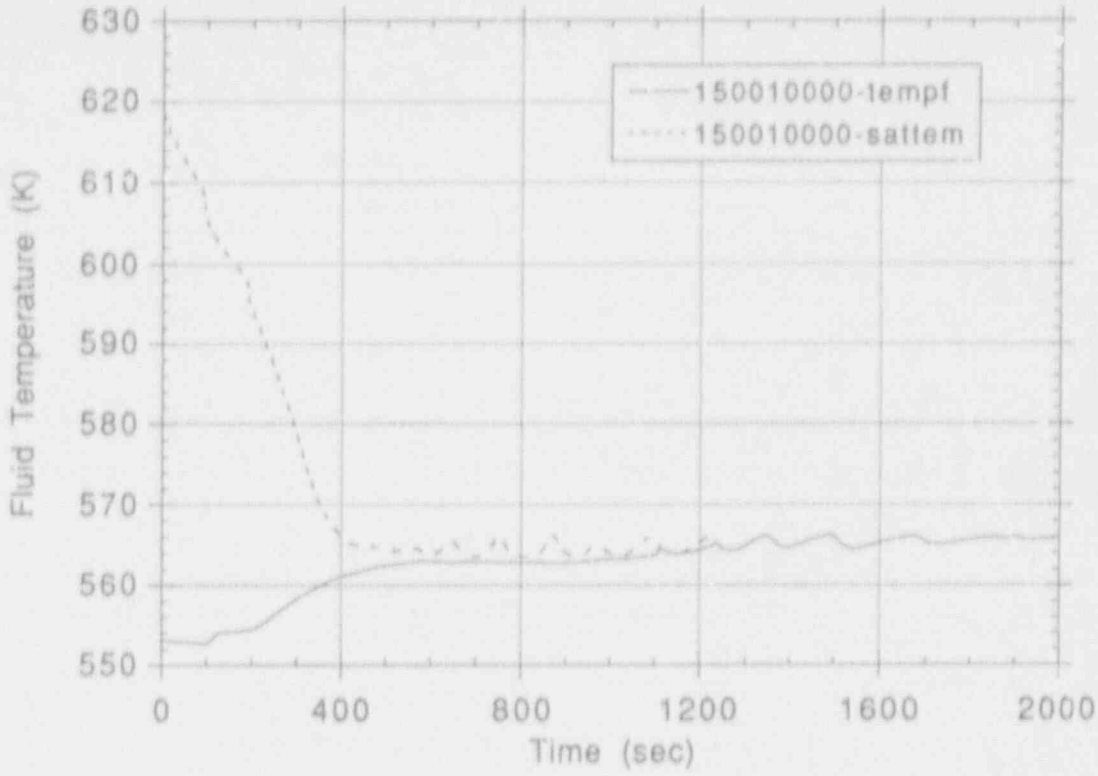

Figure 55. Upper head top volume fluid and saturation temperature for AP600 1-inch CLB calculation.

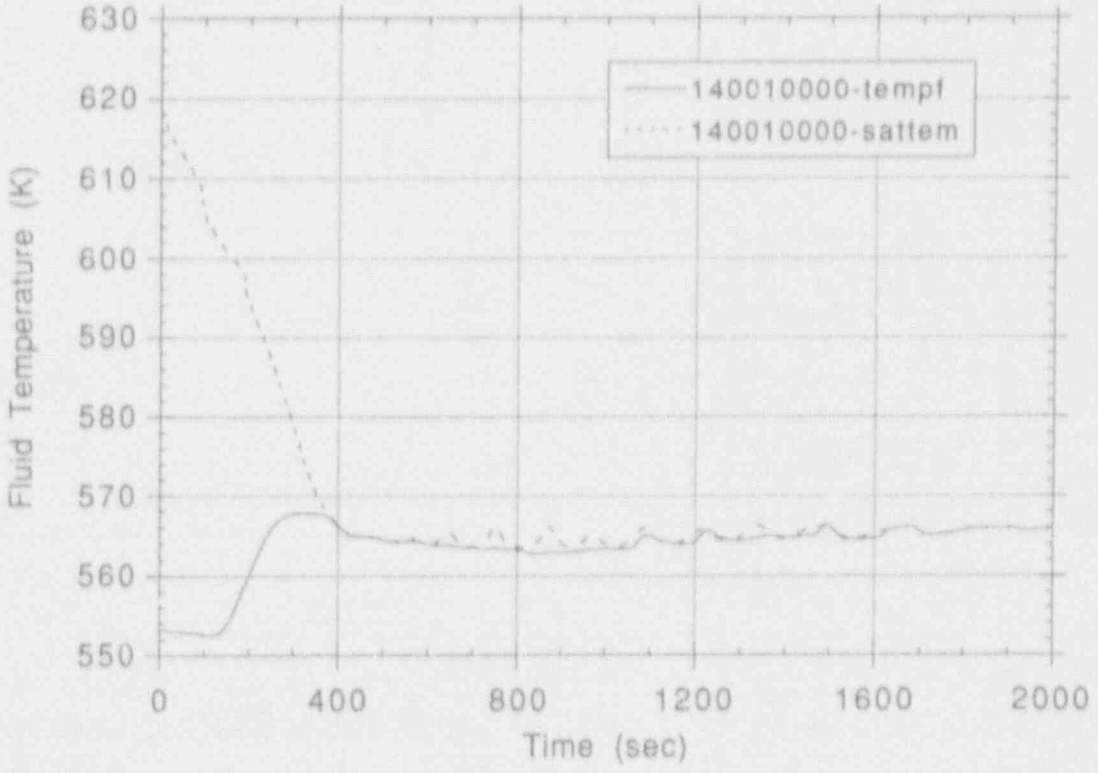

Figure 56. Upper head bottom volume fluid and saturation temperature for AP600 1-inch CLB calculation.

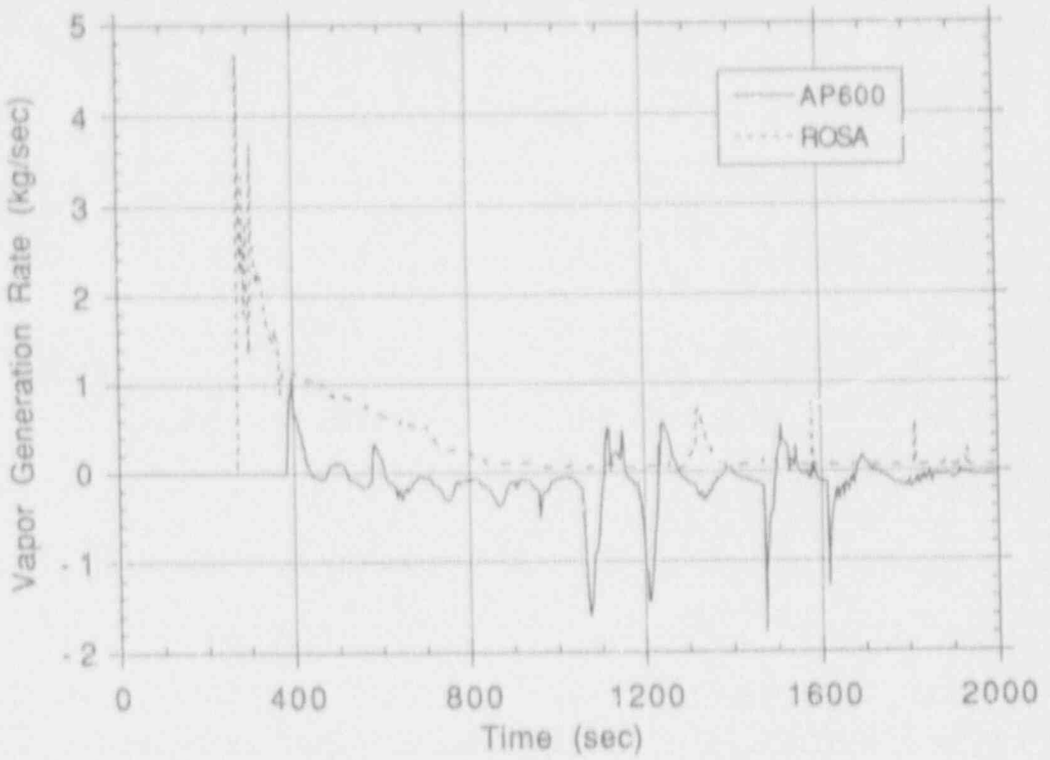

Figure 57. Total upper head vapor generation rates for 1-inch CLB calculations.

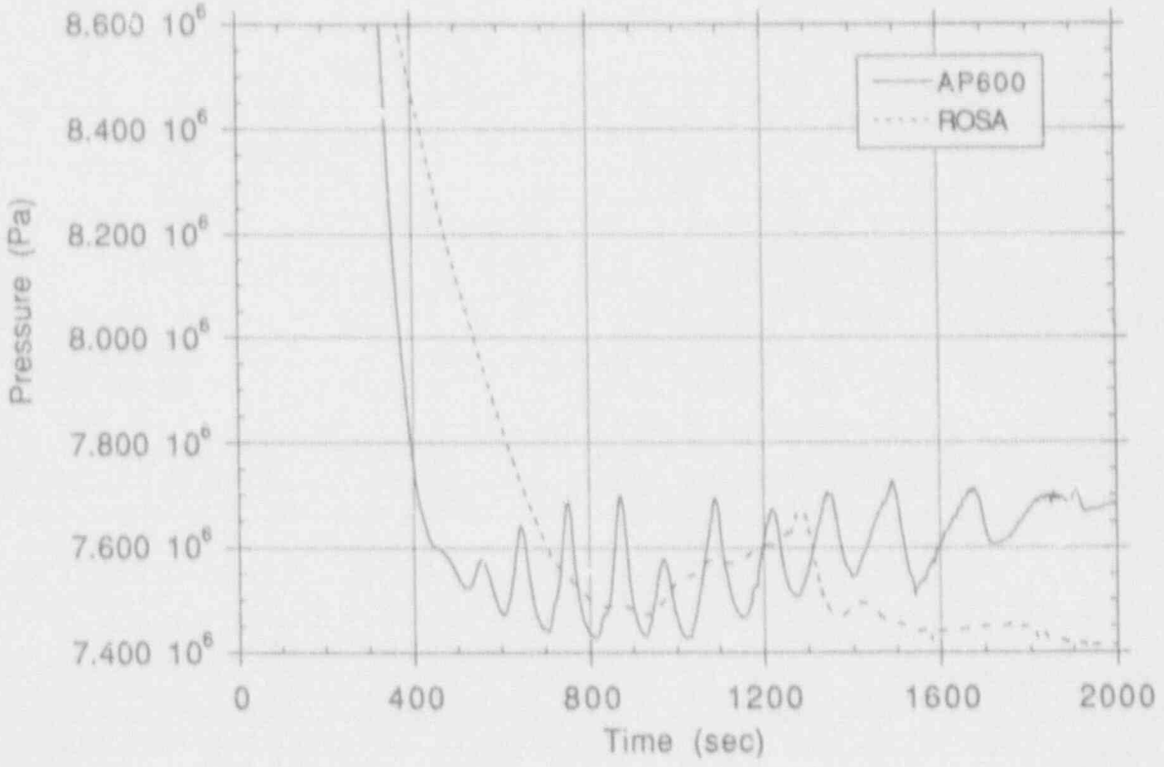

Figure 58. Pressurizer pressures for 1-inch CLB calculations.

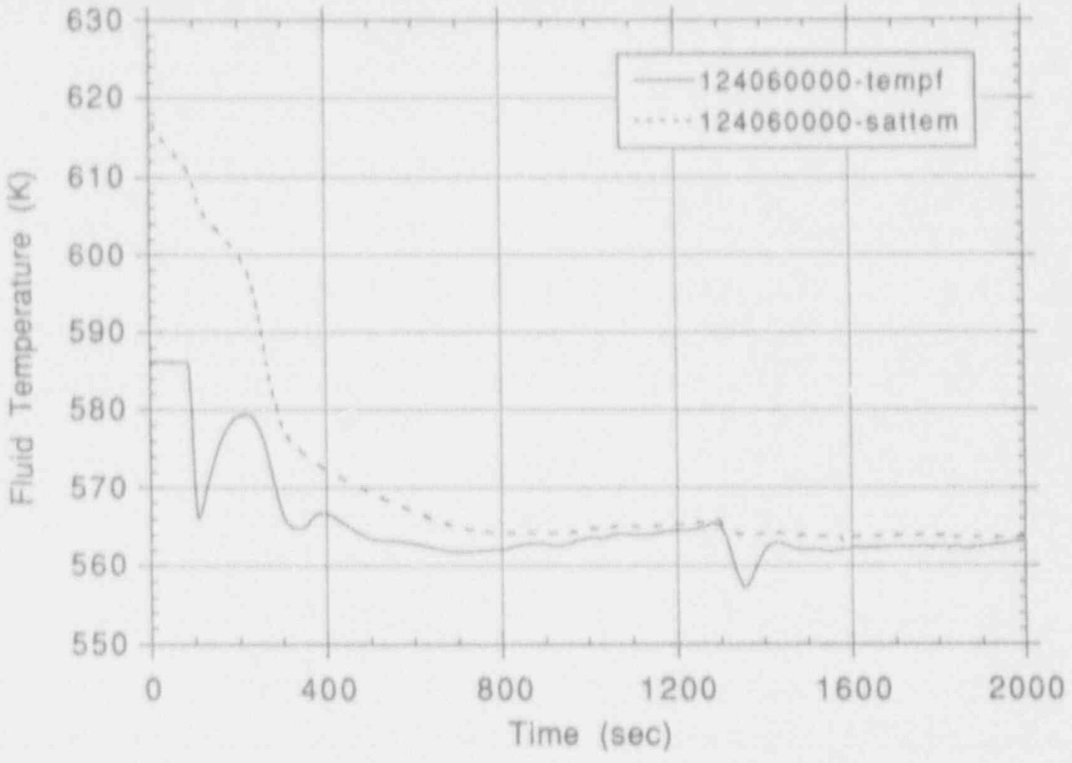

Figure 59. Core outlet fluid temperature and saturation temperature for ROSA 1–inch CLB calculation.

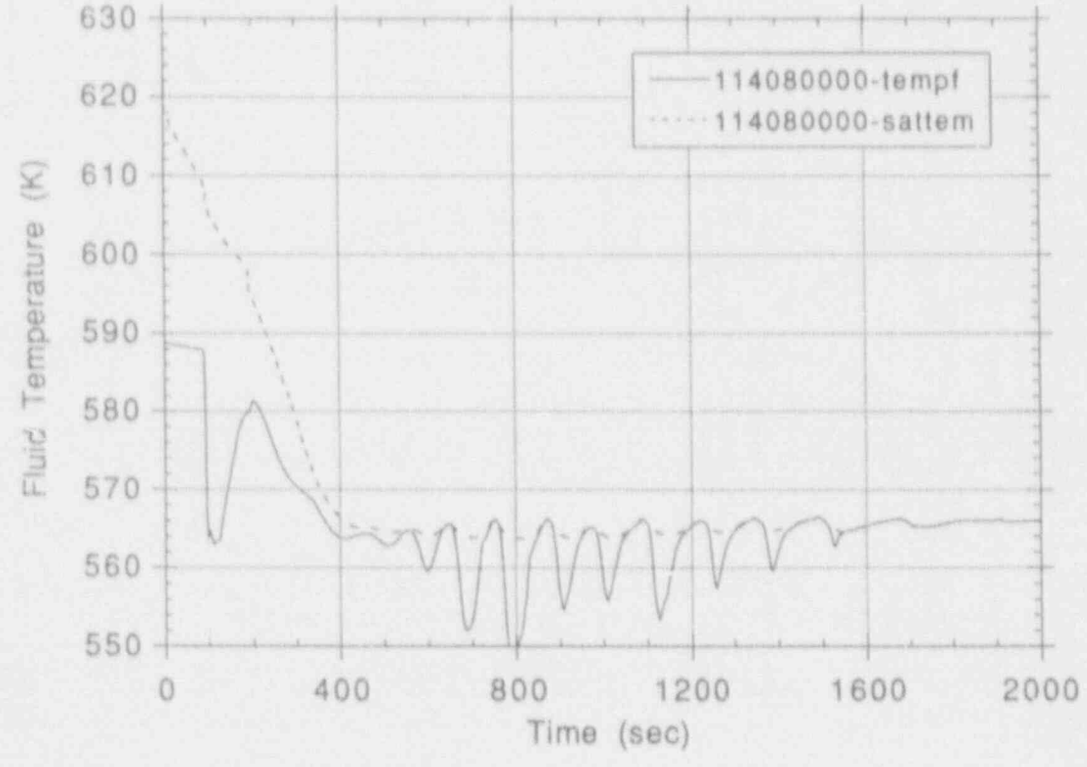

Figure 60. Core outlet fluid temperature and saturation temperature for AP600 1–inch CLB calculation.

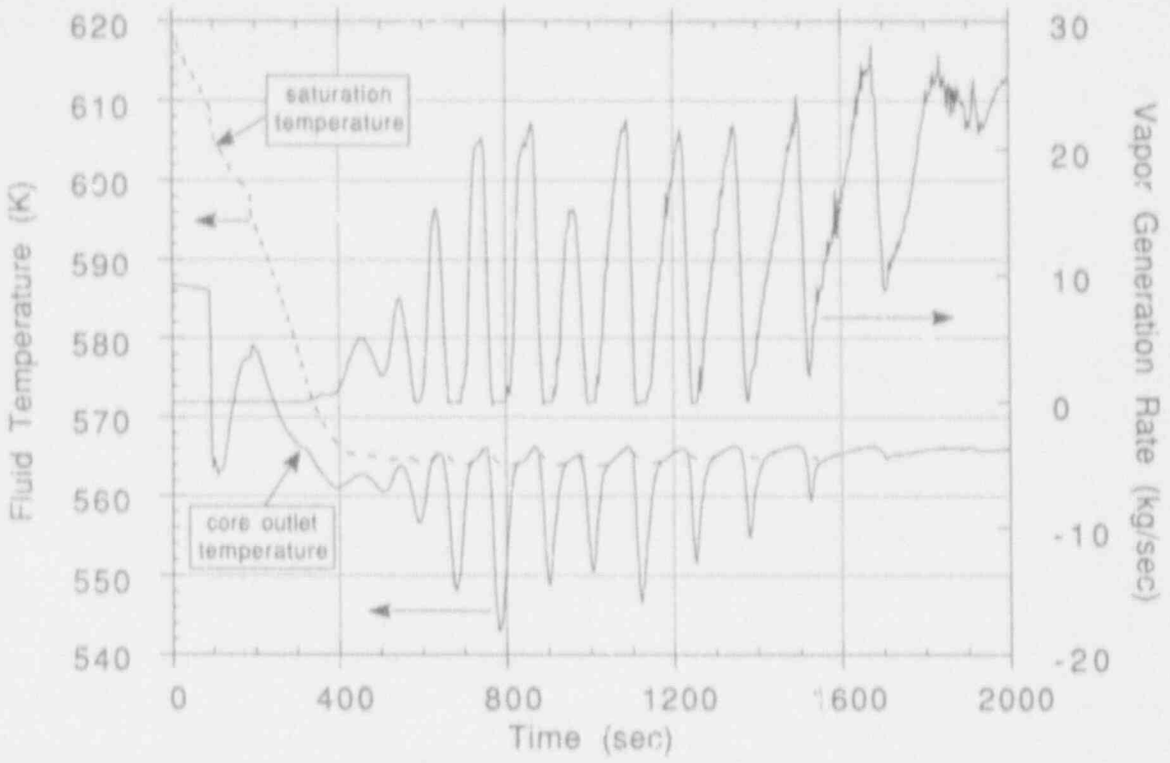

Figure 61. Core outlet fluid temperature and vapor generation rate for AP600 1–inch CLB calculation.

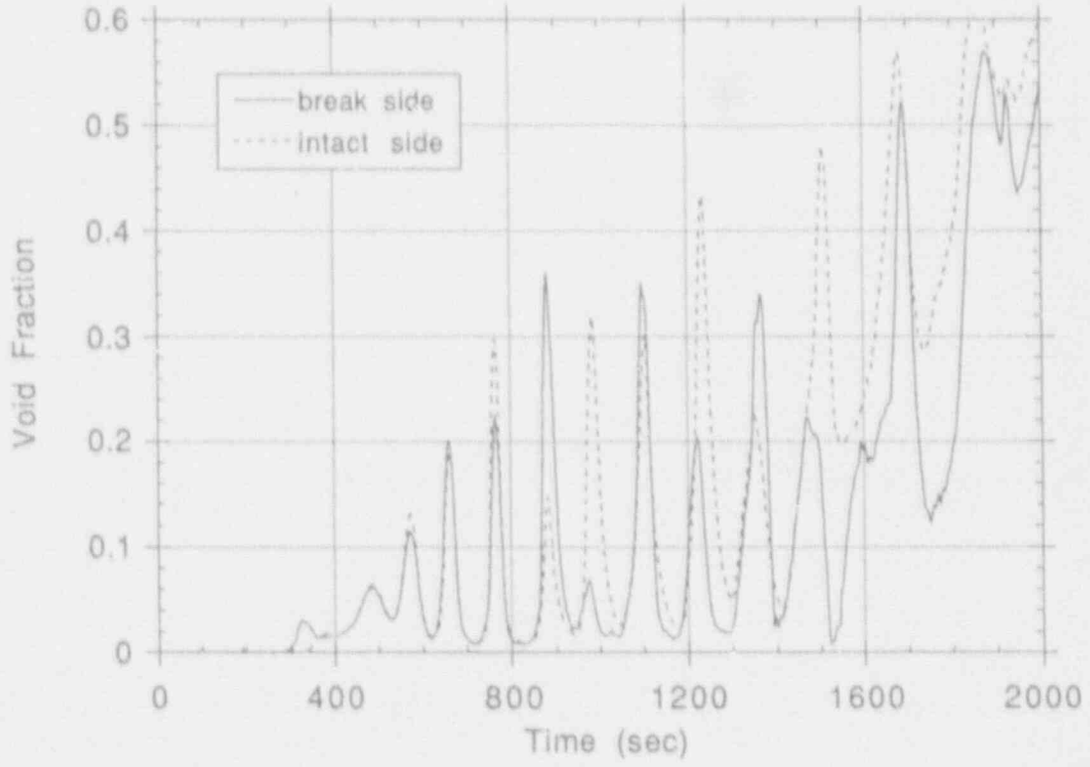

Figure 62. Hot leg vapor void fraction for AP600 1–inch CLB calculation.

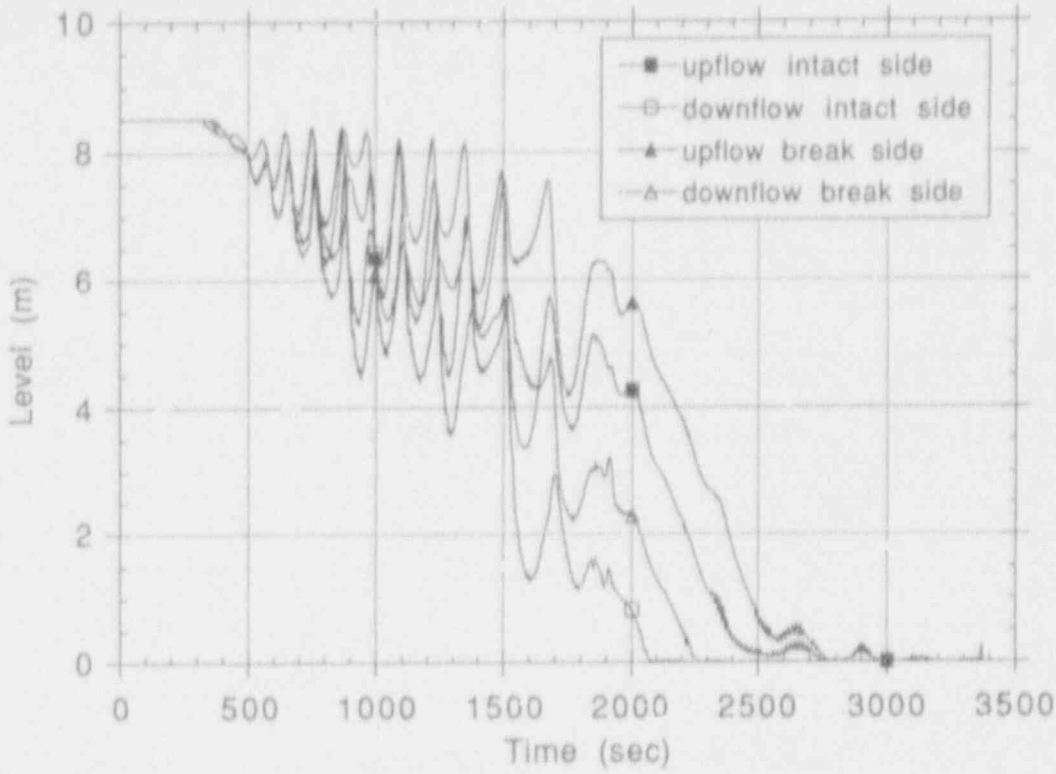

Figure 63. Steam generator U–tube collapsed liquid level for AP600 1–inch CLB calculation.

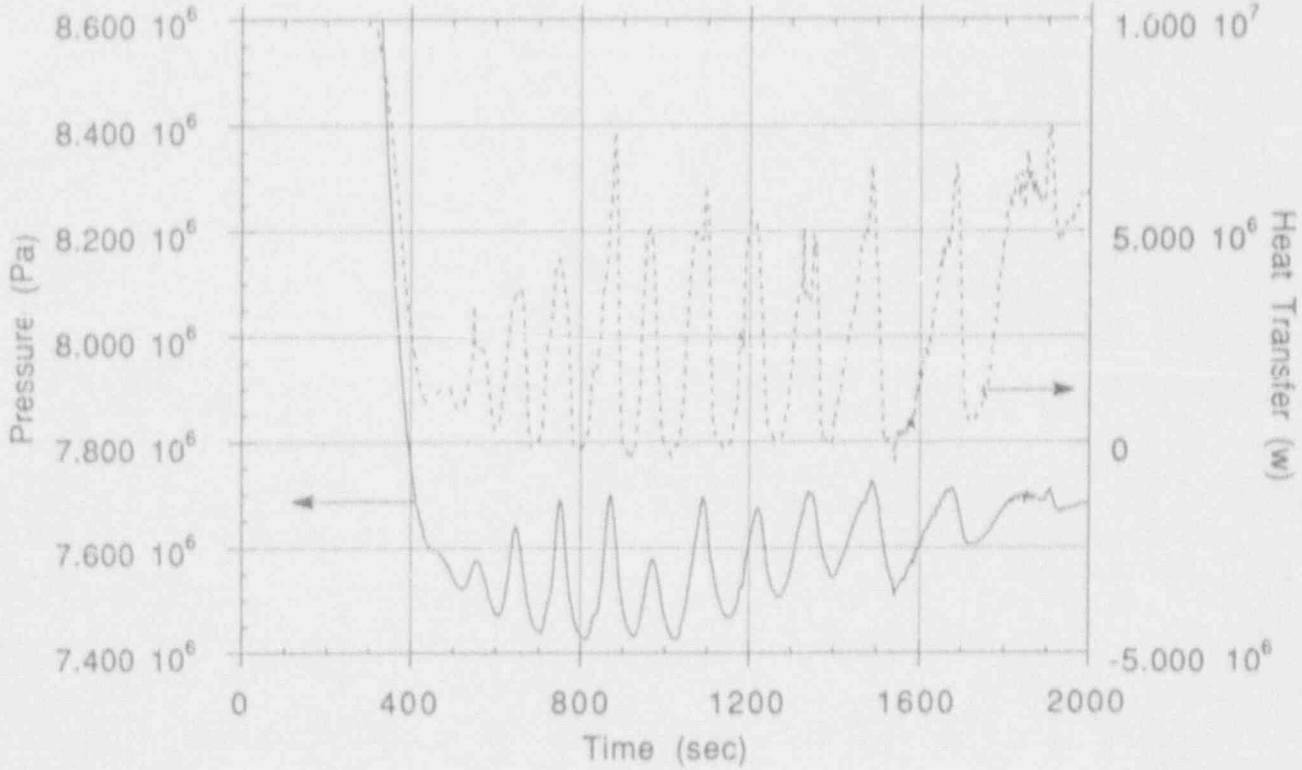

Figure 64. Primary pressure and break side SG heat transfer to secondary for AP600 1–inch CLB calculation.

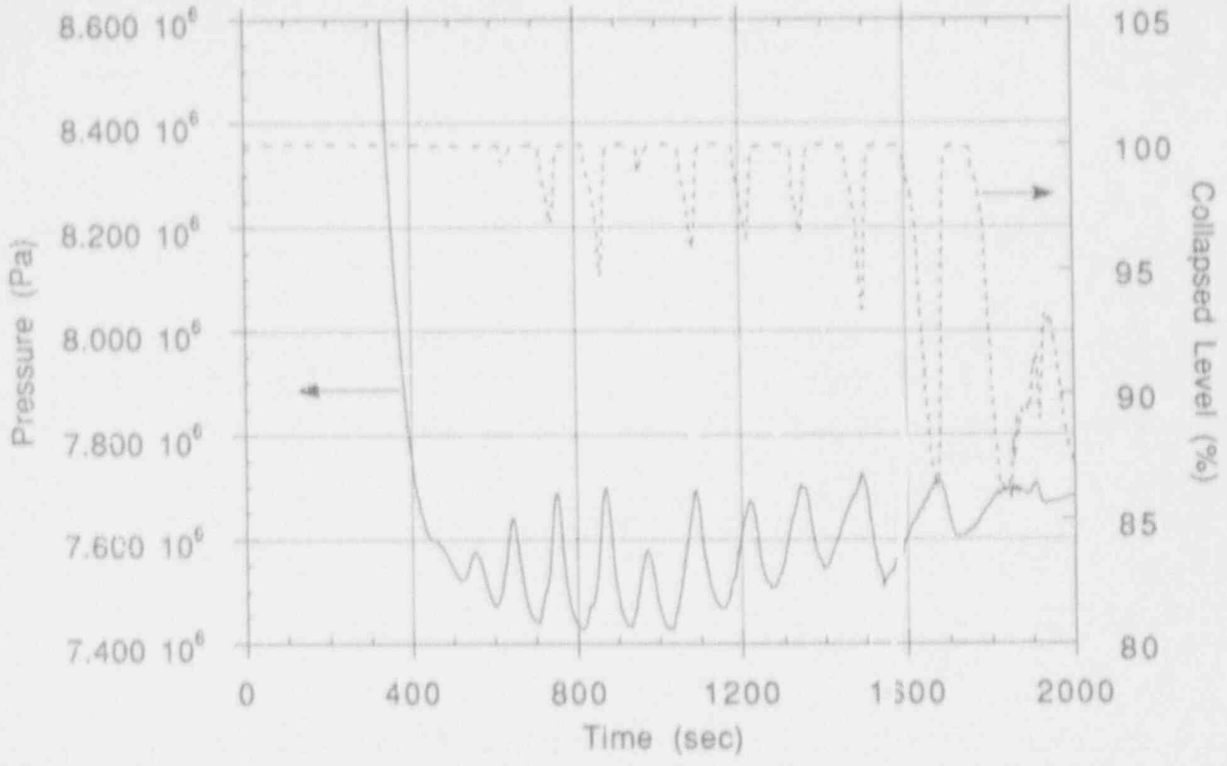

Figure 65. System pressure and core collapsed liquid level for AP600 1–inch CLB.

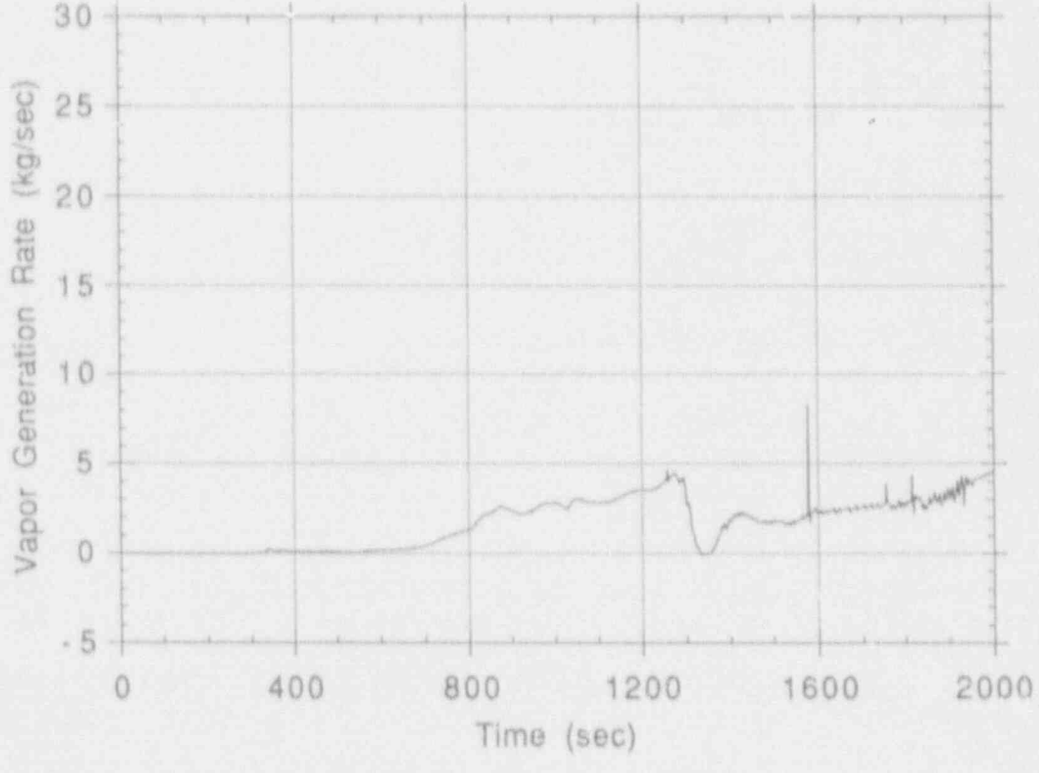

Figure 66. Total vessel vapor generation rate for ROSA 1–inch CLB calculation.

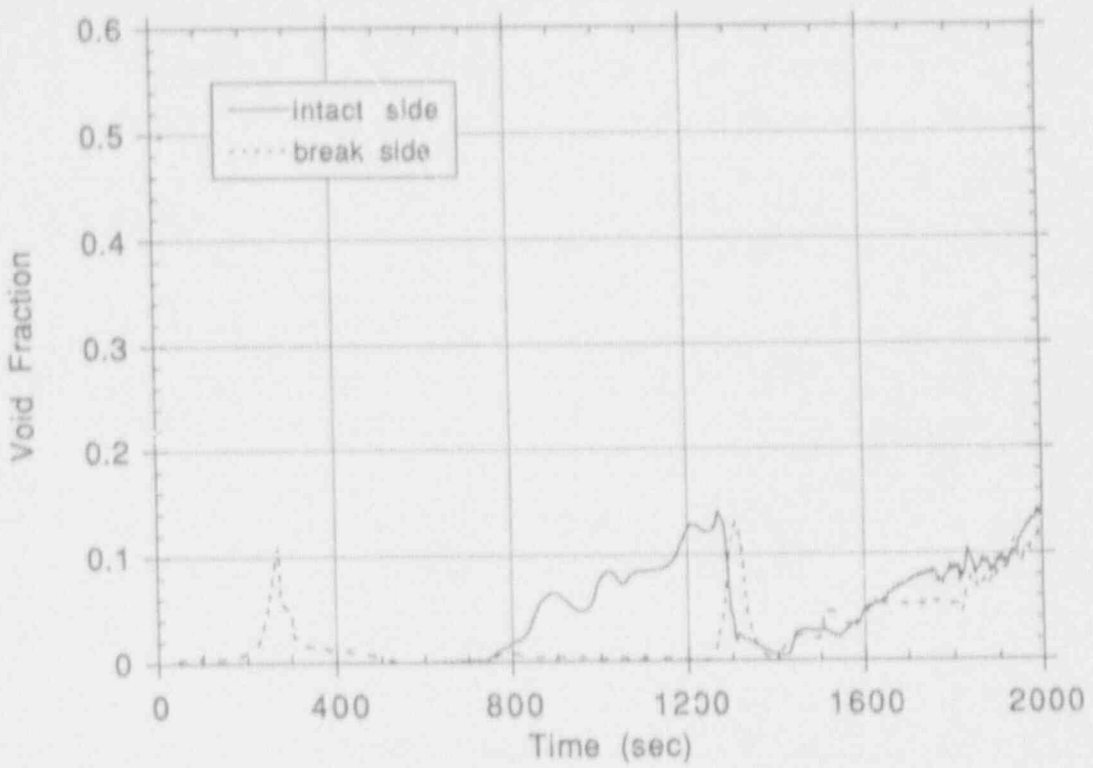

Figure 67. Hot leg vapor void fraction for ROSA 1–inch CLB calculation.

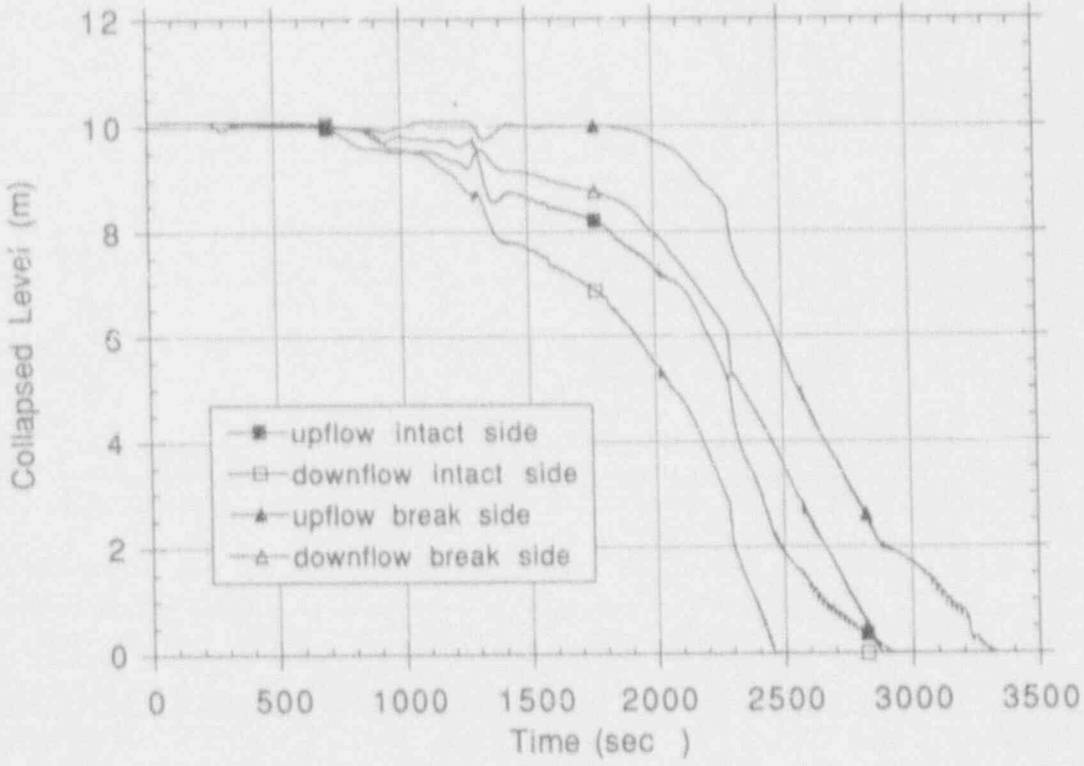

Figure 68. Steam generator U–tube collapsed liquid level for ROSA 1–inch CLB calculation.

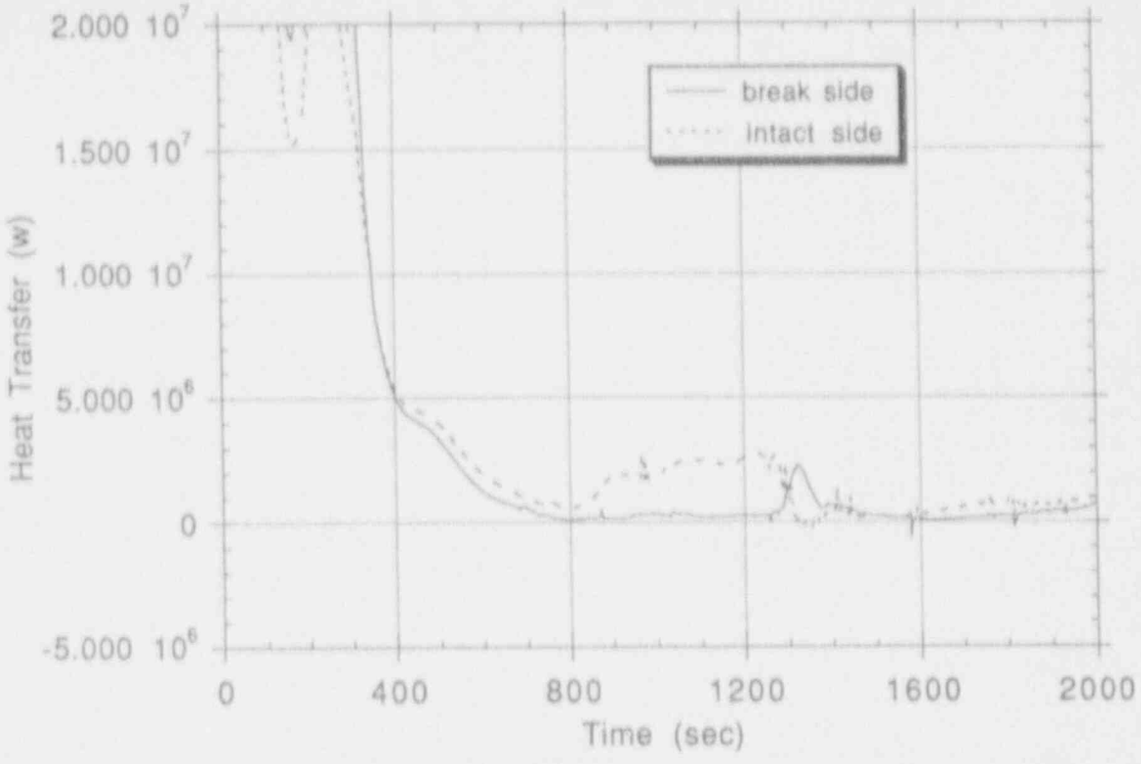

Figure 69. Intact and break side SG primary-to-secondary heat transfer for ROSA 1-inch CLB calculation.

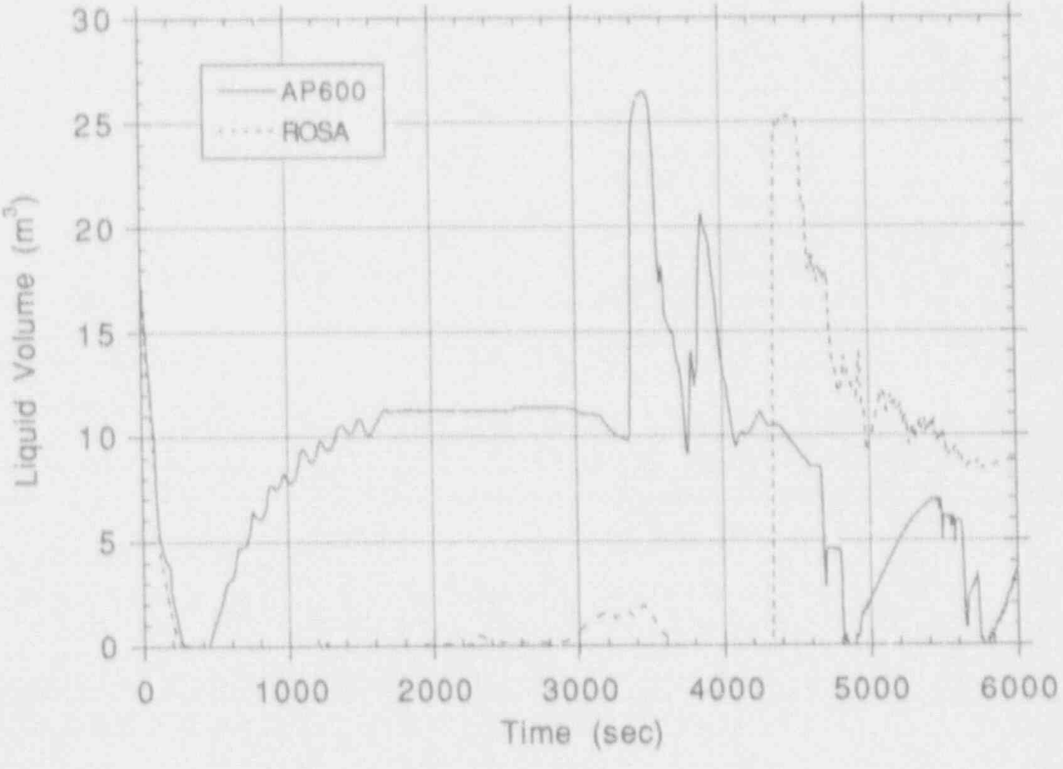

Figure 70. Pressurizer liquid volume for 1-inch CLB calculations.

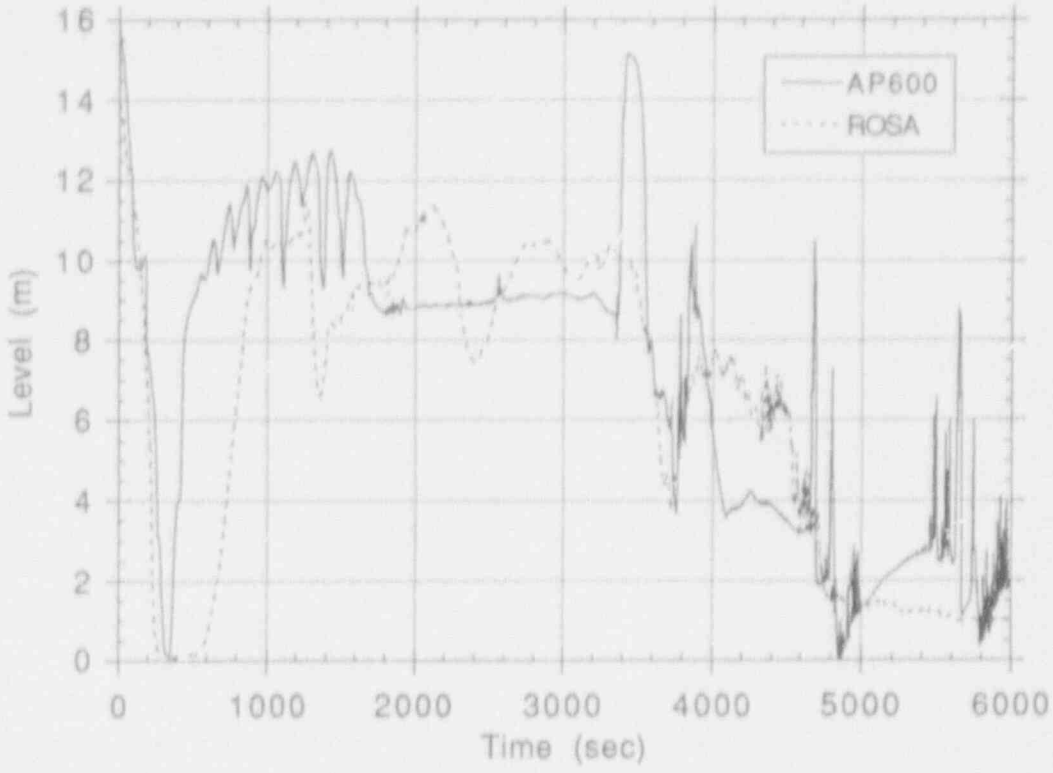

Figure 71. Pressurizer and surge line combined collapsed liquid level for 1-inch CLB.

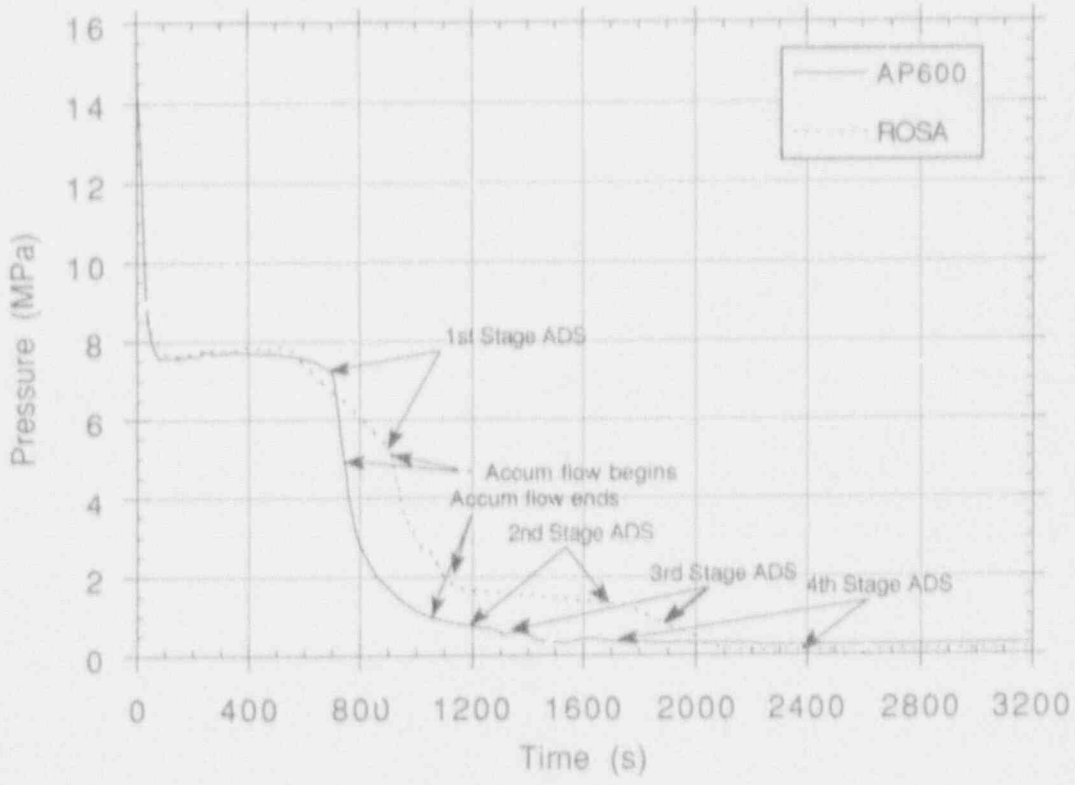

Figure 72. Pressure at the top of the pressurizer for the pressure balance line break.

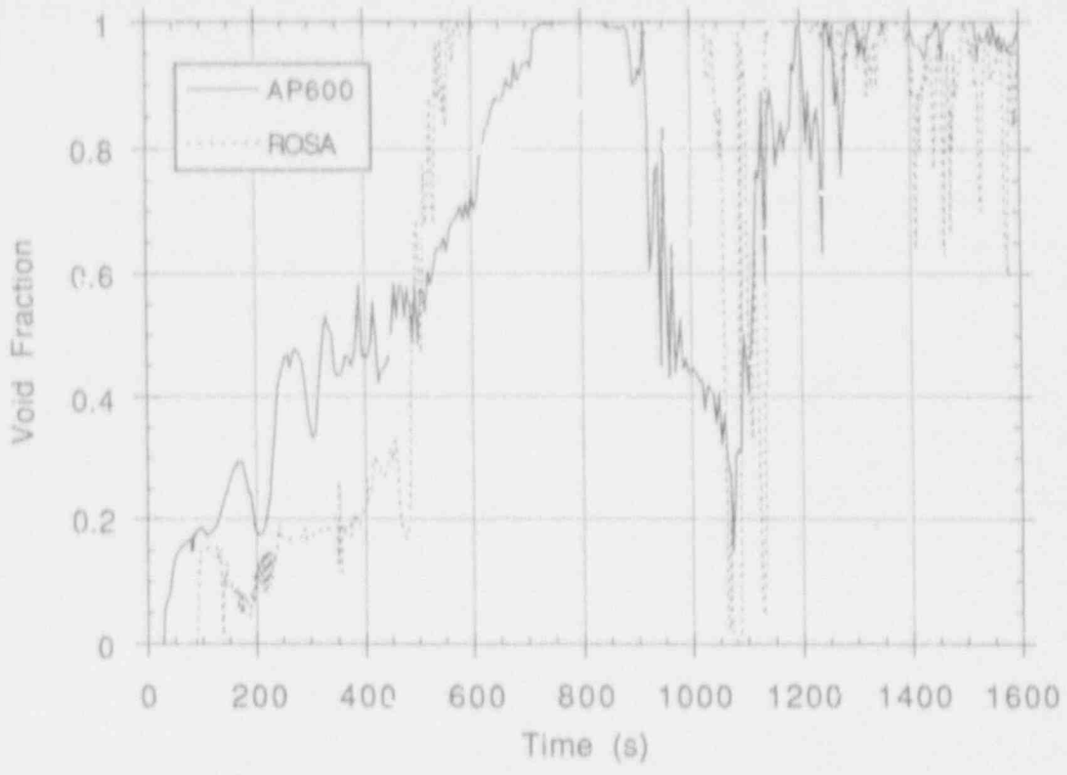

Figure 73. Void fraction of the fluid discharged through the break for the pressure balance line break.

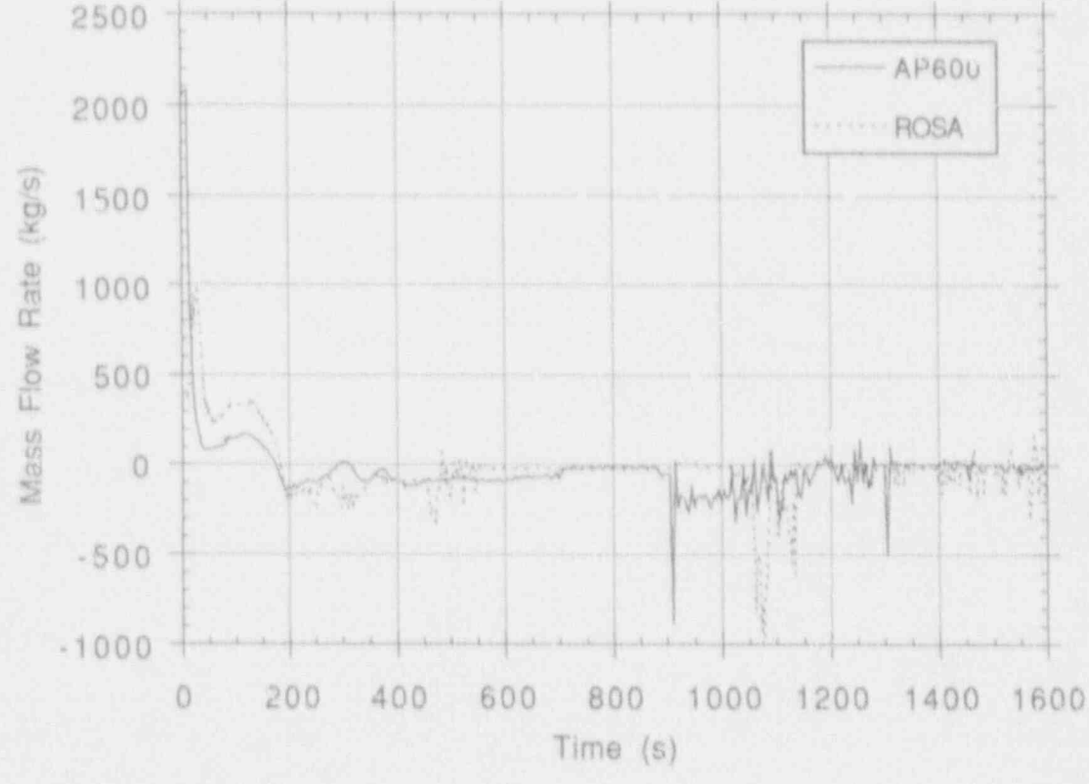

Figure 74. Mass flow rate at the connection of the affected cold leg to the reactor vessel downcomer for the pressure balance line break.

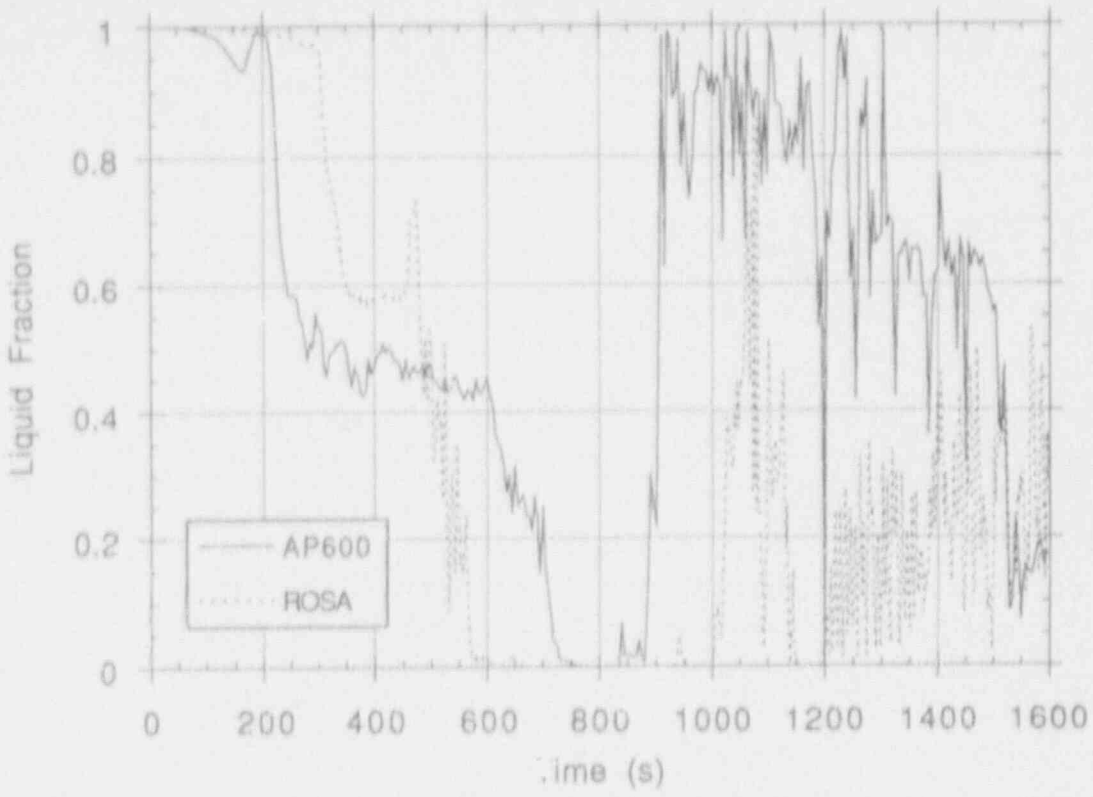

Figure 75. Liquid fraction (one minus the void fraction) in the downcomer volume connected to the affected cold leg for the pressure balance line break.

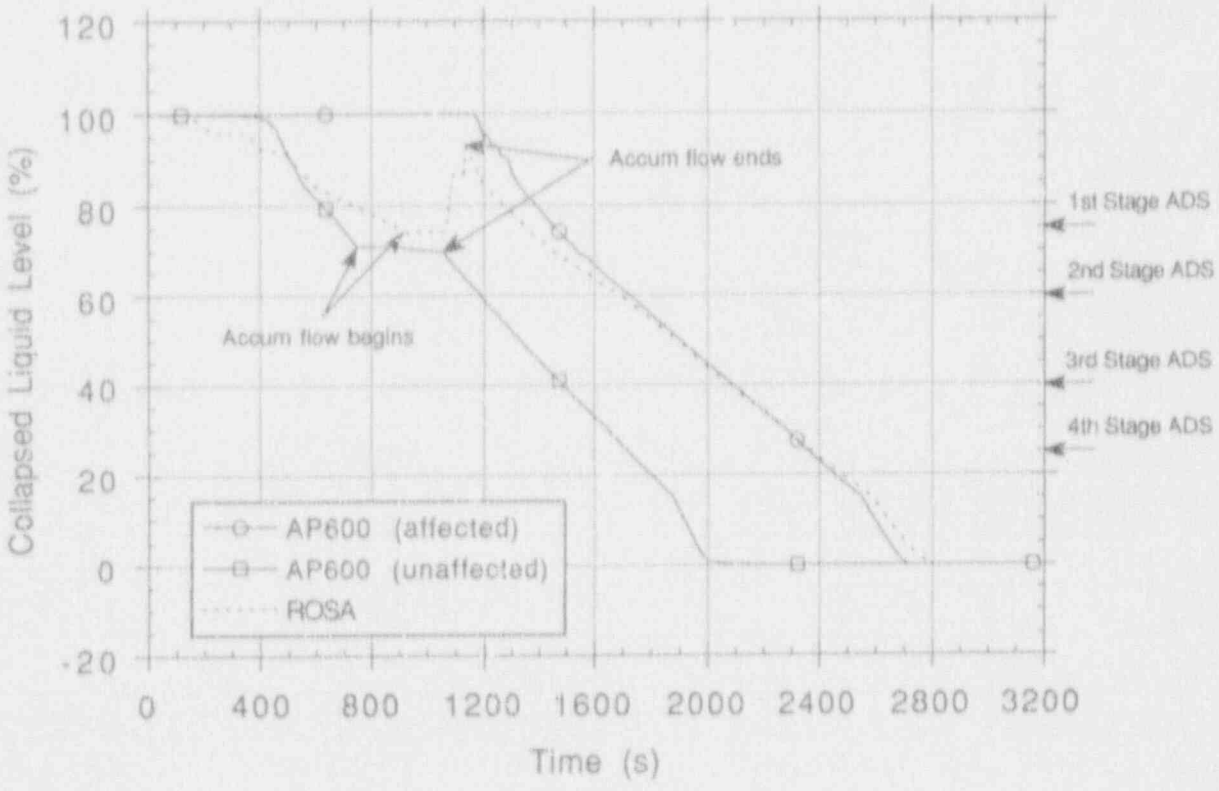

Figure 76. Collapsed liquid level in the CMTs for the pressure balance line break.

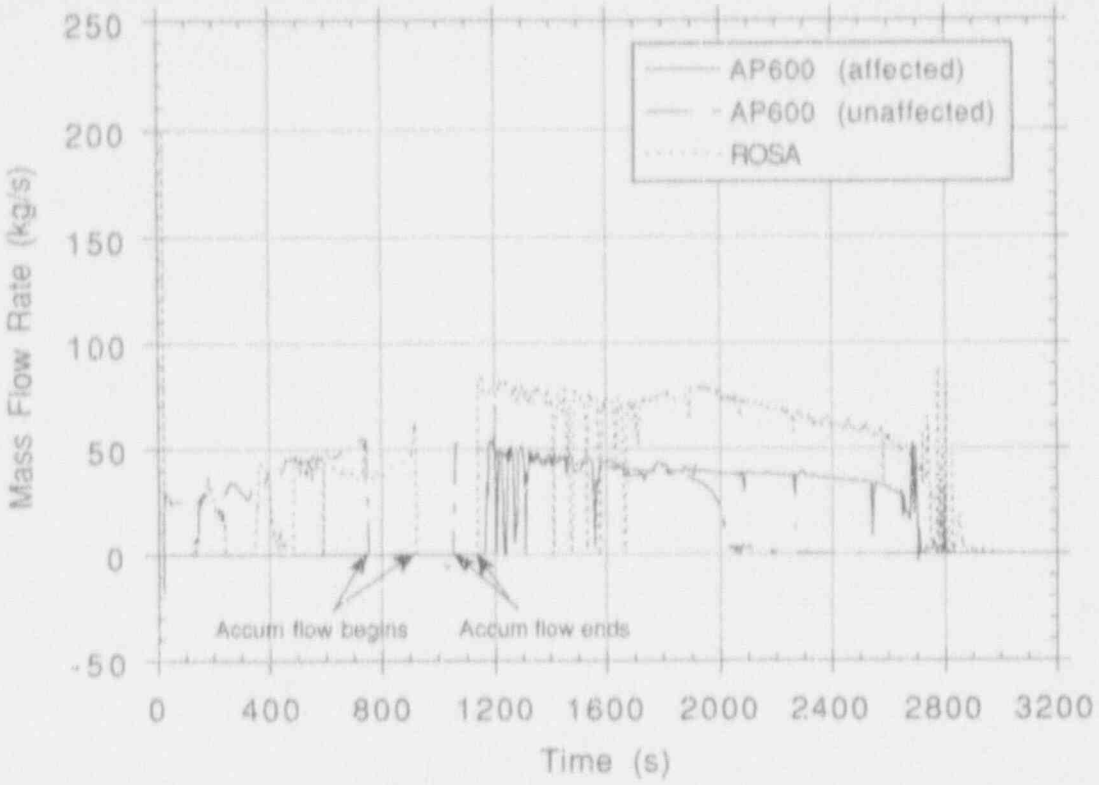

Figure 77. CMT injection flow rate for the pressure balance line break.

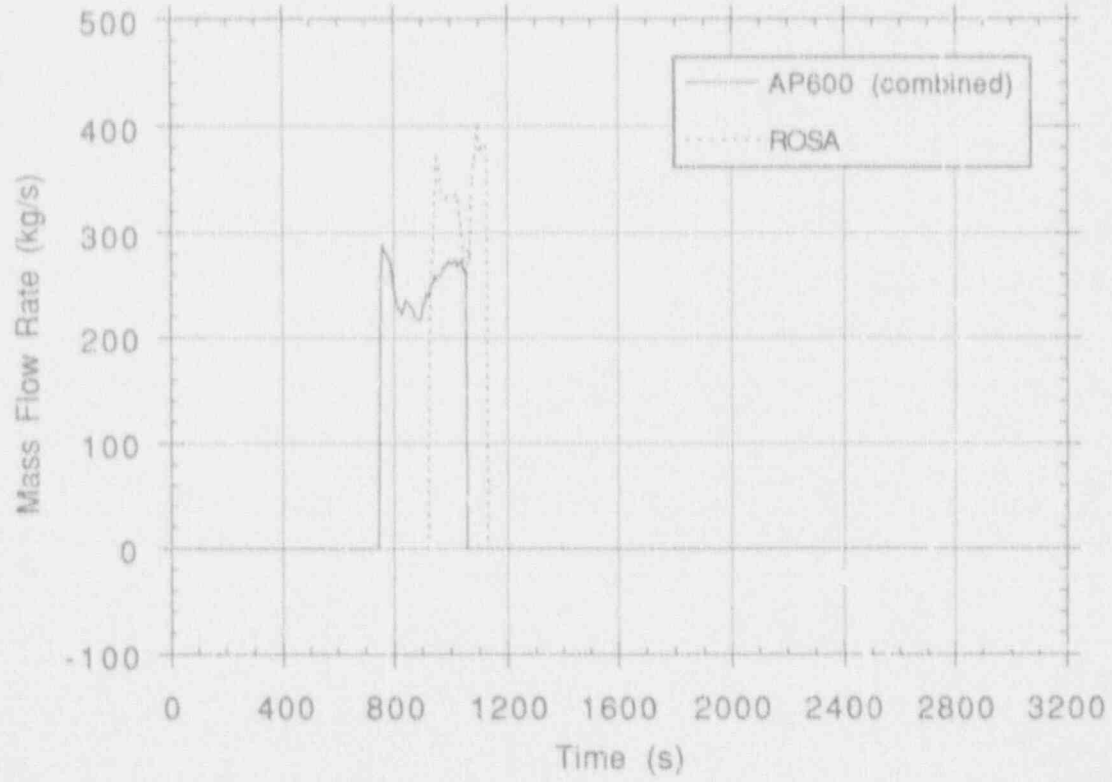

Figure 78. Accumulator injection flow rate for the pressure balance line break.

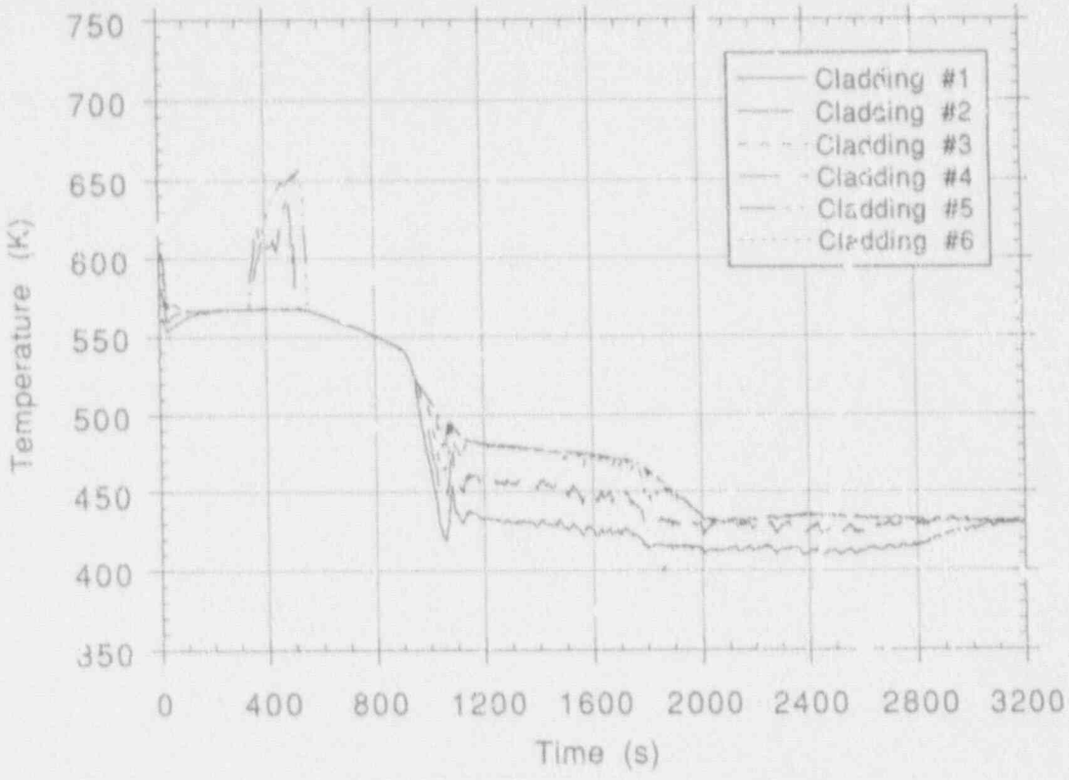

Figure 79. ROSA cladding surface temperature for the pressure balance line break.

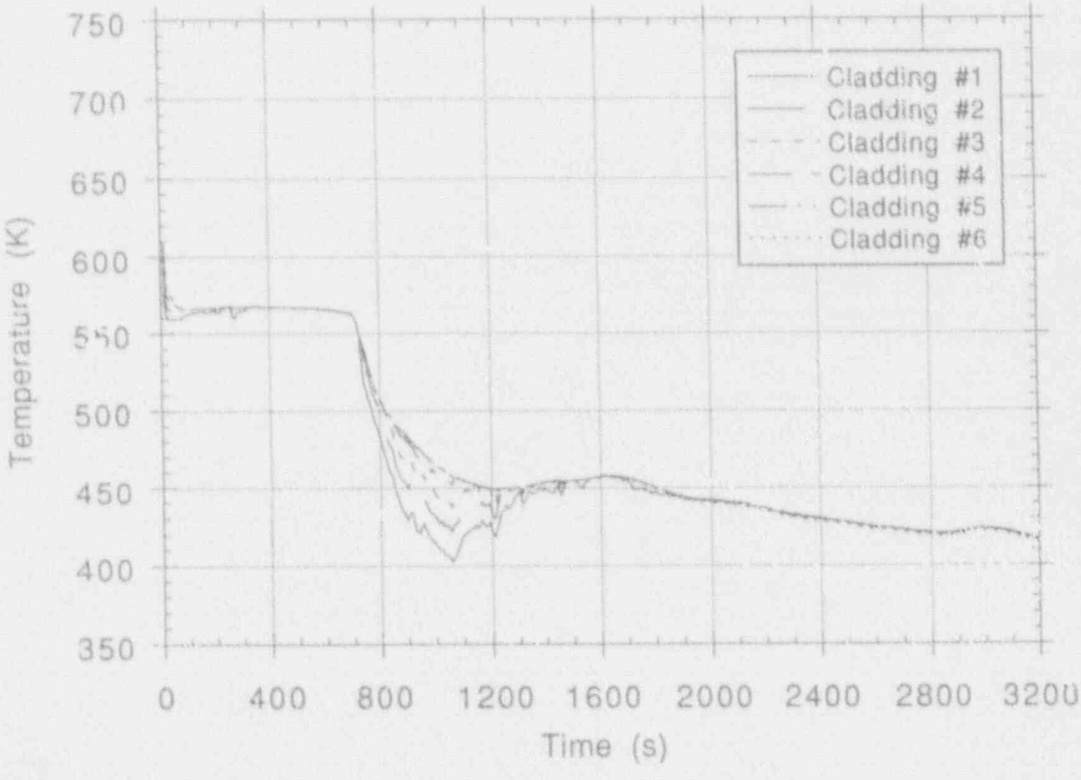

Figure 80. AP600 cladding surface temperature for the pressure balance line break.

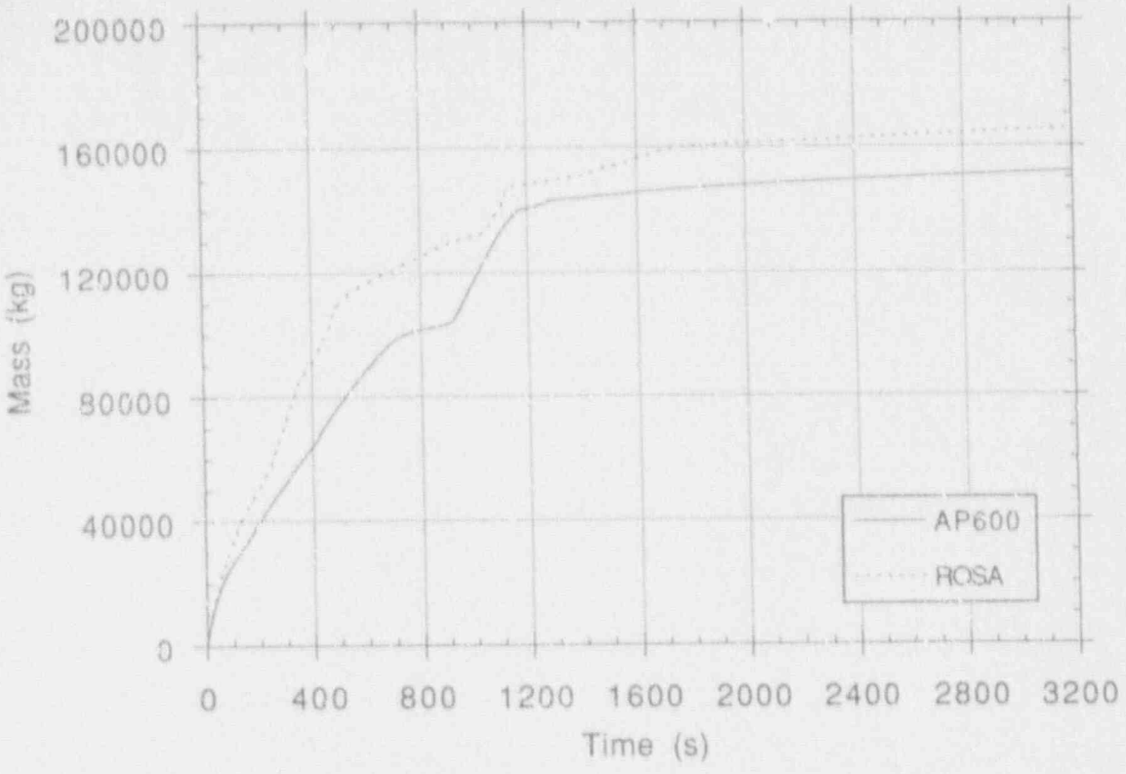

Figure 81. Integrated break mass flow rate for the pressure balance line break.

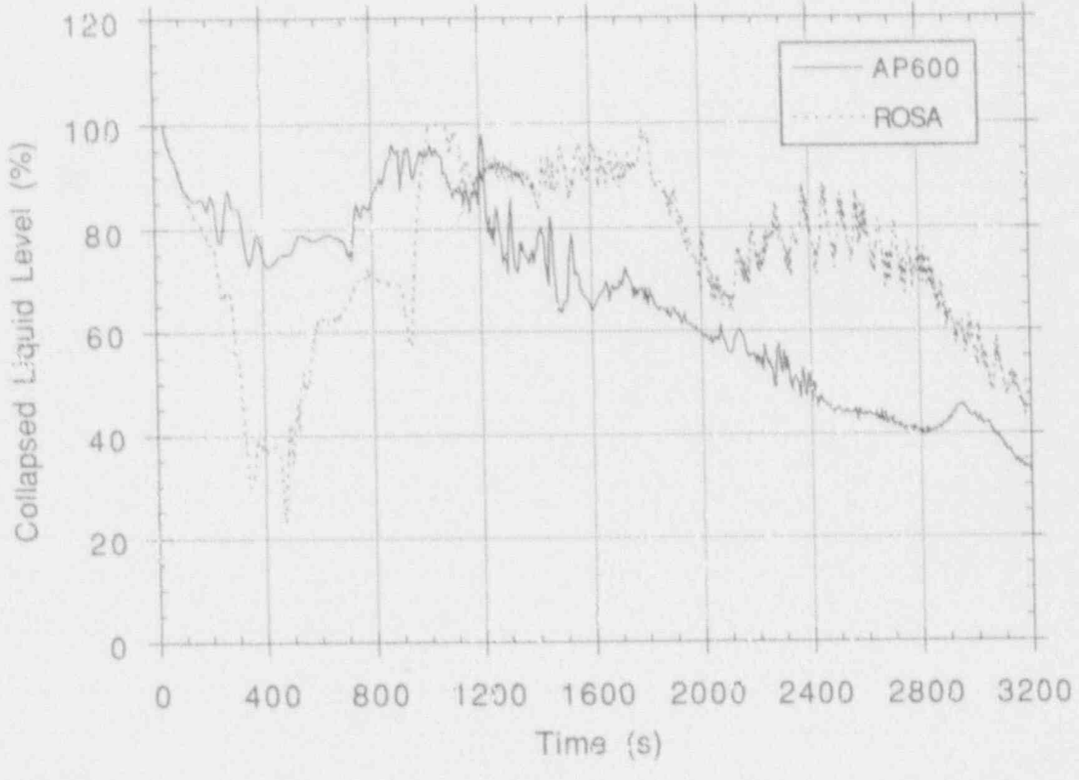

Figure 82. Collapsed liquid level in the core for the pressure balance line break.

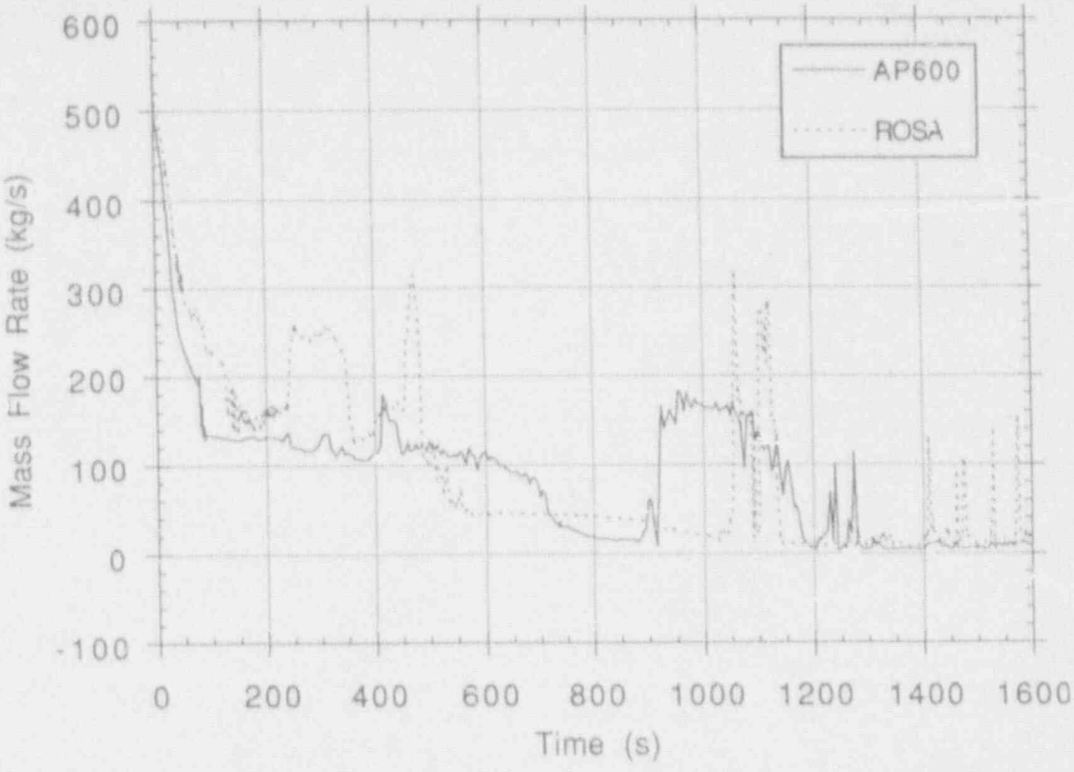

Figure 83. Break mass flow rate for the pressure balance line break.

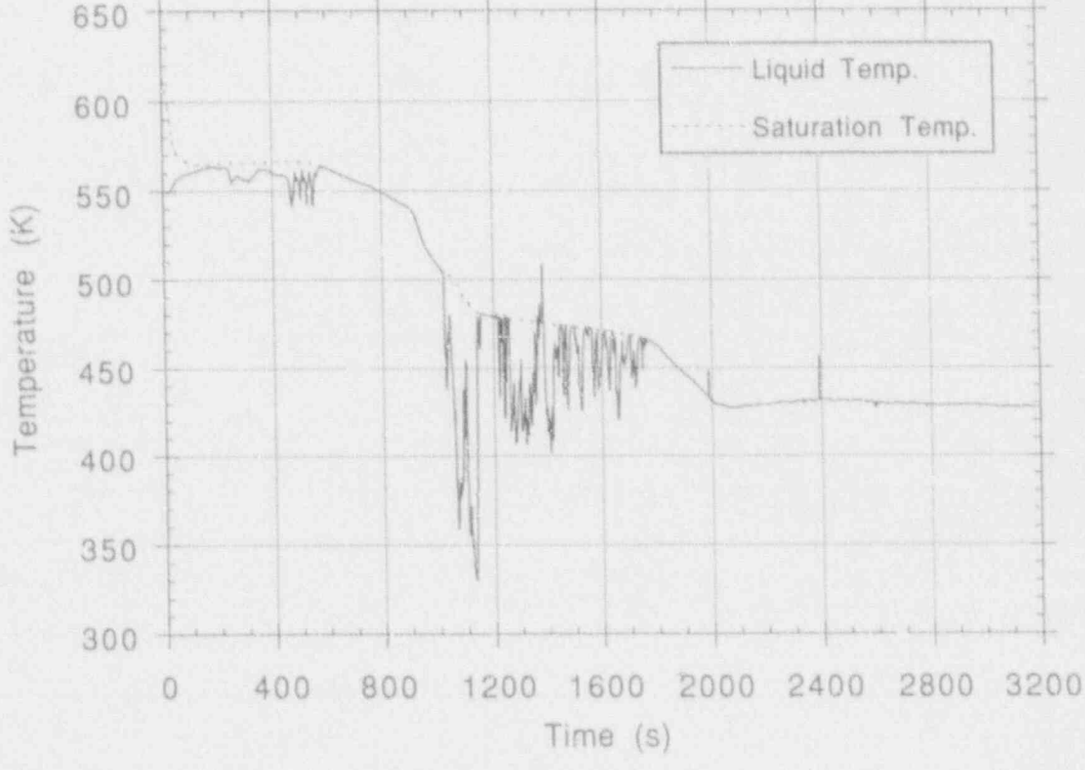

Figure 84. ROSA affected cold leg liquid and saturation temperatures for the pressure balance line break.

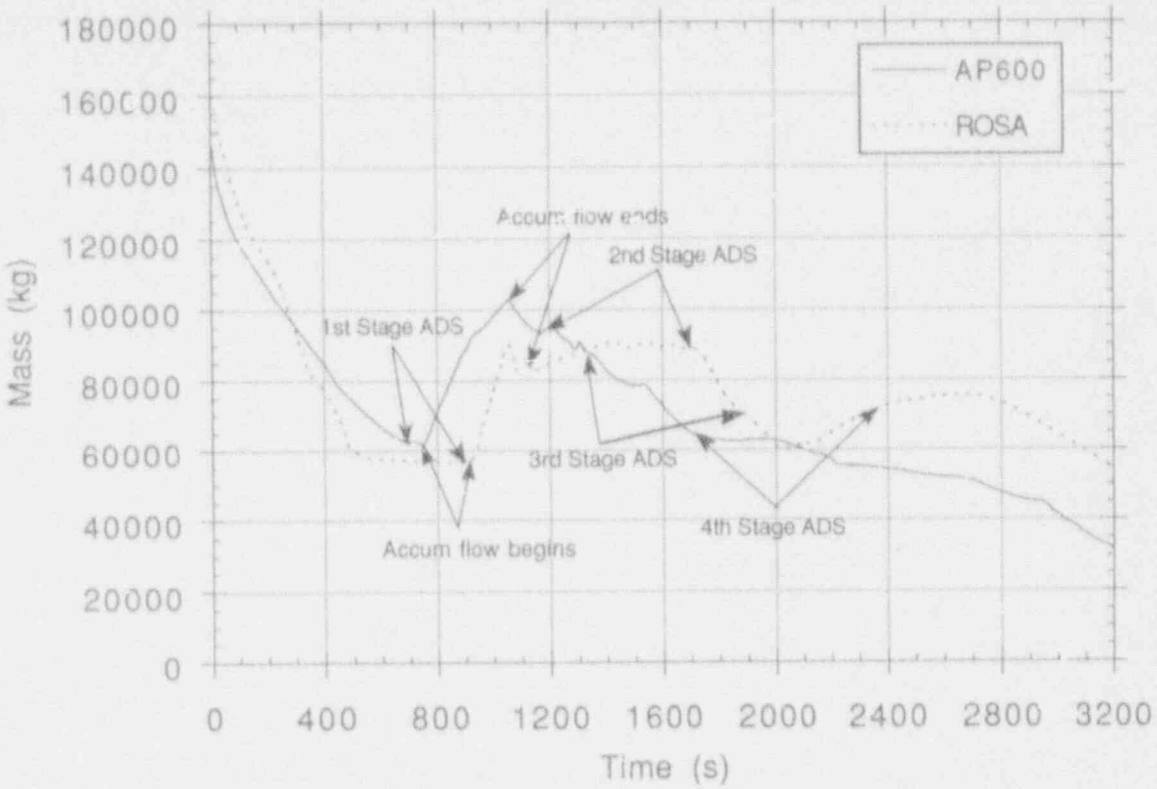

Figure 85. Total primary system mass inventory for the pressure balance line break.

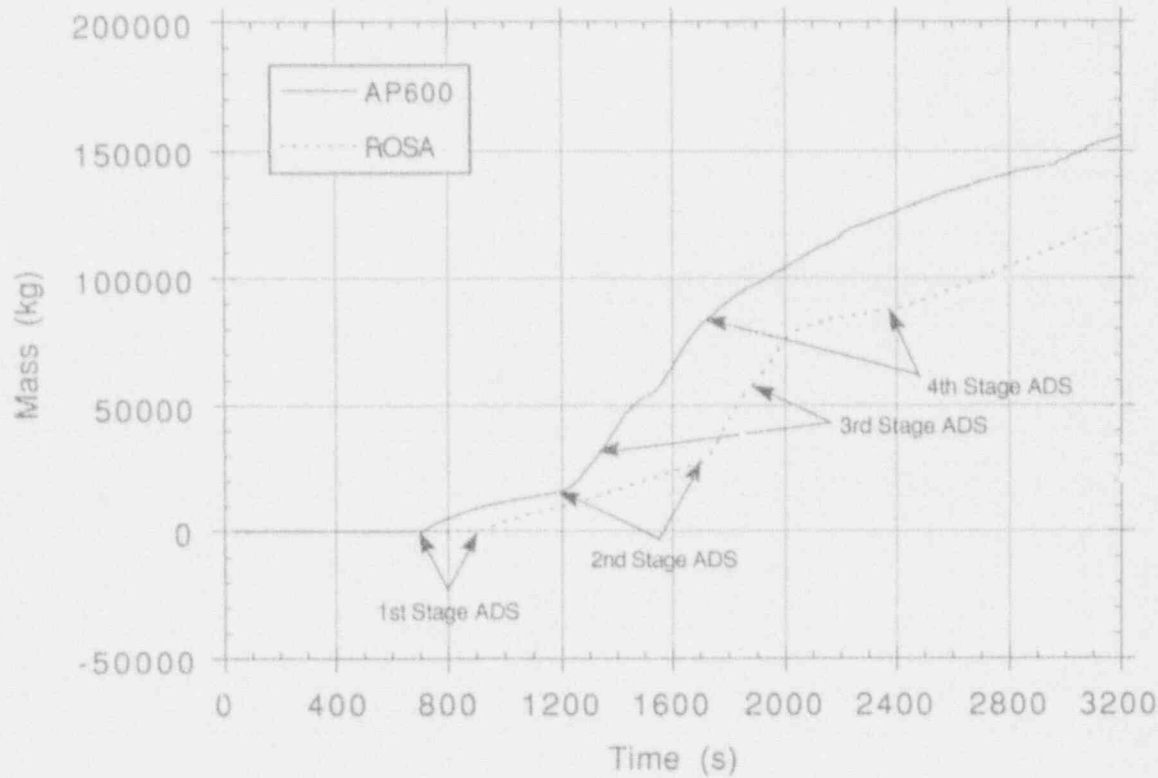

Figure 86. Integrated ADS mass flow rate for the pressure balance line break.

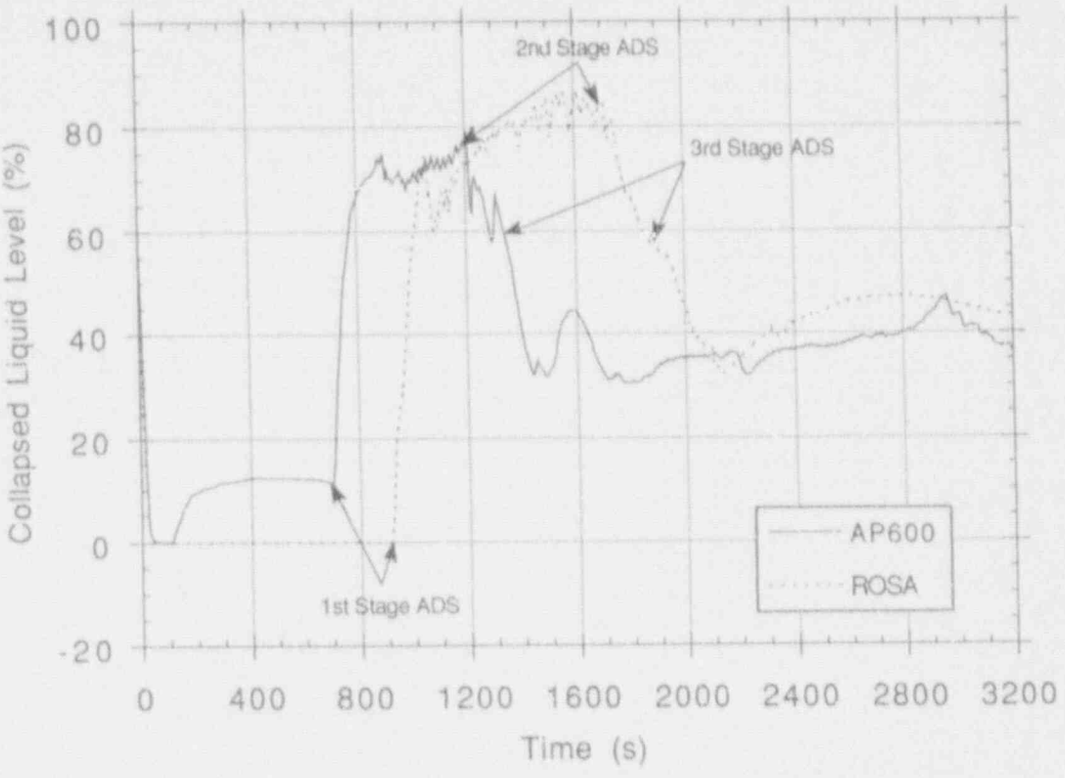

Figure 87. Collapsed liquid level in the pressurizer for the pressure balance line break.

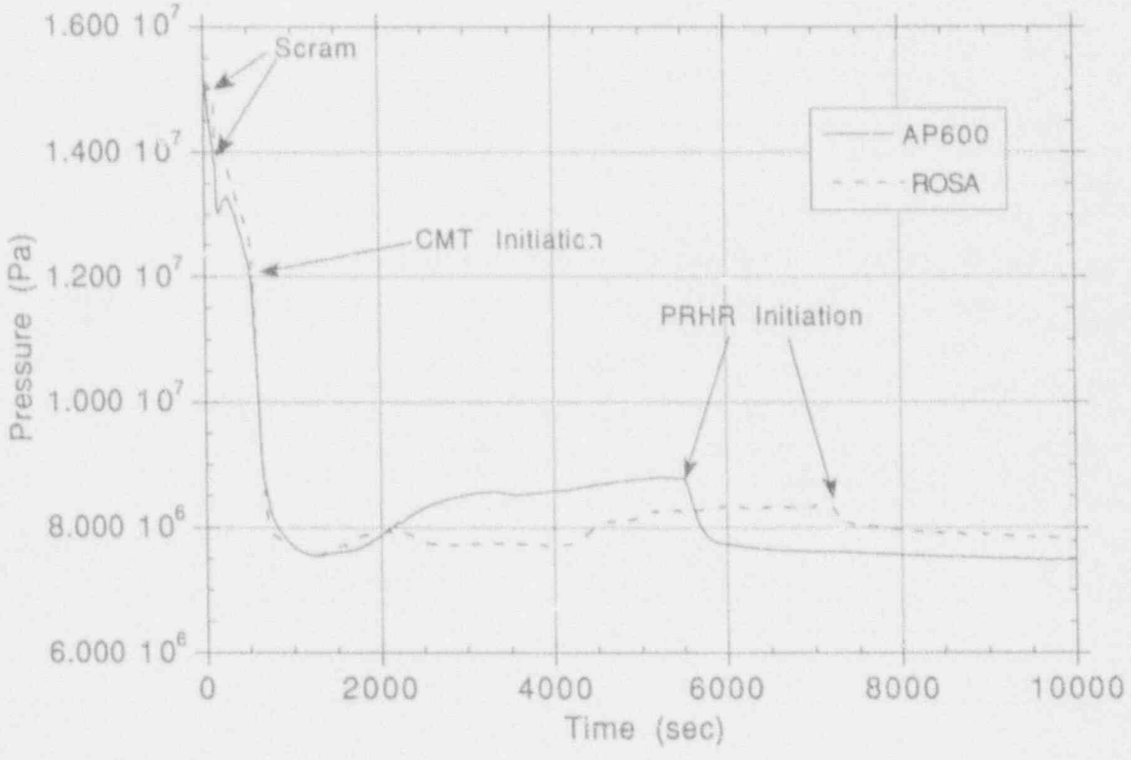

Figure 88. Pressurizer pressure for single–tube SGTR calculations.

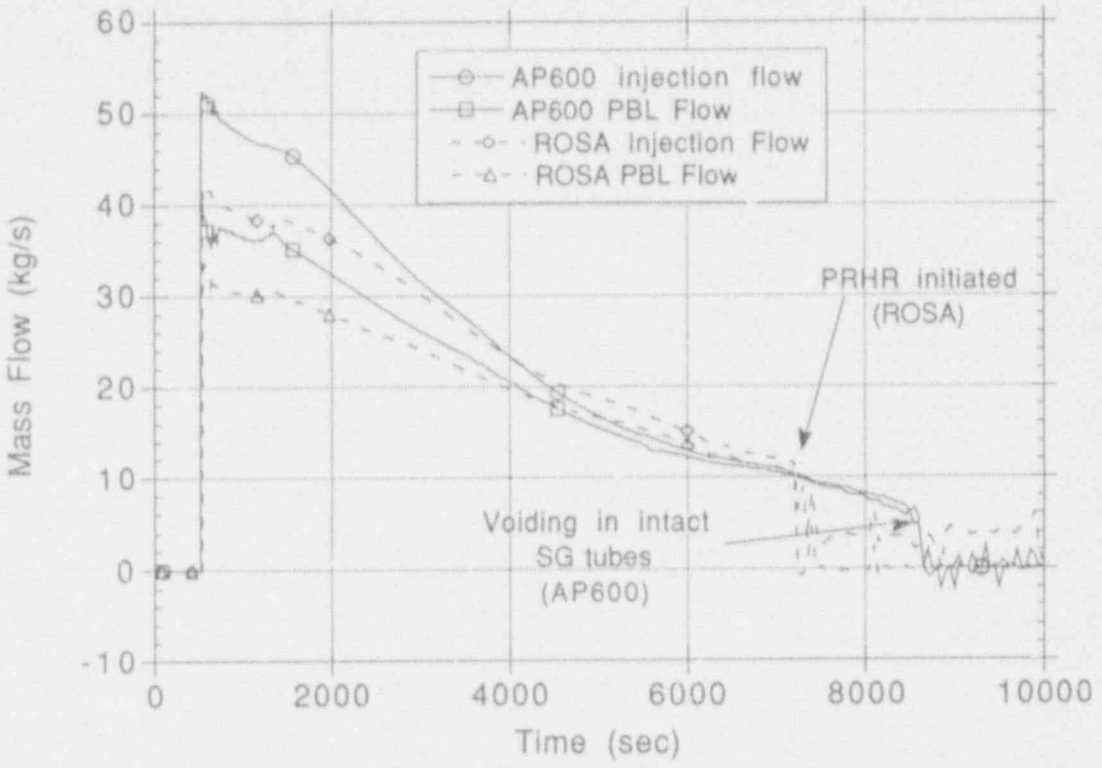

Figure 89. CMT mass flow rate for single–tube SGTR calculations.

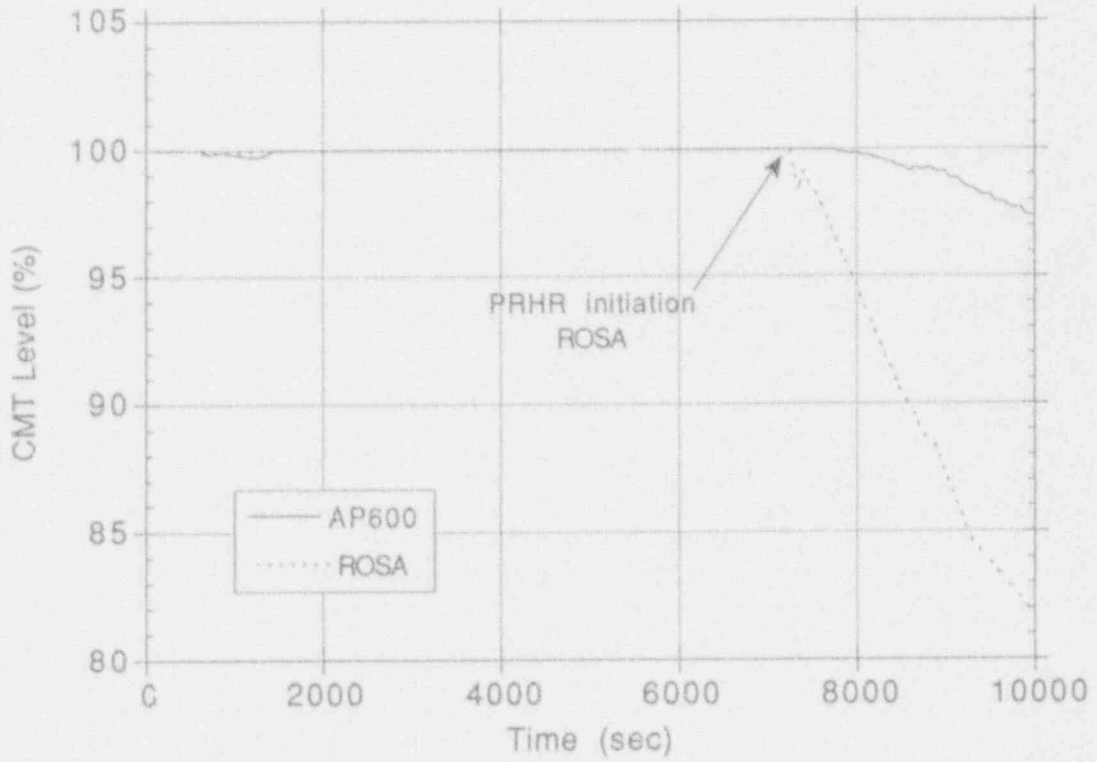

Figure 90. CMT level for single–tube SGTR calculations.

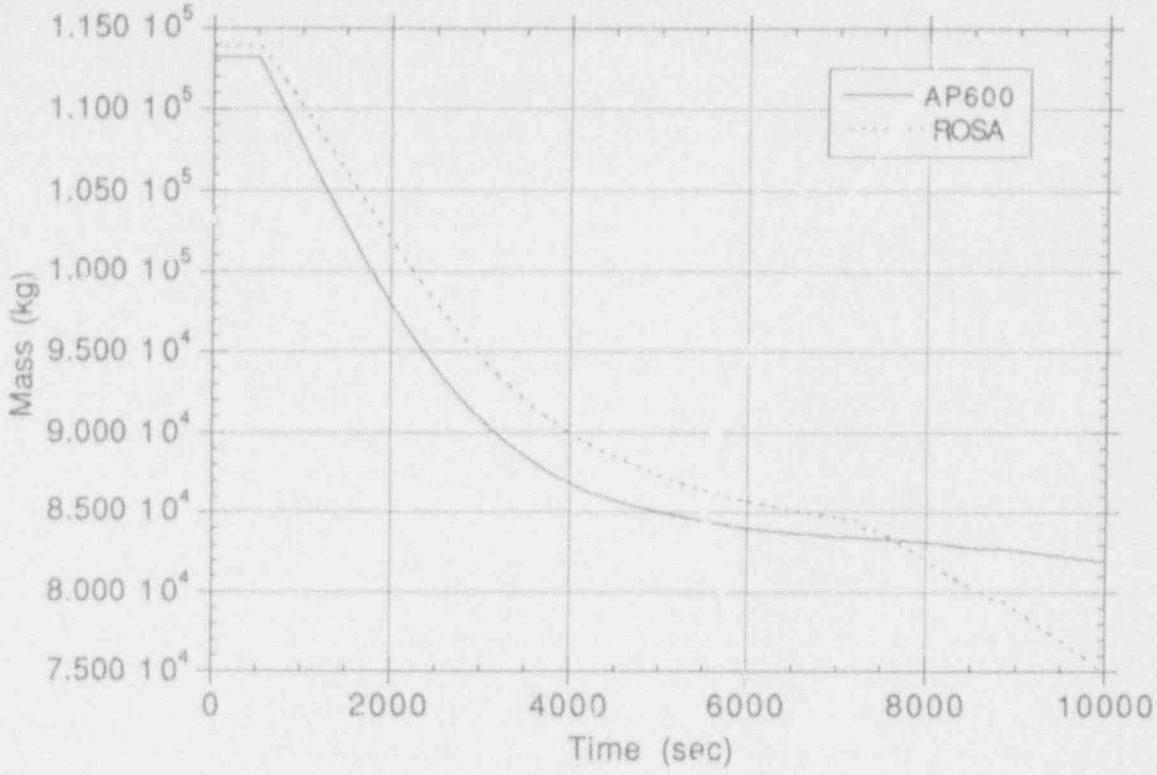

Figure 91. CMT mass inventory for single–tube SGTR calculations.

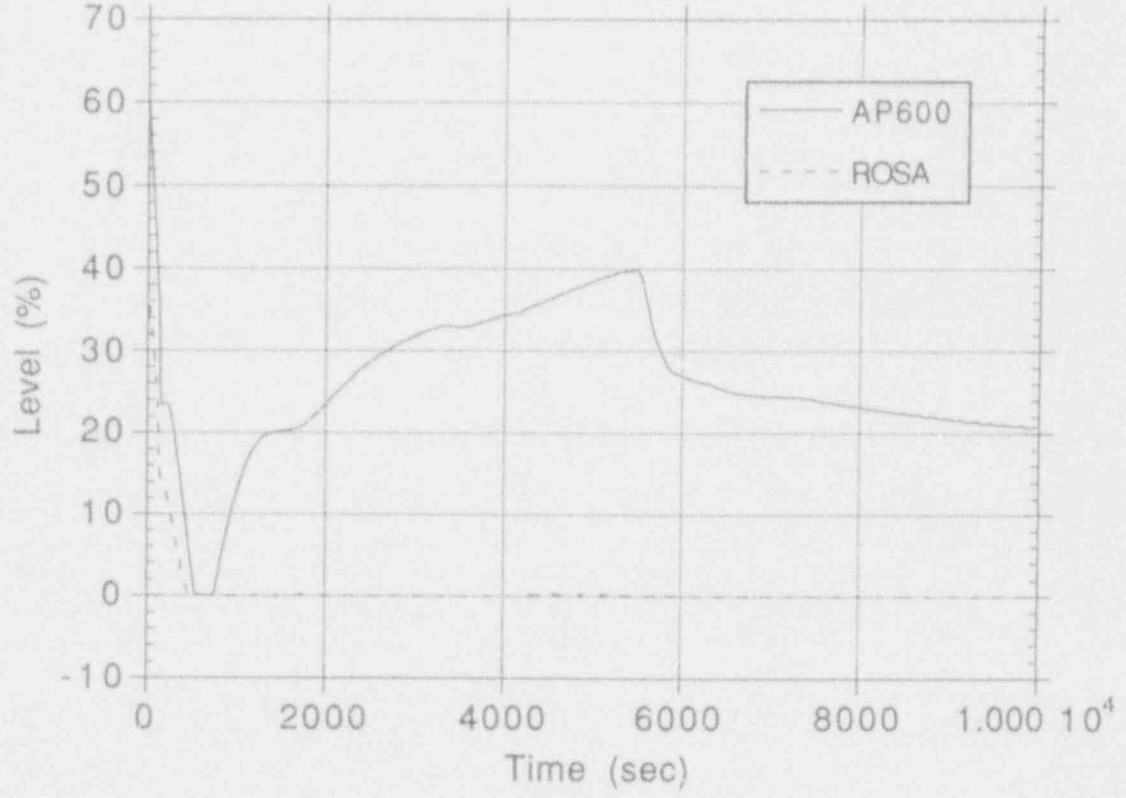

Figure 92. Pressurizer collapsed liquid level for single–tube SGTR calculations.

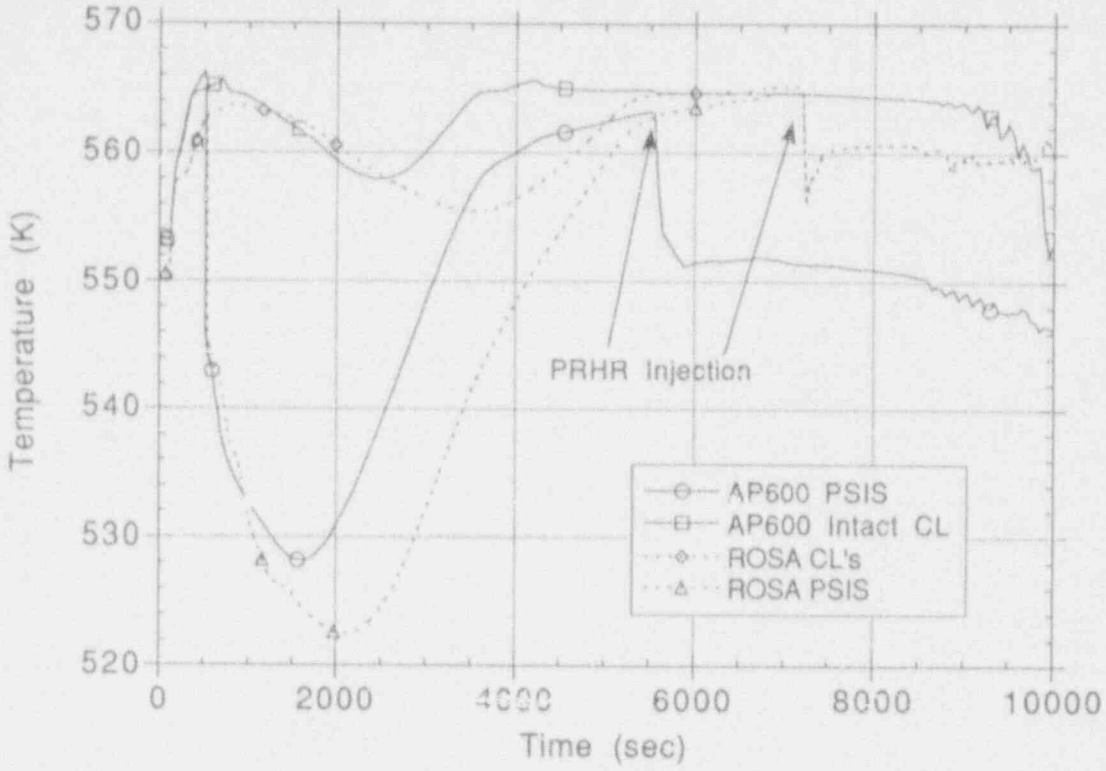

Figure 93. Downcomer cell fluid temperatures for single–tube SGTR calculations.

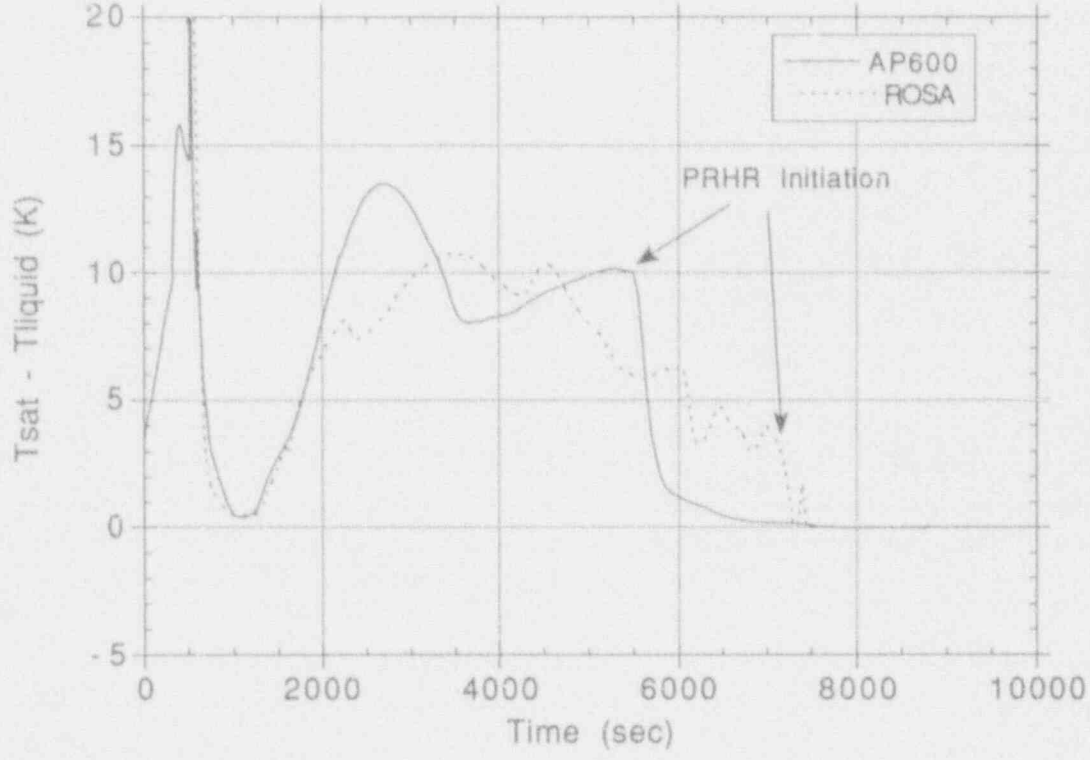

Figure 94. Liquid subcooling in pressure balance line tee for single–tube SGTR calculations.

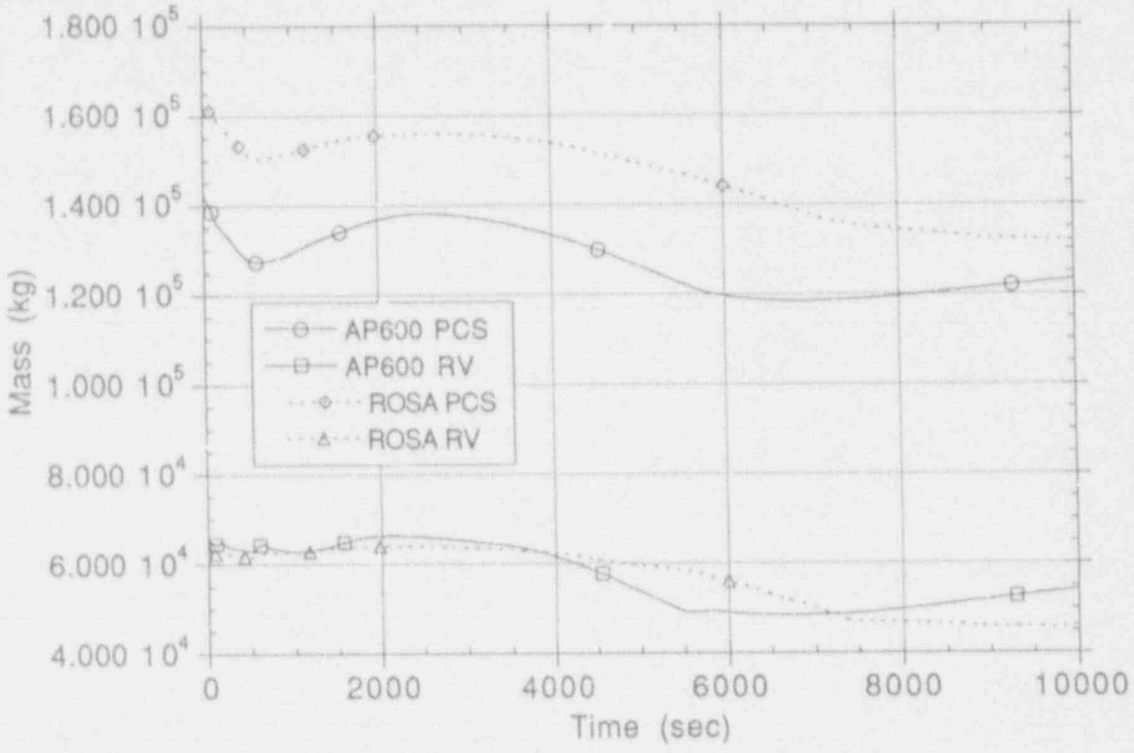

Figure 95. Primary system mass inventory for single–tube SGTR calculations.

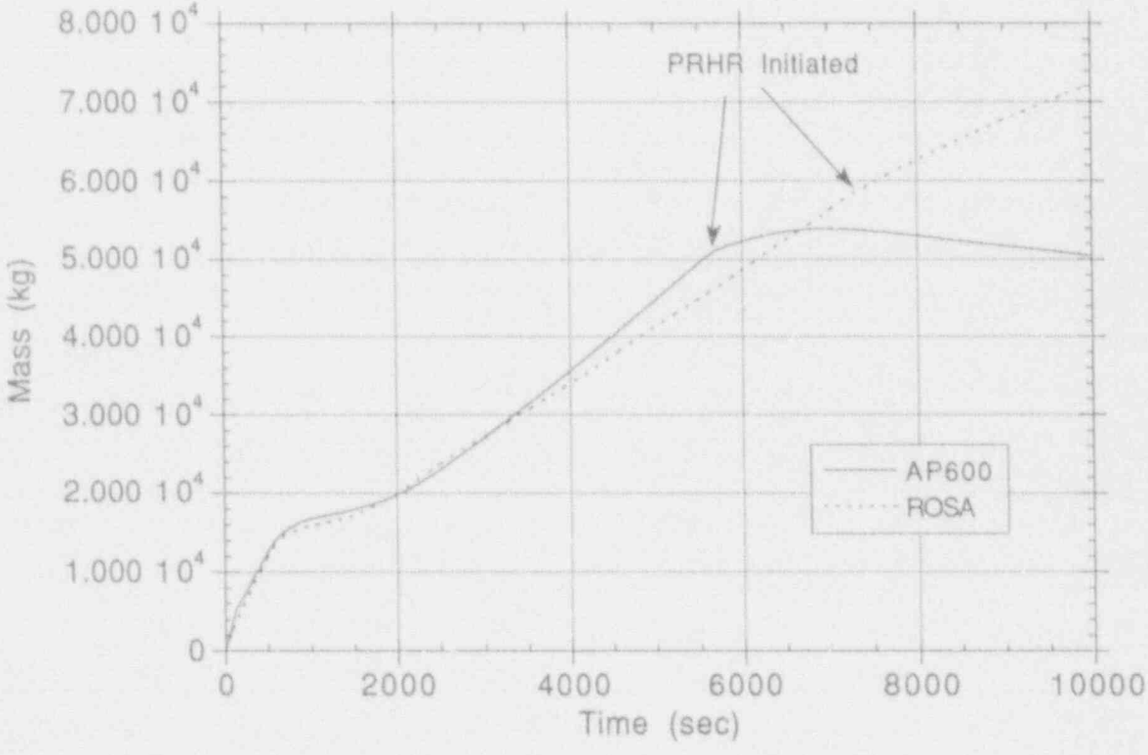

Figure 96. Integrated break mass flow rate for single–tube SGTR calculations.

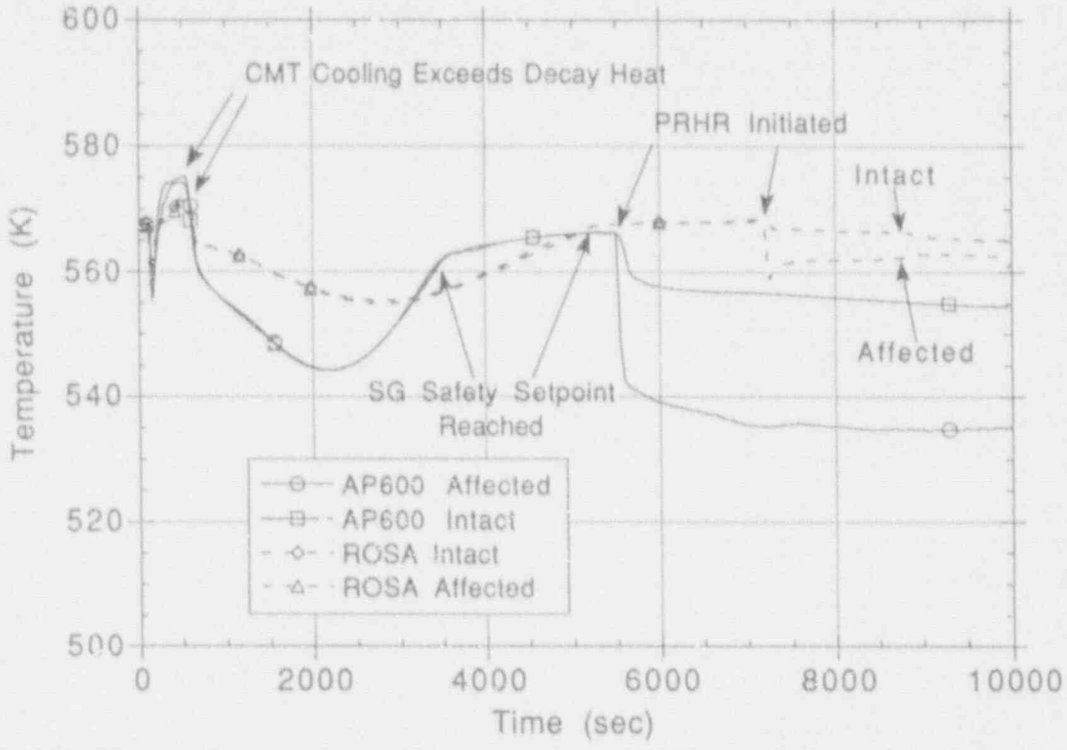

Figure 97 Loop average temperature for single–tube SGTR calculations.

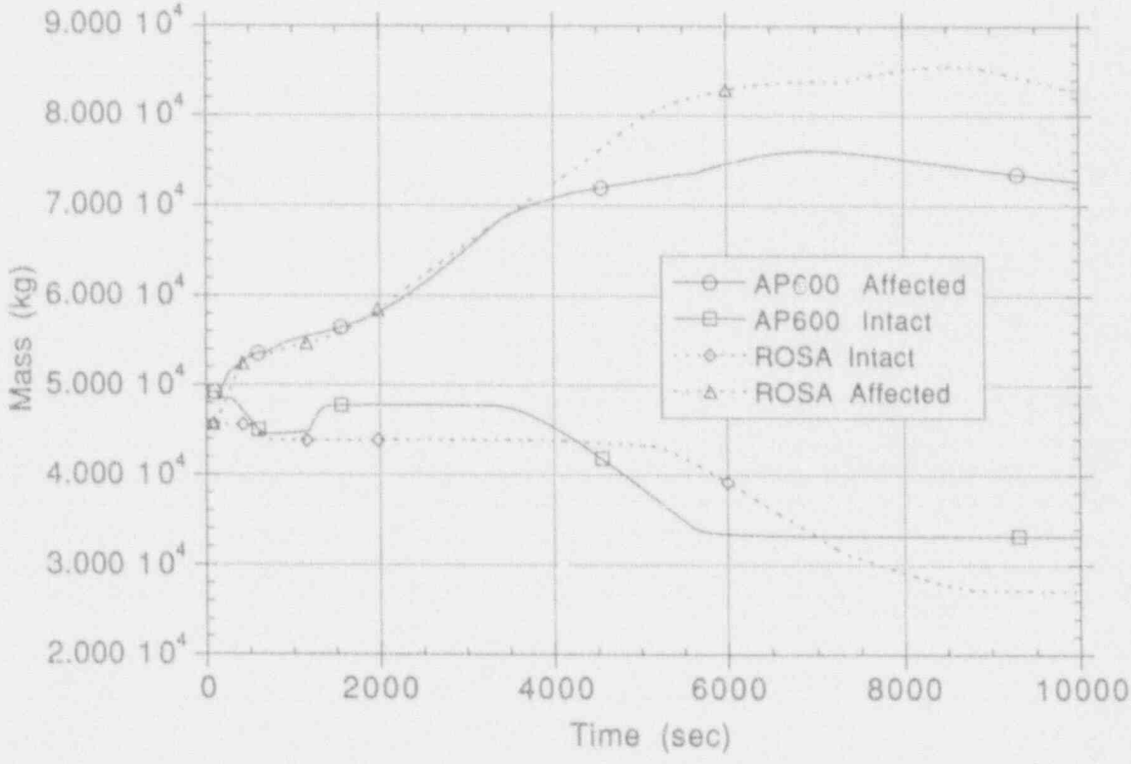

Figure 98. Steam generator secondary mass for single–tube SGTR calculations.

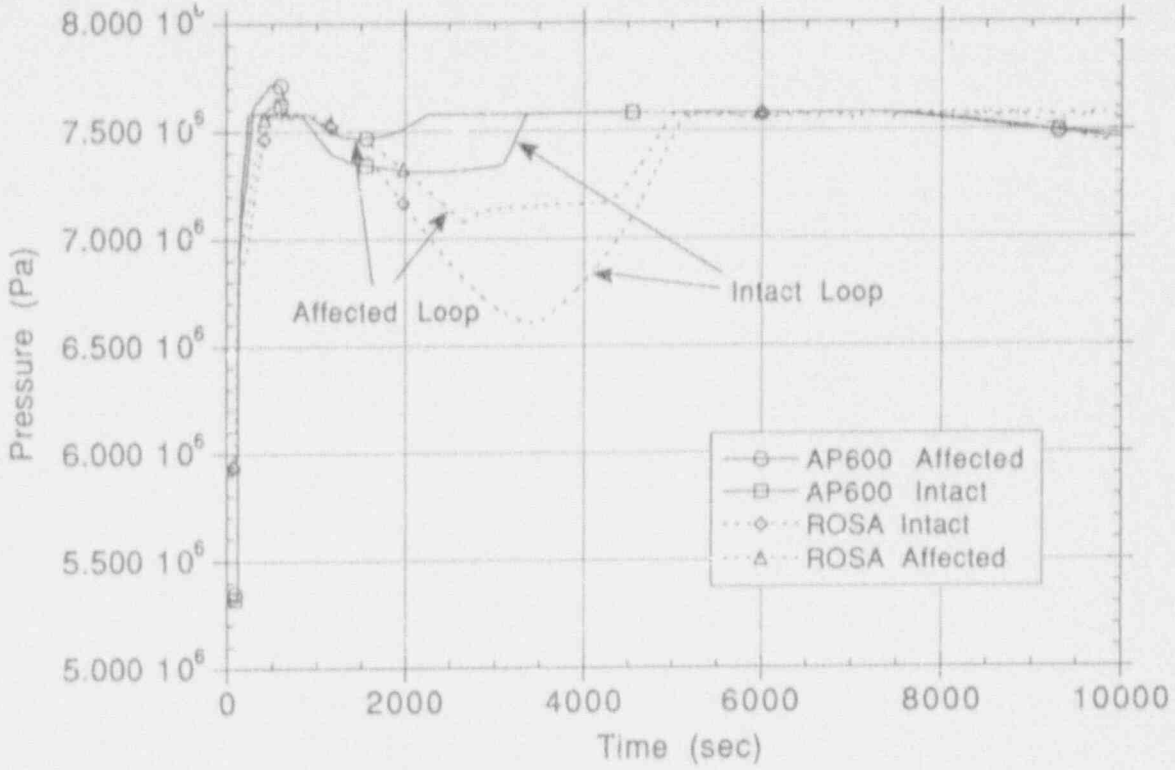

Figure 99. Steam generator secondary pressure for single–tube SGTR calculations.

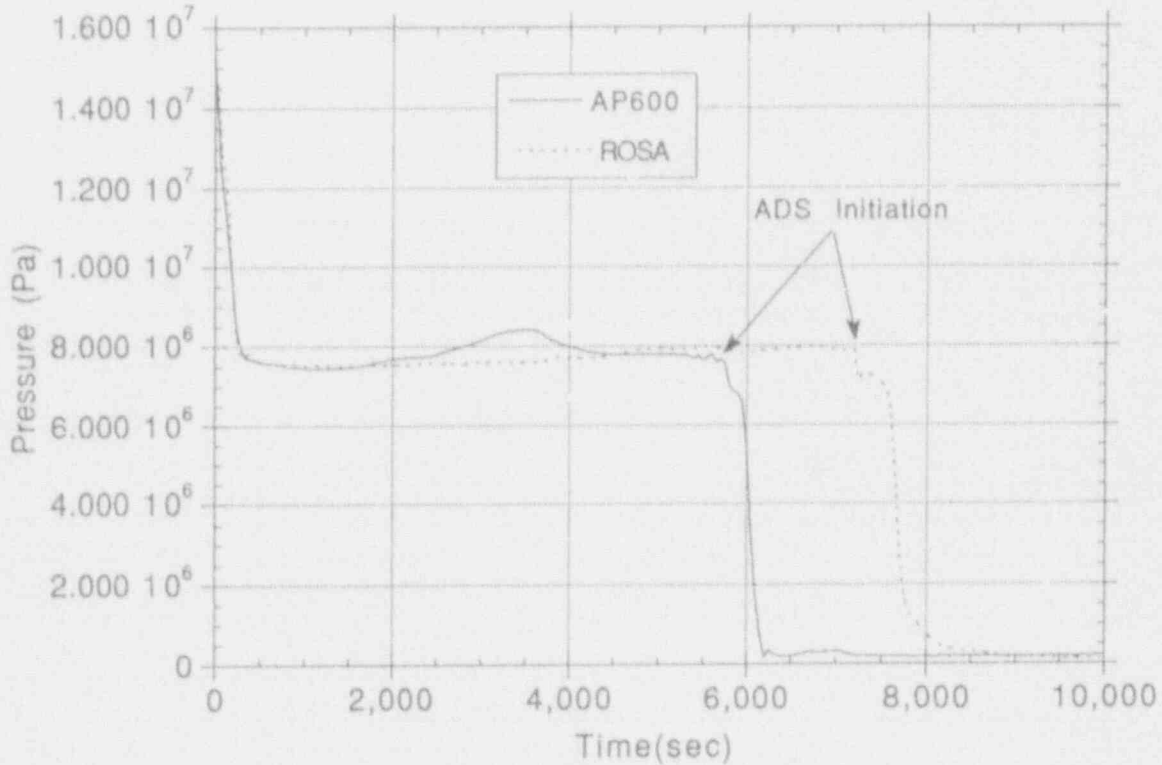

Figure 100. Pressurizer pressure for three–tube SGTR calculations.

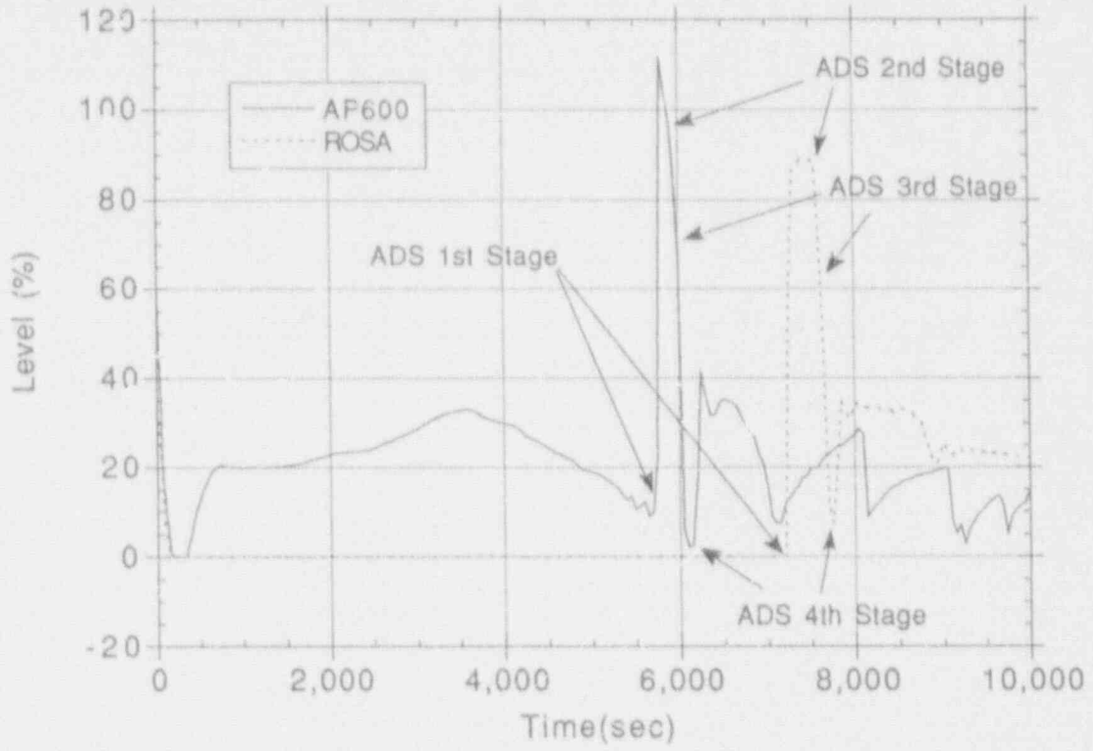

Figure 101. Pressurizer collapsed liquid level for three–tube SGTR calculations.

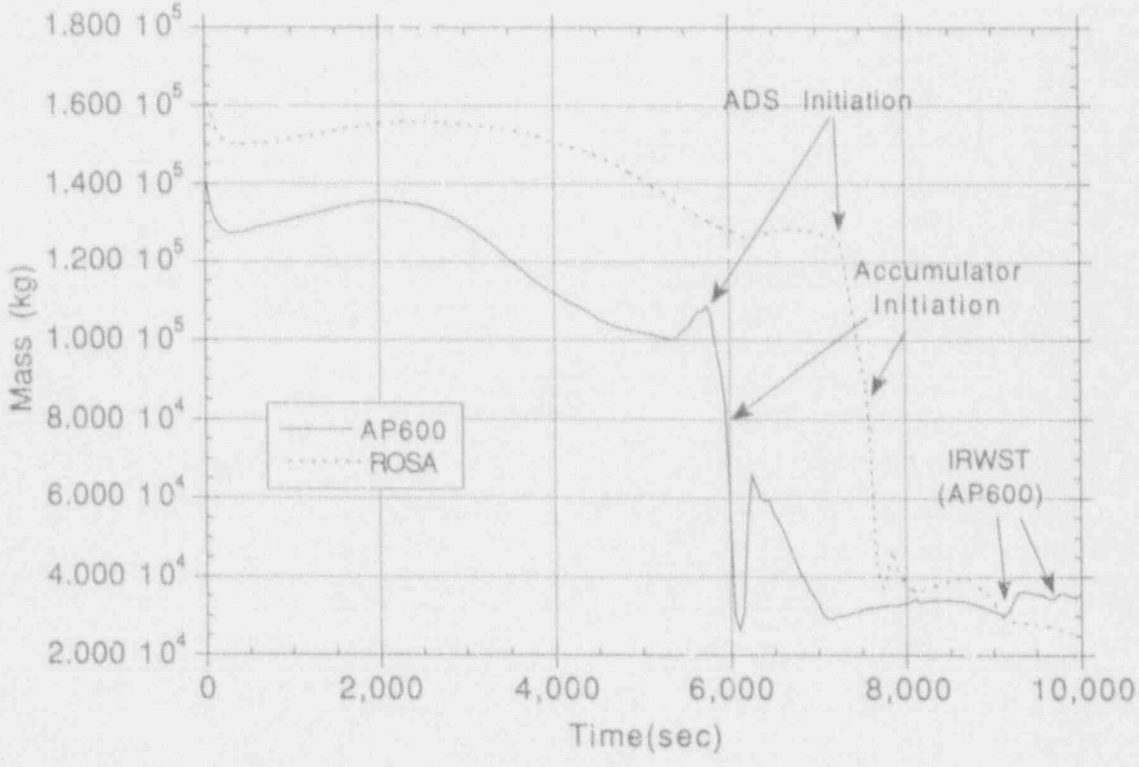

Figure 102. Primary system mass inventory for three–tube SGTR calculations.

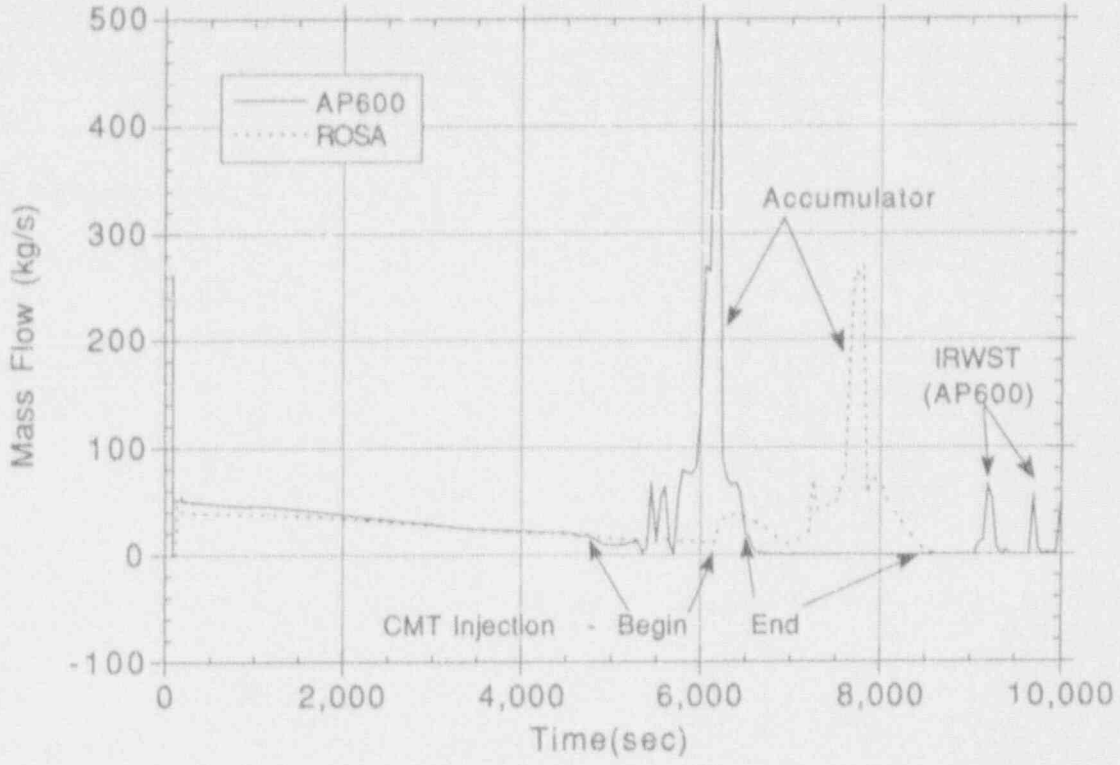

Figure 103. Total ECC system mass flow rate for three–tube SGTR calculations.

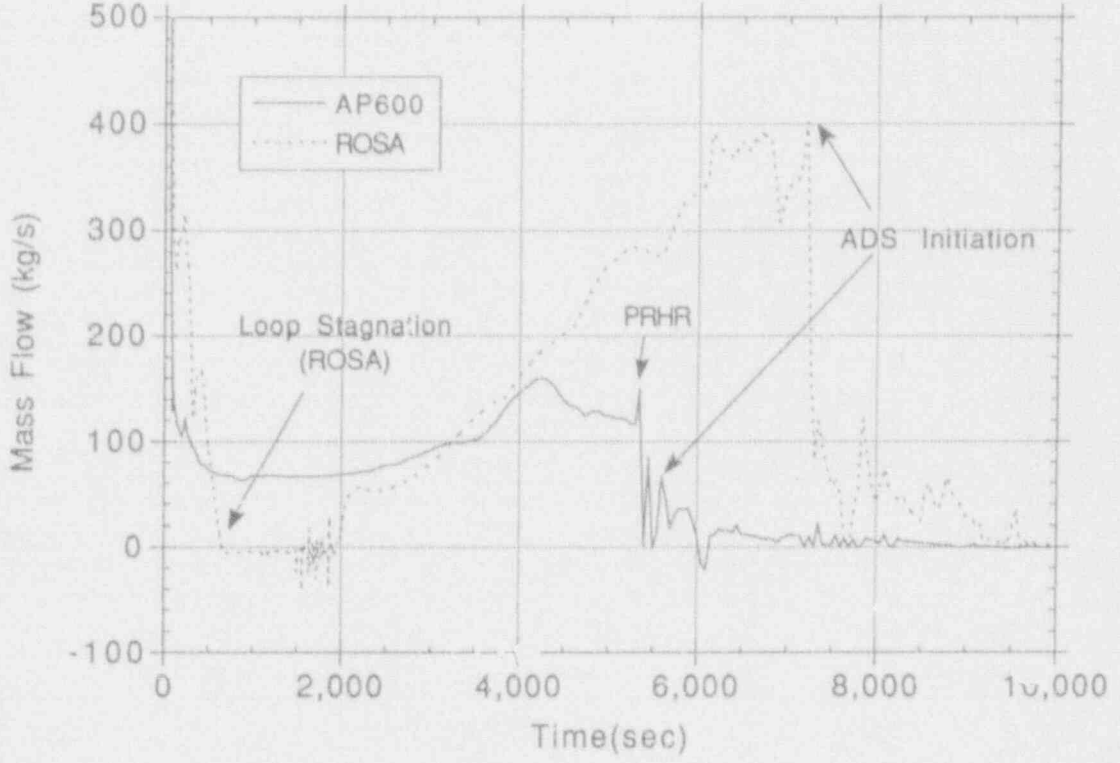

Figure 104. Intact cold leg mass flow rate for three–tube SGTR calculations.

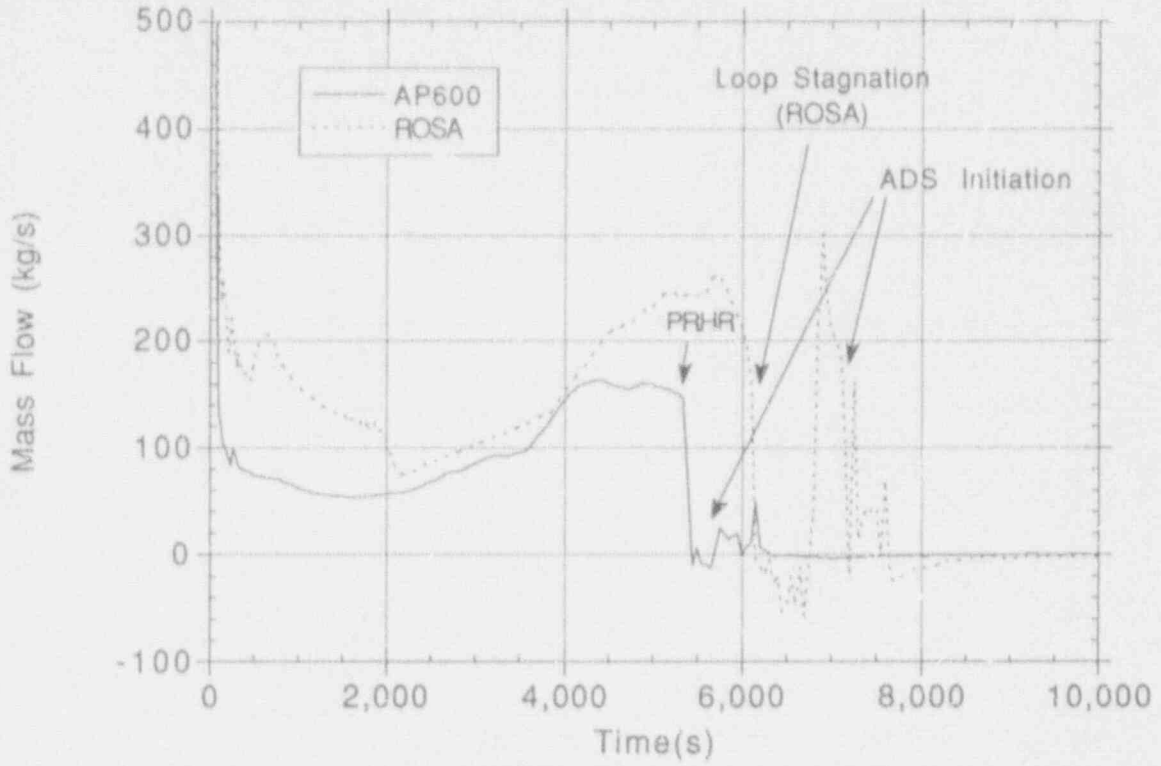

Figure 105. Affected cold leg mass flow rate for three–tube SGTR calculations.

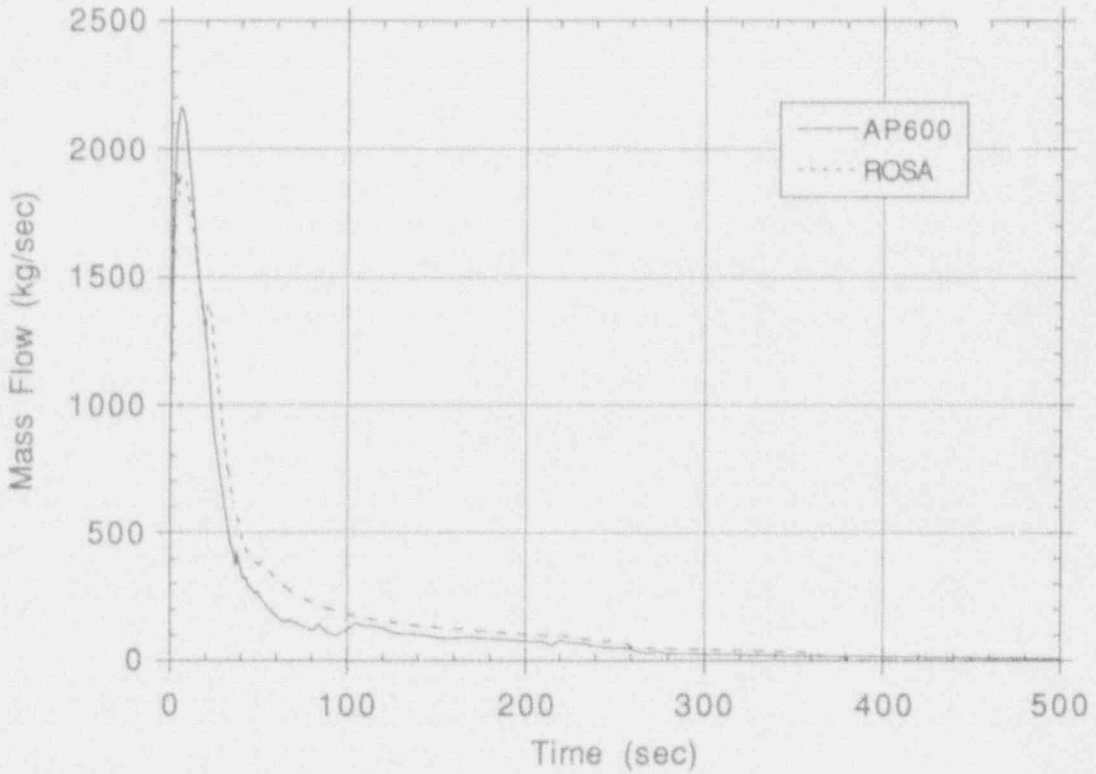

Figure 106. Steam line break mass flow rate for ROSA and AP600 MSLB calculations.

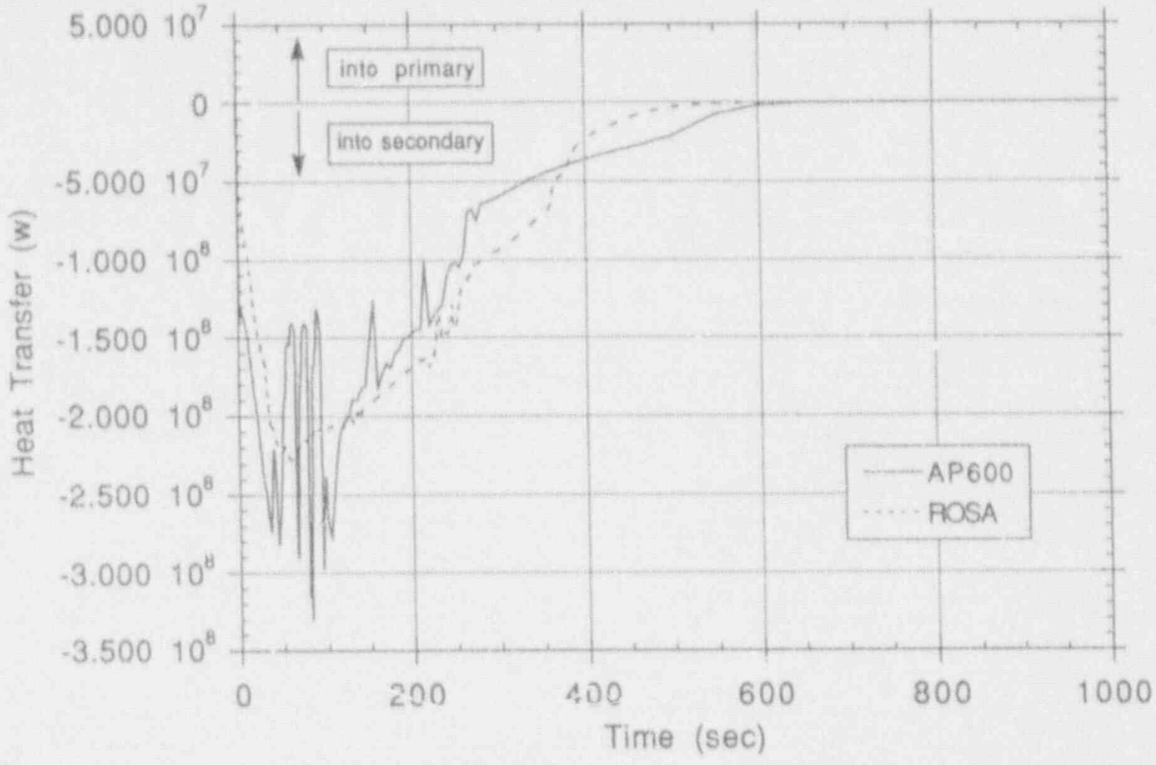

Figure 107. Break side steam generator heat transfer for ROSA and AP600 MSLB calculations.

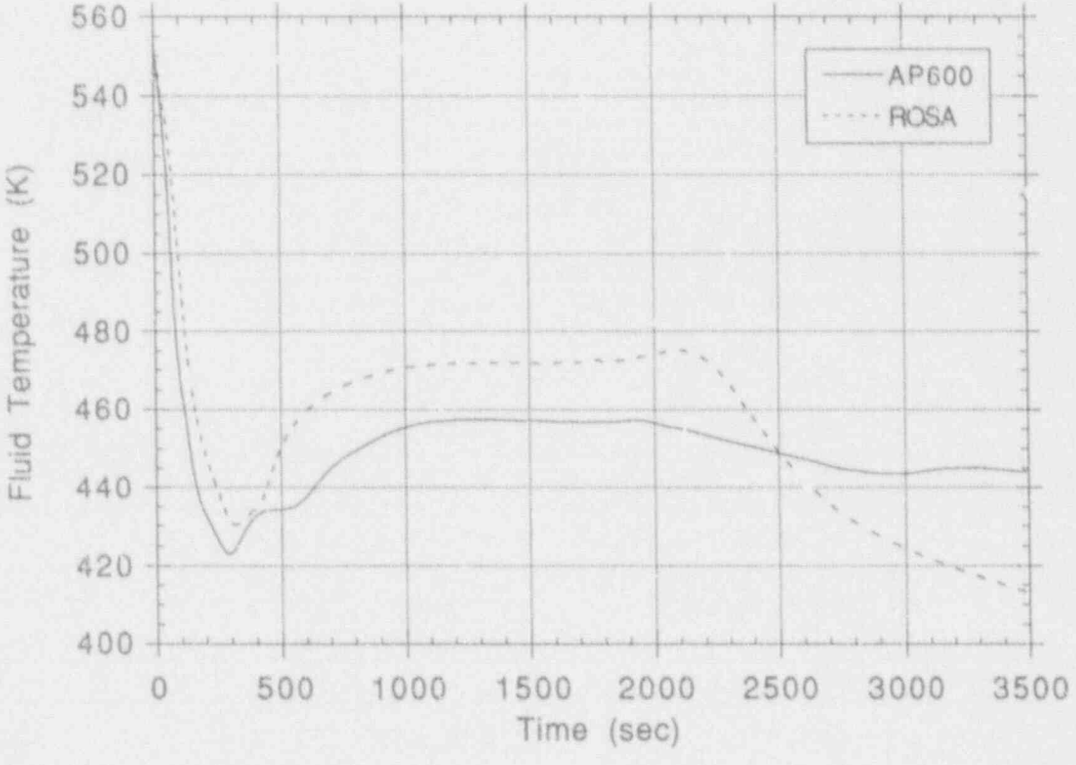

Figure 108. Break side vessel inlet fluid temperature for ROSA and AP600 MSLB calculations.

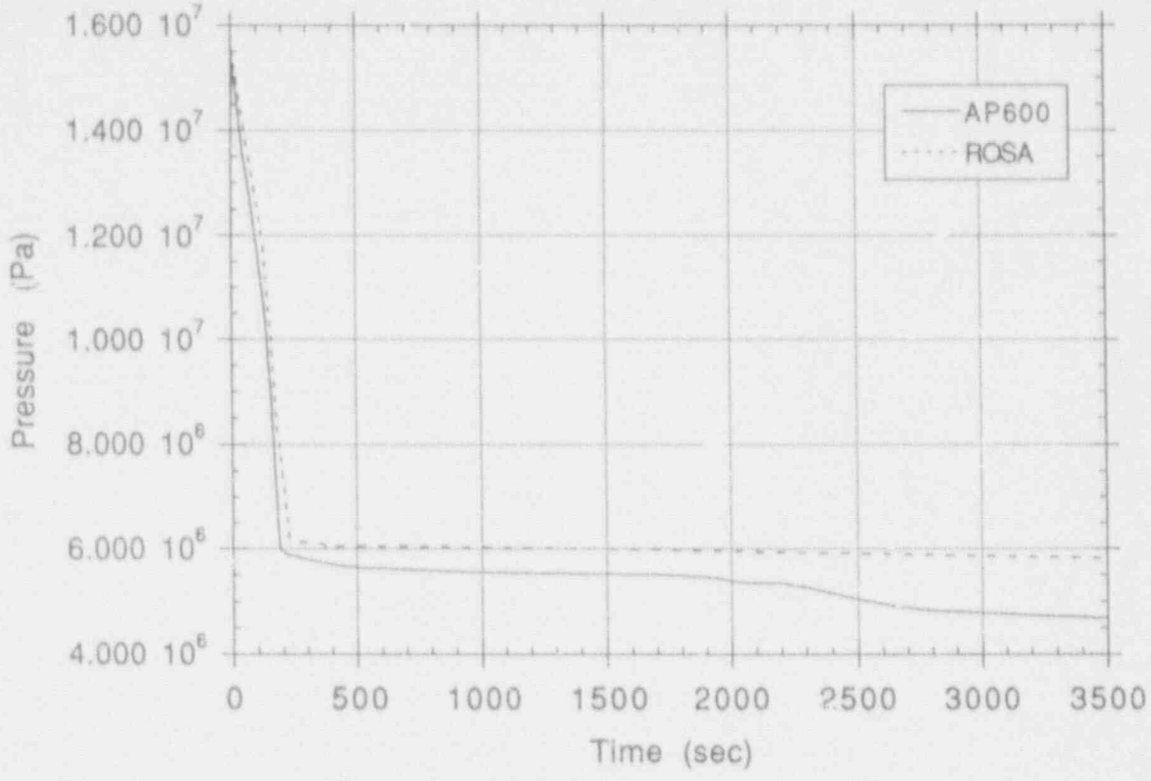

Figure 109. Pressurizer pressure for ROSA and AP600 MSLB calculations.

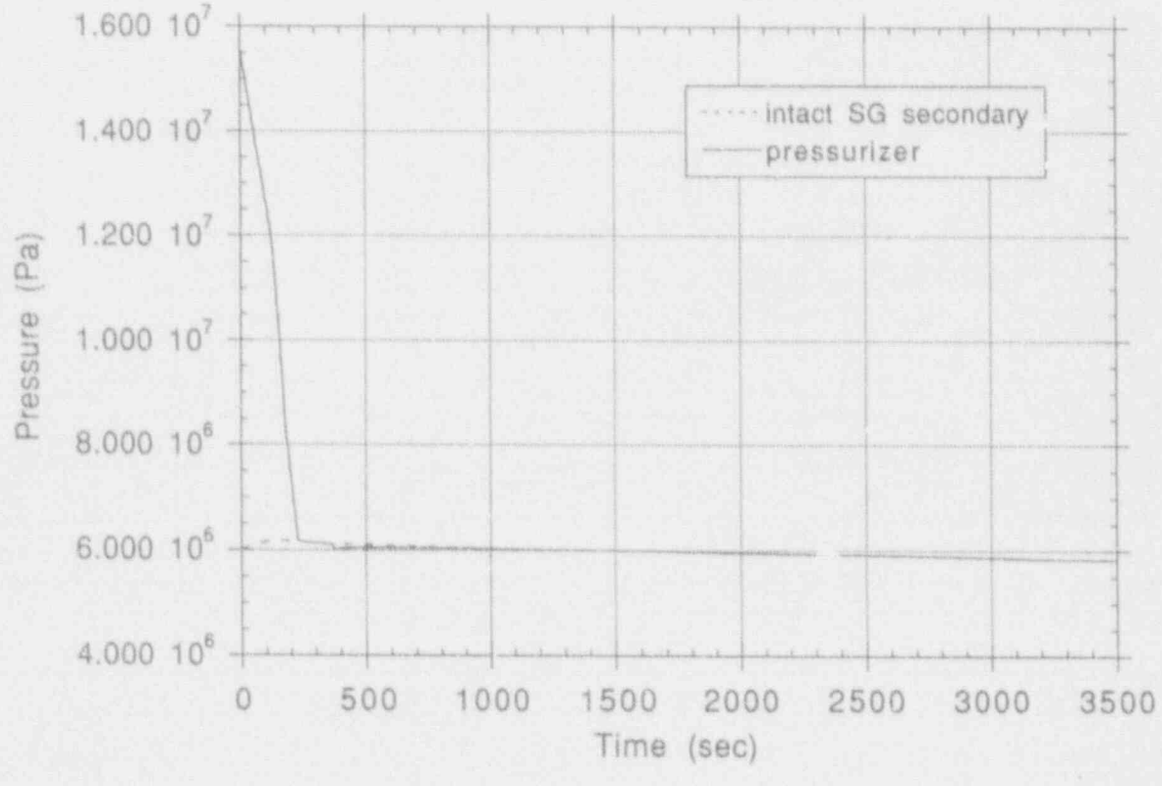

Figure 110. Pressurizer and intact steam generator secondary pressure for ROSA MSLB calculation.

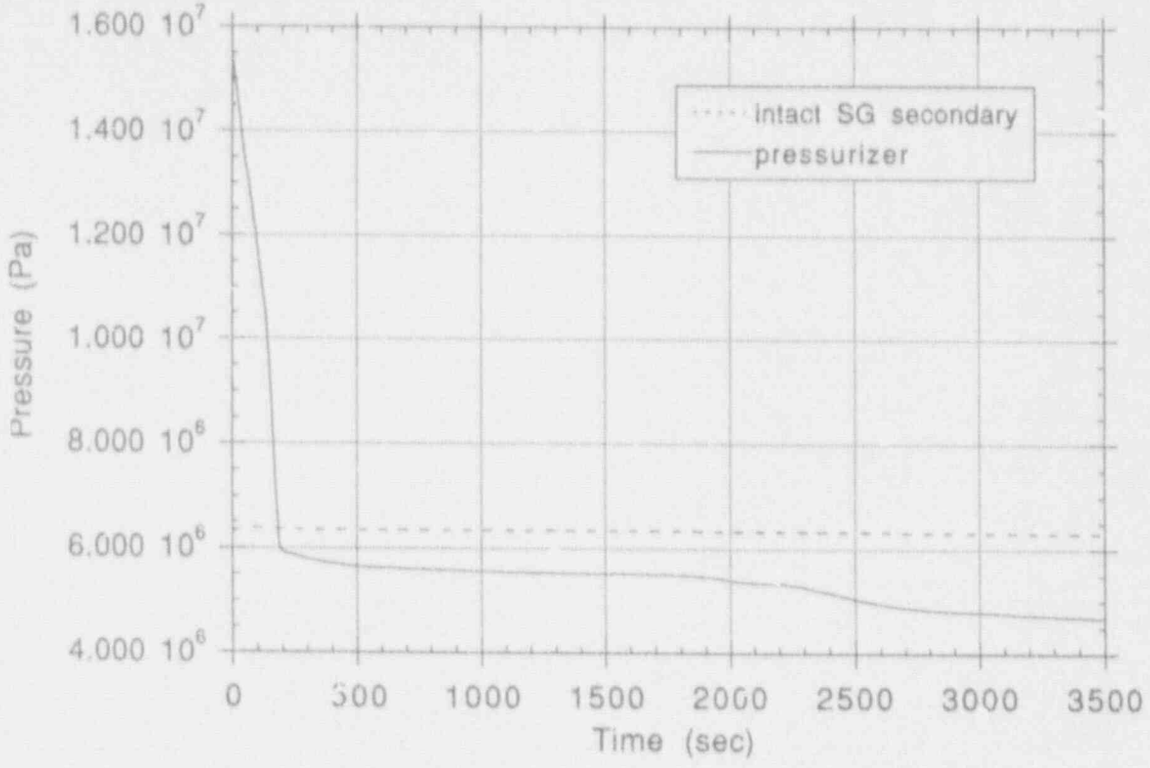

Figure 111. Pressurizer and intact steam generator secondary pressure for AP600 MSLB calculation.

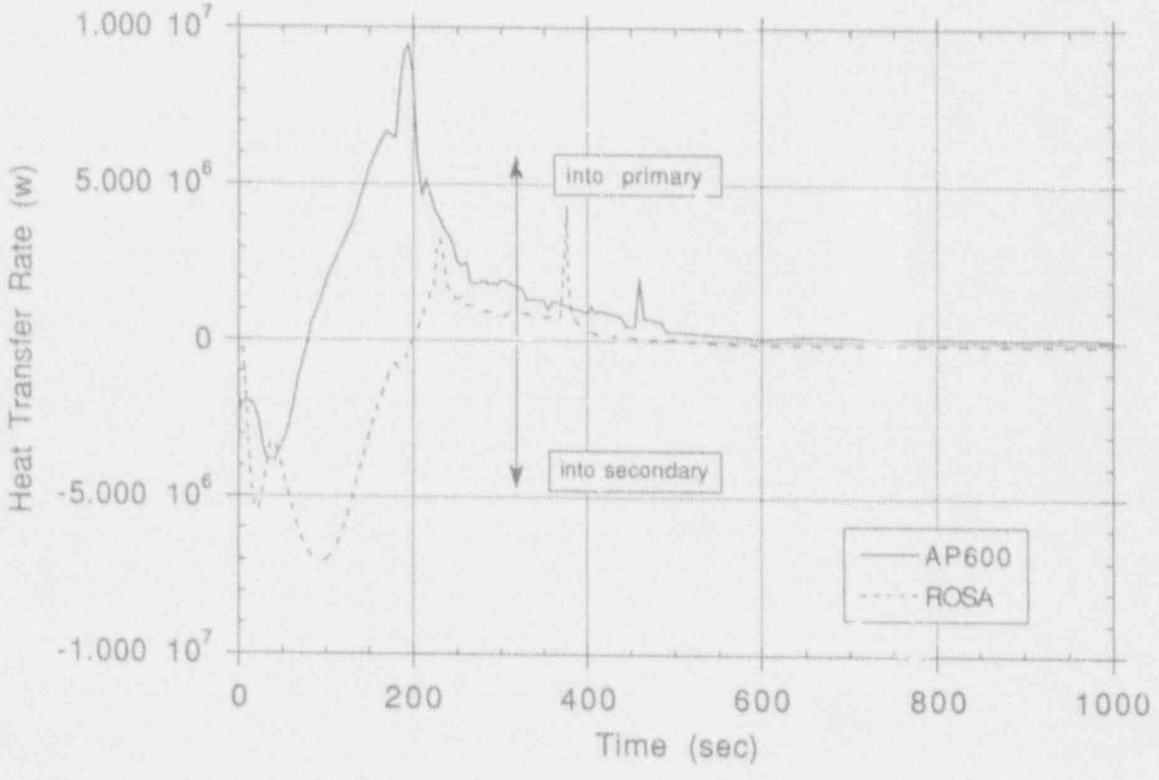

Figure 112. Intact side steam generator heat transfer for ROSA and AP600 MSLB calculations.

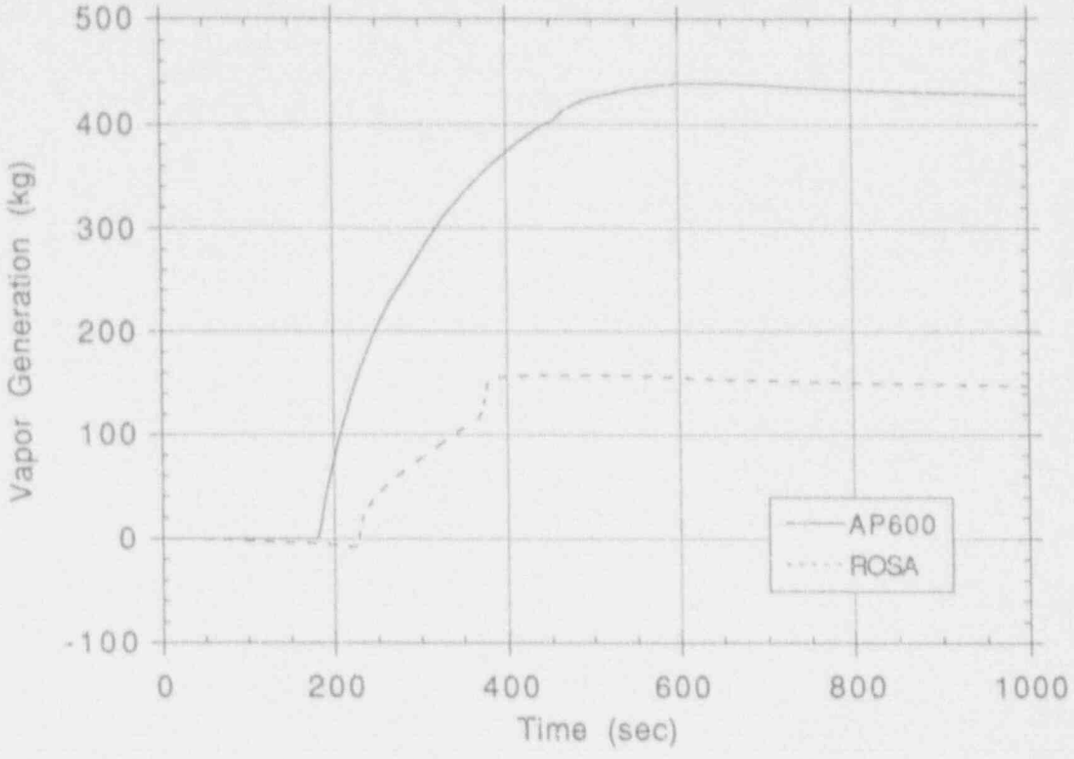

Figure 113. Intact side steam generator total vapor generation for ROSA and AP600 MSLB calculations.

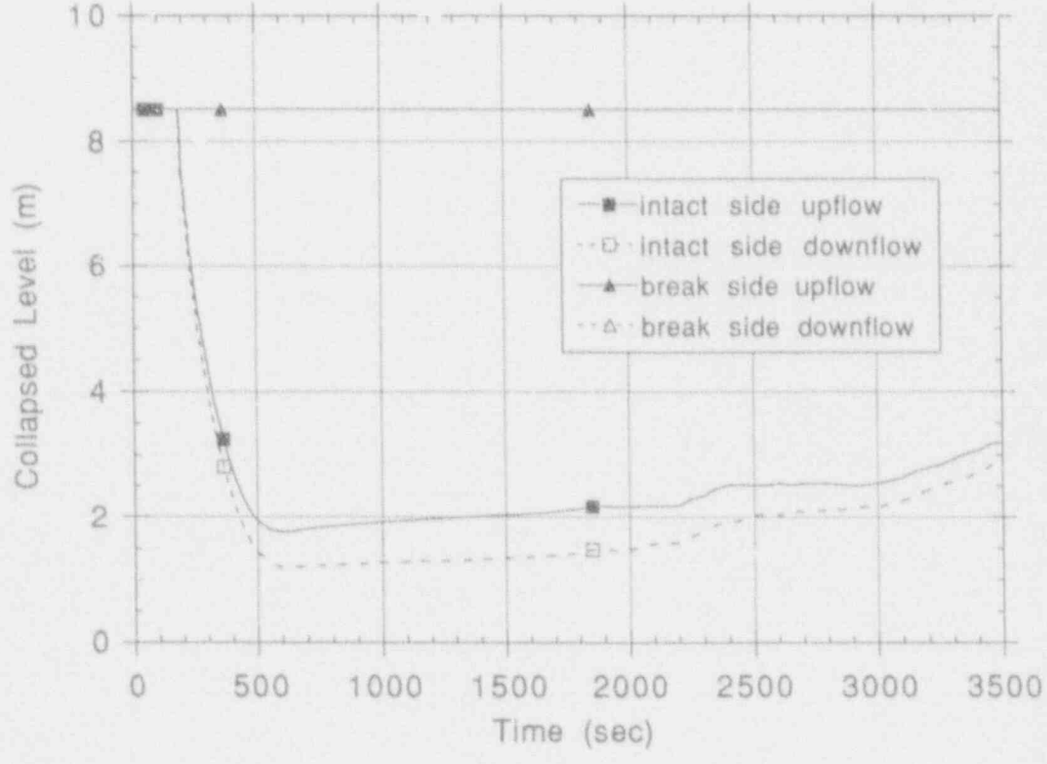

Figure 114. Steam generator U-tube collapsed liquid level for AP600 MSLB calculation.

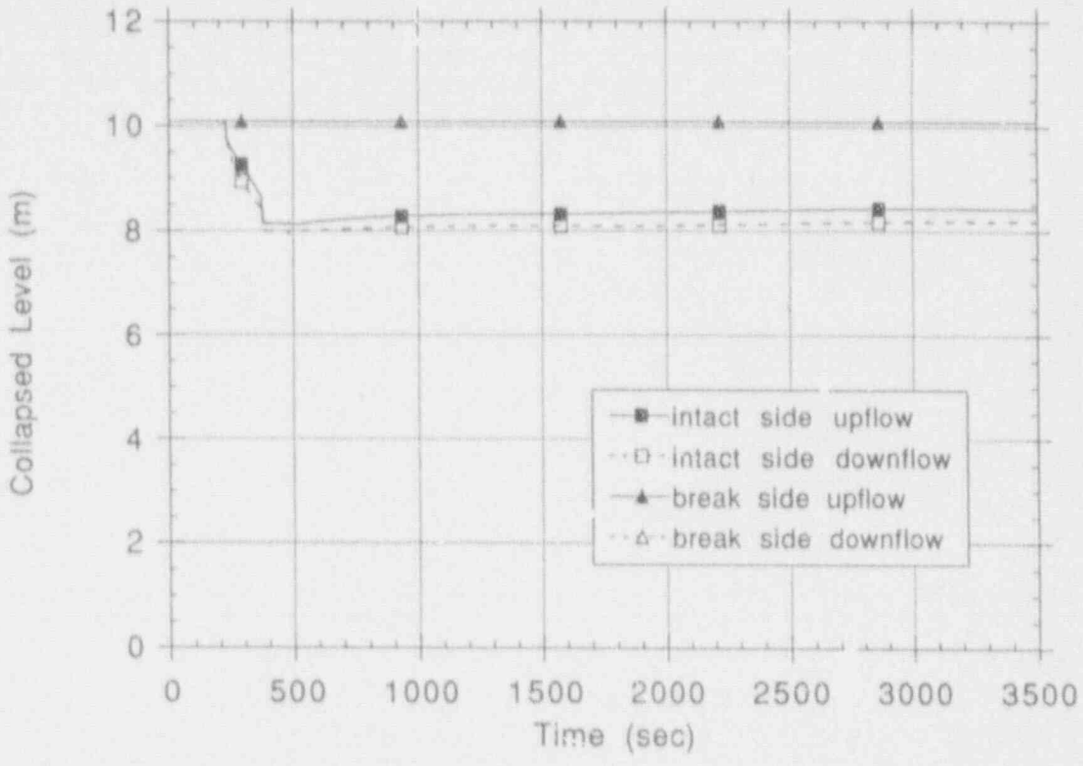

Figure 115. Steam generator U–tube collapsed liquid level for ROSA MSLB calculation.

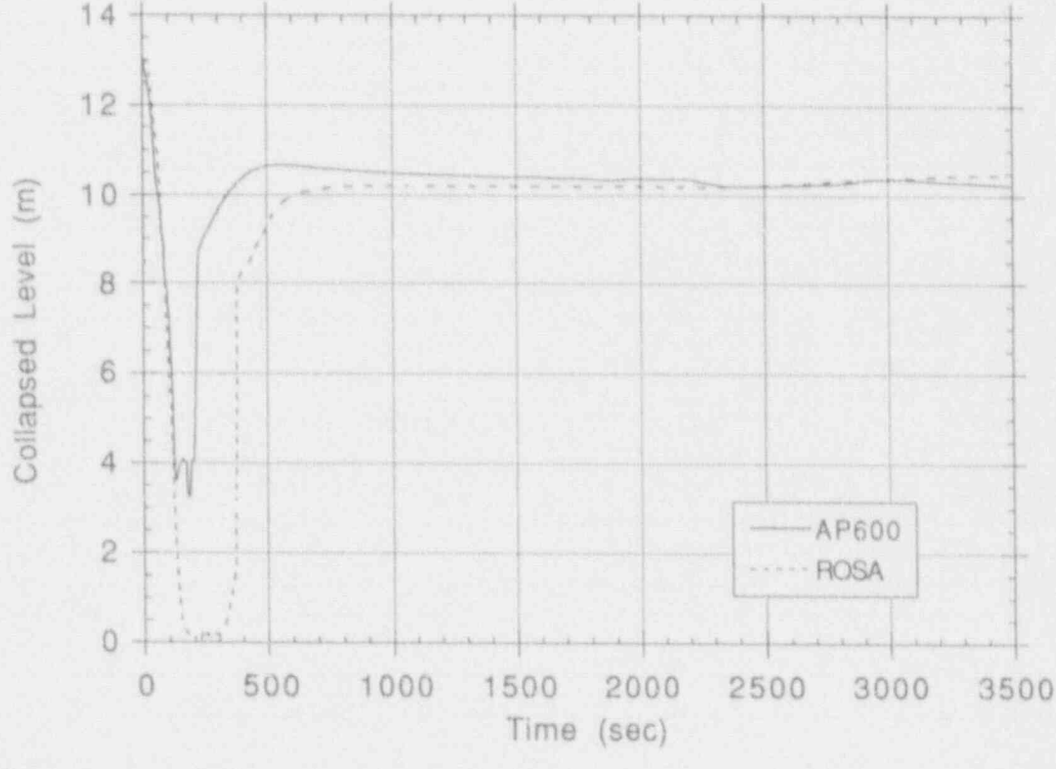

Figure 116. Combined pressurizer/surge line collapsed liquid level for ROSA and AP600 MSLB calculations.

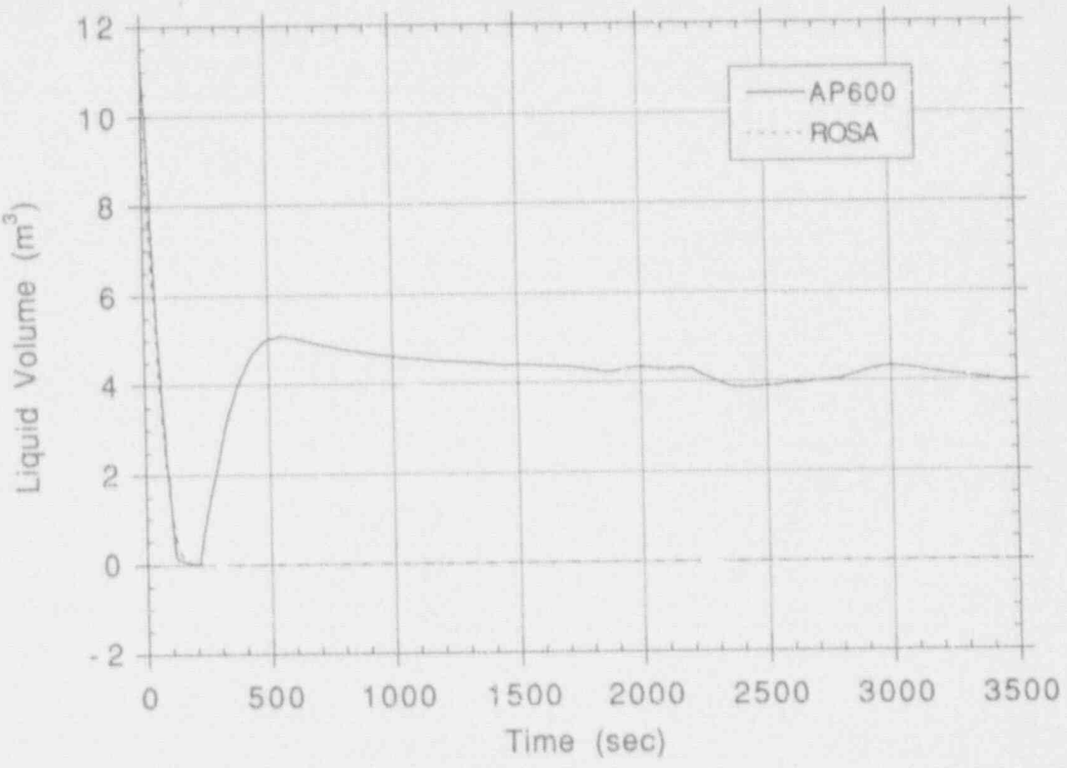

Figure 117. Pressurizer liquid volume for ROSA and AP600 MSLB calculations.

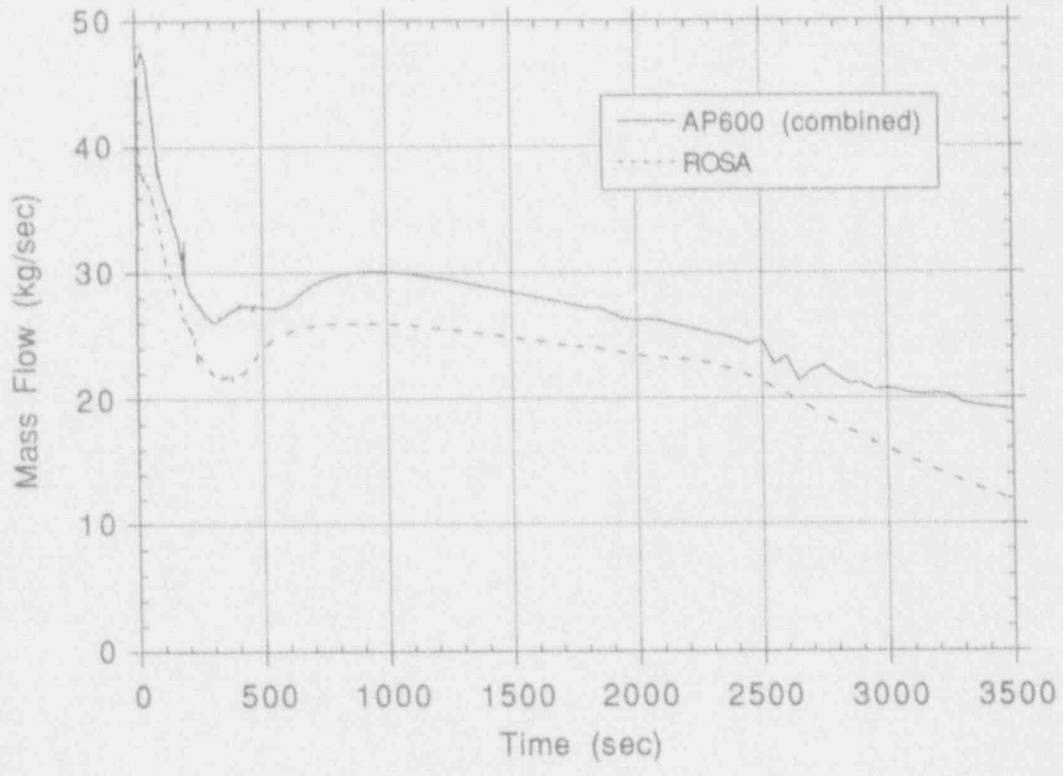

Figure 118. CMT mass flow rate for ROSA and AP600 MSLB calculations.

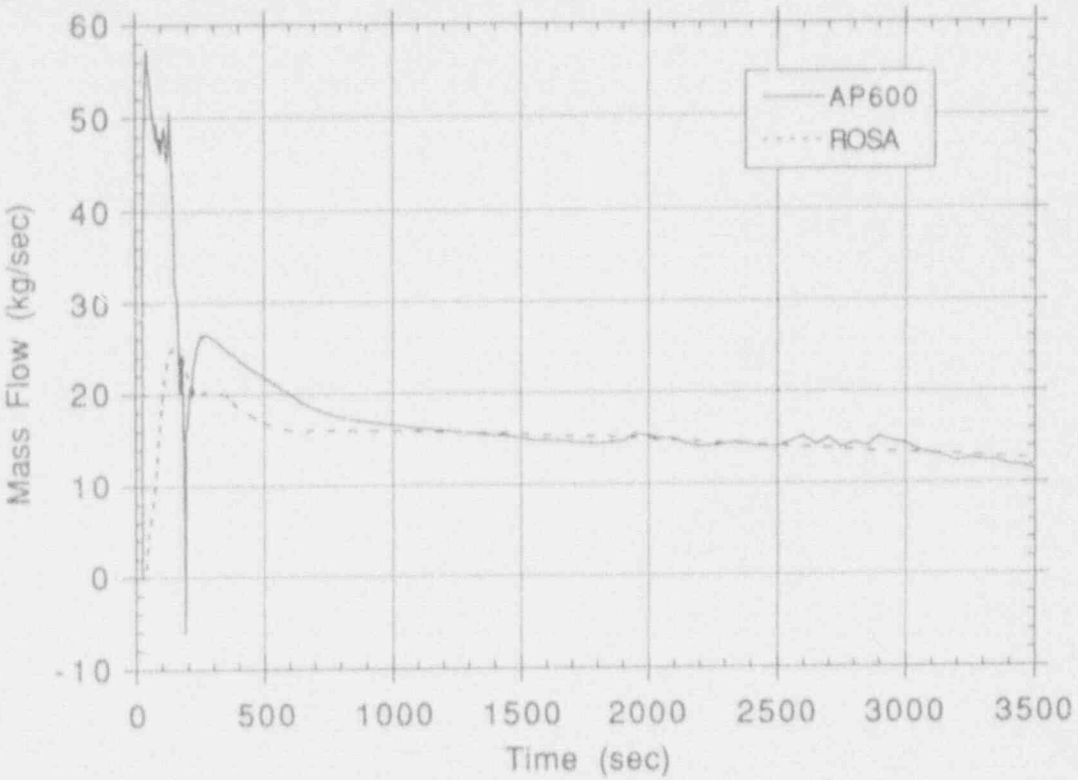

Figure 119. PRHR mass flow rate for ROSA and AP600 MSLB calculations.

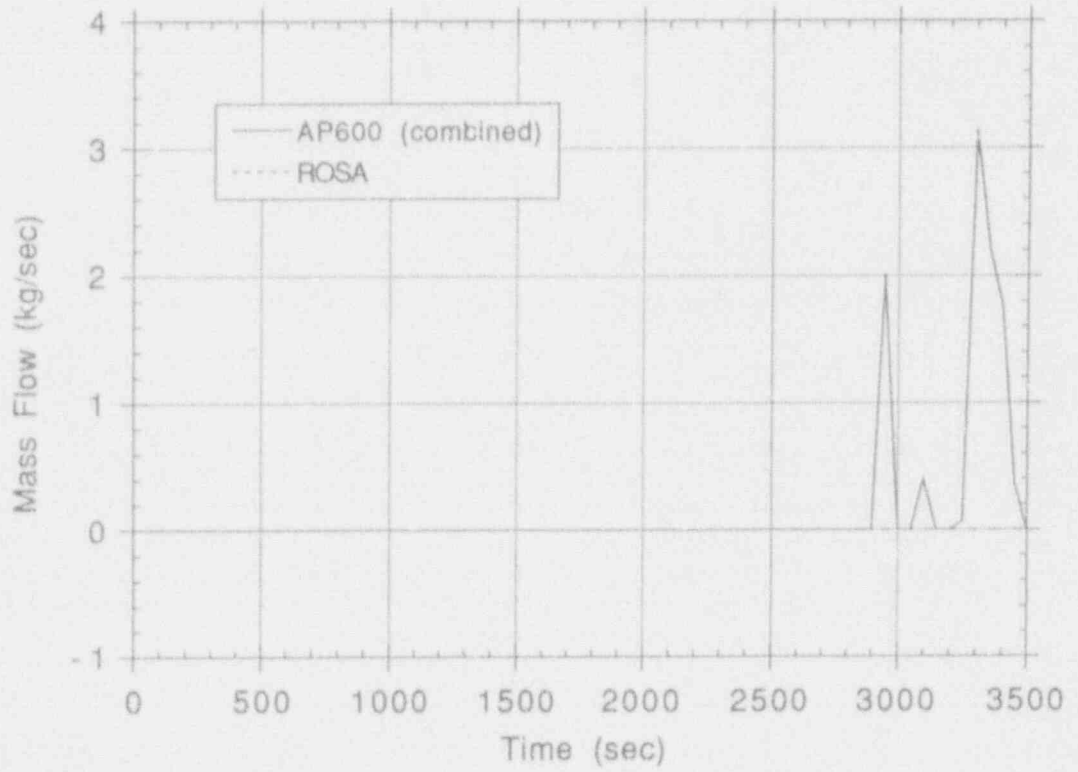

Figure 120. Accumulator mass flow rate for ROSA and AP600 MSLB calculations.

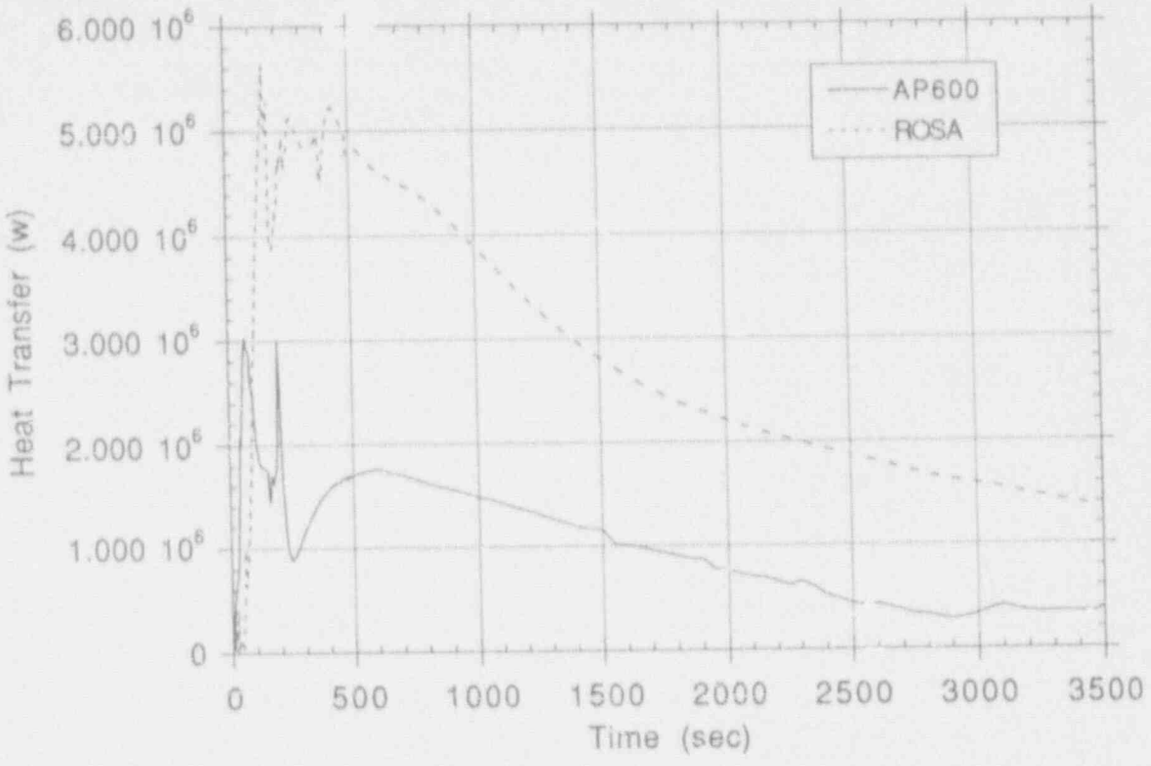

Figure 121. Total intact loop piping heat transfer for KOSA and AP600 MSLB calculations.

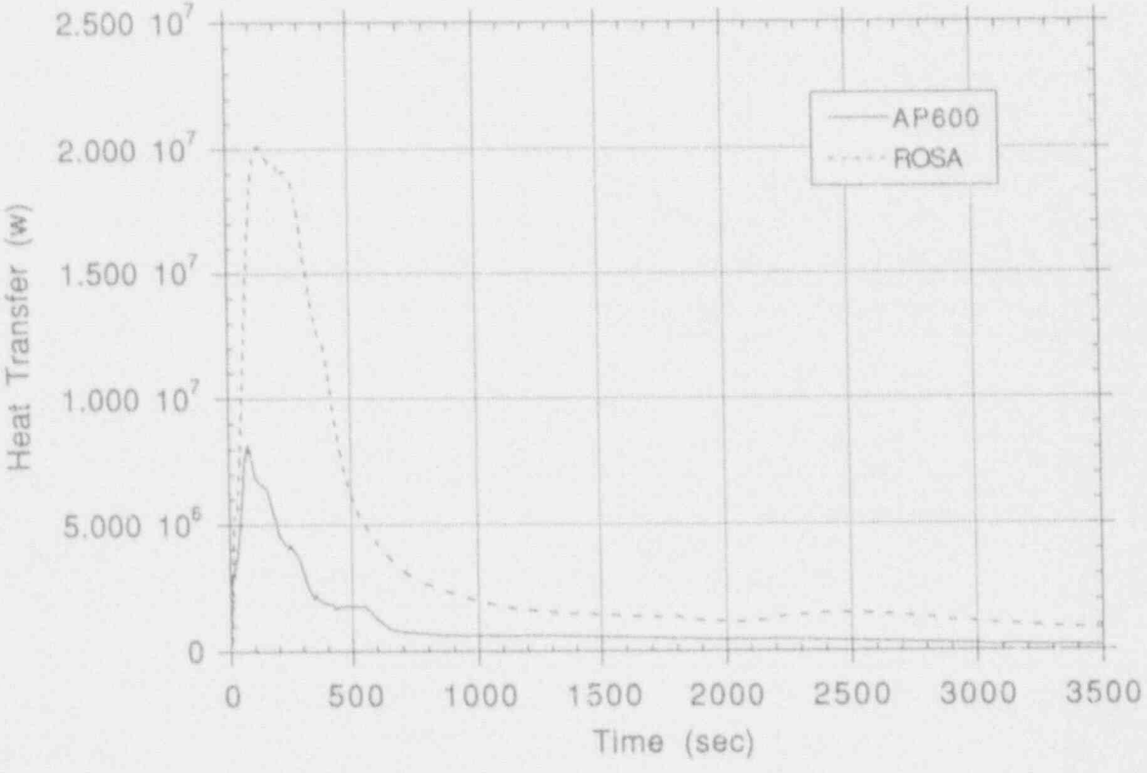

Figure 122. Total broken loop piping heat transfer for ROSA and AP600 MSLB calculations.

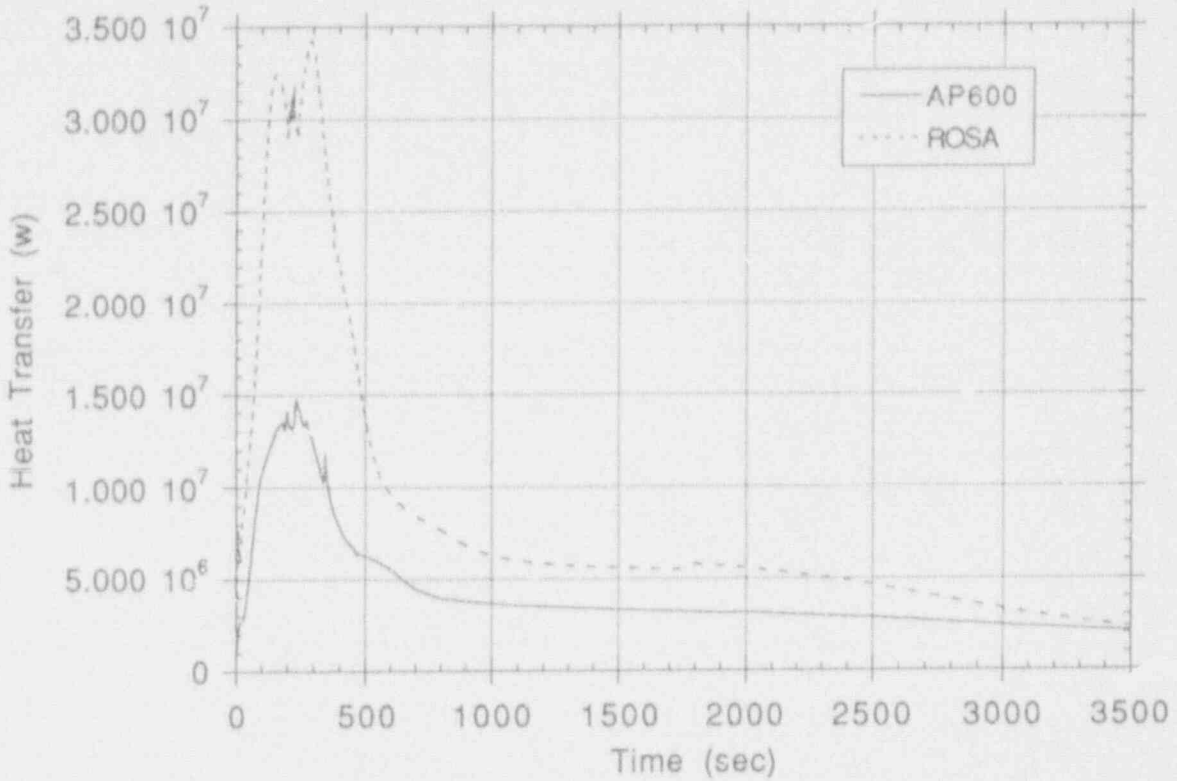

Figure 123. Total vessel heat transfer (excluding core) for ROSA and AP600 MSLB calculations.

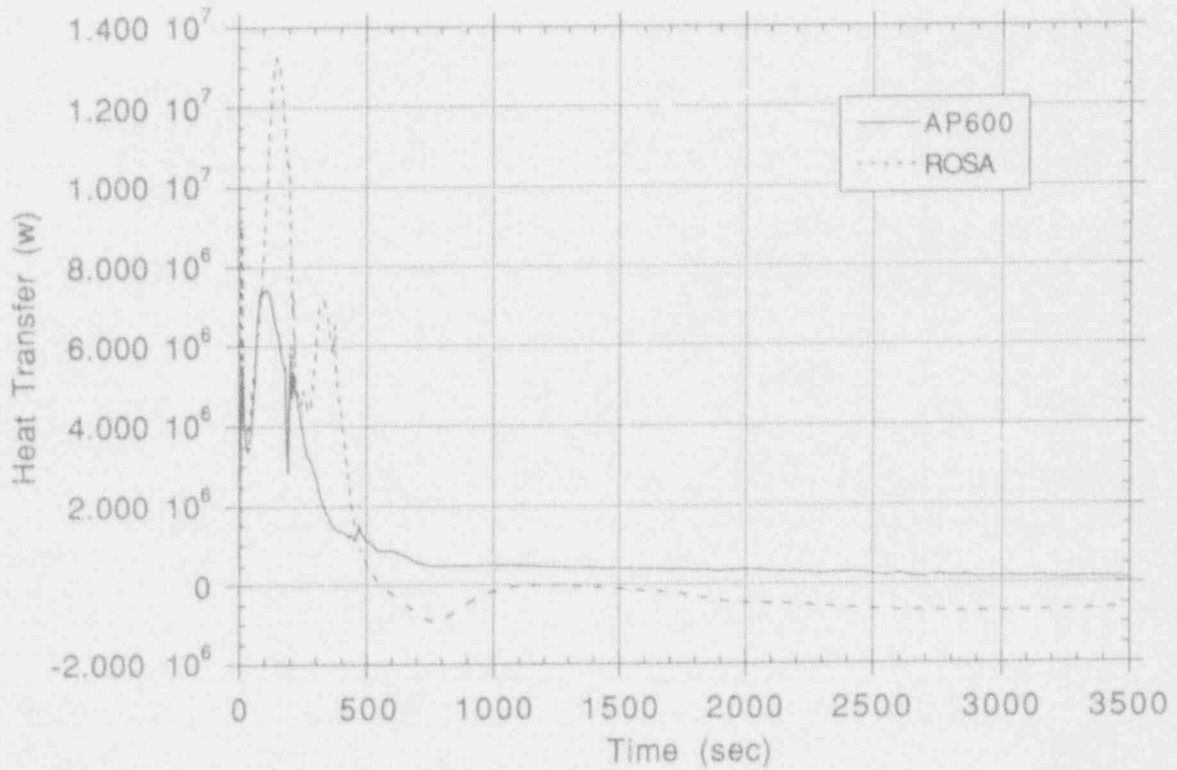

Figure 124. Total core fuel/heater rod heat transfer for ROSA and AP600 MSLB calculations.

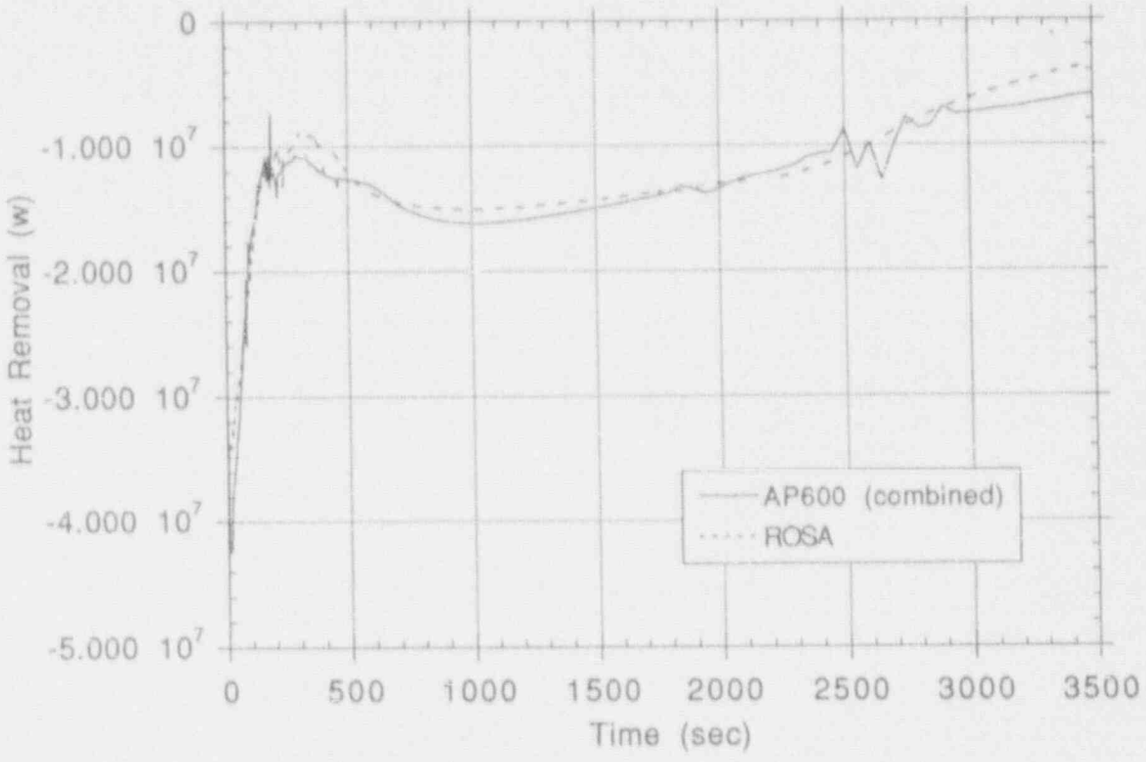

Figure 125. Total energy removal through CMT circulation for ROSA and AP600 MSLB calculations.

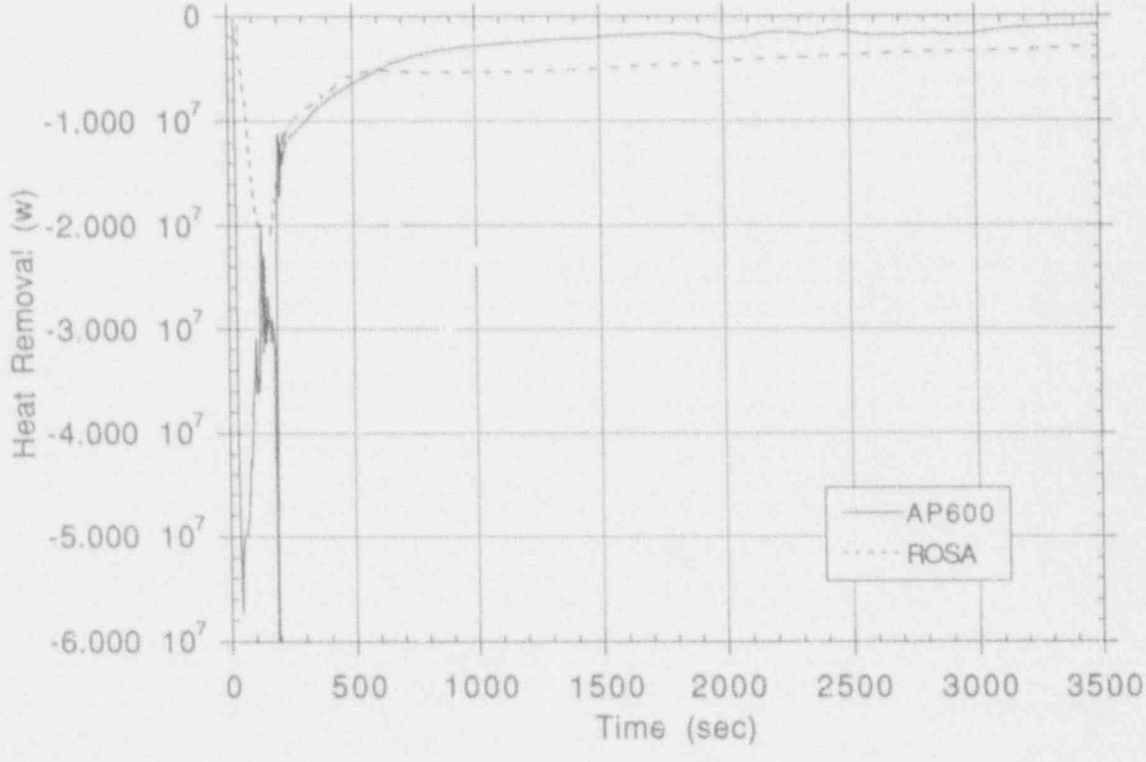

Figure 126. Total energy removal through PRHR system for ROSA and AP600 MSLB calculations.

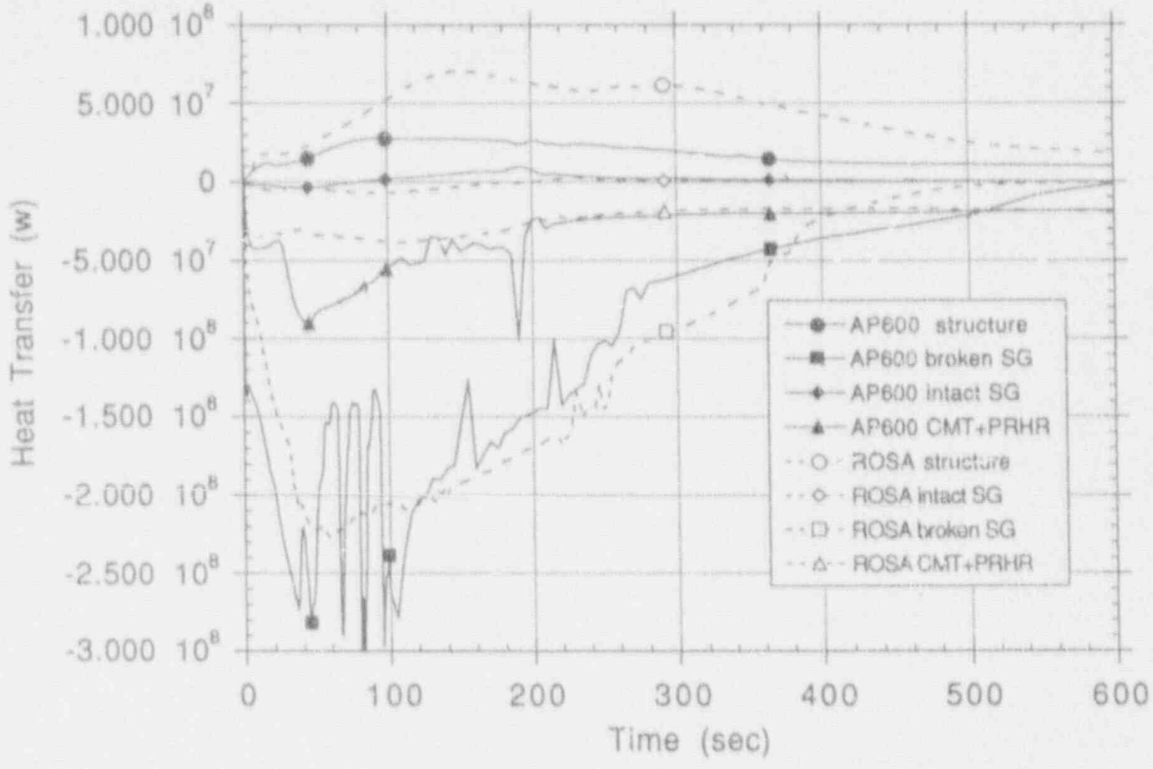

Figure 127. System heat transfer components (short term) for ROSA and AP600 MSLB calculations.

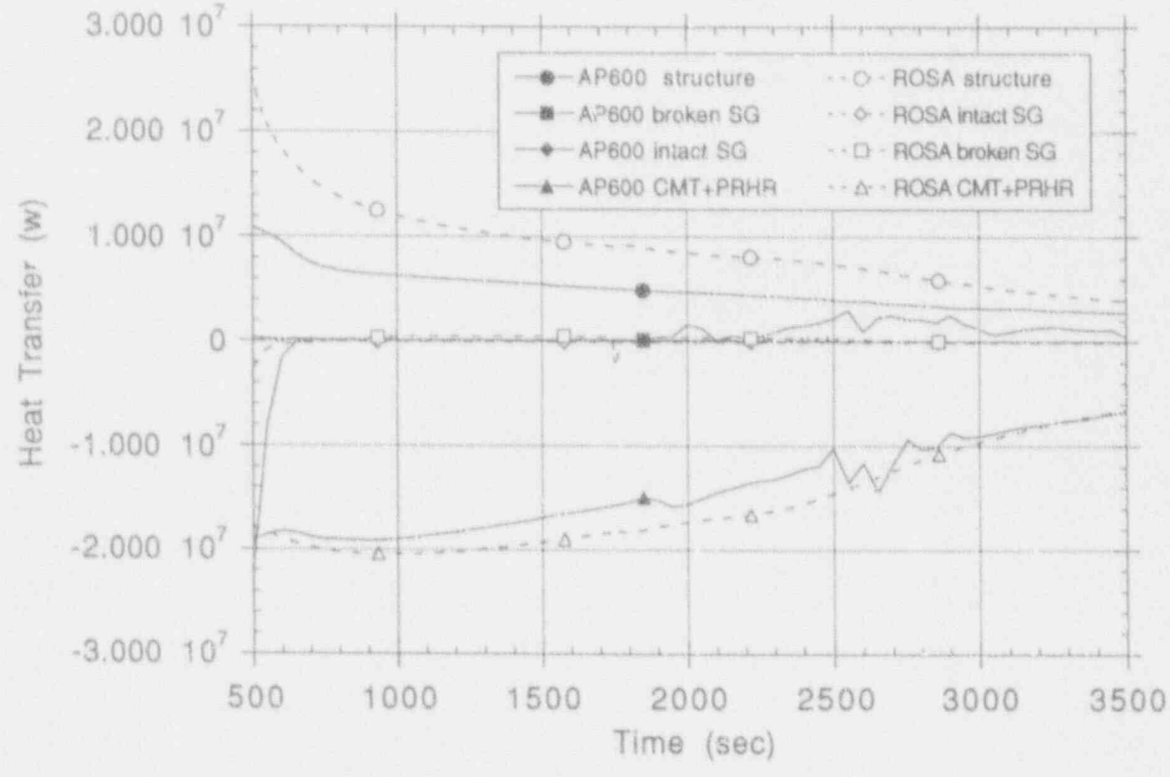

Figure 128. System heat transfer components (long term) for ROSA and AP600 MSLB calculations

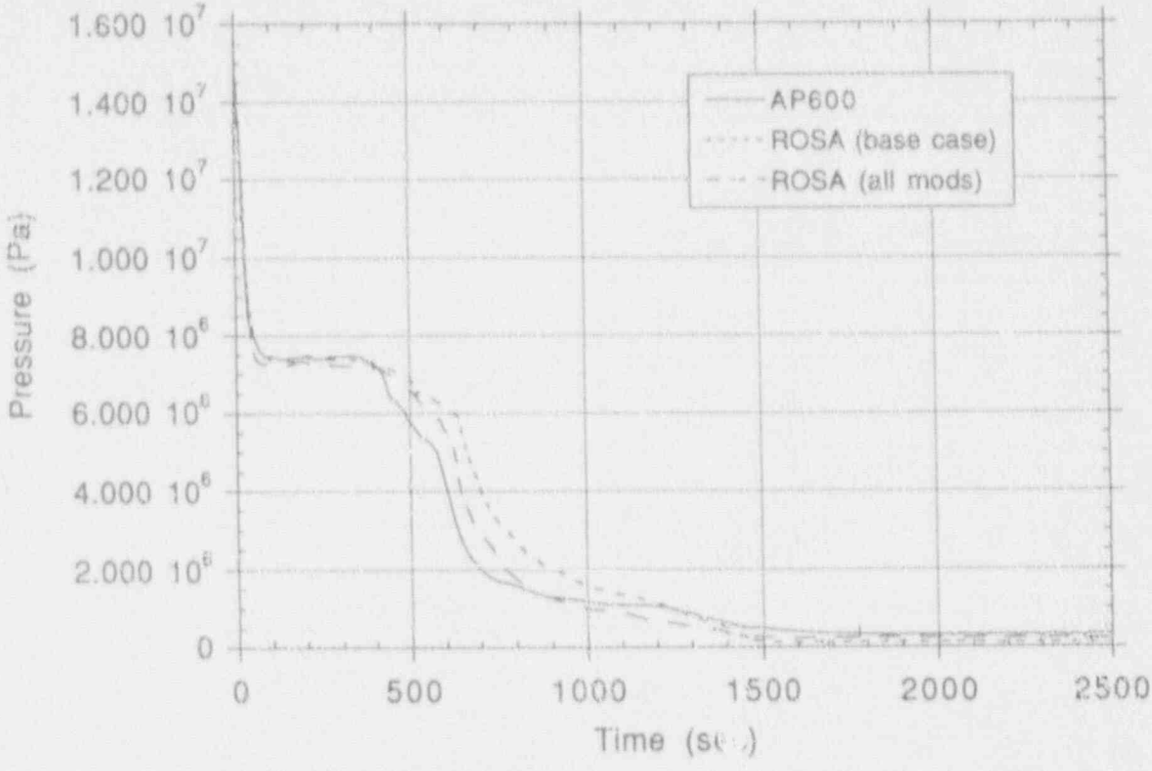

Figure 129. Pressurizer pressure for 3-inch CLB calculations.

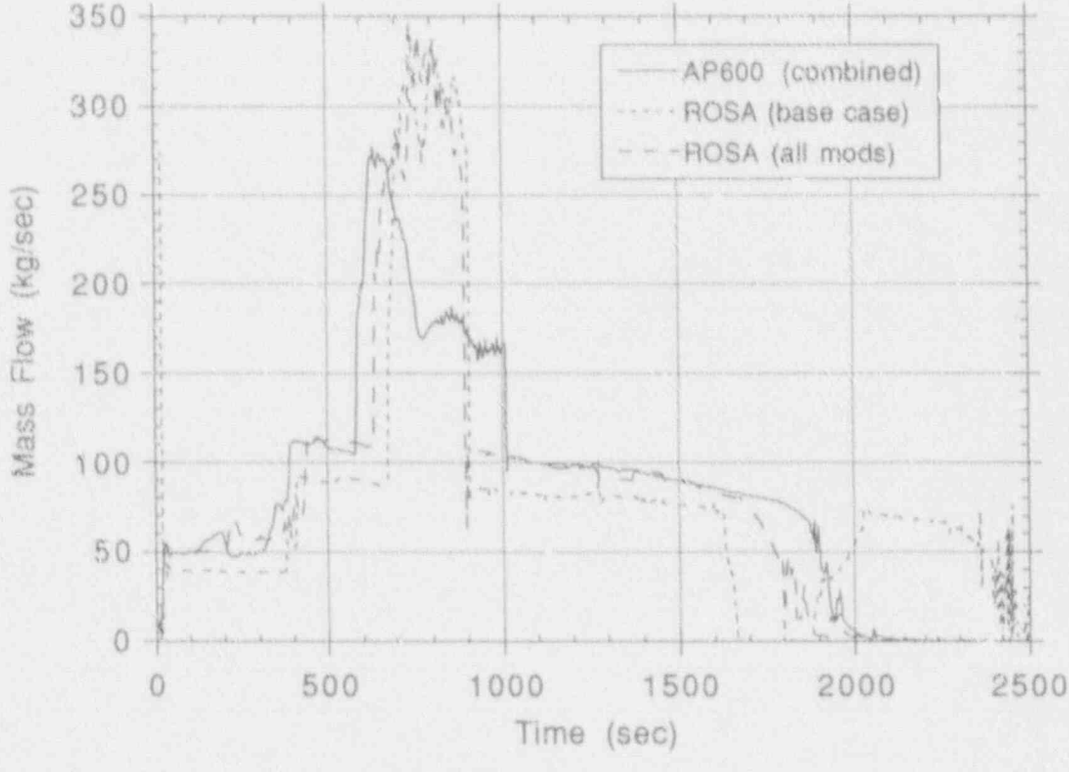

Figure 130. ECC mass flow rate for 3-inch CLB calculations.

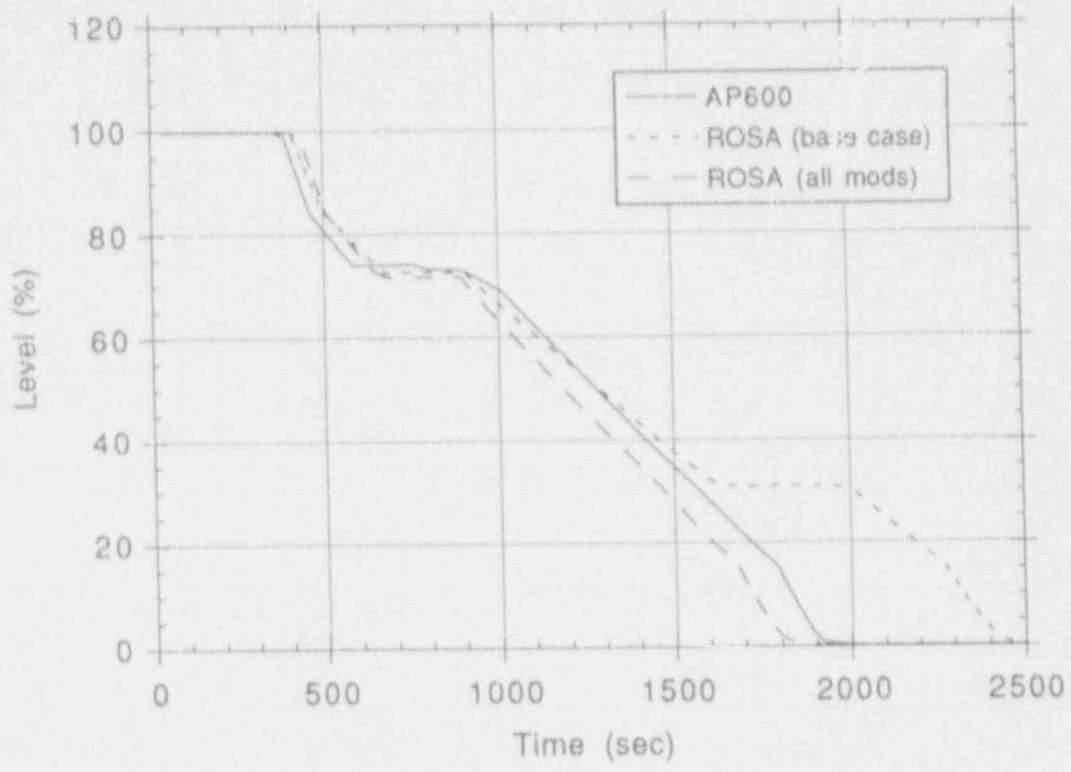

Figure 131. CMT liquid level for 3–inch CLB calculation.

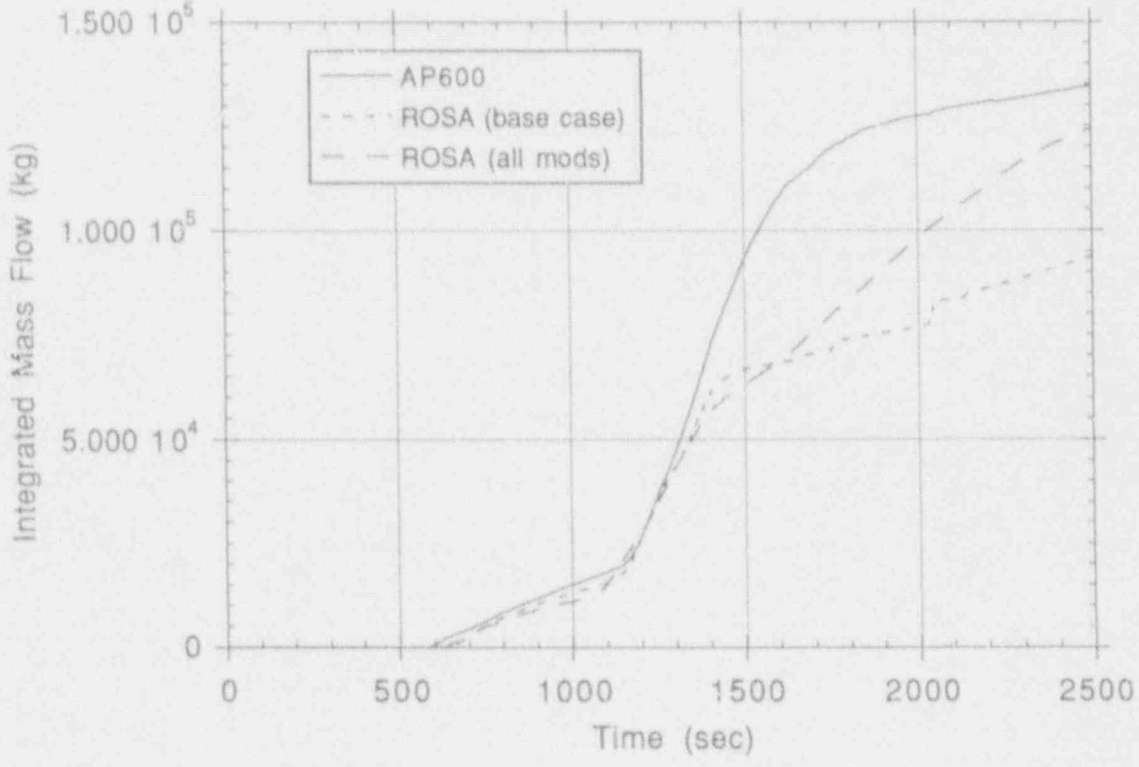

Figure 132. Total integrated ADS mass flow (Stages 1, 2, 3, and 4) for 3–inch CLB calculation.

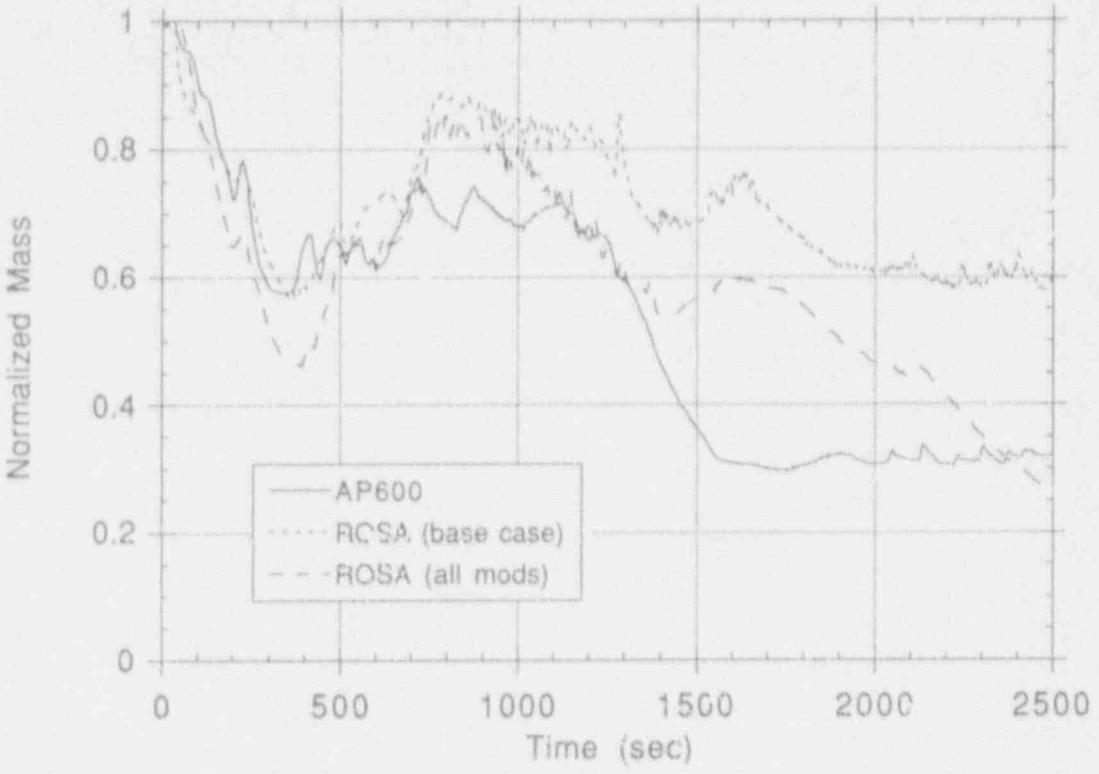

Figure 133. Vessel normalized mass inventory for 3–inch CLB calculations.

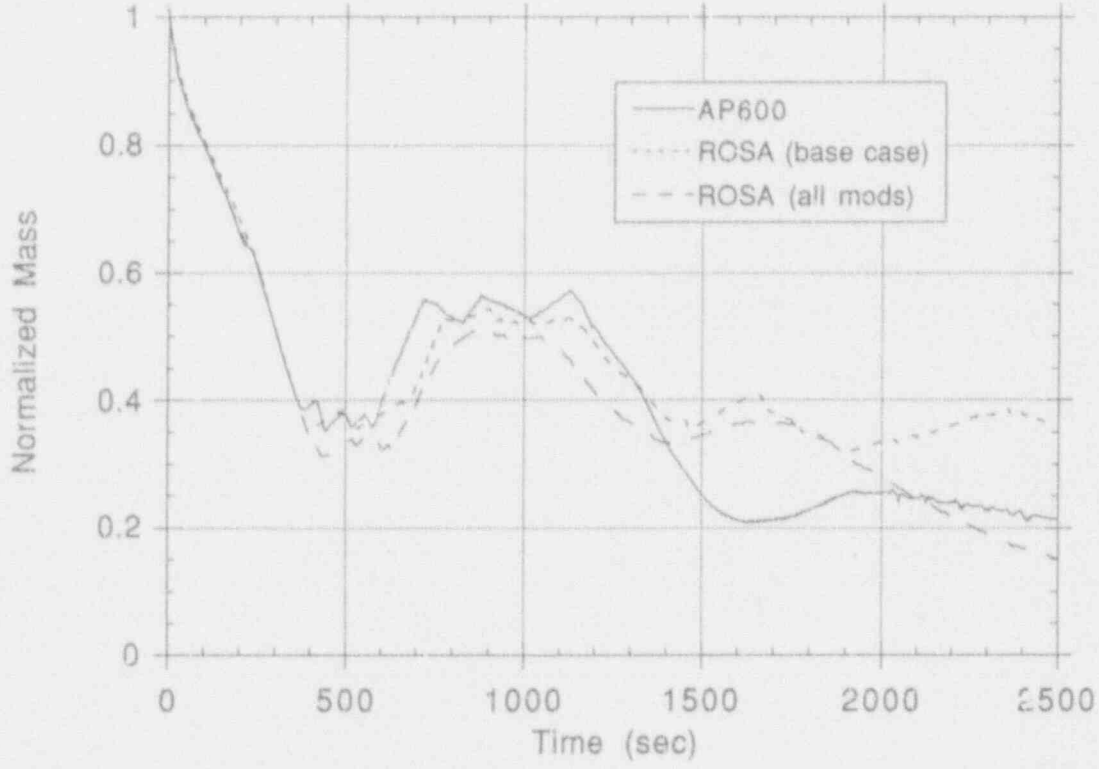

Figure 134. System normalized mass inventory for 3–inch CLB calculations.

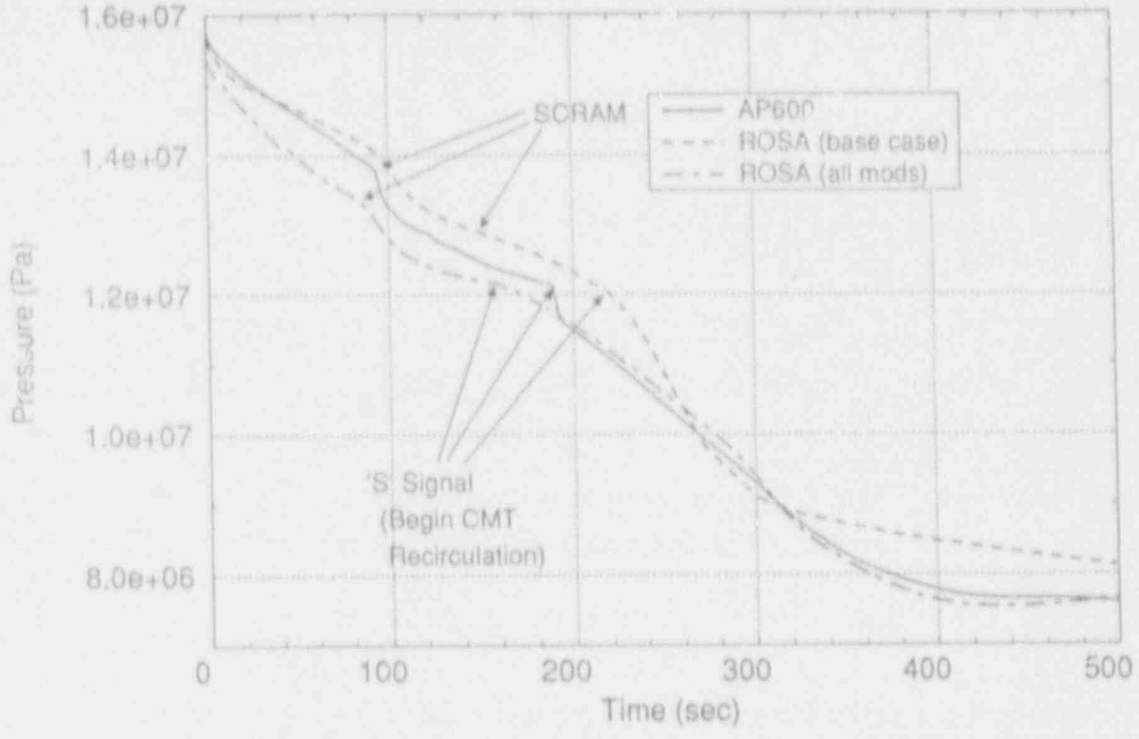

Figure 135. Pressurizer pressure (short term) for 1–inch CLB calculations.

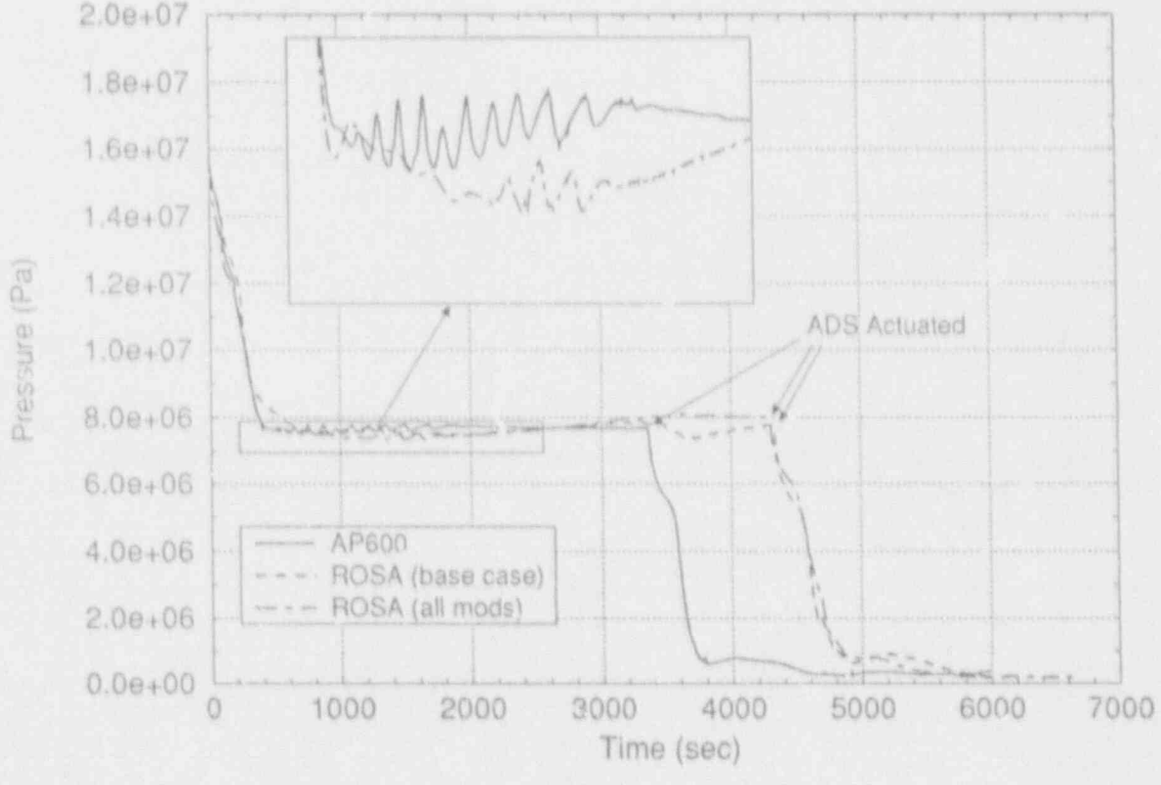

Figure 136. Pressurizer pressure for 1–inch CLB calculations.

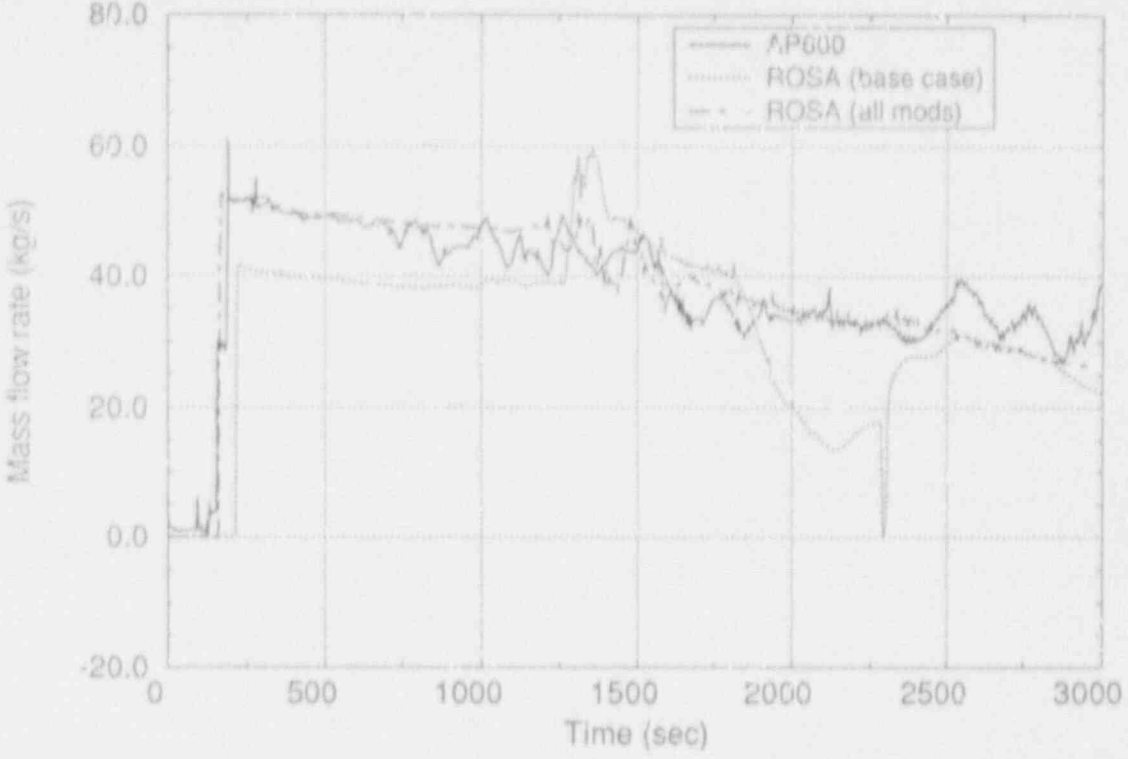

Figure 137. CMT mass flow rate for 1–inch CLB calculations.

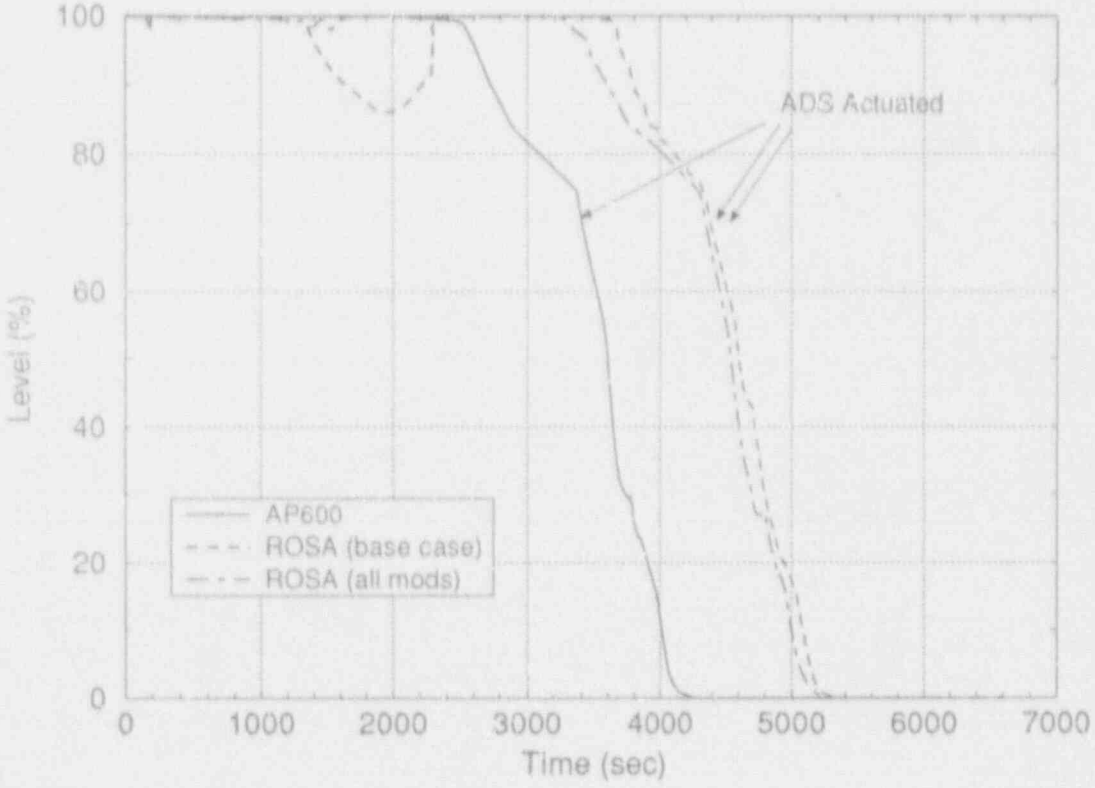

Figure 138. CMT level responses for 1–inch CLB calculations.

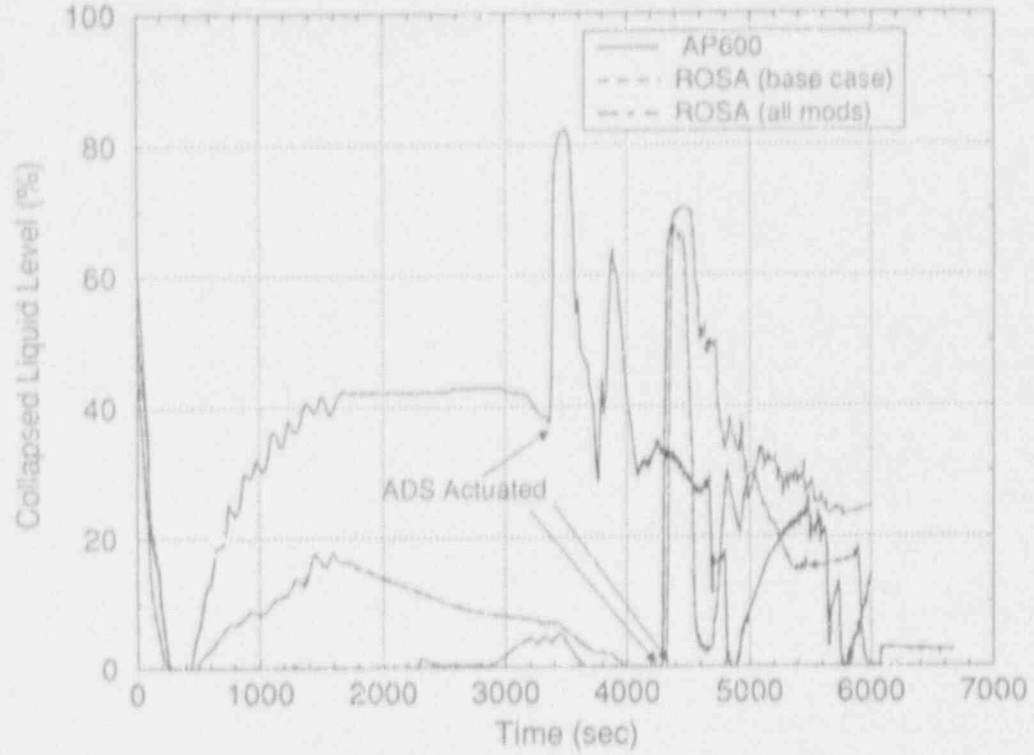

Figure 139. Pressurizer collapsed liquid level for 1-inch CLB calculations.

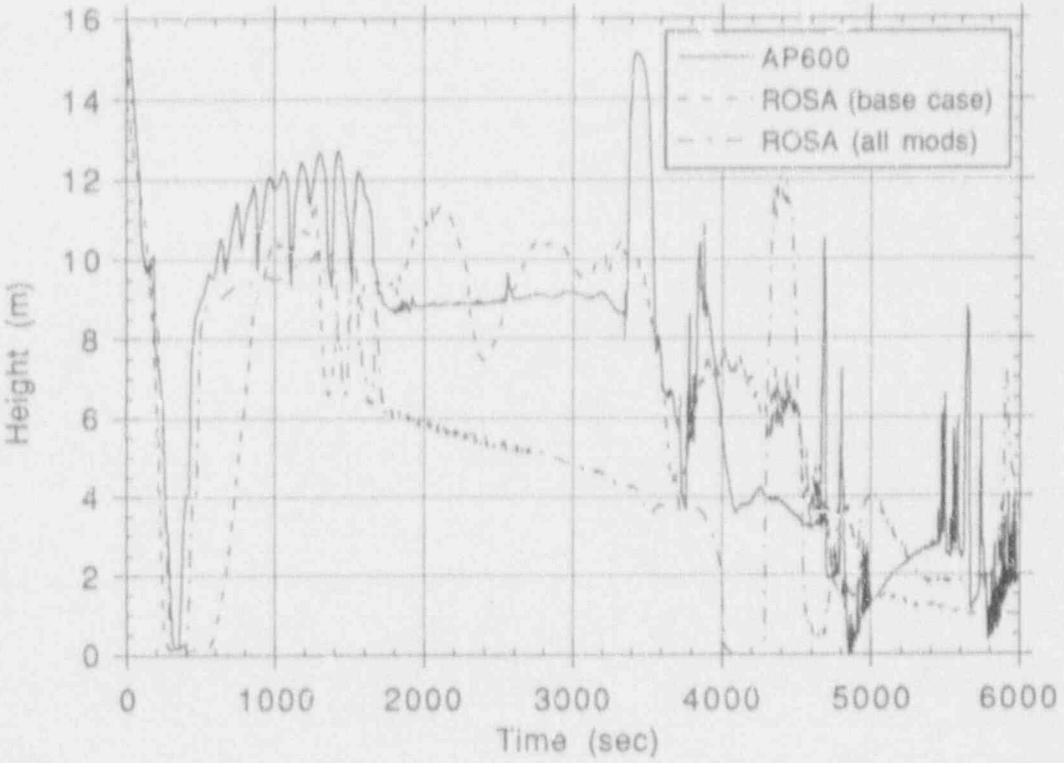

Figure 140. Combined pressurizer/surge line collapsed liquid level for 1-inch CLB calculations.

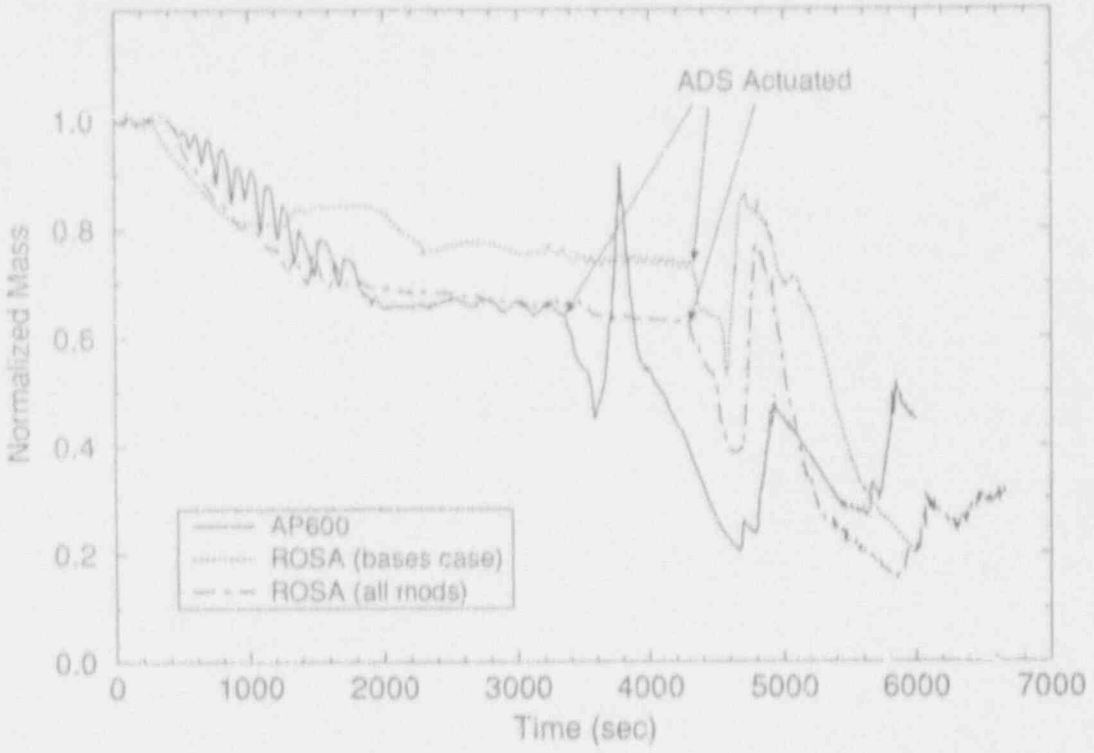

Figure 141. Vessel normalized mass inventory for 1-inch CLB calculations.

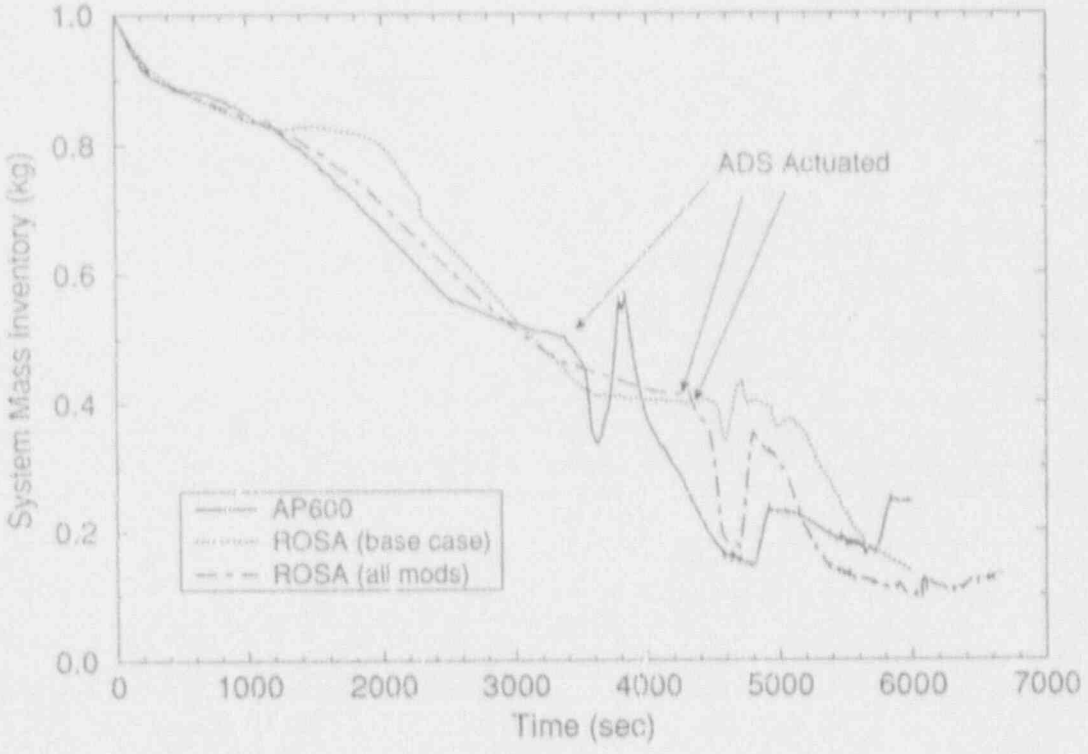

Figure 142. System normalized mass inventory for 1-inch CLB calculations.

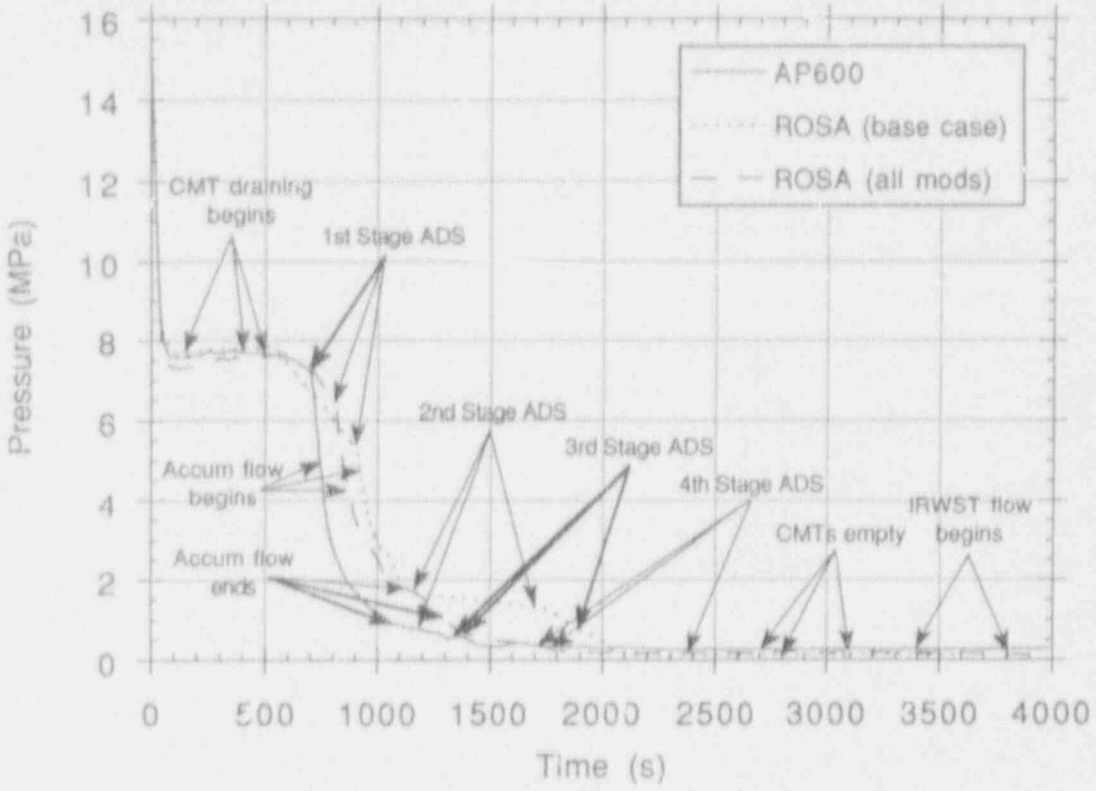

Figure 143. Pressure at the top of the pressurizer for the pressure balance line break.

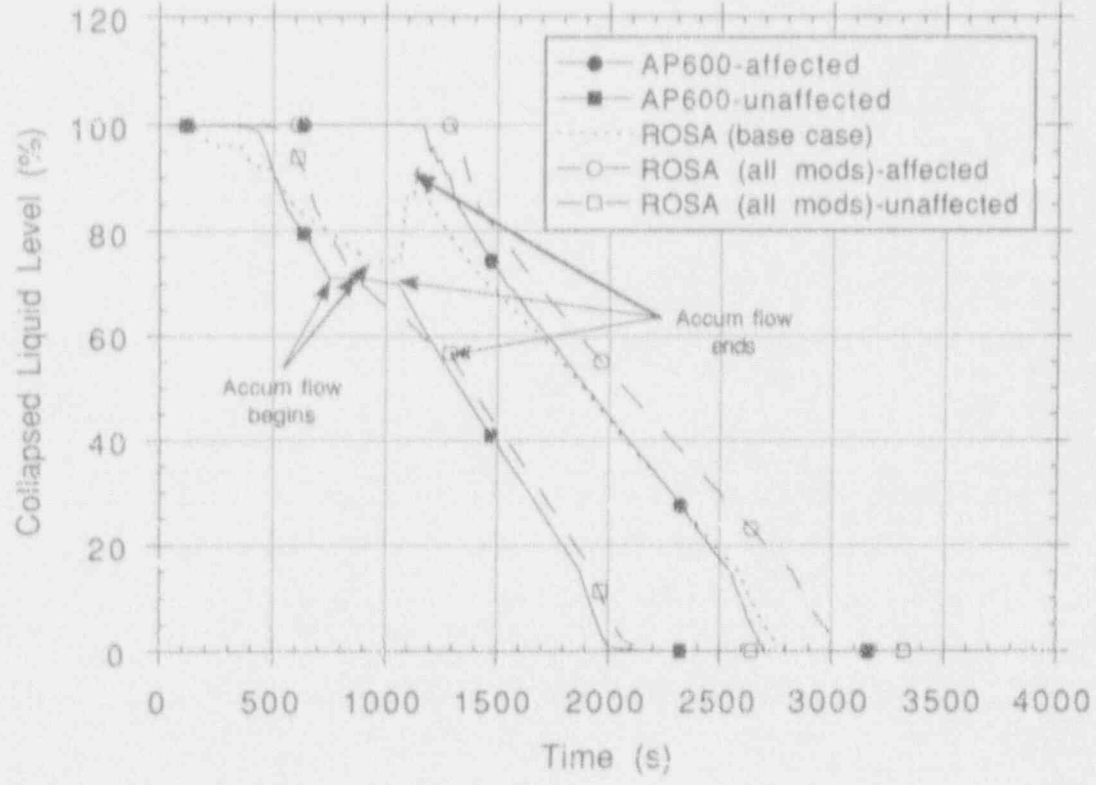

Figure 144. Collapsed liquid level in the CMTs for the pressure balance line break.

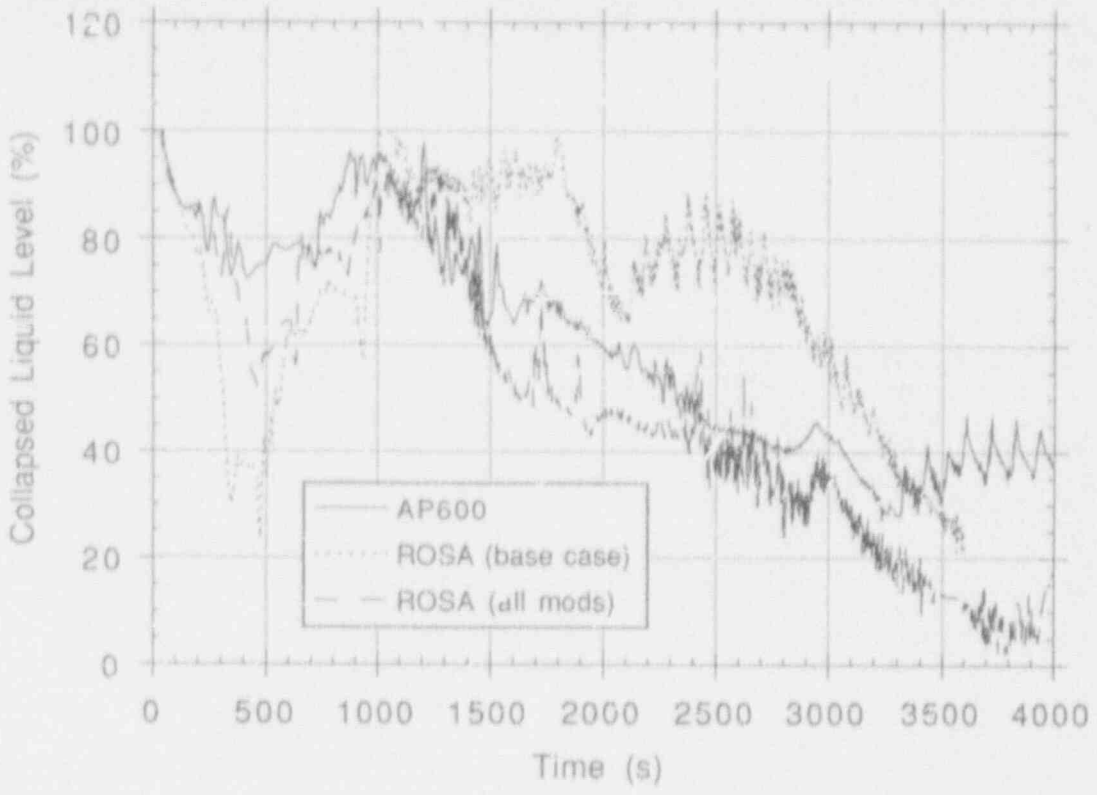

Figure 145. Collapsed liquid level in the core for the pressure balance line break.

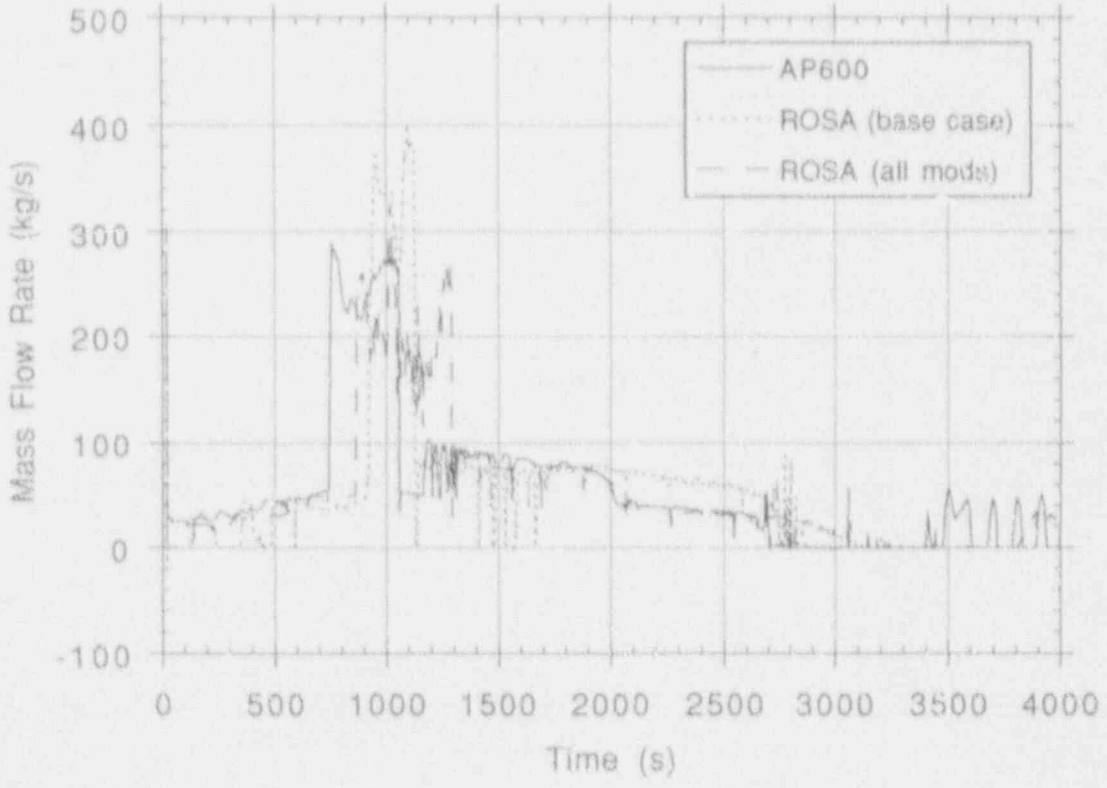

Figure 146. ECC injection flow rate into the reactor vessel for the pressure balance line break.

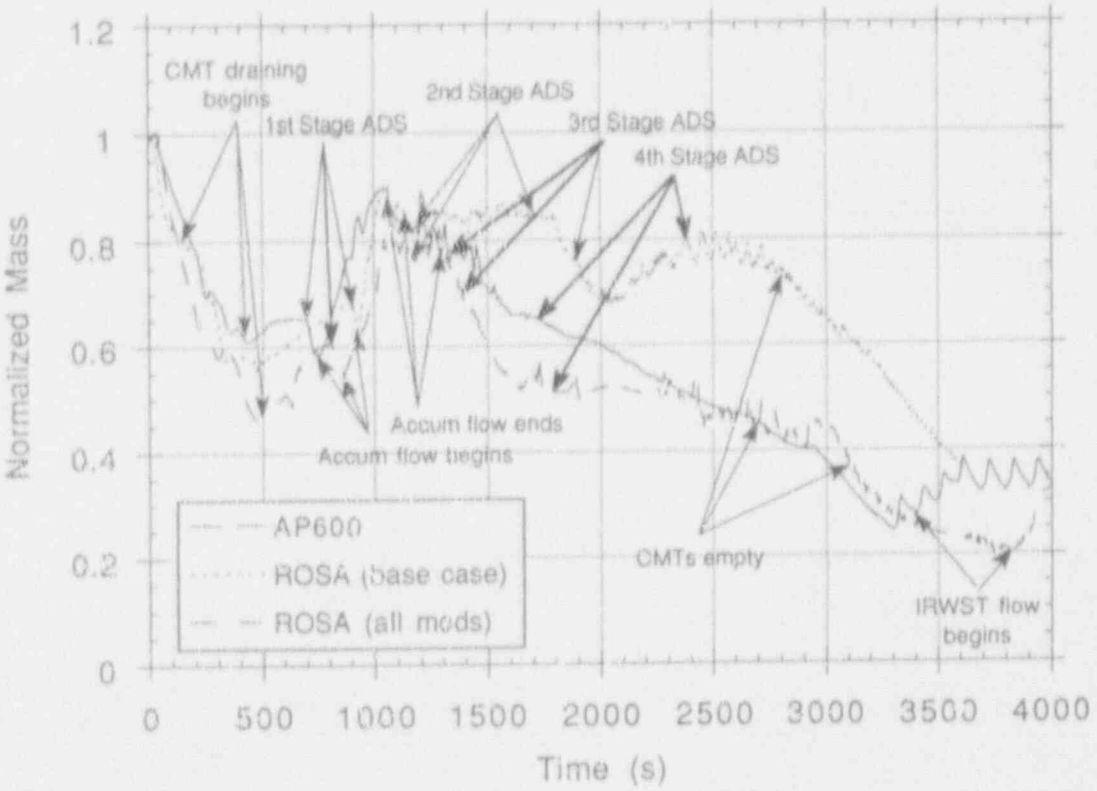

Figure 147. Normalized reactor vessel mass inventory for the pressure balance line break.

Appendix

Sensitivity Study of Pressure Balance Line with Two Cold Legs and CMTs

Appendix

Sensitivity Study of Pressure Balance Line with Two Cold Legs and CMTs

A.1 INTRODUCTION

A sensitivity study was conducted for the pressure balance line 3-in. break case to evaluate the potential benefit of including third-level modifications in the ROSA facility. These modifications comprised the addition of two separate core makeup tanks (CMTs) and associated accumulators and piping. Separate pressure balance lines were required, which were connected to separate branches of the cold leg. Thus, the cold leg was modeled as two branches of piping between the pump and the downcomer penetration. This model included all the first and second level modifications as well; plus, the ROSA downcomer model was changed to a pseudo-two-dimensional representation to make it similar to the AP600 model.

A.2 ROSA CORE UNCOVERY

As shown by Figure A-1, the initial scaled break flow rate was higher in ROSA, particularly during the early response (prior to 600 seconds). This was attributed to the difference in cold leg elevations, which apparently caused the differences in break void fraction which occurred between 50 and 500 seconds. This was the same as the base case (Section 4.3). During the first 500 transient seconds, void fraction in the downcomer cell connected to the affected cold leg was lower in ROSA than in AP600. This resulted in a lower cold leg void fraction and higher break flow in ROSA. The atypically high break flow, coupled with other factors, was responsible for a predicted core liquid level depression in ROSA that was not seen in AP600, shown in Figure A-2. These other factors include differences in static and friction head in the steam generator tube bundle upflow sides and differences in the upper head configuration and initial conditions. First, as shown in Figure A-3, the steam generator upflow side tubes in AP600 cleared of liquid more quickly than in ROSA, starting at about 300 seconds, roughly corresponding to the time the core level depression began in ROSA. Second, ROSA had an inverted top hat upper head design, which could only drain via the guide tubes or to the downcomer. The guide tube path was much more restrictive than in AP600, and the downcomer leakage path was much smaller; initial temperature was thereby the same as core outlet temperature, and with decreasing system pressure, the ROSA upper plenum became a supply of saturated steam, not a source of liquid. Conversely, the AP600 upper head obtained cooling spray from the downcomer, was initially at cold leg temperature, and was a source of liquid to the core. Therefore, the core collapsed liquid level responses of the two models were significantly different. In ROSA, the reactor core became the source of water for the break flow, whereas in AP600, the core collapsed liquid level was maintained greater than about 75%.

The ROSA core uncovery caused a heatup (Figure A-4) not seen in AP600. The energy release into the coolant during the fuel quench delayed the pressure decay response in ROSA. It also resulted in higher energy steam flow through the broken loop following the quench. This steam was condensed by the cold accumulator liquid flowing up the downcomer and back into the cold liquid. Substantially, more condensation was predicted by the code for this case than for the comparison AP600 calculation and occurred in the period between 1,200 and 1,400 seconds.

A.3 DELAYED CMT RESPONSE IN ROSA

The overall progression or timing of the transient was controlled in both cases largely by the draining characteristics of the intact CMT because the opening of the ADS valves, and sub-

sequently the actuation of the accumulators, was dependent upon the level decrease in the intact CMT. Thus, the major differences shown in the ROSA calculation were attributable to delayed draining of the intact CMT (Figure A-5). These differences included late ADS actuation and accumulator injection. Also, late accumulator injection resulted in delay of the draining of the affected CMT (the CMTs could not flow while the accumulators were injecting).

The delay in intact CMT draining occurred primarily because voids appeared in the cold leg to which the PBL was connected about 300 seconds later in ROSA (Figure A-6). As long as the cold leg contained mostly liquid, the CMT continued to operate in recirculation mode and did not drain. For the first 400 seconds of the transient, both the ROSA and AP600 intact CMTs operated in recirculation mode. During this period, the intact CMTs were providing flow to the downcomer, but most of that liquid was recirculated via the cold leg and PBL back to the CMT to keep it full. Later, when a significant amount of void appeared in the cold leg (to which the PBL to the CMT was attached), this recirculation ceased and the CMT level began to drop. In AP600, this cold leg began to contain voids at 100 seconds; ROSA started to contain voids at 409 seconds. As a result, the AP600 intact CMT began to drain sooner than that of ROSA.

Although a single root cause of the later voiding of the cold leg to which the intact CMT pressure balance line was connected has not been conclusively identified, the major contributors are believed to be the upper head response and the split cold leg geometry. Of these two factors, the upper head response appeared to have the most impact on the cold leg void fraction.

Differences in the flow paths out of the upper head caused the draining rate of the ROSA upper head to be slower than that of AP600 (Figure A-7). It can be seen in the ROSA nodalization diagram (Figure 4) that the upper head had only two possible drain paths: to the downcomer and through the guide tubes to the core region. Furthermore, the scaled area of the upper head to downcomer flow path was only about 12% of the area of the same flow path in AP600. Since there was no direct drain path from the upper head to the upper plenum as in AP600 (Figure 2) and the drain path to the downcomer was much smaller, the ROSA upper plenum took much longer to empty than that of AP600. As seen in Figure A-7, the AP600 upper head was completely drained by 400 seconds; the ROSA upper head Volume 148 was not completely drained until after 600 seconds. (In ROSA, upper head Volume 152 voided quickly because it is initialized 34 K hotter than upper head Volume 150 in AP600.) Because the AP600 had an additional drain path from the upper head to the upper plenum and the path the downcomer was larger, the upper head emptied sooner, and consequently, the downcomer level began to increase earlier and the cold legs were uncovered sooner.

The "Y" configuration of the split cold leg geometry also contributed to the sustained recirculation mode in the intact CMT because it distorted the magnitude of the flow rate toward the intact CMT once cold leg flow had reversed (Figure A-8). In both cases, the break caused the cold leg flow at the vessel to reverse at about 200 seconds. In AP600, since the two cold legs were connected at separate locations to the downcomer, the flow in the intact cold leg did not tend to stay reversed. In ROSA, however, the break caused the flow to be reversed in cold leg Volume 252 and stay reversed for about 400 seconds. Since the cold legs to which the intact and affected PBLs were attached were both connected to the vessel through a single pipe (Volume 252), flow also stayed reversed into the volume connected to the intact PBL (Volume 248) and contributed to continued CMT recirculation.

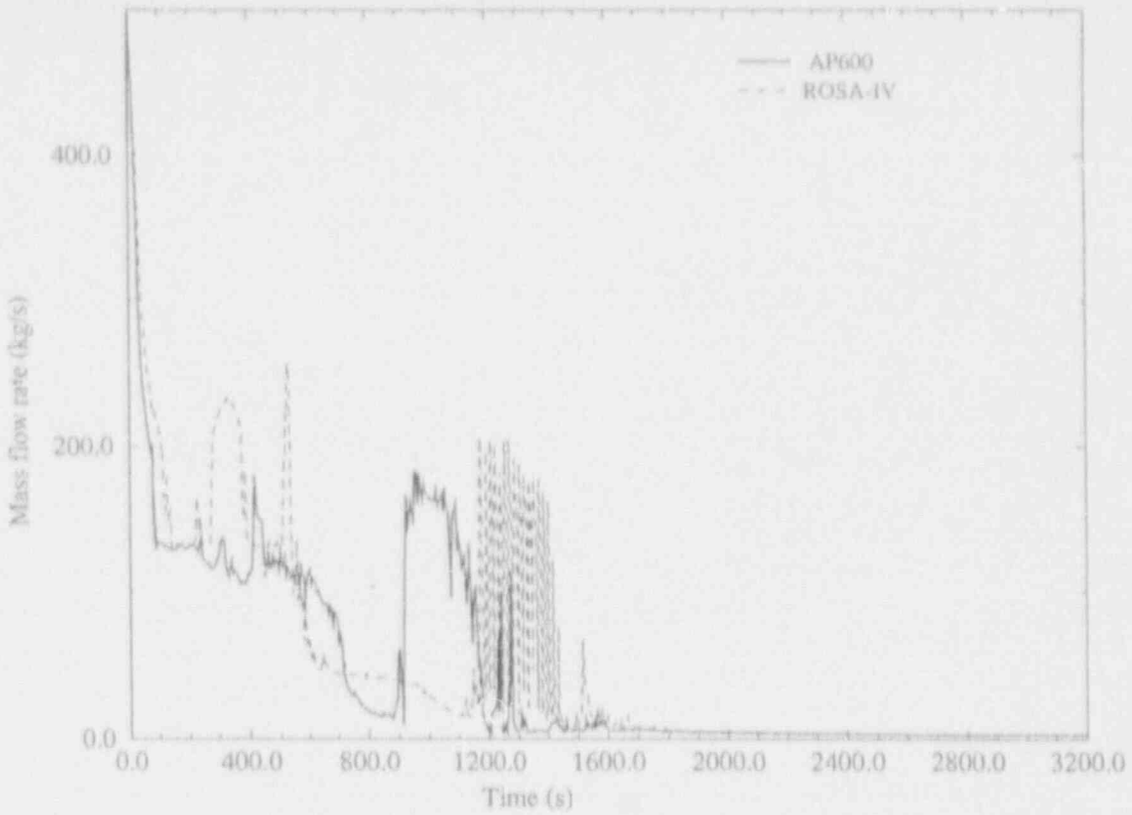

Figure A- 1. Pressure balance line 3–in. break—break flow rate responses.

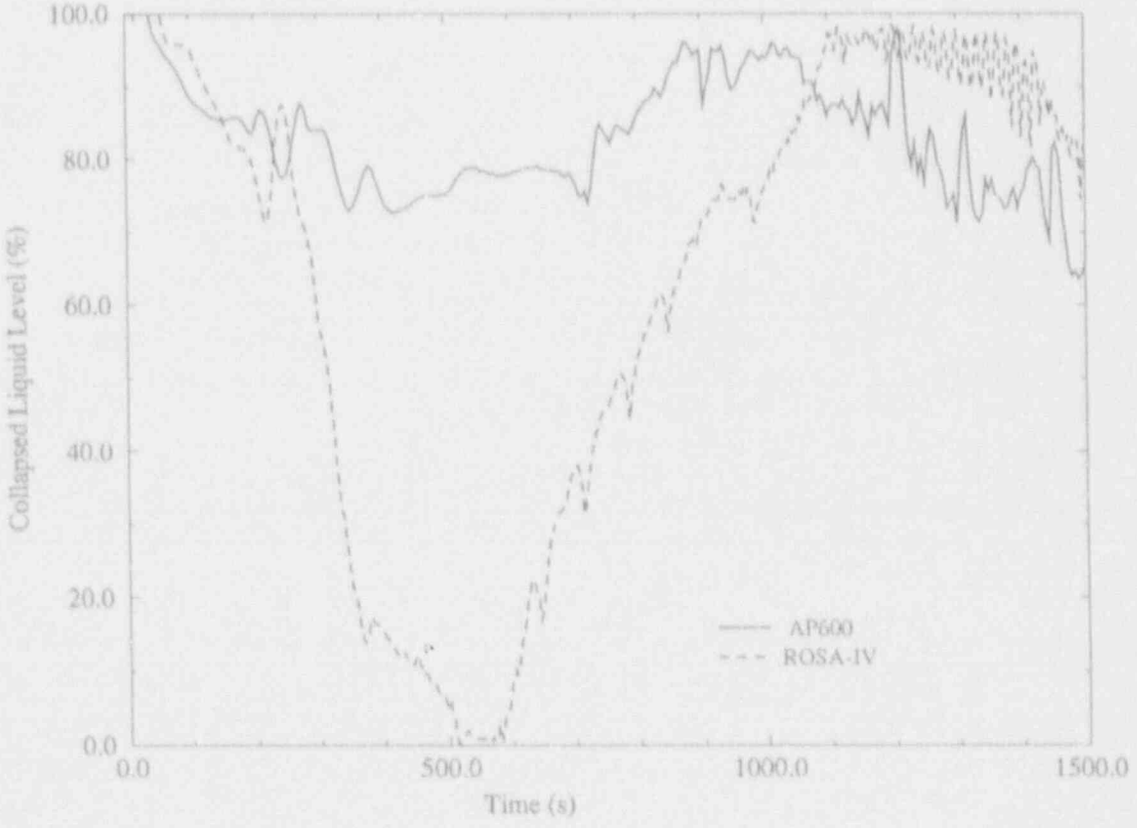

Figure A- 2. Pressure balance line 3–in. break—core collapsed liquid level (%).

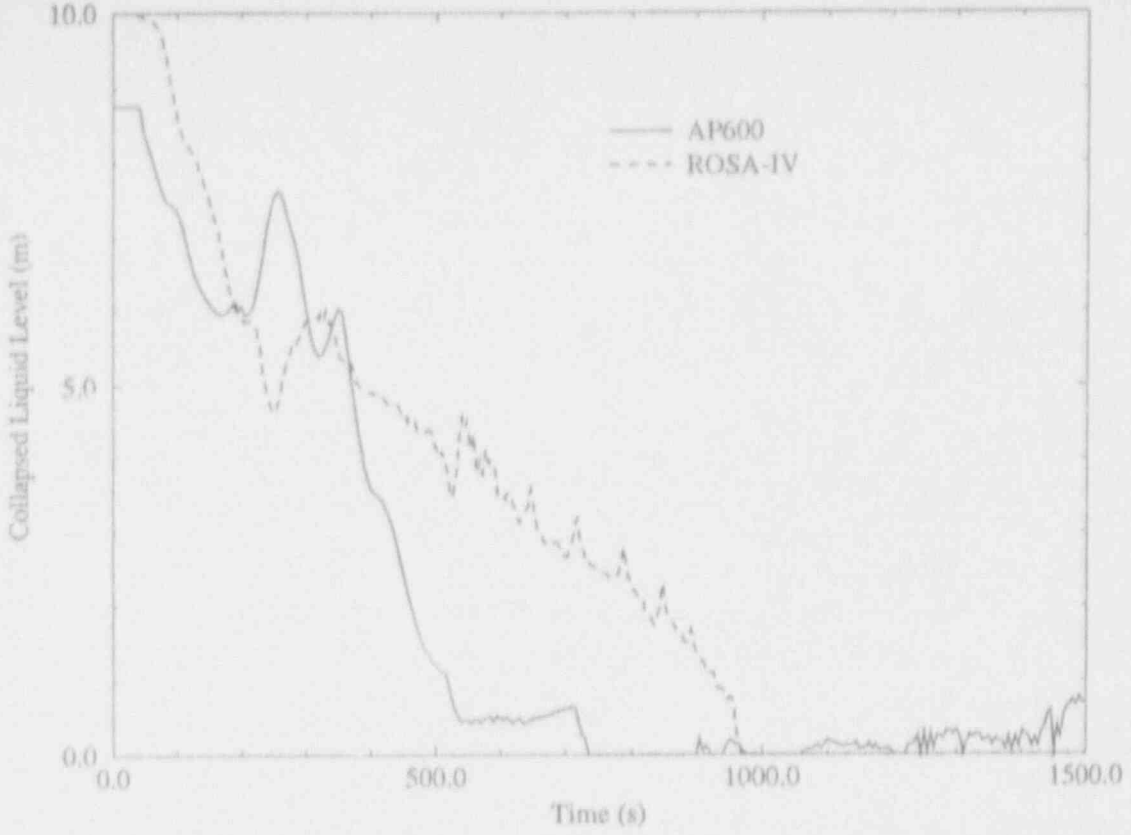

Figure A- 3. Pressure balance line 3–in. break—steam generator tube upflow side collapsed liquid level.

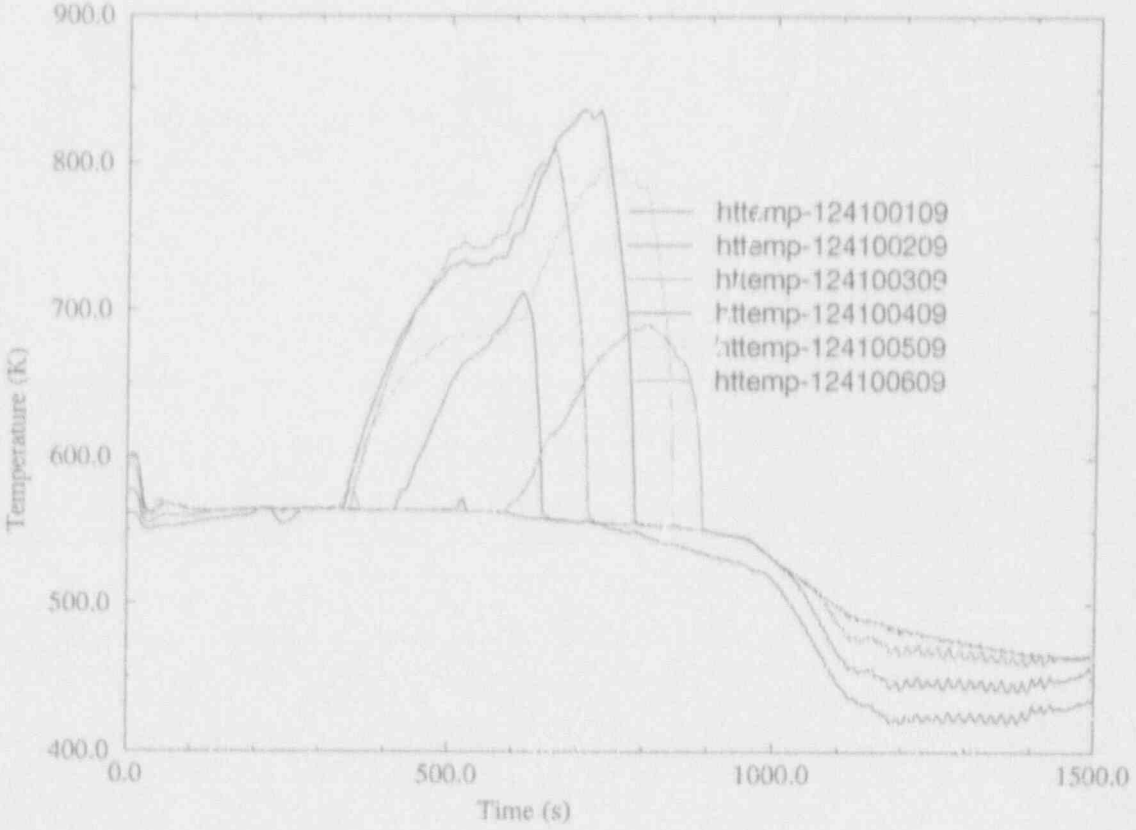

Figure A- 4. ROSA pressure balance line 3–in. break—fuel cladding temperature (K).

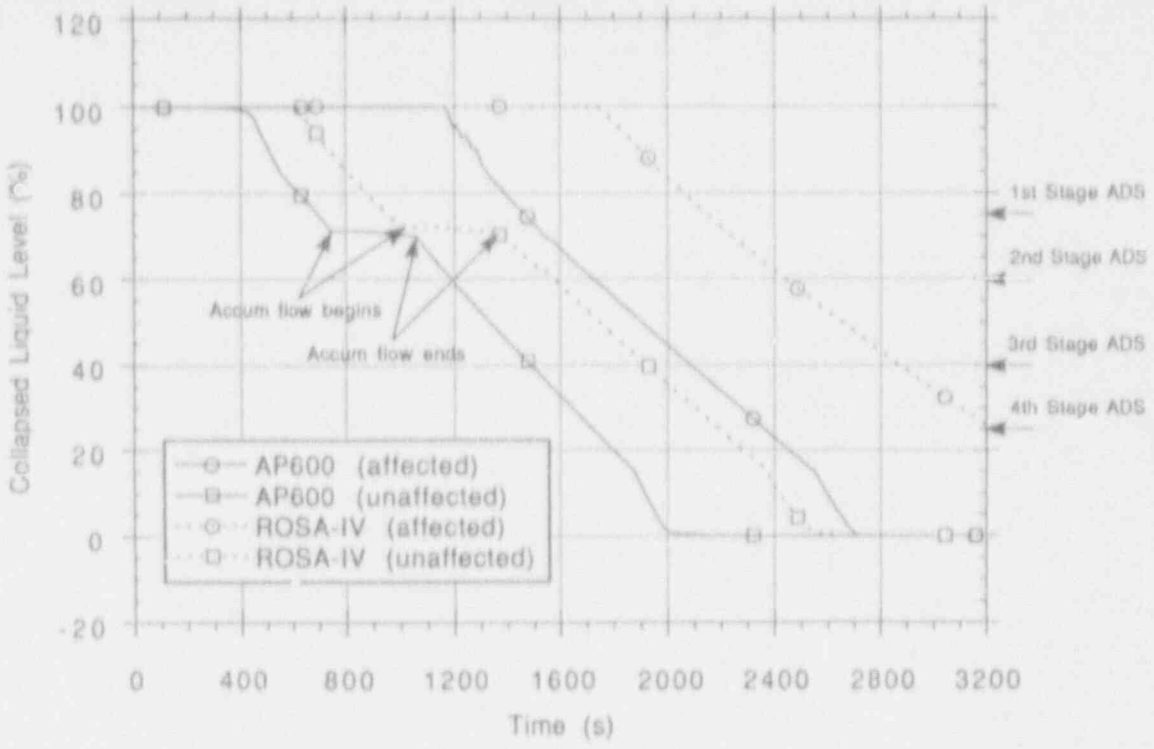

Figure A- 5. Pressure balance line break (two cold legs): collapsed liquid level in the core makeup tanks shows that the ROSA CMTs drained later than those of AP600.

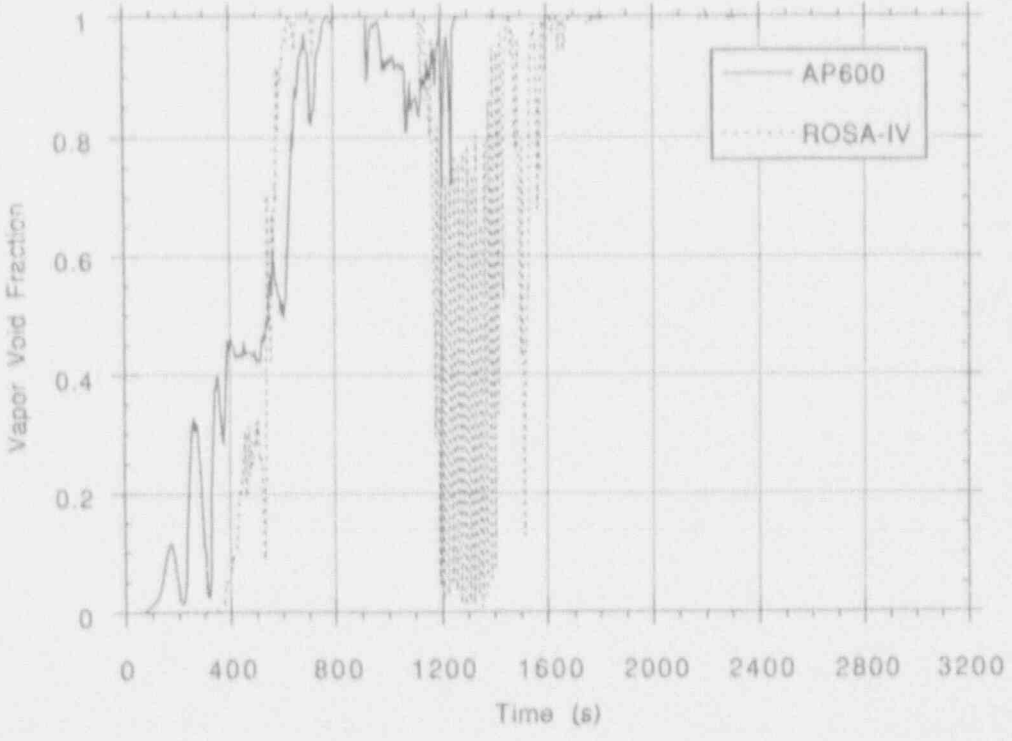

Figure A- 6. Pressure balance line break (two cold legs): void fraction in the cold leg volume connected to the intact CMT pressure balance line (Volume 375 for AP600, Volume 249 for ROSA) shows that voids appeared later in the ROSA cold leg.

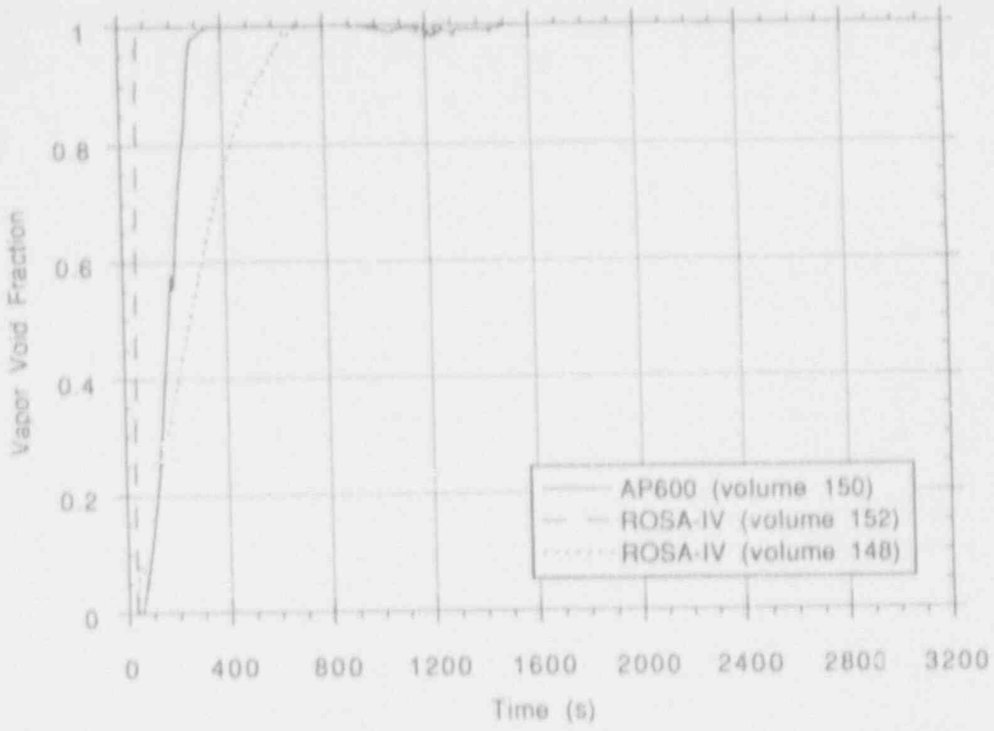

Figure A-7. Pressure balance line break (two cold legs): void fraction in the upper head volumes (Volume 150 for AP600, Volumes 152 and 148 for ROSA) shows that the upper head drained later in ROSA.

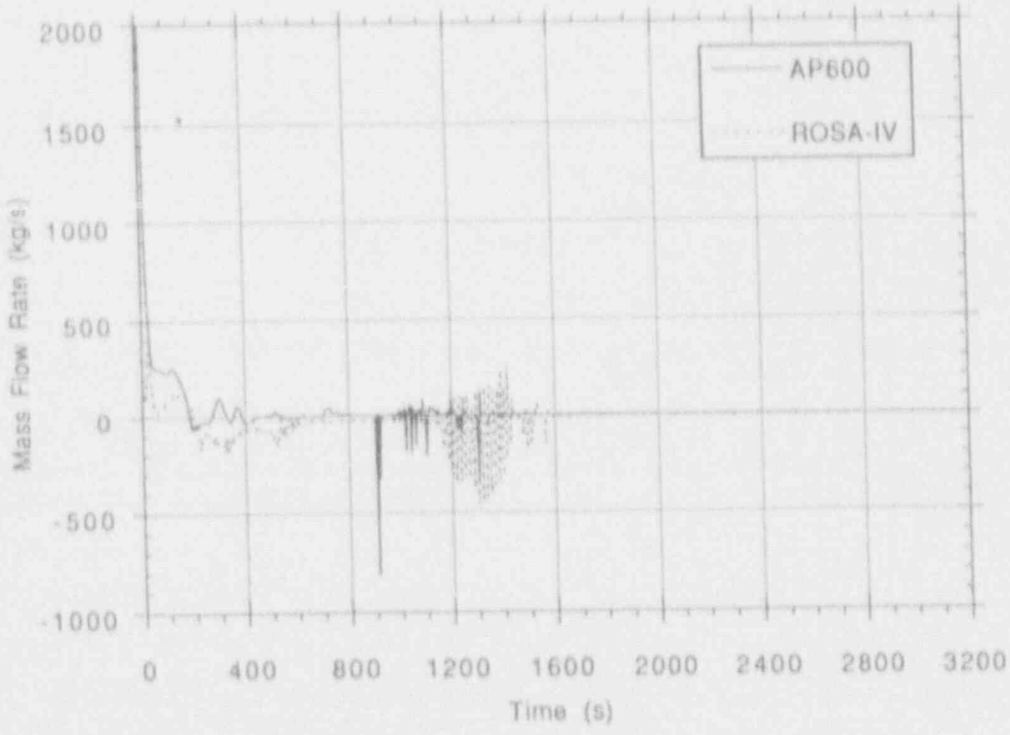

Figure A-8. Pressure balance line break (two cold legs): Mass flow rate in the affected cold leg (from Volume 380 to Volume 102–2 in AP600, from Volume 249 to Volume 252 in ROSA) shows that although both reverse at about the same time, only the ROSA flow tended to stay reversed.

NRC FORM 335 (2-89) NRCM 1102, 3201, 3202

U.S. NUCLEAR REGULATORY COMMISSION

BIBLIOGRAPHIC DATA SHEET

(See instructions on the reverse)

1. REPORT NUMBER (Assigned by NRC, Add Vol., Supp., Rev., and Addendum Numbers, if any.)

NUREG/CR-5853
EGG-2670

2. TITLE AND SUBTITLE

Investigation of the Applicability and Limitations of the ROSA Large-Scale Test Facility for AP600 Safety Assessment

3. DATE REPORT PUBLISHED

MONTH	YEAR
December	1992

4. FIN OR GRANT NUMBER

L2513

5. AUTHOR(S)

Marcos G. Ortiz, James E. Fisher, James M. Cozzuol, Timothy J. Boucher, Sandra M. Sloan, S. Mike Modro

6. TYPE OF REPORT

Technical

7. PERIOD COVERED (Inclusive Dates)

8. PERFORMING ORGANIZATION – NAME AND ADDRESS (If NRC, provide Division, Office or Region, U.S. Nuclear Regulatory Commission, and mailing address; if contractor, provide name and mailing address.)

Idaho National Engineering Laboratory
EG&G Idaho, Inc.
P.O. Box 1625
Idaho Falls, Idaho 83415

9. SPONSORING ORGANIZATION – NAME AND ADDRESS (If NRC, type "Same as above"; if contractor, provide NRC Division, Office or Region, U.S. Nuclear Regulatory Commission, and mailing address.)

Division of Systems Research
Office of Nuclear Regulatory Research
U.S. Nuclear Regulatory Commission
Washington, D.C. 20555

10. SUPPLEMENTARY NOTES

11. ABSTRACT (200 words or less)

A comparison of the thermal hydraulic behavior of the Advanced Passive 600 MW(e) (AP600) and the Rig of Safety Assessment (ROSA) Large-Scale Test Facility (LSTF), under similar initial and boundary conditions, was developed through computer simulations of selected accident scenarios for the Nuclear Regulatory Commission. The purpose of the comparison was to develop criteria to evaluate the capability of a scaled integral facility to perform an AP 600 safety assessment. It was concluded that ROSA LSTF, with a minimum of required modifications is capable of reproducing most of the phenomena and behavior expected of AP600; distortions become important for slow transients and cases in which the nonsymmetric behavior of AP600 is relevant.

12. KEY WORDS/DESCRIPTORS (List words or phrases that will assist researchers in locating the report.)

AP600 safety assessment
ROSA
passive safety
RELAP5
transient simulation
thermal hydraulic behavior

13. AVAILABILITY STATEMENT

Unlimited

14. SECURITY CLASSIFICATION

(This Page)
Unclassified

(This Report)
Unclassified

15. NUMBER OF PAGES

16. PRICE

NRC FORM 335 (2-89)

Federal Recycling Program

UNITED STATES
NUCLEAR REGULATORY COMMISSION
WASHINGTON, D.C. 20555-0001

OFFICIAL BUSINESS
PENALTY FOR PRIVATE USE, $300

SPECIAL FOURTH-CLASS RATE
POSTAGE AND FEES PAID
USNRC
PERMIT NO. G-67